Kinetic modelling simulation and optimal operation of fluid catalytic cracking of crude oil: Hydrodynamic investigation of riser gas phase compressibility factor, kinetic parameter estimation strategy and optimal yields of propylene, diesel and gasoline in fluid catalytic cracking unit

KINETIC MODELLING, SIMULATION AND OPTIMAL OPERATION OF FLUID CATALYTIC CRACKING OF CRUDE OIL

Y M JOHN

Ph.D

UNIVERSITY OF BRADFORD

2018

Kinetic modelling simulation and optimal operation of fluid catalytic cracking of crude oil

Hydrodynamic investigation of riser gas phase compressibility factor, kinetic parameter estimation strategy and optimal yields of propylene, diesel and gasoline in fluid catalytic cracking unit.

Yakubu Mandafiya JOHN

BEng Chem. Eng., MEng Chem. Eng.

Submitted for the Degree of

Doctor of Philosophy

Chemical Engineering, School of Engineering, Faculty of Engineering, and Informatics.

University of Bradford

United Kingdom

2018

Kinetic Modelling Simulation and Optimal Operation of Fluid Catalytic Cracking of Crude Oil

By Yakubu Mandafiya John

***Key words*:** FCC riser; modelling and simulation; six-lumped model; parameter estimation; maximisation; propylene; optimisation; gasoline; diesel; CO_2; Compressibility Factor.

Abstract

The Fluidized Catalytic Cracking (FCC) is known for its ability to convert refinery wastes into useful fuels such as gasoline, diesel and some lighter products such as ethylene and propylene, which are major building blocks for the polyethylene and polypropylene production. It is the most important unit of the refinery. However, changes in quality, nature of crude oil blends feedstock, environmental changes and the desire to obtain higher profitability, lead to many alternative operating conditions of the FCC riser.

There are two major reactors in the FCC unit: the riser and the regenerator. The production objective of the riser is the maximisation of gasoline and diesel, but it can also be used to maximise products like propylene, butylene etc. For the regenerator, it is for regeneration of spent or deactivated catalyst.

To realise these objectives, mathematical models of the riser, disengage-stripping section, cyclones and regenerator were adopted from the literature and modified, and then used on the gPROMS model builder platform to make a virtual form of the FCC unit. A new parameter estimation technique was developed in this research and used to estimate new kinetic parameters for a new six lumps kinetic model based on an industrial unit. Research outputs have resulted in the following major products' yields: gasoline (plant; 47.31 wt% and simulation; 48.63 wt%) and diesel (plant; 18.57 wt% and simulation; 18.42 wt%) and this readily validates the new estimation methodology as well as the kinetic parameters estimated. The same methodology was used to estimate kinetic parameters for a new kinetic reaction scheme that considered propylene as a single lump. The yield of propylene was found to be 4.59 wt%, which is consistent with published data.

For the first time, a Z-factor correlation analysis was used in the riser simulation to improve the hydrodynamics. It was found that different Z factor correlations predicted different riser operating pressures (90 – 279 kPa) and temperatures as well as the riser products. The Z factor correlation of Heidaryan et al. (2010a) was found to represent the condition of the riser, and depending on the catalyst-to-oil ratio, this ranges from 1.06 at the inlet of the riser to 0.92 at the exit.

Optimisation was carried out to maximise gasoline, propylene in the riser and minimise CO_2 in the regenerator. An increase of 4.51% gasoline, 8.93 wt.% increase in propylene as a single lump and 5.24 % reduction of carbon dioxide emission were achieved. Finally, varying the riser diameter was found to have very little effect on the yields of the riser products.

Acknowledgement

I deeply express my profound gratitude to my supervisor Prof. Iqbal Mujtaba, whose inestimable fatherly and professional guidance, support, encouragement, wisdom and instructions made this work a reality.

I am genuinely grateful to my co-supervisor Dr. Raj Patel for his invaluable assistance, guidance and support, making my work to be effective and efficient.

My sincere gratitude to my lovely wife Dorcas Osarugue Yakubu John and son Favour Yakubu John for their so much joy, love and patience expressed towards me as I worked on this research. They are treasures of inestimable price.

I am grateful to God for my Pastors and their families: Pastor Chris Oyakhilome, Pastor Light Morafa and Pastor Andrew Abraham for their invaluable love and leadership, which help me to chart the course of my life.

To my father, late Ex-Cpl John Mandafiya and Mother, Mrs Elsin Mandafiya John, you are the giants on whose shoulders I stand to be what I am today. You are symbols of strength, courage and greatness. I love you!

My special love and thanks to my brothers and sisters, and their families; Justina, Noel, Amos, Kauna, Ibrahim, Markus, Rebecca, Sarah, Naomi and Josephine, for their love and prayers. So much love to my Father in-law; Samson Enadeghe and Mother In-law; Helen Enadeghe. A big thanks to my brothers and sisters in-law, and their families; Terry, Kate, Ken, Deborah, Smart and Martins; for their kindness and love. Special thanks to my relatives, colleagues and friends.

Finally, I thank the Federal Government of Nigeria and Petroleum Technology Development Fund (PTDF) for sponsoring my PhD programme.

Above all, honour and praise to God Almighty for the avalanche of grace unleashed in me and towards me. I dedicate this work to Him alone, the strength and quality of my life.

Table of contents

List of Figures

List of Tables

Nomenclature

A	Surface area, m^2
A_{lg}, B_{lg}, C_{lg}	Coefficients of the Antoine equation for gas oil feedstock
A_{ptc}	Effective interface heat transfer area per unit volume, m^2/m^3
C	Mole concentration, kg mole/m^3
C_{ck}	Coke on catalyst, kg coke/kg catalyst
C_{ckSTO}	Minimum coke content attainable by stripping, kg coke/kg catalyst
C_d	Drag coefficient
C_f	Catalyst-gas friction coefficient, kg/m^3 s
C_{p_g}	Gas heat capacity, kJ/kg K
C_{p_s}	Solid heat capacity, kJ/kg K
D	Diameter, m
d_c	Catalyst average diameter, m
E	Activation energy, kJ/kg mole
F	Mass flow rate, kg/s
f	Mole fraction or friction coefficient
H	Specific enthalpy, kJ/kg
ΔH	Heat of reaction kJ/kg
ΔH_{vlg}	Heat of vaporisation of liquid feedstock in the feed vaporisation section, kJ/kg
h	Height (m)
h_p	Interface heat transfer coefficient between the catalyst and gas phases, kJ/m2 s K
k_{i0}	Frequency factor in the Arrhenius expression, 1/s
k_i	Rate coefficient of the four-lump cracking reaction, 1/s
K_g	Thermal conductivity of hydrocarbons
L	Length, m
M_w	Molecular weight
P	Pressure, kPa

P_{pr}	Pseudo-reduced pressure
Q_{react}	Rate of heat generation or heat removal by reaction, kJ/s
R	Overall rate of reaction
R_g	Ideal gas constant, 8.3143 kPa m^3/-kg mole K or kJ/kg mole K
RAN	Aromatics-to-Naphthenes ratio in liquid feedstock
S_c	Average sphericity of catalyst particles
S_g	Total mass interchange rate between the emulsion and bubble phases, 1/s
T	Temperature, K
T_{pr}	Pseudo-reduced temperature
u	Superficial velocity, m/s
V	Volume, m^3
y	Weight fraction
Z	Gas compressibility factor or Z factor

Greek

Ω	Cross-sectional area, m^2
ρ	Density, kg/m^3
∅	Catalyst deactivation function
ε	Voidage
α	Catalyst deactivation coefficient
α_C^*	Exponent for representing α
μ_g	Viscosity, kg/m s
Φ	Maximum likelihood objective function
$M\alpha$	Number of experiments performed
$M\beta_i$	Number of variables measured in the *i* th experiment
$M\gamma_{ij}$	Number of measurements of the *j*th variable in the *i*th experiment
σ_{ijk}^2	Variance of the kth measurement of variable j in experiment *i*.

$\hat{y}_{ijk}$	This is determined by the measured variable's variance model kth measured value of variable j in experiment *i*
y_{ijk}	kth (model-)predicted value of variable *j* in experiment *i*

Subcript

a	air
cc	Coke on catalyst
CL1	Cyclone 1
cL2	Cyclone 2
ck	Coke
dg	Dry gas
ds	Disperse steam
dz	Diesel
FS	Feed vaporisation section
g	Acceleration m/s^2
gl	gasoline
go	Gas oil
gs	Gas
j	Reaction path
lg	Liquid feed
MF	Main fractionator
MABP	Molal average boiling temperature, K
MeABP	Mean average boiling temperature, K
P_c	Pseudo-critical
P_r	Pseudo-reduced
Rs	Riser
RT	Disengager-stripping section
ss	Steam

Abbreviations

C/O	Catalyst-to-oil ratio
CCS	Carbon capture and storage
CSTR	Continuous stirred tank reactor
FCC	Fluid catalytic cracking
GA	Genetic algorithm
GOP	Global optimisation problem
gEST	parameter estimation tool in gPROMS
HCO	Heavy cyclic oil
HFO	Heavy fuel oil
HOC	Heavy oil cracker
IPCC	Intergovernmental panel on climate change
KRPC	Kaduna refinery and petrochemical company
LCO	Light cyclic oil
LFO	Light fuel oil
LCO	Light cycle oil
MABP	Molal average boiling temperature
MeABP	Mean average boiling temperature
MINLP	Mixed-integer non-linear
MOO+GA	Multi-objective optimisation and genetic algorithm
MXLKHD	Maximum Likelihood formulation technique
NLP	Non-linear optimisation
PFR	Plug flow reactor
PSO	Particle swarm optimisation
RCC	Residual catalytic cracking
SLP	Successive linear programming
SQP	Successive quadratic programming
SRQPD	Successive reduced quadratic programming
SSE	Sum of square errors
Texaco	The Texas company
UOP	Universal oil products

VGO	Vacuum gas oil
VR	Vacuum residue
WHSV	Weight hourly space velocity

Chapter 1

Introduction

1.1 Background

A fluidized catalytic cracking (FCC) unit is a process which is at the heart of a modern refinery and converts refinery residues such as vacuum and atmospheric gas oil, and in recent time co-processed with biofuel (Pinho et al. 2017; Ma et al. 2018) to maximise the production of gasoline, jet fuel and diesel. Its operation is central to the effective performance of a refinery. This process is achieved using a cracking catalyst that cracks different feeds to products. These products serve as the source of feedstock for the main downstream processes that also contribute to the gasoline pool (Bollas et al. 2007a). Gasoline and diesel are fuels produced by many processes in the downstream sector of the petroleum industry; however, not all the processes are as efficient as the FCC unit to meet the high demand for fuels. For instance, a typical barrel of crude contains approximately 20% straight run gasoline, but the demand for gasoline is nearly 50% per barrel, which is met using an efficient FCC unit.

A typical FCC unit receives different types of feedstocks containing high boiling point constituents from several other refinery process units and cracks these streams into lighter and more valuable components. The hydrocarbon feed comes into a transport bed tubular reactor (riser) through feed atomizing nozzles and is exposed to the high enthalpy rich catalyst from the regenerator. The feed is subjected to vaporisation and cracks down into middle distillates as it journeys upwards along with the catalyst in a fluid-like fashion (Gupta et al. 2007). After further processing, the FCC unit products are mixed with products from other refinery units to produce useful products, e.g. distillate and different grades of gasoline (Grosdidier et al. 1993).

In any refinery, the quantity of low market-value feeds accessible for catalytic cracking is high and a typical FCC unit exemplifies a volume that is one-third the crude units. Its enormous throughput and capability to produce gasoline, diesel and other useful middle distillates makes the FCC unit a major player in the overall economic performance of a refinery. This is the reason that the FCC is an

eye-catching unit for advanced computer controls, simulation and optimisation (Grosdidier et al. 1993).

The FCC technology continues to evolve even though the first commercialization occurred more than a half century ago (Gao et al. 2006). This is because of the thoughtfulness many researchers have given to the unit owing to its importance as the workhorse of the modern refinery. According to Lan et al., (2009) about 45% of worldwide gasoline production comes from the FCC process and its ancillary units. Especially for China, due to the lack of hydrocracking and hydro-conversion units, FCC remains the most important and profitable heavy oil conversion process in the Chinese petroleum refining industry (Lan et al. 2009).

Looking at the entire refinery process system, FCC unit (Figure 1.1) presents the maximum potential for accumulative profitability; because little improvement in the gasoline, diesel and in recent time, propylene yields entails a large economical profit where large production units of millions of barrels of these products per day (Zeydan 2008; Alvarez-Castro et al. 2015a).

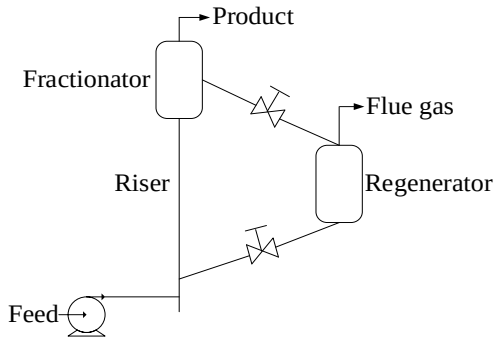

Figure 1.1: Schematic diagram of the FCC unit

1.2 Current challenges in the FCC unit

The FCC unit is made up of the riser unit where catalytic cracking of gas oil is carried out and the regenerator where the deactivated catalyst is regenerated (Wilson 1997). Many FCC units are in operation all over the world. In China alone, about 190 FCC units are in operation with a total capacity of 210 million metric tonne per year (Xie et al. 2018). Even though this process is one of the most significant achievements of chemical engineering of the last century, catalytic cracking technologies are having new opportunities and challenges because of the necessities for high product yields, better fuel quality, increased propylene production and low carbon dioxide (Xie et al. 2018). In addition, the challenge of

modelling the system which is due to its complex internal feedback loop fashioned by the circulating catalyst and its complex dynamic responses. However, due to the high production capacity of the FCC unit, great investment in research and technology is made over the years to develop new expertise that improve productivity of the unit. The total economic advantages of a refinery could be improved greatly if proper modelling, control and optimisation techniques are employed. This can be achieved by first developing an accurate model that describes the dynamics of the process (Han and Chung 2001a).

An adequate model acts as a virtual form of a physical system making it possible to investigate the system response under various conditions. Simulations can be carried out rapidly, cheaply, safely and without tampering with the actual process system, which may be used for plant design, design of open loop and close loop control systems, optimisation, trouble-shooting, debottlenecking and performance evaluation. It can also serve for monitoring and evaluation, forecasting of future system behavior, hazard analysis and training of staff.

Most industrial FCC units have little or no simulation models in the open literature that adequately represent the performance of an FCC unit, which is dependent on many parameters. These parameters are feed composition, residence time, reaction temperature, catalyst-to-oil (C/O) ratio, hydrocarbon partial pressure, catalyst properties, and riser hydrodynamics, all of which influence the conversion process in their own way (Dupain et al. 2006). These parameters vary from one technology or design of the FCC unit to another, which means that no two FCC units are the same. For some, the riser comprises of a number of equal sized compartments (or volume elements) of circular cross section (Gupta et al. 2007) whilst, for others, it comprises of a cylindrical vertical vessel where cracking of gas oil is done using catalyst in a vaporised formed (Han and Chung 2001a). Again, some regenerators are two-stage side-by-side while others are single stage units. Therefore, there is a need for a suitable dynamic model for specific FCC units. This is even more so as some FCC units like that of Kaduna Refinery and Petrochemical Company (KRPC) Nigeria, was built over 40 years ago with little maintenance carried out over the years that resulted in its incessant operational fluctuations or breakdown. Equipment wear, exchanger fouling and catalyst deactivation all contribute to an ever-changing processing capability, meaning that a lot of deviations from the original design must have taken place

considerably which will eventually affect the production efficiency of the FCC. With an adequate model of the response and capability of FCC unit, the planning group can confidently generate processing targets knowing that the optimised solution is founded on real capability.

1.3 Scope of the research

The FCC unit is one of the most important processes in the petroleum refining industry where heavy petroleum fractions are catalytically cracked to lower molecular weight products such as gasoline (Heydari et al. 2010a). To emphasize the importance of the FCC unit, currently, 80% of automobile gasoline in China is produced by the FCC unit (Zong et al. 2010). The scope of this research is as follows:

- There are various types of FCC units in operation all over the world. This work is mostly focused on some units of the M. W. Kellogg Orthoflow 'F' unit of KRPC Kaduna, however, some model similarities can be adopted from other FCC units; hence the model will be applicable to other FCC units.
- The FCC Unit plays a dominant role in most refinery operations, representing above 45 percent of product value. Such large complex equipment, high throughput and economic significance means that it is essential that it should operate at the highest level of performance, not just at steady state but throughout the production cycle. Therefore, this work will model the unit in both steady state and dynamic mode.
- The unit is made up of the riser, regenerator, disengager, stripper, catalyst transport lines, plug/slide valves and several auxiliary units (pre-heater, catalyst cooler, and blowers). Only the riser, regenerator, cyclones and the stripper will be considered in this work because they constitute the major hydrodynamics of the FCC Unit.
- The riser of the Orthorflow 'F' FCC unit of KRPC is uniquely designed. It is a vertical cylinder, but it is with varied diameters. This design is such that the reaction proceeds as the catalyst and vapour mixture flow up through the riser. The lower part of the riser is sized to provide enough pick-up velocity. As cracking proceeds, the riser diameter is increased to handle the increasing volume and provide the desired reaction time. The

mixture flows through the remainder of the vertical riser. A lot of work has been carried out on the modelling of the riser as a uniform unvaried diameter vertical tube or cylinder. However, this work will consider the riser as a varied diameter riser. Therefore, the various effects of the riser geometry on the conversion of gas oil and yield of gasoline will be determined while optimal operating parameters through optimisation studies for different modes of operation will be carried out using the gPROMS software.

- The cyclones of the FCC regenerator will be modelled and simulated.
- The riser and the regenerator are generally modelled along with the catalytic cracking reactions of heavy hydrocarbons on zeolite catalysts which is described as complex parallel series reaction in carbonium ion mechanism (Wang et al. 2005). This unit offers a unique challenge by virtue of its complex process dynamics and severe operating restrictions because of the interactions between variables from both regenerator and riser (Vieira et al. 2005). The effective interactions of the process variables of FCC unit play key role in the overall economic performance of a refinery (Grosdidier et al. 1993). Therefore, any change in process variables can change the economics of the entire plant. To better study the effect of the severe operating restrictions, concurrent simulation and optimisation of the riser and the regenerator will be carried out in this work, which is not common in the open literature. Concurrent simulation gives better insight into the overall performance of the FCC unit.
- Simulation of FCC has been carried out with several software, such as Aspen HYSYS®, Matlab®, and Ansys Fluent®. This work focuses on the development of steady state and dynamic model of the FCC unit and to simulate it using gPROMS (5.0.0 version) Software.
- This work will investigate the dynamic and steady state responses of the FCC unit to various plant input variables and validates using operational log data from some industrial FCC units and literature data.

1.4 Aim and objectives of the research

The aim of this research is to model, simulate and optimise a FCC unit, which consists of a varied diameter riser, regenerator, stripper and cyclones.

The model will act as a “surrogate” or virtual form of the FCC system making it possible to investigate the system response under various conditions. The objectives of this work can be summarized as follows:

- To carry out extensive literature survey on the various types and sections of the FCC Unit
- To develop a detailed model of the riser, stripper, regenerator and cyclones unit using momentum, mass and energy balances, by reviewing the over simplified assumptions modelling the unit. This is mostly done by improving the FCC model presented in the literature (Han and Chung 2001a; Han and Chung 2001b)
- To simulate the riser and regenerator using gPROMS and investigate the effect of varying diameters and compressibility factor
- To simulate the cyclone and stripper using gPROMS
- To carry out optimisation of the riser and regenerator: to maximise gasoline and propylene and minimise CO_2 emissions
- To carry out parameter estimation for kinetic lumps
- To carry out concurrent simulation of the riser and regenerator.

1.5 gPROMS software for modelling, simulation and optimisation

The software general Process Modelling System (gPROMS) Model Builder is a powerful modelling platform for simulation and optimisation of both steady state and dynamic systems. Unquestionably, it can be successfully used for any process system if accurate mathematical models are available. Among many modelling software, the gPROMS suits has several key advantages, which include easy to use interface, capability of handling both steady and dynamic state operation, design of experiments, drag and drop flowsheets to MS Excel to examine the results, and sensitivity analysis. Furthermore, it provides the model validation scheme, which enable the user to fit the model prediction to match the experimental data (parameter optimisation). In addition, it provides the degree of freedom, which is useful to examine the model structure and investigate the problem specification. Most importantly, the model equations can be built in any hierarchy. In other words, the order in which the equations are written is of no importance. gPROMS can handle many algebraic, differential, and partial differential equations with a high execution speed with high accuracy.

1.5.1 gPROMS model builder platform

The gPROMS suite (Process System Enterprise Ltd 2001) was used to simulate the FCC unit using the mathematical models developed as described earlier. The FCC unit model developed is a set of algebraic, differential and partial differential equations written in model entity. The model variables are declared in lower and upper bounds and their default values specified in variable type's entity. Whereas, the process entity includes the setting of process parameters (module specifications) and assigned variables. Once the model is built in gPROMS, it can be used to carry out several simulations such as experimental design, parameter estimation, and process optimisation. The optimisation entity enables the user to carry out a non-linear optimisation (NLP) and Mixed-Integer non-linear (MINLP) optimisation. The gPROMS project tree with the provided entities are shown in screenshot picture of Figure 1.2.

The MODEL platform has several requirements to build the model as follows:

- PARAMETER: This is used to declare the real, integer and constants. The values of the parameters are declared in the PROCESS entity.
- VARIABLE: This is used to declare the model variables, whose lower and upper limits, and default values are specified in the Variable Type entity. The specified variables are assigned in the PROCESS entity.
- EQUATION: This section is used to specify the model equations.

Figure 1.2 shows the screenshot of the model entity section.

The PROCESS platform contains several sections as follows:

- UNIT: This is used to link the process and the model.
- SET: This is used to declare the model parameters.
- ASSIGN: This is used to declare the specified variables. The degree of freedom is related to the number of variables that should be assigned to make the model successfully well posed or to satisfy the degree of freedom.
- INITIAL: This is used to declare the initial conditions of the differential variables at time = zero.

- SOLUTIONPARAMETER: This is used to control various aspects of model-based activities, which include types of solvers (Numerical methods) and their settings, and drop and drag flowsheets etc.
- SCHEDUALE: This is used to implement a variable disturbance for a specified period.

Well-posed models enable the user to plot the simulation results using gRMS plotting channel in 2D and 3D graphs. In addition, the Microsoft Excel output channel can be used to generate an Excel file of the simulation results.

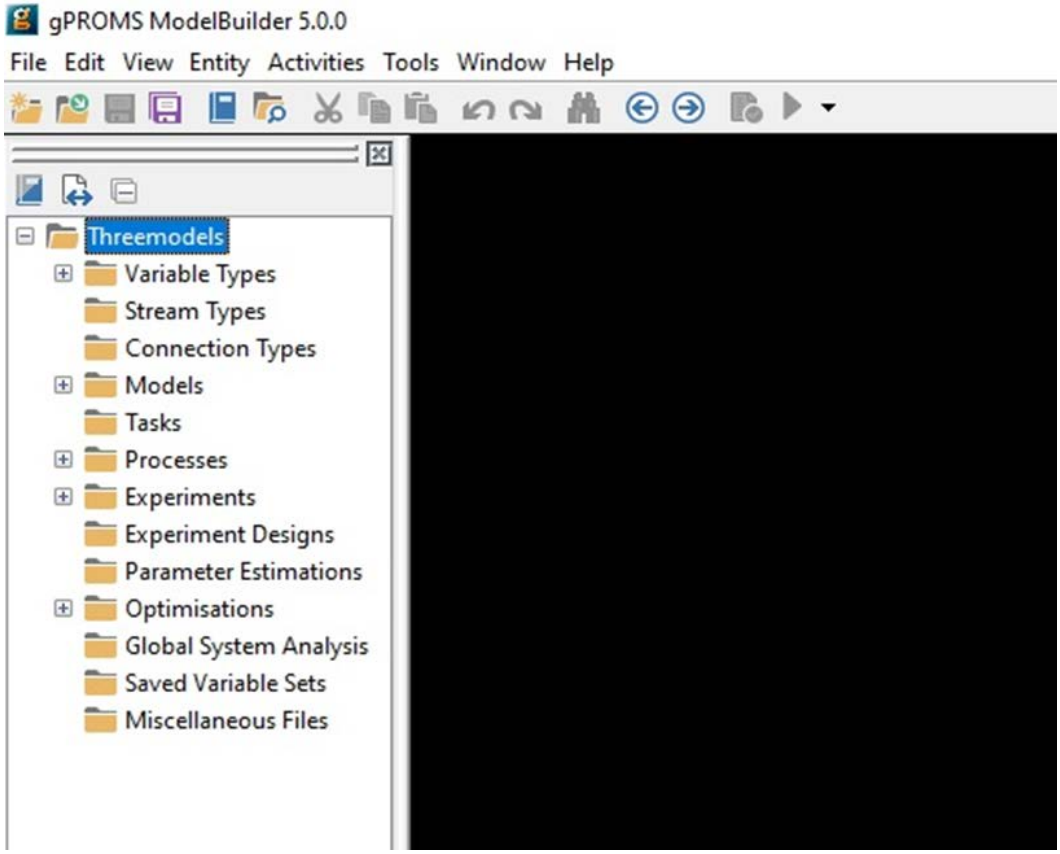

Figure 1.2: Screenshot of the project entities for the gPROMS

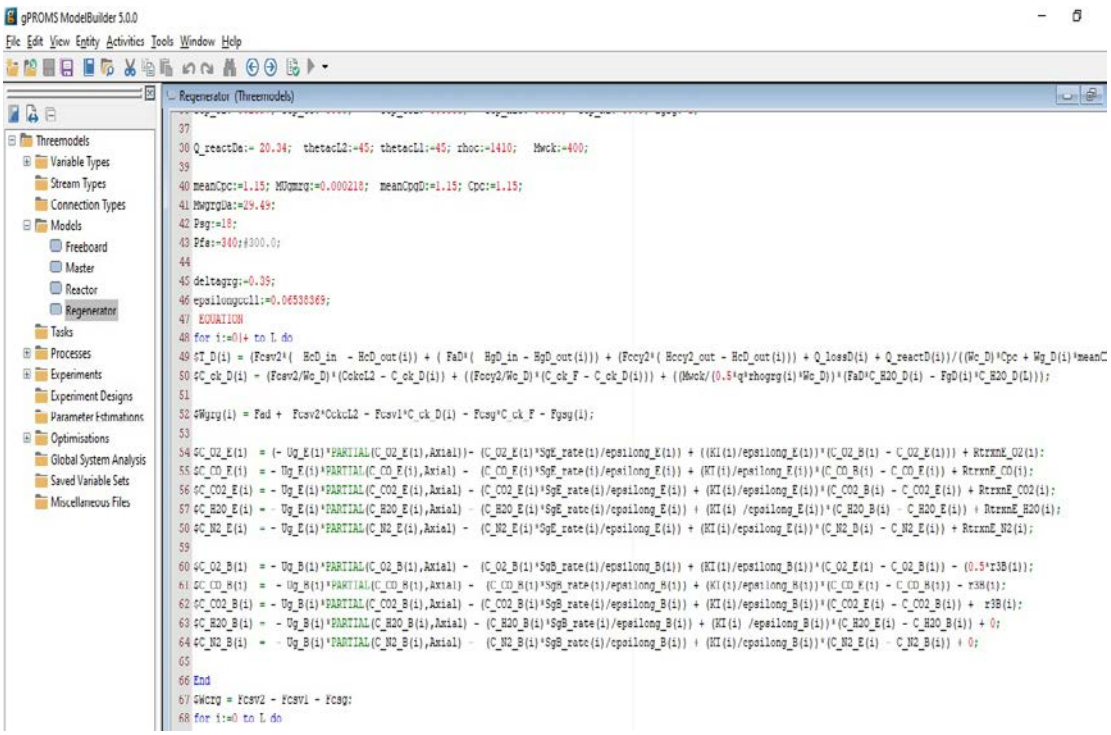

Figure 1.3: Screenshot of the model entity

There are three sections in the optimisation entity: General, Controls and Constraints. The objective function (maximise or minimise) is declared in the General section. The bounds on the optimisation decision variables are declared in the Controls section, while the Constraints section is used to declare other constraints type as follows:

- End-point constraints: These are conditions of the operating variables that the system must satisfy at the end of the operation. These constraints include equality and inequality constraints type. The inequality constraints are within lower and upper limits. Figure 1.3 shows a screenshot of optimisation entity.

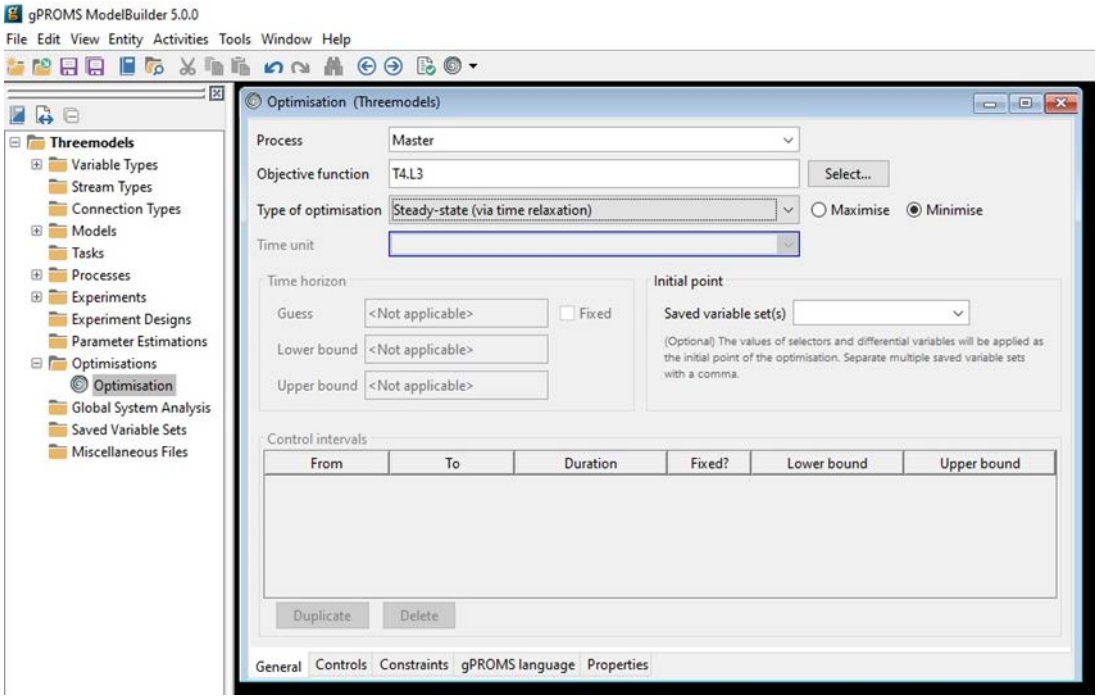

Figure 1.4: Screenshot of the optimisation entity

1.5.2 Simulation solver

gPROMS is designed to use several types of simulation solvers they are basically numerical method solutions for different types of PDAE. These solvers are in the SOLUTIONPARAMETER section of the PROCESS entity. The simulation solver type DASOLVE is usually the default solver, however, gPROMS has the capability to check the level of stiffness of the set of equations and call for the appropriate solvers. In this research, gPROMS can solve mixed sets of non-linear algebraic and differential equations.

1.6 Thesis structure

This work is done in stages based on the various tasks outlined in the chapters. The thesis consists of eight chapters and the next chapters are presented as follows:

Chapter Two: Survey of Literature

The history of FCC units and types are discussed. Kinetic models of the riser and regenerator have been reviewed. Also presented are the riser, stripper, disengager and regenerator hydrodynamics. Process optimisation and parameter estimation techniques are discussed.

Chapter Three: Mathematical models of different units of FCC unit

Detailed mathematical models of the FCC riser, stripper, cyclones and regenerator are presented. The riser model incorporates the mass, energy and momentum balance equations. A parameter estimation technique was proposed to estimate kinetic parameters of the riser kinetic reactions, as well as optimisation procedure for maximizing gasoline and propylene are also presented.

Chapter Four: Parameter estimation of riser kinetic model

Parameter estimation for six lump kinetic model involving the cracking of gas oil was carried out to estimate kinetic parameters of the riser kinetic reactions. Propylene as a single lump has also been proposed in a kinetic scheme and the kinetic parameters estimated. The kinetic data were used for riser simulation and the results were shown and validated against literature and plant data.

Chapter Five: Effects of Compressibility factor on FCC riser hydrodynamics

A model of the riser is used to predict the Z factor in the riser. Different Z factors proposed by many authors were tested and the best, which is consistent with the riser hydrodynamics, was chosen and used for riser simulation with results validated against literature and plant data.

Chapter Six: Optimisation of gasoline and propylene in FCC unit

Optimisation of riser operational variables was carried out to maximise gasoline and propylene in riser unit. Mass flowrates of gas oil and catalyst were used as decision variables while the model equations and some process variables that represent some limitations were used as constraints. The results were validated against literature and plant data.

Chapter Seven: Varied riser and regenerator simulation.

Varied diameter riser and regenerator were concurrently simulated and used for minimisation of CO_2 in the regenerator, while the effect of the varying diameter was evaluated. The dynamic simulation of the stripper-disengager section was also incorporated. The results were validated against literature and plant data.

Chapter 2:

Literature Survey

2.1 Introduction

The history of FCC has been discussed in detail and presented in this chapter. The different kinetic models of riser and regenerator, including the hydrodynamics, have also been presented clearly showing the differences of some commercial FCC units. Parameter estimation, optimisation and Z factor determination have been discussed in this chapter.

2.2 History of FCC units

The French engineer, Eugene Houdry, inventor of catalytic cracking of petroleum in 1915 (Carlisle 2004) developed the first commercial catalytic cracking process in the 1920s. This was done as a result of some experiments on catalysts while sulfur was being removed from oil vapours (Grace 1993). As the catalysts undergo cracking reactions, it became deactivated due to the buildup of a carbonaceous deposit from the cracked oils. Soon after, Houdry found that the catalyst could be regenerated by burning off the carbon deposit using air, thereby restoring the catalyst activity. The idea eventually gave birth to the first continuous cracking of gas oil because of catalyst circulation and made a commercially viable process possible. The Vacuum Oil Company in a joint venture with Standard Oil of New York formed the Mobil Oil and became a strong support for Houdry in the development of this commercially viable process. Sun Oil later became part of them (Blazeck 1993; Grace 1993; Wilson 1997).

Due to careful engineering development on the commercial FCC unit, the first commercially viable Houdry unit came on stream in 1936 with distinguished yields that was vastly superior to those from competitive thermal cracking processes, hence, making catalytic cracking quickly acceptable. By 1943, 24 of these units were in operation or under construction. The combined capacity of these units was 3.815695 x 107 L/d (Blazeck 1993; Grace 1993).

The Houdry process was made up of several reactors, some of which were used for catalyst regeneration while others were for gas purging in a cyclic, fixed bed configuration. According to Grace (1993) and Blazeck (1993), each reactor was

equipped with a molten salt heat removal system, this was because the regeneration of catalyst is an exothermic reaction and heat removal is necessary. The molten salt is a nitrate salt (sodium, potassium or calcium nitrate) which removed and transferred the heat to the reaction step. The molten salt is non-flammable and nontoxic and is used in the chemical and metals industries as a heat-transport fluid (Menéndez et al. 2014). The original catalyst used in the Houdry units were acid-treated bentonite clays (Magee 1993).

The fixed bed catalytic cracking unit was known for handling of large catalyst particles which was not a possible in the past (Grace 1993). Even though, the fixed bed catalytic cracking unit was far superior to thermal processes, the issue of handling large particles was difficult. This eventually led to the development of two continuous processes, moving bed catalytic cracking (MBCC) and fluid catalytic cracking (FCC).

Houdry and Socony-Vacuum Oil Company developed the moving bed process. This process addressed the earlier challenge of handling large particles in the fixed bed catalytic crackers by providing for continuous movement of catalyst from the riser to regenerator. The catalysts pellets were introduced at the top of the reactor along with the feed and flowed co-currently downward through the reaction zone. This is the case of the down-flow risers. As the catalyst contacted the feed, it vapourized and flowed along as the cracking reaction gets the catalyst deactivated by depositing carbonaceous materials on its surface and requiring the regeneration of the catalyst. The catalyst is thus sent to the regenerator to be contacted with air for regeneration as the coke deposit is burned off. Instead of the standpipes of the current FCC unit, the early units used bucket elevators to move the catalyst to the top of the vessels. Later development introduced air lift. The first of these units was a 57,813-liter test unit in New Jersey, the Socony-Vacuum Paulsboro refinery commissioned in 1941 (Sadeghbeigi 2012a). A larger unit processing 1,156,271 l/d was commissioned in 1943 in Magnolia Oil's Beaumont, Texas refinery (Grace 1993).

Catalyst handling was a major challenge for the circulating bed due to the use of those bucket elevators, and to overcome that challenge, the fluid catalytic cracking was developed as an outgrowth of work by Standard Oil of New Jersey (Exxon). In 1938, Catalytic Research Associates (CRA) was formed to develop catalytic cracking technology (Sadeghbeigi 2012a). The original members of CRA

were: Standard of New Jersey (Exxon), Standard of Indiana (Amoco), M.W. Kellogg and I.G. Farben. The Texas Company (Texaco), Anglo Iranian Oil Company (BP), Royal Dutch Shell and Universal Oil Products (UOP) joined the group in 1940. I.G. Farben was dropped from the group at this time (Grace 1993).

The use of both pelleted and powdered catalyst got the attention of the early catalytic cracking technology but by mid – 1940, the pelleted catalyst approach was avoided due to difficulty in the catalyst handling. Initial work with powdered catalyst used long folded reactor lines. Screw conveyors though not quite effective, were used to move the catalysts from region of low pressure to higher pressure (Grace 1993). This led to the discovery of the use of catalyst flowing down a vertical standpipe against a pressure gradient and eliminated need for screw conveyors and greatly simplified the process. This discovery gave birth to the FCC technology in 1940 and the first FCC was commissioned in 1942 in Esso's Baton Rouge refinery. This unit used up-flow reactors. Both the catalyst and air flowed upward through the reactor vessel and exited through the vessel overhead lines. External cyclones were used to collect the catalyst. In this first unit, the feed was vaporised at the vaporisation zone where the catalyst first contacts the feed before being fed to the reactors. Heat removal was achieved from the unit by coiled pipes as catalyst coolers (Montgomery 1993). Later units charged liquid feed, which was vaporised by the hot catalyst from the regenerator. This reduced or eliminated the need for external heat removal.

Again, because of the need to produce more gasoline to meet market demand, even as the first unit was under construction, effort was directed to the development of the next generation of FCC unit. In this unit, a reverse to the down-flow systems consisting of a dense fluid bed topped by a dilute phase emerged to replace the up-flow reactors in existence. These were the model of the Model II FCCs. Cyclones inside the regenerators were used to collect entrained catalyst and return it to the catalyst bed. The first of these Model II units came on stream in 1943 (Grace 1993).

In the early 1960s, M.W. Kellogg and Phillips Petroleum began the development of what was to eventually become the next frontier in catalytic cracking-residual oil cracking. The first purpose built resid cracker, or heavy oil cracker (HOC), was built in Phillips' Borger, Texas refinery (Grace 1993). The original concept was to operate the HOC as a feed preparation unit for the conventional gas oil cracker

already in the refinery. The HOC would feed atmospheric bottoms and operate at low conversion. Heavy gas oils produced in the HOC would then be fed to the existing FCC where they would be converted further.

Kellogg and Phillips anticipated that the high carbon residue present in residual feeds would result in high coke yields, which would generate large amounts of heat energy when the coke was burnt. They realized that some form of regenerator heat removal would be necessary. To meet this, the HOC was equipped with regenerator bed coils submerged in the regenerator bed and boiler feed water was circulated through the coils. Steam generation in the coils absorbed heat from the regenerator bed. In addition, the HOC technology produced a great productive outcome.

This first HOC was a great success and is still in operation today. Despite this, residual oil cracking did not gain significant interest until the mid-1970s. At that time, increases in the price of crude oil, decreasing demand for heavy fuel oil and a decrease in the availability of light crudes increased pressure on refineries to increase the yield of transportation fuels from each barrel of crude oil. This in turn led to renewed interest in cracking the “bottom” of the crude barrel.

In response to these pressures, two new residual oil cracking technologies-the UOP residual catalytic cracking (RCC) technology and the Total Residual fluid catalytic cracking technology were developed to compete with heavy oil cracking (Magee 1993). Both technologies used two–stage regeneration to cope with the problem of excess coke production and were commercialized in the 1970s.

Today, FCC technology is available from a variety of licensors. The major licensors are Exxon, M.W. Kellogg, Stone & Webster/IFP (Total Technology), ABB Lummus Global (Texaco Technology) and UOP (Magee, 1993).

It is interesting to note that four of these five major licensors were members of CRA or rely on technology developed by an original CRA member. In addition, the other CRA members (Shell, Amoco, BP) have continued to develop FCC technology for their own use and/or for limited licensing. Thus, the Stone & Webster /IFP joint licensing effort of the Total RFCC technology is the only significant new entry into the field of FCC development. The fact means that most FCC technologies are the result of more than 50 years of continuing development involving both improved understanding of the chemical and physical processes

involved as well as the equipment needed to control and direct the process to the desired goals. This has produced a technology that is mature in many ways but that continues to evolve to meet the changing needs of petroleum refining.

In summary, the developments and commercialization of both fluid catalytic cracking and moving bed cracking continued in parallel for some time. Eventually, however, the FCC process proved to be a more flexible, efficient, reliable technology and came to dominate the field with currently over 400 units in operation around the world (Clough et al. 2017), and of the over 400 units, 190 units are in china having a total production capacity of 210 MMtpy (Xie et al. 2018).

2.3 Different commercial FCC designs

The reactor/regenerator system has been the dominant feature of the FCC unit since the first commercial FCC came on stream in 1942. Individual FCC configurations differ considerably and results in the differences in the overall performance of various FCC units across the world today. Different FCC units are designed for different feeds and products. It is their designs that affect the operations and performance of each FCC unit. Their designs differ from one another and have their own strengths and weaknesses. There are little changes in the design of the FCCs, which affects their overall operation and reliability, therefore, the need to know the differences in most of the FCC units.

This section summarizes the outstanding features of the common FCC designs in their original form before they underwent revamping and have modern features assimilated.

There are basically two types of FCC units in use today; the side-by-side type where the reactor and the regenerator are separate vessels adjacent to each other, and the stacked or orthoflow type, where the reactor is mounted on top of the regenerator. The Exxon (Esso) designs are typical examples of the side-by-side type (Wilson 1997).

2.3.1 Exxon (Esso) designs

The first commercial FCC was an Esso Model I up-flow unit (Figure 2.1); not many of this design were built and none remain in operation today. This design has historical significance because some of its features can be found in designs that

are more recent. For instance, its feed first went through preheat furnace and vaporised outside the riser reactor. It has up-flow design, one of the features retained by many FCC units today. The risers operated at velocities higher than fluidization velocities causing the up-flowing or fast fluid bed flow. It has external cyclones (a feature still present today) where the spent catalyst was separated from the products. It uses slide valves. The next generation of the Esso FCCs was the Esso Model II, which differ from Esso Model I because it was the first down-flow design that incorporated most of the features found in today's FCC units. In addition, the feed was fed into the riser in a liquid phase. This reduced the necessary feed preheat duty and also served to absorb some of the heat evolved during catalyst regeneration (Wilson 1997). Due to the challenges of using long standpipes experienced with the Model II units, researchers moved to shorten the regenerated catalyst standpipes and ended up with the Model III unit. This attempt reduced the erosion effect of the catalyst on the walls of the standpipes. However, the units still struggled with erosion in the control slide valves and were subject to rapid erosion and became a major maintenance problem, hence the need to have a solution. Esso Model IV was the solution, being a complete departure from these earlier designs, which eliminated this problem by removing the catalyst control valves. Model IV was an up-flow riser, utilizing the advantage of gravity to create pressure differential between the riser and the regenerator as catalyst from the regenerator overflows into the overflow well and down the regenerated catalyst standpipe, through the regenerated catalyst U-bend and into the riser again.

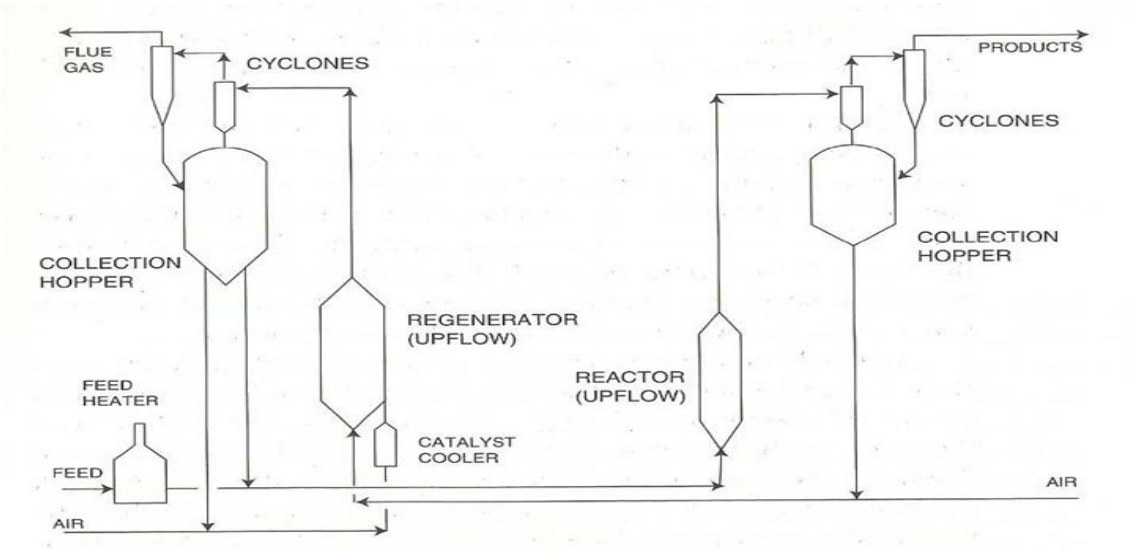

Figure 2.1 Esso Model I (Wilson 1997)

The U-bend as shown in Figure 2.2 was the undoing of the Model IV FCC unit. This is because catalyst flow horizontally at the bottom of the bend and cause some region of defluidization, which require intensive maintenance. A J-bend of Exxon Flexicracker design replaced the difficult-to-operate U-bends of the Model IV FCC unit, with a standpipe and an upwardly sloped laterals making these transfer lines easier to operate (Wilson 1997).

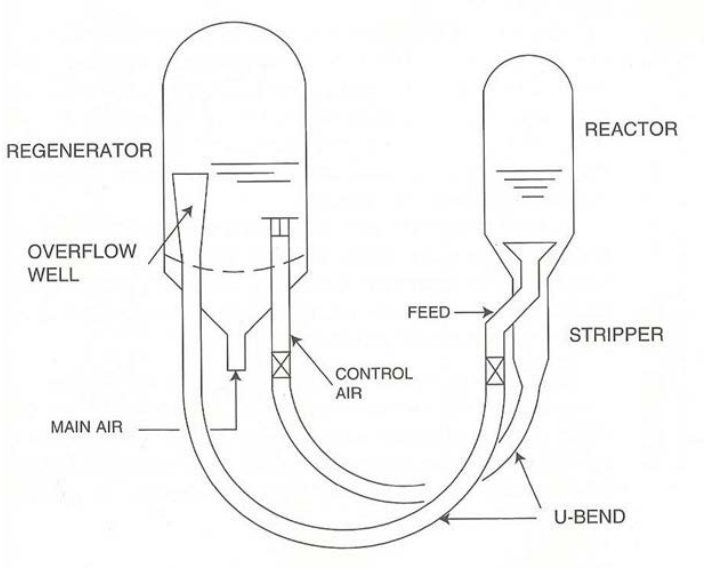

Figure 2.2 Esso IV (Wilson 1997)

2.3.2 M.W. Kellogg designs

Orthoflow A is the first stand-alone Kellogg design. It was a stacked unit (a feature that Kellogg has retained to this day), with the reactor located above the regenerator vessel. There were no slide valves of the former models and plug valves regulated catalyst flow. It is all vertical flow, which earned the name orthoflow. The regenerated catalyst standpipes of former unit are replaced with plug valves and both the riser and the spent catalyst standpipe were internal to the regenerator. Orthoflow B was created without a riser; hence, it was the only true bed cracker ever built. It has a reactor stacked with a regenerator (Wilson 1997). Feed was never in contact with hot catalyst from the regenerator because the feed was injected directly into the bed; hence, the Orthoflow B worked very well as a bed cracker. This reduced thermal cracking reaction and gave improved yields. The Orthoflow C brought back the more conventional design of having the reactor on top and the regenerator on the bottom. It has two risers: one riser for fresh feed and the other for recycle. The Orthflow C configuration holds the distinction of being the first FCC design used in a purpose build resid cracker.

The UltraOrthoflow and Orthoflow F design are similar. Orthoflow F is a type of the KRPC FCC unit; it has the first and second stages side-by-side in the regenerator while the riser is located outside of the reactor and regenerator. Early Orthoflow F designs used a simple inertial separator on the riser termination but currently use riser cyclones or rough-cut cyclones. This unit has an improved plug valve design that eliminated erosion and sticking problems of earlier units.

2.3.3 Lummus (Texaco) Design

Early Texaco designs were catalyst bed equipped with a slide valve to control the flow of catalyst from the reactor to the stripper. The Modern designs use a vertical external riser and have multiple feed injection nozzles with closed cyclone riser termination. The units have a relatively high velocity turbulent bed in the regenerator.

2.3.4 UOP Designs

The UOP stacked unit was a contemporary of the Esso Model III unit and the Orthoflow A. The riser and spent catalyst standpipe were external. These units were designed as bed crackers. The UOP stacked unit was easy to convert to all riser cracking and many of these units are still in operation today (Wilson 1997).

2.3.5 High efficiency regenerator

This design uses a high velocity regenerator against the conventional fluid bed. The high velocities effectively increased burning kinetics in the regenerator due to very good mixing of the spent catalyst and air. Hence, it allows for a lower regenerator volume and thus a greatly reduced catalyst inventory. This design has no significant weakness.

2.3.6 Residual catalytic cracking (RCC) Units

The first purpose built residual catalytic cracking unit brought on-stream in 1961 was a joint development between M.W. Kellogg and Phillips Petroleum. This is a type of the Orthoflow F unit, having two stages in the regenerator but not one stage on the other. This is basically, an Orthoflow C unit and the first heavy oil cracking (HOC) unit. It used steam coils for temperature control by removing excess heat from the regenerator bed. It is a high conversion unit and modern designs incorporate external dense phase catalyst coolers to remove the excess

heat of regeneration. The RCC regenerators are stacked with the first stage on top of the second stage (James and Glenn 2001; Xu et al. 2006; Behjat et al. 2011). The second stage regenerator does not have any cyclones, and flue gas from this stage passes into the bed of the first stage. Thus, there is only one flue gas system.

2.4 Mathematical modelling

The application, maintenance and conservation of model-based engineering tools are scarce due to inexperienced workforce in the refineries (Moro 2003). Therefore, it is expedient for refiners to use costly hand-in-hand solutions from companies who have expertise or are specialized in the development of these engineering applications (Pinheiro et al. 2012). At the level of the industry, model synthesis and process identification are perhaps the most time-consuming steps in the practical application of many advanced process-engineering approaches. For instance, advanced control strategies generally depend on linear “black box” process simulations and even though the models are well developed, they are only useful for the processes where they were acquired. Hence, they are generally unable to represent the nonlinearities of the industrial processes (Pinheiro et al. 2012). These limitations make it difficult when there is need to use wider operating conditions in tasks such as plant optimisation, which require accurate and rigorous models. The production of laborious and detailed FCC models is generally challenging due to the complex nature of the industrial FCC processes. These inaccurate and poorly detailed models are accompanied with the challenge of inadequate and limited classification of the FCC feedstock, the almost nonexistent true steady states in conventional FCC plants and sometimes, the difficulty in accessing plant data for validation of the models. Therefore, to properly implement plant simulation and real time optimisation, more detailed and accurate models including the right feed characterization data are needed (Moro 2003). In the next sections of this work, different mathematical models describing the FCC process simulation and optimisation are presented.

2.4.1 Riser mathematical model

The modelling of the FCC unit is quite difficult because of the presence of all three phases (solid, liquid, and vapour) inside the riser/reactor, involvement of physical and chemical rate steps, and its strong interaction between the riser and the

regenerator. Nevertheless, considerable efforts are being made by various workers in all the above aspects of riser/regenerator modelling (Gupta et al. 2005).

2.4.1.1 Riser kinetics

Gas oil, a feedstock to commercial FCC unit is a complex mixture, which is made up of thousands of different chemical compounds with a wide range of temperature (Souza et al. 2003; Bollas et al. 2007a; Gupta et al. 2007). It is this complex nature of the feedstock and the hydrodynamics of the riser that makes the detailed FCC simulations very challenging (Gupta et al. 2007). The complexity of the gas oil mixture makes the kinetics of the cracking reactions difficult to characterize.

An FCC process model has proven to be useful for control studies, choosing of optimal operation plan, and optimisation of operating conditions, catalysts selection and even staff on the job training. Zong et al. (2010) identified three different types of models that are popularly in use for the cracking reactions in the riser, they are semi-empirical models (Gupta et al. 2005), the lumping kinetic models, and the molecular-level kinetic models (Dewachtere et al. 1999). The semi-empirical models are easy to estimate, nevertheless, they do not replicate the reaction mechanism of catalytic cracking and have poor extrapolation. They are also considered to be of limited application (Hernandez-Barajas et al. 2009). Molecular-level kinetic model is exactly consistent with the reaction mechanism; however, the models are too problematical to calculate and analyse. Lumping kinetic models take the best of the above two models: the lumping models give acceptable and reasonable estimated and calculated parameters. The lumping technique has been shown to be suitable and applicable to the simulation of all kinds of catalytic reactions of hydrocarbon which include catalytic cracking (Zong et al. 2010). Therefore, lumping strategy is considered in this work.

Numerous efforts have been made to describe a perfect reaction scheme for the riser cracking reaction. Wei and Kuo (1969) and Kuo and Wei (1969) presented what they referred to as “principle of invariant response” to describe the dynamics of lumping approach. This is to say that species are classified as single lump due to their invariant dynamic behaviour (similarity in physical properties, such as boiling points and those components of similar chemical properties) on the

composition of species (Kuo and Wei 1969; Wei and Kuo 1969). This approach uses low-order, linear differential equations having lumped pseudo-species to typify large monomolecular reaction systems (Coxson and Bischoff 1987). This strategy gave birth to the lumping methodology as Weekman and Nace (1970), being considered as the pioneers, evolved the simple kinetic lump model for modelling purposes.

Weekman and Nace (1970) carried out some work based on the theory of Wei and Prater (1962) which can be considered as a pioneering work in developing the simple kinetic mechanism for modeling purposes. Weekman and Nace (1970) developed the three lump model where the scheme was divided into the original feedstock (gas oil), gasoline and, dry gas and coke as shown in Figure 2.3.

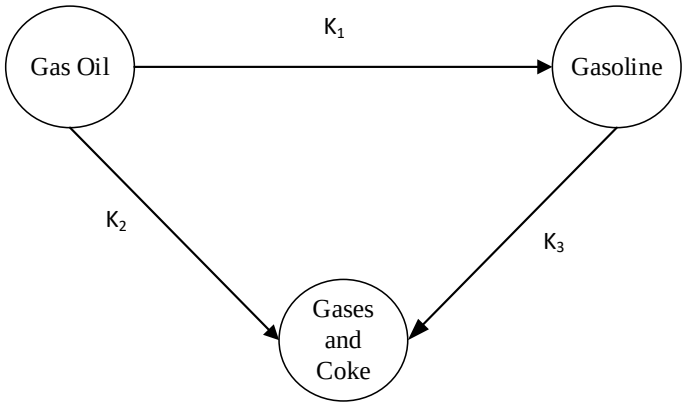

Figure 2.3 Three lump kinetic scheme of Weekman and Nace (1970)

Table 2.1 shows the three paths of the reactions for the three-lump parameters shown in Figure 2.3, and their corresponding order of reactions.

Table 2.1: Reaction Order and Path for three lump model (Cristina 2015)

Reaction	Path	Order
Gas Oil - Gasoline	1	2
Gas Oil - C_1-C_4 gases + Coke	2	2
Gasoline - C_1-C_4 gases + Coke	3	1

The three lump kinetic model has been used by several researchers to estimate the conversion of gas oil and yield of other FCC unit products such as gasoline using various reactor types such as fixed bed, continuous and fluid reactors under isothermal and non-isothermal conditions. Weekman and Nace (1970) estimated the kinetic parameters of the model using the experimental data under isothermal

reactor condition while an optimum reactor temperature was also estimated for the system. The three lump kinetic model has been used extensively because of its simplicity, which led many investigators, such as Lee et al. (1989c) and Theologos and Markatos (1993) to carry out the simulation of the riser reactor with three lump model. Many other users found the three lump model useful (Novia et al. 2007; Ahsan 2012). The three lump model can be used with all feedstock of the FCC unit (Gupta et al. 2005).

The three lump model was further extended to form several other kinetic models, such as the four-lump model. Lee et al. (1989c) took the first step to separate the lump light gas plus coke into two different lumps of C_1-C_4 gas and coke, developing the first 4-lump models for fluid catalytic cracking (Lee et al. 1989c).

The three lump model had a disadvantage, since it could not predict coke concentration independently. The endothermic heat needed in the riser for the cracking is supplied by burning coke in the regenerator, which is formed and deposited on the catalyst. Thus, the accurate prediction of coke concentration that is formed will a benefit for heat integration and reactor temperature control. This formed the basis for the four-lump model.

According to (Lee et al. 1989a), the four lump model cracks gas oil into gases, coke and gasoline as shown in Figure 2.4 and it is known for consolidating the very important refinery fractions. Over the years, the four-lump model is considered the most widely used and acceptable for its accuracy to predict the coke fraction.

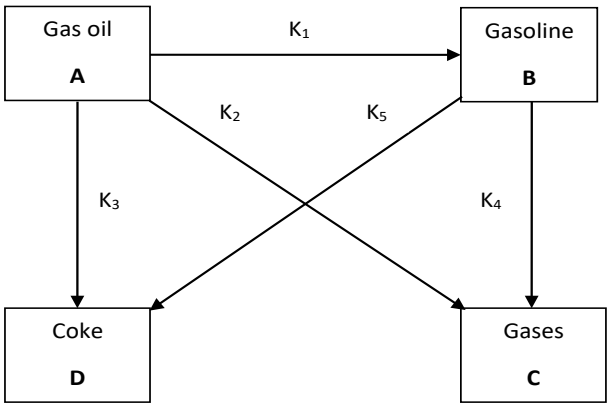

Figure 2.4: Four-lump model for gas oil cracking reactions (Lee et al. 1989a)

Table 2.2 shows the five paths of the reactions for the four-lump parameter presented in Figure 2.4, and their resulting order of reactions.

Table 2.2: Order of the gas oil cracking reactions for four lump model

Reaction	**Path**	**Order of reaction**
Gas oil – Gasoline	A-B	2
Gas oil –C_1-C_4 gases	A-C	2
Gas oil- Coke	A-D	2
Gasoline –C_1-C_4 gases	B-C	1
Gasoline- Coke	B-D	1

The most important kinetic model of the FCC unit is one that has the ability to predict important components of the unit, particularly coke formation. Voorhies (1945) was first to relate the coke formation equation and gas oil conversion. The equation proposed was:

$$Cf = Btx^m \tag{2.1}$$

Where *Cf* is ratio of coke formed to feed in weight percent, *t* the gas oil conversion percent, and *B* and *m* the parameters which depend on temperature, feed composition, and catalyst type (Voorhies 1945). Voorhies (1945) equation is very simple but lacks practical application because it only relates coke formation and extent of gas oil conversion while other important refinery products are not characterized. Hence, further analysis cannot be done using this equation. The three and four lump models were studied, and the conclusion was that the use of the four-lump kinetic scheme gives more reliable and better prediction of the plant data (Ali et al. 1997; Cristina 2015)**.**

Many researchers have used the four-lump model with satisfactory results (Han and Chung 2001a; Han and Chung 2001b; Nayak et al. 2005; Ahari et al. 2008b; Baudrez et al. 2010; Heydari et al. 2010a; Zhu et al. 2011; Lopes et al. 2012; Shayegh et al. 2012; Chen et al. 2013; Ahsan 2015; Cristina 2015; He et al. 2015). According to Ancheyta-Juarez, et al., (1997), if the interest is the subdivisions of the important refinery fractions, then more fractions can be derived from the various lumps. This is the reason why many lumps began to come up from the four lump kinetic model. The five-lump scheme of Corella and Frances (1991b) consists of Heavy Cycle Oil (HCO) lump as the feedstock, which

cracks into heavy and light fractions consisting Light Cycle Oil (LCO) and Coke, and Gasoline and Gas. Corella and Frances (1991b) five lump model is shown in Figure 2.5.

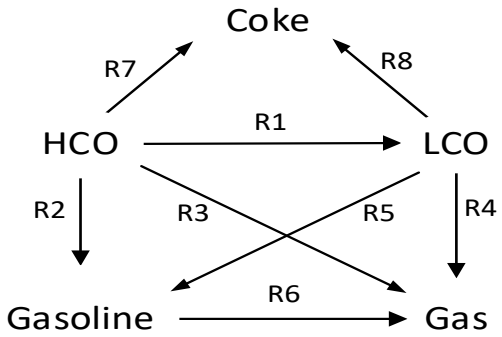

Figure 2.5: Five lump model (Corella and Frances 1991b)

The drive to bring down the maximum concentration of aromatics in gasoline from 40 vol% to 35 vol% in future years makes refiners to seek for the reduction of aromatics, sulfur, and olefins in fuels. In a determination to attain the decrease in aromatic content of gasoline, Dupain et al. (2006) improved the 5-lump model of Corella and Frances (1991b) by reducing the reactions involved in the lumping scheme as shown in Figure 2.6. Larocca and Delasa (1990) improved the 3-lump model to obtain another 5-lump model by separating the gas oil lump into aromatic, paraffinic and naphthenic lumps (Larocca and Delasa 1990; Ancheyta-Juarez et al. 1997). Ancheyta-Juarez et al. (1999) developed a different 5-lump model by treating the gas oil as single lump but separated the gas lump into two lumps (liquefied petroleum gas and dry gas) as shown in Figure 2.7. The advantage of their model is that the three products (coke, LPG and dry gas) can be predicted independently (Ancheyta-Juarez et al. 1999).

Figures 2.6 and 2.7 are five lump models.

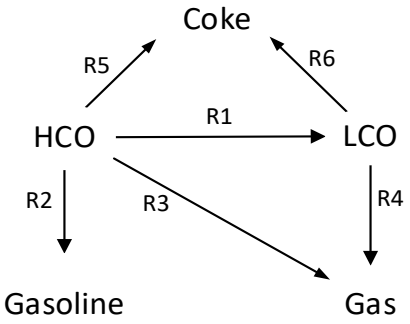

Figure 2.6: Five lump model of Dupain et al. (2006)

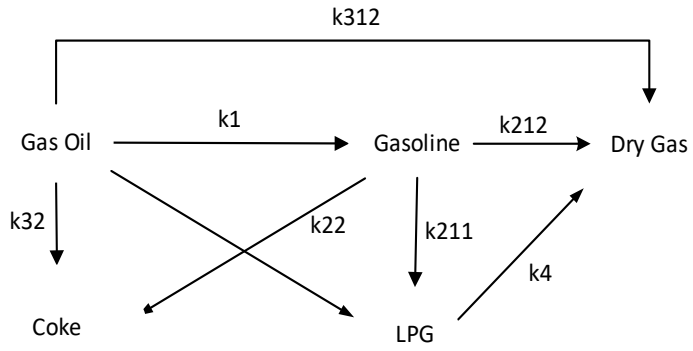

Figure 2.7: Five lump model of Ancheyta et al. (1999)

Many researchers have used the five lump model to simulate the riser reactor (Dupain et al. 2003b; León-Becerril et al. 2004; Al-Sabawi et al. 2006b; Dupain et al. 2006; Bollas et al. 2007a; Roman et al. 2009; Sadighi 2013)

The six (gas oil, LCO, gasoline, fuel gas, LPG and coke) lump model was developed by Coxson and Bischoff (1987) and was used by Takatsuka et al. (1987) to estimate the catalytic cracking of residual oil. The six lumps kinetic model was used to crack from the heavy feedstock, vacuum residue (VR) and the vacuum gas oil (VGO) to heavy cyclic oil (HCO), light cyclic oil (LCO), gasoline, light gases, and coke (Takatsuka et al. 1987). The six-lump model for the riser cracking has been variously and extensively used (Ancheyta and Rogelio 2002; Souza et al. 2003; Souza et al. 2006; Fernandes et al. 2007b; Du et al. 2014). The six-lump kinetic model as presented by Coxson and Bischoff (1987) is shown in Figure 2.8.

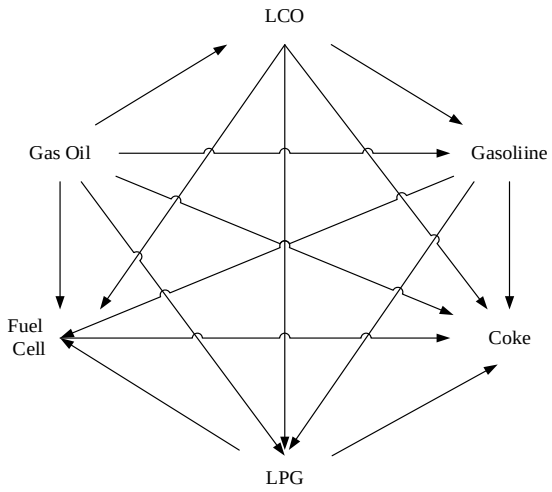

Figure 2.8: Six-lump as presented by Coxson and Bischoff (1987)

In another attempt to obtain suitable kinetic model for the riser reactor, Heydari et al. (2010b) presented a seven lump model and their motive was to maintain a good balance between kinetics and applicability of the model to predict the behaviour of the FCC unit. The seven lump model was divided into Vacuum Residue (VR (>500°C)) and vacuum gas oil (VGO (350-500°C)), heavy fuel oil (HFO (350-500°C)), light fuel oil (LFO (200-350°C)), gasoline (C_5-200°C), LPG (C_3-C_4), dry gas (C_1-C_2) and C (coke). Some researchers (Sugungun et al. 1998; Al-Khattaf and de Lasa 1999; Villafuerte-Macías et al. 2004; Xu et al. 2006; Heydari et al. 2010b; Zong et al. 2010) also used the seven-lump model for the simulation of the riser unit. Figure 2.9 shows a schematic diagram of the seven-lump model.

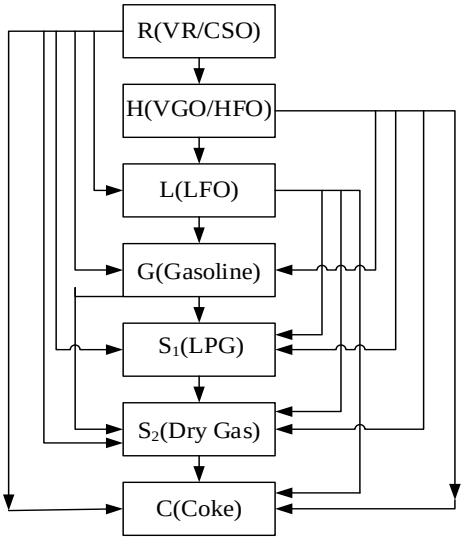

Figure 2.9: Seven lump model (Heydari et al. 2010b)

Hagelberg et al. (2002) extended the 5-lump model of Ancheyta-Juarez et al. (1999) to an eight-lump model by sub-dividing the gasoline lump into paraffins, olefins, naphthenes and aromatics.

In the reaction scheme shown in Fig. 2.10, LPG fraction was formed principally by the cracking reaction of gas oil, which was followed by the cracking reaction of the olefins present in the gasoline fraction. The olefins in the gasoline fraction were chosen as the only lump to form LPG, because olefins crack faster than naphthenes and paraffins with the same molecular weight (Hagelberg et al. 2002).

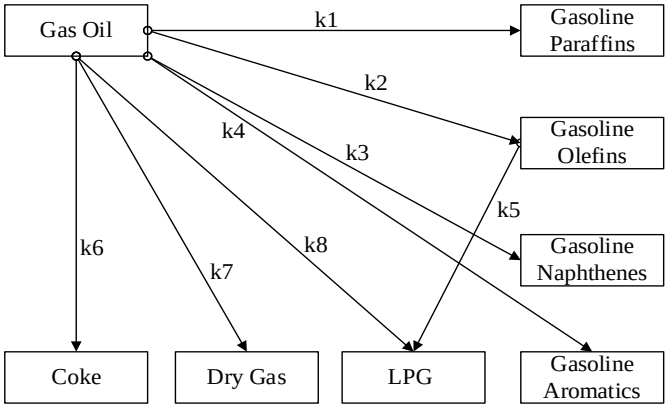

Figure 2.10: Eight lump model (Hagelberg et al. 2002)

The same eight lump model of Hagelberg et al. (2002) was used to describe a new kinetic model for the riser, however, it considered gasoline cracking into LPG and dry gas (Wang et al. 2005).

A nine-lump reaction network model for the aromatization reaction of gasoline, not gas oil, was considered (You 2013). The model considered the cracking of gasoline as the first-order irreversible reaction. The essence was to study the performance of FCC gasoline and catalyst in a restricted fluidized bed reactor in a plug flow, non-axial diffusion, non-radial concentration, and non-temperature gradient. The nine-lump model is presented in Figure 2.11.

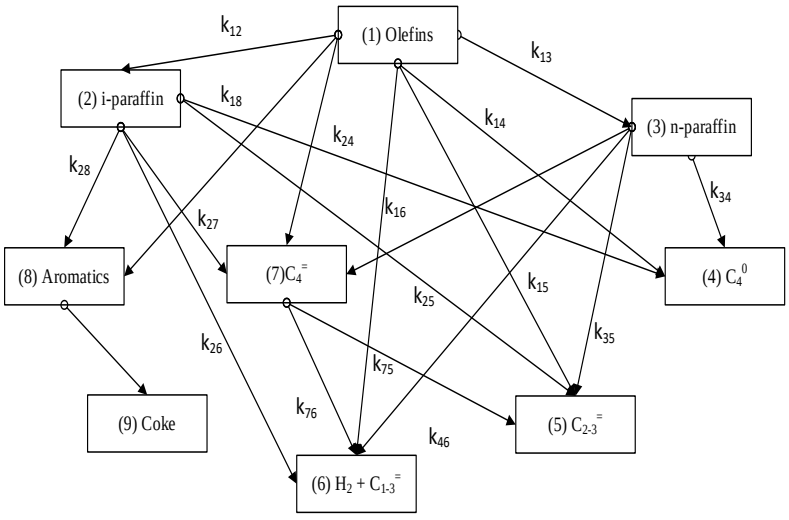

Figure 2.11: Nine lumps web models of FCC gasoline (You 2013)

The aromatization reaction firstly put the lump into n-paraffins, i-paraffins, olefins, aromatics, coke, $C_4^=$, C_4^0, $C_{2-3}^=$ and H_2+ C_{1-3}^0 . The aromatization reaction network

considered three core reactions type; paraffin dehydrogenation and cyclization, paraffin isomerization, and cracking to low carbon hydrocarbon (You 2013).

Jacob et al. (1976) presented a more advanced 10 lump model that distributed the feed and products into a ten-lump kinetic reaction scheme, which comprised light and heavy gas oil paraffinic, naphthenic and aromatic rings and substituent. The advantage of this model, which also made is so distinctive is that it took account of the feed properties with various boiling ranges. It also accounted for the nitrogen poisoning, aromatic adsorption and time dependent catalyst decay (Gupta et al. 2005).

(Du et al. 2015a), presented another ten-lump kinetic model for a two-stage riser catalytic cracking (TMP) process. The feedstock and products were divided into ten lumps; heavy oil, diesel oil, gasoline olefins, gasoline aromatics, gasoline saturates, (butane + propane), butylene, propylene, dry gas and coke. The ten lump model according to Jacob et al. (1976) is in Figure 2.12.

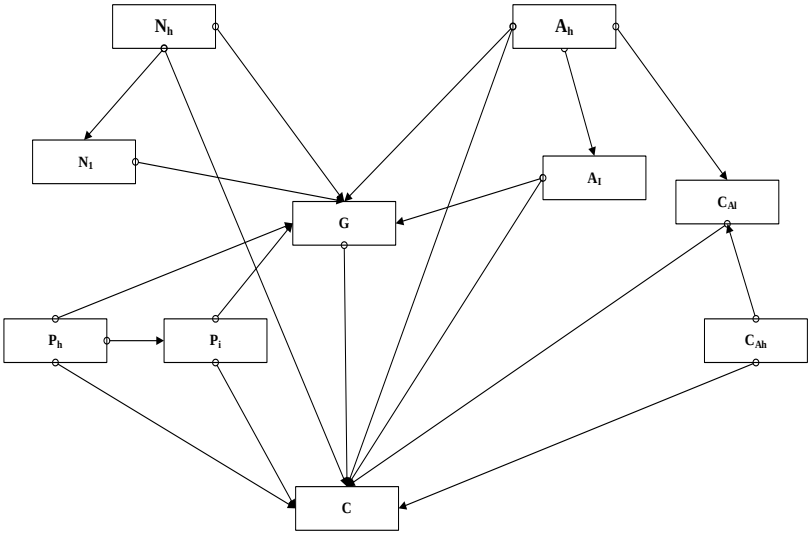

Figure 2.12: Ten-lump kinetic scheme (Jacob et al. 1976; Gupta et al. 2005)

Where:

P_l = wt% paraffinic molecules, 221.1 ^oC – 343.3 ^oC

N_l = wt% naphthenic molecules, 221.1 ^oC – 343.3 ^oC

C_{Al} = wt% carbon atoms among aromatic rings, 221.1 ^oC – 343.3 ^oC

A_l = wt% aromatic substituent group, 221.1 ^oC – 343.3 ^oC

P_I = wt% paraffinic molecules, 221.1 ^oC – 343.3 ^oC

P_h = wt% paraffinic molecules, 343.3 $^oC^+$

N_h = wt% naphthenic molecules, 343.3 $^oC^+$

C_{Ah}, = wt% carbon atoms among aromatic rings, 343.3 $^oC^+$

A_h = wt% aromatic substituent groups, 343.3 $^oC^+$

G = Gasoline lump (C5 - 221.1 ^oC)

C = Coke lump (C1 to C4 and Coke)

$C_{Al} + P_l + N_l + A_l$ = LFO 221.1 ^oC – 343.3 ^oC

$C_{Ah} + P_h + N_h + A_h$ = HFO 343.3 $^oC^+$

An eleven-lump model (Mao et al. 1985; Sa et al. 1985; Zhu et al. 1985; Sa et al. 1995) was proposed which was a division of the six lump model of Gan et al. (2011). The eleven lump is divided into heavy oil (HO), diesel oil (DO), gasoline [olefin (G^O), aromatic (G^A), saturates (G^S)], LPG [butane + propane ($C_{3,4}{}^0$), butylene ($C4^=$), propylene $C_3{}^=$)], dry gas [ethane ($DG^=$), ethane + methane + H_2 $(DG)^0$)] and coke (CK) (Gan et al. 2011). The lump keeps dividing and multiplying based on the requirements of the researchers. Oliveira and Biscaia (1989) improved on the ten-lump model of Jacob et al. (1976) by supposing the C-lump divided into primary gaseous products (Gas1), secondary gaseous products (Gas2) and coke itself (Oliveira and Biscaia 1989; Peixoto and de Medeiros 2001).

A twelve lump model used by Alvarez-Castro et al. (2015b), was presented by Wu et al. (2008). The lumps are saturates in feedstock (613.15 K), aromatics in feedstock, resin and asphaltene in feedstock, diesel without pretreating LCO (477.15 – 613.15K), saturates in gasoline (C_5 - 477.15K), olefins in gasoline, aromatics in gasoline, low carbon alkanes ($C_3 + C_4$), propylene, butene, dry gas ($C_1 + C_2 + H_2$) and coke (Alvarez-Castro et al. 2015b). Another 12-lump kinetic model was also established to simulate catalytic cracking reactions in the Maximizing Iso-Paraffin (MIP) process (Zong et al. 2010). This lumping strategy was because of the demands for numerous lumps. Structural property differences were used on gas oil or heavy oil as feedstock that was subdivided into three groups. The groups are alkyl group carbon, cycloalkyl group carbon, and aromatic

group carbon. The division of diesel oil into another three lumps using the same strategy was carried out. The MIP process decreases the alkenes component in gasoline, hence, the quantity of alkenes needs to be estimated in the model. As a result, the gasoline is further separated into three lumps: saturated hydrocarbons, alkenes, and aromatics. Finally, gases as a lump was considered and coke is treated as another lump (Zong et al. 2010). The twelve lumps are alkyl group carbon of heavy oil (HP), cycloalkyl group carbon of heavy oil (HN), aromatic group carbon of heavy oil (HA), alkyl group carbon of diesel (DP), and cycloalkyl group carbon of diesel (DN). Others in the twelve lumps are aromatic group carbon of diesel (DA), saturated hydrocarbons of gasoline (GP), alkenes of gasoline (GO), aromatics of gasoline (GA), propylene (C3), other gases (LG), and coke (C) (Zong et al. 2010). The rising demand for propylene was also a need, hence, it is required that propylene be accounted for as a single lump to calculate the amount of propylene. This was achieved in the case of the twelve-lump model of Zong et al. (2010), although, it was based on the MIP process. For the normal FCC riser cracking with pneumatic flow, in most cases, propylene is lumped with other gases, thereby making it difficult to improve on the yield of the product. This has been a challenge that require urgent attention to meet the demand for propylene. The twelve lump model was quite exciting to many researcher (Chang et al. 2012b; Dutta et al. 2012). Other widely used kinetic lump models are the thirteen-lump model (Sa et al. 1995) and the nineteen lump model (Pitault et al. 1994; Gupta et al. 2005).

A method called structure-oriented lumping (SOL) (Quann and Jaffe 1992) was presented and used for relating the composition, reactions and properties of complex hydrocarbon mixtures in the riser. The strategy presented each hydrocarbon molecule as a vector of incremental structural features. This means that a mixture of hydrocarbons can be characterized as a collection of these vectors, each with a linked weight percent. This lumping method offers the possibility for developing reaction networks of random size and complexity, which can be used to develop correlations on the basis of molecular properties and captures existing group contribution methods for the valuation of molecular thermodynamic properties (Gupta et al. 2005). Christensen et al. (1999) used over sixty reaction rules to produce a network of 30,000 elementary chemical reactions with the SOL method and described fundamental cracking chemistry of

FCC feeds. They included the monomolecular reactions (cracking, isomerization, and cyclization), bimolecular reactions (hydrogen transfer, coking, and disproportionation), and the impact of thermal cracking and metal-catalyzed dehydrogenation for the reaction network generation (Christensen et al. 1999). The model's kinetic parameters were obtained using regression from a wide range of FCC process conditions, feed compositions, and catalyst formulations. The detailed FCC process model presented by the authors using the kinetic model is said to have the ability to predict the complex non-linear behavior of FCC units (Christensen et al. 1999).

An alternative technique for developing kinetic models known as the 'single-events' method was advanced. This strategy defines a mechanistic dimension of catalytic cracking reactions, which incorporates carbanion ions intermediates (Feng et al. 1993). To obtain the kinetic constants for these single events models, it requires some key reactions of pure hydrocarbons. Using the single event technique, Dewachtere et al. (1999) produced a kinetic model for catalytic cracking of VGO using elementary steps of chemistry. They use a link with modern analytical techniques to describe the cracking of the VGO lump to form network of other lumps, while they considered and accounted for each chemical species. Fifty single event rate parameters were obtained from a detailed experimental work on catalytic cracking of main components with appropriate structures (Dewachtere et al. 1999).

2.4.1.2 Propylene as single lump

Light olefins such as ethylene and propylene are major sources of the raw materials for the polyethylene and polypropylene industries. In recent times, there has been an increase in the demand for propylene, a petrochemical industry feedstock (Li et al. 2007) and it is chiefly sourced from light olefins in the naphtha steam pyrolysis process. However, propylene and ethylene are sourced cheaply from the FCC unit due to the abundance and cheapness of the FCC feedstock compared with Naphtha (Li et al. 2007; Khanmohammadi et al. 2016). The recent growth in demand for propylene in the world has maintained focus on the refineries toward FCC technologies for the maximisation of propylene production in order to achieve economic profit (Berrouk et al. 2017). Currently, there is an increasing interest in maximizing propylene yield of FCC units (Liu et al. 2007; Akah and Al-Ghrami 2015).

The production of propylene is mostly achieved using catalytic reactions with special selectivity for propylene (Liu et al. 2007; Inagaki et al. 2010; Haiyan et al. 2012; Akah and Al-Ghrami 2015). A number of lumps for catalytic cracking were reported in the literature but most of them lumped the gaseous products in a single lump, thereby making it difficult to optimise or maximise a particular gas, for instance propylene. Usman et al. (2017) conducted experimental studies using three different crudes (Super Light, Extra Light and Arab Light) and catalytically cracked the feeds to produce light olefins, where they presented propane and propylene as different lumps. They used different catalysts: base equilibrated catalyst and others; (Z30 and Z1500) which are the base equilibrated catalyst + MFI Zeoliite at varying Si/Al ratio. The results show that the total weight fraction of the two lumps; propylene and propane contain about 80% to 89% propylene for all the crude oils and catalysts used (Usman et al. 2017). This percentage is high and therefore, a combined lump of propylene and propane can be treated as a single lump of propylene and the kinetic model of Ancheyta and Rogelio (2002) is a suitable scheme to achieve this objective.

2.4.1.3 Riser hydrodynamic models

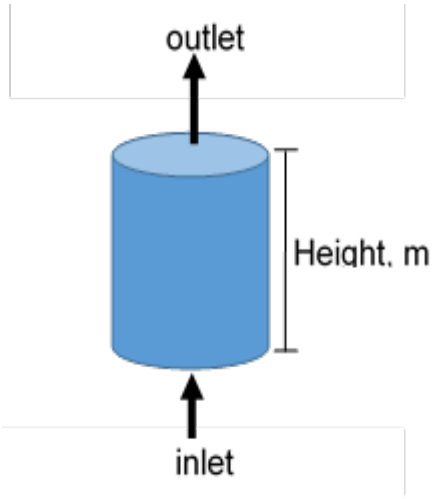

Figure 2.13: Riser diagram

The feed mixes and vaporises in the feed vaporisation section of the riser while catalytic cracking reactions take place in the riser. This happens as both catalyst and hydrocarbon liquid droplets and vapours expand and travel pneumatically upward. The expanding volume is the main driving force that enables the catalyst particles to move upward in the riser (Das et al. 2003; Dutta et al. 2012).

The FCC riser is a complex unit that involves strong multivariable interactions, complex hydrodynamics and operating restrictions, which poses as a major difficulty in the simulation of the process. Many different chemical and physical occurrences happening concurrently that need great attention.

The degree to which hydrocarbon feed vaporizes in the riser has many effects on the efficiency of the riser (Pinheiro et al. 2012). The more the reacting system is in the liquid phase, the negative effect it has on the cracking reactions, while, a sluggish vaporisation creates very high “effective Catalyst-to-Oil (C/O)” ratio. At the vaporisation section, high catalytic activity and temperature produces undesirable secondary cracking reactions, increases catalyst deactivation due to high coke formation while gasoline yield decreases (Han and Chung 2001a; Deng et al. 2002). As a result, extensive research has been and is ongoing in the development and production of effective nozzles and feed injection systems which are capable of atomizing hydrocarbon feed that aid fast vaporisation and influence short, effective surface area contact between catalyst and oil (Vieira et al. 2004).

When simulating the riser, many authors hardly model the feed vaporisation section even though it is an important component of riser. Most times, instantaneous vaporisation concept eliminates its consideration. Nevertheless, when it is modelled, it can be useful for optimisation and design studies of the feed injection systems and nozzles. Vaporisation takes place in the first 1.5 - 3 m of most risers, corresponding to about 5 - 10% of the riser total length (30 - 40 m) (Theologos and Markatos 1993). In addition, Ali et al. (1997) state that it takes 0.1 sec for the feed to fully vaporise, which is about approximately 3% of the mixture residence time in the riser. For the remaining 97% of the residence time, the feed remains vaporised which supports the cracking reactions, because cracking only takes place in the vaporised region (Sadeghbeigi 2000; Gupta et al. 2010), and this is a justification for assuming instantaneous vaporisation at the vaporisation section. This will not result in a ‘weighty’ error in yield or conversion calculation (Pinheiro et al. 2012).

Three phases are involved in the modelling of the riser vaporisation section: catalyst particles, hydrocarbon liquid droplets, and hydrocarbon vapours. Modelling also needs to consider both the sensible heat gain and vaporisation of the liquid droplets along with mass transfer from the droplet to the gas phase.

Modelling also needs to consider the heat transfer between the solid (catalyst) and gas phases after vaporisation is complete. Modelling of the vaporisation section is with much difficulty, because it requires calculating the diameters of the liquid droplets and connects the rate of vaporisation to the sizes of the droplets along with the mass transfer being connected to the gas phase. It also includes calculating the heat transfer coefficients between the two phases. This could be the simple reason many authors model the riser without the feed vaporisation section (Pinheiro et al. 2012), and only a few do (Theologos and Markatos 1993; Ali and Rohani 1997; Gupta and Rao 2001; Martignoni and de Lasa 2001; Nayak et al. 2005; Araujo-Monroy and López-Isunza 2006). The most common modelling approach for the riser is the one-dimensional (1-D) model, even though many others can be found in the open literature (Ali et al. 1997; Ahari et al. 2008b). The others include the more complex 3-D models, which uses two different kinds of modelling approaches to represent the riser hydrodynamics. These methods are the Eulerian-Eulerian and the Eulerian-Lagrangian methodologies. These approaches use the computational fluid dynamics (CFD) modelling techniques. The Eulerian - Eulerian approach uses both gas and solid continuum phases, for each phase, while using conservation of mass, momentum, and energy equations to model the riser. For the Eulerian - Eulerian approach, kinetic theory of granular flow is used to describe the particle flow characteristics (Benyahia et al. 2000; Lan et al. 2009; Pinheiro et al. 2012). The Eulerian-Lagrangian method describes the gas phase as a continuum phase. This the approach represents the particles in the solid phase by Lagrangian equations of motion for each particle of the system. Each particle in the Lagrangian equations is prescribed a set of initial conditions (Lan et al. 2009; Behjat et al. 2011). The overall efficiency of the riser can be precisely estimated with a 1-D mass, energy, and chemical species models, but, to evaluate heat transfer, chemical reaction, and effects of geometry of the riser at the feed vaporisation and injection section, a 3-D model has to be used (Theologos et al. 1999; Das et al. 2003; Gupta et al. 2010). In addition to the 1-D plug-flow and 3-D model approaches, the core annulus model (Bolkan-Kenny et al. 1994; Derouin et al. 1997; Deng et al. 2002) that is established on the hydrodynamic correlations that estimates the slip velocity and the porosity profiles both radially and axially was presented. It comprised two zones; a central core for an upward flowing gas at high velocity, which entrains dilute solid with a small slip velocity, as the particle

terminal velocity. The other zone is a peripheral annulus having a downward flowing concentrated solid with a gas velocity close to zero.

There are common assumptions in the use of the 1-D model; that is, they are plug flow for both vapour and catalyst phases, the operation is adiabatic, and there is no mass or heat transfer resistances between the catalyst and gas phases. Some authors commonly neglect the ratio between the velocities of the phases, the slip factor. Nevertheless, considering the existence of a slip velocity between the phases is useful due to its effects on the contact time between the vapour phase and catalyst flows, as well as the conversion of the feed. There are several assumptions that pertains the slip factor; a constant slip factor (Pathanjali et al. 1999), and a varying slip factor (Corella and Francés 1991). Han and Chung (2001a) used momentum equations for the catalyst and gas phases to obtain velocity profiles along the riser reactor, which allows for the estimation of the slip velocity. Gupta and Rao (2001) equate the slip velocity to the terminal velocity of a single particle.

Besides the usefulness of the slip factor in obtaining different velocity profiles for the catalyst and gas/vapour phases, it determines the diameter of the solid particles. For particles with diameters as those of the FCC catalysts, the slip factor equals unity, meaning that the gas and solid velocities are practically equivalent (Han and Chung 2001b). However, this disagrees with other authors that have presented slip factors close to two (Fligner et al. 1994; Pathanjali et al. 1999; Das et al. 2003). For some authors, the slip factor is as large as 4, which is linked to clusters (aggregate of particles moving together with the same velocity) formation along the riser reactor (Fligner et al. 1994; Harriott 2003). The higher the clusters, the higher the slip factor, and the lower the clusters, the lower the slip factor. From simulated results, the catalytic cracking of VGO to gasoline, gas, and coke of individual particles in the cluster are slower than those of the isolated particles, but faster for the reaction from gasoline to gas and coke. Clusters decrease the rates of reaction from VGO to gasoline, gas, and coke and increase the rates of reaction from gasoline to gas and coke (Shuyan et al. 2008). Common cluster sizes reported for the FCC catalyst is between 2 and 15 mm.

Some authors (Ali and Rohani 1997; Han and Chung 2001a; Martignoni and de Lasa 2001) have treated the gas compressibility of the vaporised fluid in the riser as unity. Others have assumed that the compressibility or Z factor can be a

dimensionless value of one because the riser operates at low pressure and high temperature (Ali et al. 1997; Fermoselli 2010), even though, at low pressure 2 - 3% error is prevalent (Ahmed 2001). There is also an assumption that the density relationship of the gas phase model in the riser behaves as an ideal gas at any position in the riser even for a heavy oil feedstock (Martignoni and de Lasa 2001). Another researcher treated the gas phase in the riser as an ideal gas with the assumption of constant enthalpy (Li et al. 2009). However, enthalpy is not constant in the riser (Han and Chung 2001b).

The Z-Factor is very significant in characterising the fluid flow of oil and gas in the upstream and downstream sector of the petroleum industries (Heidaryan et al. 2010a; Heidaryan et al. 2010b). The process that the fluid undergo describes whether it is compressible or non-compressible and if there is a density change, as is possible in the riser, then the compressibility factor changes. Hence, treating the gaseous phase as an ideal gas in the case of changing density system will not be accurate. In addition, as velocity increases, the density of the fluid varies and can be a compressible fluid (Balachandran 2007). Some process variables such as density (Lopes et al. 2012), viscosity and the void fraction would vary when change in mass (or moles) occur due to cracking reactions and when operating conditions such as temperature, mass flowrate and/or pressure (a function of gas compressibility) are altered. Since these changes in the operating conditions of the riser are considered when modelling risers (León-Becerril et al. 2004), the variation in the compressibility factor of the fluid needs to be considered too.

The summary of the riser model is presented in Table 2.3.

Table 2.3: Comparative summary of main features of some FCC riser models

	(Corella and Frances 1991a)	(Martin et al. 1992)	(Fligner et al. 1994)	(Ali et al. 1997)	(Derouin et al. 1997)	(Theologos et al. 1999)	(Han and Chung 2001a)
Vaporisation	Instantaneous	Instantaneous	Instantaneous	Instantaneous	Instantaneous	Vaporisation then cracking	Vaporisation then cracking
Temperature Variation	Adiabatic	Isothermal	Isothermal	Adiabatic	Isothermal	Adiabatic	Adiabatic
Molar expansion	Considered	Considered	Not considered	Not considered	Considered	Not considered	Considered
Axial catalyst holdup	Slip factor varied between values 1.15 and 1.05 along riser height	Correlation relating slip factor to riser height fitted to plant data	Cluster model approach	Constant	Correlation relating slip factor to riser height fitted to plant data	Single particle dynamics	Slip factor maintained within 0.25 m/s along riser height
Mass transfer resistance	Not considered	Not considered	Fitted to plant data	Not considered	Not considered	Not considered	Not considered
Kinetic model	Five lumps	Five lumps	Three lumps	Four lumps	Nineteen lumps	Three lumps	Four lumps
Deactivation	Non-selective. Based on the time-on-stream of catalyst	Non –selective. Based on the coke concentration on catalyst	Non –selective. Based on the time-on-stream of catalyst	Variation along riser height not considered	Non –selective except reactions leading to coke formation. Based on the coke concentration on catalyst	Non –selective. Based on the time-on-stream of catalyst	Non –selective. Based on the coke concentration on catalyst

2.4.1.4 Catalyst deactivation

Besides the complexities in the modelling of the catalytic cracking kinetics of FCC, there is the challenge of catalyst deactivation as a result of coke formation and deposition on the surface of the catalyst (Guisnet and Magnoux 2001). Voorhies (1945) made the first attempt to model the coke formation on cracking catalyst using an empirical correlation, which relates its dependency on the catalyst residence time.

There are two different methods to modelling catalyst deactivation. They are the time-on-stream and the coke-on-catalyst functions (Pinheiro et al. 2012). Nam and Kittrell (1984) addressed one of the advantages of the time-on-stream functions in having the deactivation mechanisms (for instance, simultaneous titration of basic nitrogen along with coking) concurrently with the mechanistic kinetics of coke formation. Different types of coke in the catalyst were recognised (whisker like, pyrolytic, polymeric, in multilayers, etc.) and their respective varying contributions to deactivation. Therefore, (Corella and Monzon 1988) recommended that, it is better to use time-dependent relationships in the presence of multiple sources of deactivation. On the other hand, Froment et al. (2011) disapprove the use of time-on-stream functions because of its over simplistic approach. Both the function of time-on-stream and coke-on-catalyst coke content function requires an additional rate equation for the coke formation, to introduce the process time and characterization data from spent catalyst (Froment et al. 2011). However, the use of coke-on-catalyst relationships was highly recommended by Nam and Kittrell (1984), because it offers extra understandings into the deactivation mechanism due to the presence of microbalance data and coke-bed profile data. Moreover, coke-on-catalyst relationships can be used to study catalyst regeneration since it determines the effect of non-regenerated coke at the riser inlet (Nam and Kittrell 1984; Corella et al. 1985). According to Jiménez-García et al. (2010), the two separate approaches for the modelling of catalyst deactivation can be combined by monitoring catalyst activity as a function of the decline in the effective diffusivity of the reactants because of the blockage of the external surface of the catalyst pore by coke. This was considered the main reason for catalyst deactivation, and consequent increase of the Thiele modules but decrease of the effectiveness factor of each reaction.

Apart from those basic methods for estimating the catalyst deactivation rates, other correlations based on exponential and power laws are common in the literature (Weekman 1968a; Corella et al. 1985; Pitault et al. 1994; Froment et al. 2011). Although their mathematical equations are not similarities, good modifications against experimental data was achieved. However, accurate validation of the functions was challenging because of different experimental conditions at which deactivation occur, which are mainly dependent on operating conditions, feedstock, and catalyst properties. In support of the foregoing fact, Larocca et al. (1990) and Corella et al. (1985) noted that there are variations in the catalyst residence times used by different researchers and pointed at the difficulty in acquiring data at very low residence times in conventional bench-scale reactors. They noted a different deactivation behaviour in the first few seconds resulting in a different decay order (Corella et al. 1985; Larocca et al. 1990), which is dependent on the feedstock and catalyst used (Corella and Francés 1991), or a different decay coefficient in the exponential function (Larocca et al. 1990). A generalised equation for catalyst deactivation considering variations in the decay order, which represents various deactivation mechanisms for all reactions, is presented as:

$$\frac{d\Phi}{dt} = -\alpha\Phi^{do} \tag{2.2}$$

where Φ is the average value of catalyst activity for all active site strengths present in the catalyst surface, α the kinetic deactivation constant, and *t* the time on stream or coke on catalyst. Decay order *d* relates the number of active sites and the catalyst deactivation for that reaction (Corella et al. 1985). This equation is valid for different decay orders.

2.4.2 Stripper/reactor/disengager models

The stripper is also called the reactor (Han and Chung 2001a), and along with the disengager, these units are generally studied as cold-flow units (in the absence of reactions). The unit has very high catalyst holdup, which is responsible for the transient behaviour of the FCC unit. Modelling the stripper/disengager unit is important because it calculates the proportion of hydrocarbons that are adsorbed or occluded coke in the catalyst pores after stripping. This coke is referred to as cat-to-oil coke and is responsible for the increase in the hydrocarbon molar ratio in coke that eventually increases the heat

produced in the regenerator (Koon et al. 2000; Alvarenga Baptista and Cerqueira 2004).

There are not many dynamic models of the stripper/disengager section in the literature for the dynamic simulation in an FCC unit (Arbel et al. 1995a; Ali et al. 1997; Pathanjali et al. 1999; Han and Chung 2001a; Bollas et al. 2007b). However, where such models are found, the stripper and disengager are always modelled as a singled unique unit (Han and Chung 2001a). This makes it easier for the unit to be simulated as a continuous stirred tank (CST) without reaction (Pinheiro et al. 2012). Some authors thought that linear empirical correlations to estimate the cat-to-oil coke as a function of stripping steam flowrate were adequate (Arbel et al. 1995a; Han and Chung 2001a; Hernández-Barajas et al. 2006), whilst others presented the exponential law function of catalyst, feed and stripping steam flow rates (Han and Chung 2001a). On the other hand, there are some steady-state models of the stripper/disengager section, which include mass or energy balances or both (Pinheiro et al. 2012).

2.4.3 The regenerator models

There are early records of studies of regenerator hydrodynamics and steady-state behaviour in the literature (de Lasa and Grace 1979; Errazu et al. 1979). However, areas of interest such as the CO after-burn combustion phenomena (Morley and de Lasa 1987) and the CO_2/CO ratio in the flue gas (Weisz 1966) keep growing. FCC regenerators are fluidized bed reactors with multifaceted hydrodynamics, along with strong exothermic reaction of coke combustion on catalyst surface. The combustion reaction occurs in two distinctive phases: the dense region and the dilute region (freeboard). The dense bed/region hosts most of the solids (catalyst) and gases, where both heterogeneous and homogeneous reactions take place. On the other hand, the freeboard has less catalyst and bubbles that vent at the surface of the dense fluidized bed and entrain upwards. In the freeboard, the fraction of solids diminishes gradually with height (de Lasa and Grace 1979). However, the entrained solids are returned to the dense bed using cyclones.

The two-phase theory (Faltsi-Saravelou and Vasalos 1991) is generally used for the modelling of the FCC regenerators. This theory describes the dense phase section in two folds: the bubble and emulsion phases. The emulsion phase

contains the gas that is essential to fluidize most of the solids. The bubble phase is thought to come from the excess gas that pertains to the minimum fluidization flow rate passing through the bed, since bubbles are solid free. In the two-phase theory, the bubble phase is modelled as plug flow while the emulsion phase is modelled as continuous stirred tank reactor (CSTR) or a plug flow reactor (PFR). The bubble phase is considered to have no reactions in the solid phase because it is solid free but has gas-phase reactions.

Kunii and Levenspiel (1990) presented the bubbling-bed model. They assumed that the bubbling-bed is a three-phase model with thin layer all over the bubble that has a much lower solid fraction than the emulsion (the cloud) and a similar zone being pulled up by the bubble (the wake). Two-phase models neglect the cloud and the wake, an assumption usually justified when small particles are fluidized, as in the FCC regenerators. There is a section called the grid region, which is found at the bottom of the fluidized bed and it is used as gas inlet zone. At this region, the gas flows as jets, and, emulsion and bubbles are considered perfectly mixed in the region (Filho et al. 1996). Three distinct models of the dense region (two-phase, grid, and bubbling-bed) of a classic regenerator were compared with experimental data of an industrial plant (Lee et al. 1989b). The conclusion was that the bubbling-bed model represents the experimental data with the smallest error. A steady-state application of single-phase theory and two-phase theory models on the dense region of the regenerator was modelled as a CSTR (Errazu et al. 1979). The conclusion was that there were no major differences between the predictions of the two models. This means that a simple CSTR model could estimate the overall performance of a complex fluidized bed FCC regenerator.

There is a general agreement on the modelling methodology for the dilute region (freeboard) of the regenerator. Some authors simulated the temperature profile of dilute region using a 1-D plug flow reactor model (de Lasa and Grace 1979; Krishna and Parkin 1985b; Faltsi-Saravelou and Vasalos 1991; Han and Chung 2001b; Hernández-Barajas et al. 2006). This is a consequence of both afterburning reactions and incomplete combustion in the dense bed (de Carvalho et al. 2004; Pinheiro et al. 2012).

There are several regenerator dynamic models in the literature used for the simulation of the FCC riser-regenerator system (Arbel et al. 1995a; Pathanjali et

al. 1999; Arandes et al. 2000; Han and Chung 2001b; Hernández-Barajas et al. 2006). This is because the regenerator's dynamics has more impact on the FCC unit dynamics than the riser dynamics.

2.4.3.1 Two-stage regenerators

In modern refineries, numerous types of FCC units are currently in use, using different designs. However, not all mathematical models presented in the literature can easily and adequately be applied for all units (Fernandes et al. 2007b). Some authors use single stage regenerator (Han and Chung 2001a; Pinho et al. 2017; Zahran et al. 2017), while others use two-stage regenerators (Moro and Odloak 1995; Fernandes et al. 2005; Fernandes et al. 2007a; Fernandes et al. 2007b; Cuadros et al. 2012; Cuadros et al. 2013). There are two types of the two-stage regenerators: stacked (Figure 2.14) and side-by-side.

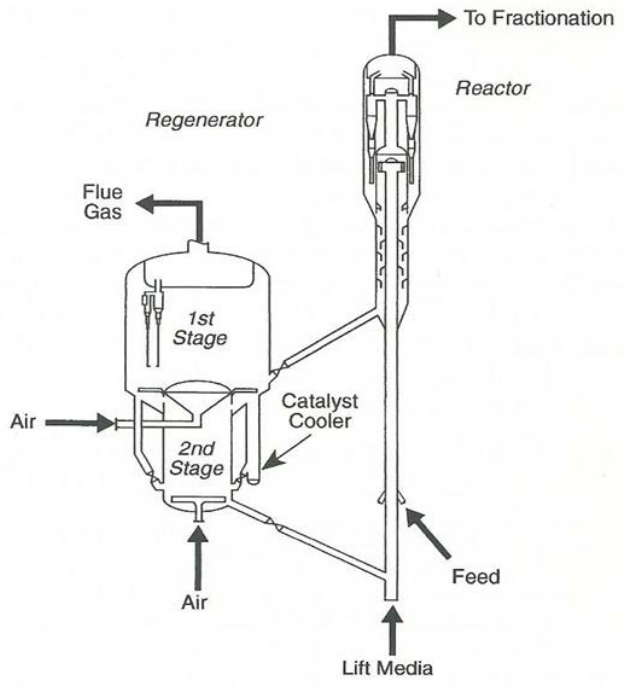

Figure 2.14: RCC Unit-stacked regenerators (Wilson 1997)

A dynamic model for a R2R FCC unit including a riser, a stripper, a disengager, two standpipes and a regeneration system with two regenerators (stacked- one on the other) connected by a lift was presented (Fernandes et al. 2005; Fernandes et al. 2007b). The other two-stage regenerator model presented in the literature is a Kellogg Orthoflow F converter by Moro and Odloak (1995), which includes a riser, a stripper, a disengager, a regeneration system with two regenerators (side-by-side) connected by perforation between the two

regenerators. The presented dynamic model was used in control applications. Although the model can represent well the important dynamic aspects of the system, it includes only the coke balance in the riser but without adequate product distribution (Pinheiro et al. 2012). This is a drawback especially for the Kellogg Orthoflow F converter, because it does not have in the open literature, the detailed model that adequately represent the unit.

2.4.3.2 Kinetic models of the regenerator

During the cracking of gas oil with catalyst in the riser, the catalyst becomes deactivated because of the deposit of coke on the surface of catalyst which reduces its activity within seconds (Arbel et al. 1995a). This coke, which is chiefly carbon and hydrogen in nature, is in the end removed from the catalyst by combustion or burning reactions taking place in the regenerator, thereby regenerating the catalyst for future use. This reaction is called catalyst regeneration reaction.

The usual coke is considered a carbonaceous material that is made up of various chemical compounds comprising hydrocarbons, sulfuric and nitrogenous compounds. These carbonaceous substances deposited on catalyst such as silica-alumina during cracking of hydrocarbons have stoichiometric compositions ranging from approximately $C_{1.0}H_{1.0}$ to $C_{1.0}H_{0.5}$, with the hydrocarbons being the dominant components in coke. Hence, it is assumed that CH_n represents the coke formula, where n is a number between 0.5 and 1.0 (Weisz and Goodwin 1963; Weisz and Goodwin 1966), while for others, n = 1.64 (Lee et al. 1989b). The combustion reaction takes the form of Arbel et al. (1995a) and Weisz and Goodwin (1966) model.

Regenerators are mainly classified as either a single or a two-stage regenerators (Moro and Odloak 1995; Fernandes et al. 2007b; Cuadros et al. 2013; Bispo et al. 2014). The regenerator is made up of two regions: dense bed and dilute region, while the dense bed is made up of the emulsion and bubble phases. This classification is due to the different amount of catalyst per unit volume in each (Arbel et al. 1995a). Hence, the model classified the reactions into two: the homogenous and heterogeneous reactions. The homogeneous reaction is carried out in all the phases of the regenerator: the emulsion and the bubble phases of first and second stage, and the dilute (freeboard) phase. The reason

for this is that homogenous reaction happens for gaseous reactions only and such gaseous reactions take place in all the phases of the regenerator. The heterogeneous reaction occurs in the presence of catalyst. This means that this reaction takes place in the three regions of the regenerator only, which is, the emulsion phases of the first and second stages of the regenerator and in the free board too. It happens in the freeboard due to catalyst entrainment, which ultimately results in after-burn reaction in the freeboard.

The heterogeneous reactions are as follows:

$$CH_{n(S\rightarrow g)} + (0.5 + 0.25_n)O_{2(g)} \overset{K_1'}{\rightarrow} CO_{(g)} + 0.5_n H_2O_{(g)} \quad (2.3)$$

$$CH_{n(S\rightarrow g)} + (1.0 + 0.25_n)O_{2(g)} \overset{K_2'}{\rightarrow} CO_{(g)} + 0.5_n H_2O_{(g)} \quad (2.4)$$

$$CO_{n(S\rightarrow g)} + 0.5O_{2(g)} \overset{K_3'}{\rightarrow} CO_{(g)} \quad (2.5)$$

The following is the homogeneous reaction

$$CO_{n(g)} + 0.5O_{2(g)} \overset{K_4'}{\rightarrow} CO_{(g)} \quad (2.6)$$

The rate of carbon combustion is first order with respect to the carbon-on-catalyst and oxygen partial pressure (Weisz and Goodwin 1963; Weisz and Goodwin 1966). The oxidation of CO takes place in both homogenous and heterogeneous phases with different first order rate constants. Equation (2.6) is the homogeneous oxidation is in the gas phase and Equation (2.5) is the heterogeneous catalytic oxidation reaction (Weisz and Goodwin 1963; Weisz and Goodwin 1966). The rate of CO oxidation is also considered as first order with respect to the partial pressure of CO and half order with respect to the partial pressure of O_2 for both homogeneous and catalytic oxidation reactions (Weisz and Goodwin 1966). The overall rate expression for the CO oxidation is the sum of the rates of homogeneous and heterogeneous oxidation reactions. The intrinsic kinetic constant for coke combustion reaction at the reaction site is the same with the global kinetic constant and it is independent of the rate equation chosen for CO post combustion reaction (Weisz 1966; Morley and de Lasa 1987). Coke burning was valued from the observed oxygen concentration and CO_2 to CO product ratio, while considering an additive relationship between the coke combustion and the CO post combustion reactions (Weisz 1966; Morley and de Lasa 1987).

There are many FCC units, but they differ in their regenerator design and configurations, which controls both the dynamic and steady state behavior of the regenerator. This is due to its adiabatic nature that require a balance between coke formation and combustion being the dominant driving force. Hence, the most significant variable in the regenerator simulation is the heat of combustion, a function of the quantity of air and gas composition. The hydrogen in the coke is converted into steam, while the carbon is converted into either CO or CO_2. The heat balance in the regenerator is controlled by the ratio of CO_2 to CO because the heat of combustion when producing CO_2 is nearly 3 times the heat of combustion when CO is produced. Hence, it is essential to model correctly the influence of operating conditions for proper energy balance (Arbel et al. 1995a)**.**

2.4.3.3 Regenerator hydrodynamics

As cracking reaction is finalized in the riser, the deactivated catalyst (spent catalyst) gets into the regenerator unit via the separator or disengager. At the bottom of the regenerator, hot air is forced in to fluidize the catalyst as well as burning off the coke thereby renewing the catalyst. The catalyst bed is made up of many different phases, which makes it difficult to model due to unclear flow pattern (Pinheiro et al. 2012).

Based on fluidization characteristics of the particles, the density difference and mean particle size, the regenerator particles are classified into A, B, C and D recognizable groups (Geldart 1973). FCC particles are known for their dense phase expansion after minimum fluidization and just before the bubbles begin to form, hence they are Geldart A type particles (Geldart 1973) as shown in Figure 2.12.

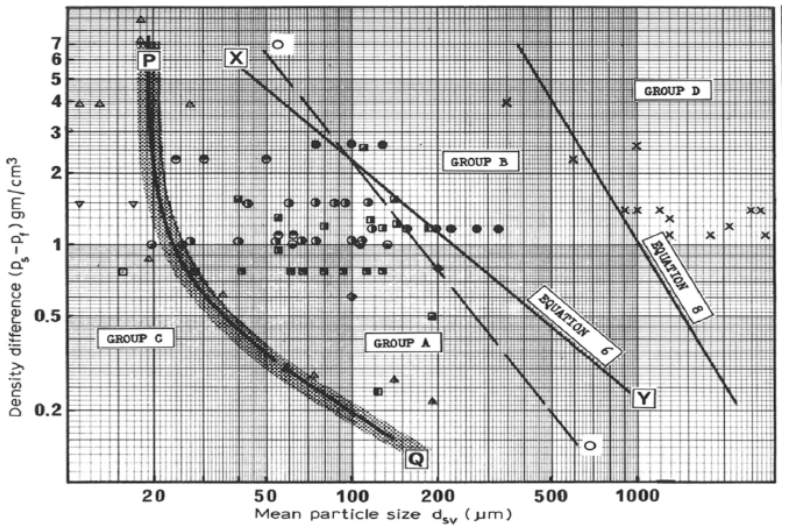

Figure 2.15: Powder classification diagram for fluidization by air (ambient condition) (Geldart 1973)

Figure 2.15: When gas velocity increases through a bed of particles in the upward direction, several fluidization regimes like bubbling, slugging, turbulent, fast fluidization bed regime and dilute transport emerge. The bubble bed regime is formed immediately as air is distributed and blown into the bed. The slugging bed regime is formed when the bubbles grow into an adequate size and easily occupy the whole cross section of the regenerator column, hence forming slug flow. The turbulent bed regime is where the superficial gas velocity is so high, that it causes turbulence in the column. The fast fluidization regime is a regime of higher velocities where particles are circulated from the bottom to the top of the regenerator and back again. Dilute transport is one in which the particles flow as fluid, such as in pneumatic transport (Grace et al. 1999).

To model the regenerator, the fluidized bed was sectioned into two beds of different densities: dense bed and dilute bed (Grace et al. 1999; Han and Chung 2001a). The dense bed having more catalyst than the dilute bed. Other thorough models like grid effect model, two-region model, and bubbling bed model were later developed.

For the grid effect model, Behie and Kehoe (1973) used a shallow bed with diameter larger than height and considered the same height and size for air columns in the bed, they also assumed that the air columns are not connected. The assumption was not valid for simulating some real processes because not many of them form this type of grid. This led to the development of two region model from the grid effect model (de Lasa and Grace 1979; de Lasa et al. 1981),

where they considered that the dense phase is divided into two phases: the bubble phase and emulsion phase. Kunii and Levenspiel (1969) considered the effect of rising air bubbles on the catalyst in the two-region model which was not considered in the earlier case (de Lasa and Grace 1979; de Lasa et al. 1981). The bubbling bed model treats the bubble phase and emulsion phase as plug flow while the grid-effect and two-region models treats the emulsion phase as a mixed flow (Kunii and Levenspiel 1969). Hence, in the bubbling bed model the oxygen concentration is a function of position in the bed (Kunii and Levenspiel 1969). Five distinct fluidized bed models were studied using experimental data from the industrial regenerator (de Lasa et al. 1981):

i. Davidson and Harrison (1963) correlation used for the measurement of bubble mass transfer coefficients in a grid model;
ii. Kunii and Levenspiel (1969) equation bubble mass transfer coefficients in a grid model;
iii. Davidson and Harrison (1963) correlation used for the measurement of mass transfer coefficient in a pure bubble model;
iv. Kunii and Levenspiel (1969) equation used for the measurement of mass transfer coefficient in a pure bubble model;
v. CSTR model was thought to be simpler and better in estimating the overall coke conversion than the other models, which become difficult on the consideration of the freeboard region effect (Davidson and Harrison 1963; Behie and Kehoe 1973).

Three distinct regenerator models (grid-effect model, two-region model, bubbling-bed model) were studied for a fluidized-bed catalyst regenerator (Lee et al. 1989b). This study was carried out using actual operating data for selecting an adequate model for regenerator simulation. The authors established that the bubbling-bed model of the fluidized-bed regenerator, along with two thermally uniform stages for heat balance, can represent the actual regenerator with minimum error. The authors also found that increasing the catalyst temperature and the airflow rate or lowering the catalyst-cycling rate would increase the degree of coke conversion and the outlet temperature. Nevertheless, there ought to be a limit on the air flow rate, because too much air lowers the regenerator efficiency (Lee et al. 1989b).

In modern regenerators, the characteristics are; dense bed with most of the regenerator catalyst and a dilute region at the top all in turbulent fluidization regime (Gupta and Subba Rao 2003). The dense bed of the regenerator is modelled based on the conclusions of the model of Arbel et al. (1995). They are:

- The regenerator is modelled as a bed of solids having two regions, a dense bed region and a dilute region (freeboard). Most of the solids in the regenerator are in the dense bed; hence, the combustion reactions take place there. The dilute region with low solids amount is considered to have little or no impact on the regenerator performance (Ali and Rohani 1997);
- Coke is assumed to have carbon and the overall rate is controlled by the intrinsic kinetics of combustion (Ali et al. 1997);
- The regeneration is assumed to operate adiabatically while heat given off during combustion reactions is considered the major reason for the increase of the temperature of the catalyst and the flue gas (Gupta and Subba Rao 2003);
- The solid phase is modelled as mixed reactor because the phase is well mixed. The gas phase is assumed to flow through the equal sized well mixed compartments in series and in the dilute phase in a plug flow (Arbel et al. 1995a);
- It is assumed that thermal equilibrium exits between the solid phase and the gas phase, and there is insignificant resistance to mass transfer of the gaseous constituents (Krishna and Parkin 1985a);
- The entrained catalyst is completely collected by cyclones and returned to the dense bed Krishna and Parkin (1985a).

2.4.4 Fluid catalytic cracking riser-regenerator models

Dynamic and steady state models have been proposed for the simulation of different types of FCC unit (riser-regenerator) depending on whether the model is used for monitoring, optimisation or control studies. Kumar et al. (1995) presented a steady state model for preliminary calculations for the design, monitoring and optimisation of FCC units. Gupta and Subba Rao (2003) presented another steady state model by extending an initial model (Gupta and Rao 2001) for the riser-regenerator simulation to study the unit's performance as they considered the impact of feed atomization at constant coke yield. Steady

state models of a model IV unit were presented and used to study the impact of the key operating parameters and feedstock compositions in the bifurcation behavior of the FCC unit and its consequences on gasoline yields (Elshishini and Elnashaie 1990a; Elshishini and Elnashaie 1990b; Elshishini et al. 1992). Many other authors developed the dynamic models of the FCC unit (Lee and Kugelman 1973; McFarlane et al. 1993; Arbel et al. 1995a; Ali and Rohani 1997; Han and Chung 2001a; Mircea V. Cristea 2003; Hernández-Barajas et al. 2006). Chiefly among these dynamic models is the one presented by McFarlane et al. (1993), which represents well the interactions between the catalyst circulation and major process parameters. Hence, it was used for identification, control, and optimisation of the entire unit. Nevertheless, its major drawback was the inability of the model to predict product distribution in the riser (Pinheiro et al. 2012). Moro and Odloak (1995) presented a dynamic model of a Kellogg Orthoflow F FCC unit, for control applications. Their model includes the riser, the disengager-stripping section, and the two-stage regenerators operating in partial combustion mode. The model can give adequate dynamic predictions of the system. Its drawback was that it contains only the coke balance in the riser and no product distribution. (Arbel et al. 1995a) presented both dynamic and steady state model for a typical side-by-side FCC unit, which was later used to study the state of multiplicity and control problems of industrial FCC units. A more comprehensive and much inclusive model was presented for a side-by-side reactor-regenerator FCC type with the aim of using it as a simulated or surrogate plant for carrying out numerous process systems studies like control and optimisation (Han and Chung 2001a; Han and Chung 2001b). Their model includes a riser, stripper/disengager, regenerator, and catalyst transport lines with slide valves. In addition to mass and energy balances for the riser, momentum equations for the gas and catalyst particles were incorporated, for the calculation of the velocity profiles along the riser height and determining the slip velocity between gas and catalyst particles which was not usually carried out in other models.

2.5 Process modelling

Process models are very beneficial because they represent a virtual process with which employee training, operator training, safety systems design, design of operation and operation control systems design are easily carried out. Construction of models is one of the major professions of engineering and

science. Models are used because it is too expensive or time consuming or risky to use real system to evaluate plant performance (Jarullah et al. 2017). Models are usually engaged in engineering design and optimisation because they offer the cheapest and faster way of studying the influences of fluctuations in design parameters on system performance. The enhancement of faster computer and advanced numerical methods has made the modelling and solution of complete processes a possibility (Jarullah 2011). System mathematical modelling handles quantitative rather than qualitative analysis of the process. Yet, mathematical modelling has wide opportunity of application and several advantages, some of these are (Khalfalla 2009):

- Using a surrogate mathematical model is cheaper and easier than using the real system. It allows a wide range of access to data and information about a system without having turn to lengthy and expensive runs on the plant.
- Simulation result is of low risk when something goes wrong during the study; hence, it is more secure.
- It is less time consuming.

Given a system to be investigated, a mathematical model could be used to represent that system. The model is a set of variables and equations that are linked in describable relationships that represent the behaviour of the real system. The variables define the nature of the process, for example, measured process outputs normally as signals, timing data and counters.

Engineering models can be very complex, given rise to sets of highly non–linear equations. For several chemical engineering models, the non–linearity is additionally complicated by the exponential dependency of the reaction rates on the temperature (Arrhenius type equations), and by the rigorousness of the rate equations used within the mass and energy balance equations. These complex models require the use of sophisticated numerical methods.

Academia and industry have enjoyed and are still enjoying the ongoing quest for better and more advanced numerical solutions and the application of the huge advancement in computing power during the past two decades. In general, three kinds of model exits (Bonvin 1998): they are data driven black box models, Knowledge driven white box models and Hybrid grey box models.

Black–box models are founded and improved on empirical observations of the relation between various process inputs and their corresponding outputs. Such models are easily developed but their exactness is limited when there is need for extrapolation. In addition, data can only exist for measurable variables; hence, no relation can be formed for variables that cannot be measured, such as heat of reaction. In describing a process using a wide group of functions, the calculation of variables are difficult when the number of variables increases (Khalfalla 2009). Knowledge driven white–box models are mechanistic first principles models, which are founded on mathematical modelling. Models are developed for any process using stoichiometric and kinetic knowledge of the mass and energy balances of the process. The influence of control variables such as temperature and concentration that are depended on the rate of each reaction is related to the kinetic model, while the reactor model connects the process state variables with other variables like inlet streams composition and system constraints. White–box models are more difficult to obtain than their black–box models, and usually exhibit high non-linear behaviour. To manage some of these complications, assumptions are usually made and consequently, oversimplified models are preferred at the expense of the very detailed ones that requires large computing time (Ekpo 2006; Khalfalla 2009). According to Ekpo (2006), a white–box model is developed from the mass and energy balances, system constraints, and thermos-physical properties of the process.

The grey – box model is a mixture of the black- and white-box models. In this study, a white–box model is used for the modelling and simulation of FCC unit.

2.6 Process optimisation

The best and most efficient solution to a problem or design is obtained using optimisation. It is a technique of choosing the best among many options and the key quantitative tools in industrial decision-making. An old saying on Roman bathhouse in relation to the choice between two aspirants for the Emperor of Rome says; "Do doubus mails, minus est simper aligendum", meaning, of two evils, all the time select the lesser (Edgar et al. 2001).

The aim of optimisation is to obtain values of the system (design) variables that represent the best value of the performance benchmark. Generally, the problems in chemical engineering operation design or plant process have numerous, and

possibly limitless solutions. Optimisation is choosing the best set of possible solutions by using efficient quantitative techniques. The power of computers and their accompanying applications packages make the desirable calculations achievable and cost effective (Edgar et al. 2001).

In all process plants, performance enhancement can bring about great benefits. For instance, improved yields of precious products or reduced yields of impurities, reduced energy consumption and higher processing rates can be achieved when performance is improved through optimisation. This can bring about reduction in operation costs and to better staff deployment (Edgar et al. 2001). Optimisation is applicable to chemical operations and plants in many ways. These include equipment used for operation such as reactors, heat exchanger, columns, etc., determination of plant data for new model development, estimation of better sites for plant location, and many more.

Every optimisation statement requires a set of independent variables (parameters) that optimise a given quantity, and subject to constrains. A typical optimisation statement involves the following (Khalfalla 2009):

- An objective function: such as maximise conversion, maximise profit, minimise cost and minimise operation time.
- Control variables: inputs that can be used as decision variables, which influence the value of the objective function.
- Uncontrolled parameters: these are fixed values that are unique to the optimisation statement.
- Constraints: these are limitations on the between the controllable and uncontrollable inputs (or between the decision variables and the parameters).

A general optimisation problem can be stated mathematically as follows:

Maximise or minimise

$$Z = f(x), \qquad x = x_1,\ x_2, \dots, x_n \tag{2.7}$$

Subject to

$$C_i(x) = 0, \qquad i = 1,2, \dots, m \tag{2.8}$$

$$C_i(x) \geq 0, \qquad x = x_1,\ x_2, \dots, x_n \tag{2.9}$$

Where $f(x)$, the objective function, x the vector of n independent variables and $C_i(x)$ the set of constraint functions. Constraint equations such as $C_i(x) = 0$ are known as equality constraints (model equations), while $C_i(x) \geq 0$ are called inequality constraints (lower and upper limits of operating variables). Different optimisation problems require different solution method or algorithm, and are based on these three factors: the nature of the objective function(s), number of dependent and independent variables, and nature of the constraints (Edgar et al. 2001):

2.7 Parameter estimation

Parameter estimation is usually carried out for a model with the aim of optimising some parameters and in some cases estimating such parameters using experimental data. The optimal estimated parameters are obtained as the best match between the experimental data and the values calculated by the model (Dobre and Marcano 2007).

The use of suitable and accurate models in advanced process analysis and optimisation is very important. The accuracy of the model for a process depends on having the right parameters. However, accurate online information of some unknown parameters is difficult to obtain even with accurate models but can be estimated using parameter estimation. It was identified that parameter estimation is not an easy task in the development of process models, whether dynamic or steady state, and that fitting a model to a set of measurement is very challenging (Soroush 1998).

There are many types of parameter estimation techniques and they are mainly based on the systems used. The parameter estimation by state estimation technique found common use in chemical and biochemical engineering in systems of dynamic models where each model represents an unknown parameter to be estimated (Soroush 1997; Tatiraju and Soroush 1997; Soroush 1998). Another parameter estimation technique is achieved through on-line optimisation. This is a case where the estimates are derived from minimisation of the sum of squared errors of the optimisation problem through comparing the experimental and calculated results within some given range of constraints (Muske and Rawlings 1995; Robertson et al. 1996). This method has gained acceptance in the parameter estimation of chemical processes (Jarullah et al.

2011) and it is the method used in this work. Another method is the parameter estimation by model inversion (Tatiraju and Soroush 1998) which comprises a parameter estimate of left inverse of process model concurrently estimating least-squared errors via on-line measurements (Tatiraju and Soroush 1998). The method of calorimetric technique for estimating kinetic parameters of process systems is achieved with the use of mass and energy balance models of the systems (Régnier et al. 1996).

Parameter estimation for kinetic and compositional values of processes is based on optimisation techniques that are either Linear (LN) or non- linear (NLN) regressions. These estimations are readily carried out using computer programs and software (Nowee et al. 2007), which makes complex NLN models much easier to solve. There are many NLN optimisation methods such as maximum likelihood estimation (Tjoa and Biegler 1992) where it seeks a weighted least square fit to the measurements with an underdetermined process model. Other methods include the Bayesian parameter estimation which uses the Bayesian regularization back propagation (Ma and Weng 2009). There is Newton-Raphson method (Souza et al. 2009) which is a robust technique for solving nonlinear problems. There is also the Genetic algorithm and its various types known to be common in academia and the industry due its insightfulness, easy applicability and effectiveness in solving highly nonlinear, mixed integer optimisation problems that are typical of complex engineering systems such as the FCC unit (Hassan et al. 2005; Kordabadi and Jahanmiri 2005; Wang et al. 2005). The Successive Quadratic Programming (SQP) (Tjoa and Biegler 1992) is readily implementable with the help of computer programming packages and software. It is very much utilized by the gPROMS software (gPROMS 2013) and it has proven to be very capable (Jarullah et al. 2011).

2.8 Summary

This chapter has reviewed many past works carried out on the FCC unit processes. It has been noticed that the FCC unit is the major source of fuels (diesel, gasoline, LPG, etc) in the petroleum refinery. Hence, little improvement in its operation or design can bring about huge benefits to the profitability of the unit.

The chapter has reviewed different types of FCC units and the different modelling approaches to the various components (riser, stripper/disengager and regenerator) units. Most mathematical models of the riser did not consider the vaporisation section. Some authors treated the vapour phase as ideal gas model; and some authors have riser models without momentum equations except for few (Han and Chung 2001a; Han and Chung 2001b). However, there is no author that considered the non-ideality of the gas phase in the riser. Most FCC units have single stage regenerators, and those that have two stage regenerators have different configurations. In addition, different models represent different unit.

For accurate estimates of the FCC unit performance under different operating conditions, it is significant to develop kinetic model that are dependable. The model should be significantly applicable to process design and operation. Therefore, a brief discussion on the kinetic parameter estimation techniques was carried out in this chapter. It can be concluded that the evaluation of the kinetic parameters in FCC unit are necessary for ensuring accurate model calculations and good model-based decision, so that the model can be effectively used for simulation and optimisation. In addition, treating the gas phase of the riser as an ideal gas phase, meaning that the compressibility factor is unity, was also discussed and the need to have an accurate estimation of the Z factor.

Chapter 3

Mathematical Models of Different Sub-Units of FCC Unit

3.1 Introduction to riser model equations

Although one, two and three-dimensional riser models exists, it was found that the overall performance of the riser can be predicted by a one-dimensional mass, energy and chemical species balances. This suggests that simplified models may be precise enough to be used for plant design and in an optimisation studies (Souza et al. 2009).

With the help of advanced technique, the one-dimensional plug flow riser reactor model can be solved adequately. It was modelled without axial and radial dispersion, and mass and energy balance equations for the catalyst and gaseous phases are obtained under the following assumptions:

- At the riser inlet, hydrocarbon feed meets the hot catalyst coming from the regenerator and instantly vaporises (taking away latent heat and sensible heat from the hot catalyst). The vapour thus formed moves upwards in thermal equilibrium with the catalyst (Ali et al. 1997).
- There is no loss of heat from the riser and the temperature of the reaction mixture (hydrocarbon vapours and catalyst) falls only because of the endothermicity of the cracking reactions (Ali et al. 1997; Gupta and Subba Rao 2003).
- The endothermicity of the cracking reactions is calculated by finding the difference in the heat of combustion of each pseudo-component involved in the reaction, thus heat effects of all other reactions such as hydrogen-shift, polymerization, condensation, etc., are assumed to be included in the overall heat of reaction (Gupta et al. 2007).
- The gas-phase velocity variation because of gas phase temperature and molar expansion due to cracking is considered (Gupta and Subba Rao 2003).
- Heat and mass transfer resistances are assumed as negligible (Ali et al. 1997).

- The cracking reactions only take place in the riser (Gupta and Subba Rao 2003);
- Dispersion and adsorption inside the catalyst particles are negligible, hence reaction occur at the surface of the catalyst (Gupta and Subba Rao 2003).
- The riser dynamics is fast enough to justify steady state model;
- The coke formed has the same properties with catalyst (Lee et al. 1989b);
- Fluid flow is not affected by coke deposit on catalyst;
- Gas oil cracking is second order (Lee et al. 1989b).

The following Equations in this section (Equations (3.1 – 3.194)) and those in the Appendix A (Equations (A.1 – A.34)), which are mostly correlations were all used in the simulation of the riser and vaporisation section of the FCC unit. Most of the equations were taken from the literature (Han and Chung 2001a; Han and Chung 2001b).

Equations 3.1 and 3.2 are derived from the energy balance of the riser showing the temperature of catalyst and gas phases respectively. They show temperature profiles of the two phases along the riser:

$$\frac{dT_c}{dx} = \frac{\Omega h_p A_p}{F_c C_{pc}} (T_g - T_c) \tag{3.1}$$

$$\frac{dT_g}{dx} = \frac{\Omega}{F_g C_{pg}} \left[h_p A_p (T_c - T_g) + \rho_c \varepsilon_c Q_{react} \right] \tag{3.2}$$

3.1.1 Kinetic equations for four-lumped model

The material balance for the reaction showing the four lumps; gas oil, gasoline, light gas and coke are given respectively as Equations (3.3 – 3.6):

$$\frac{dy_{go}}{dx} = \frac{\rho_c \varepsilon_c \Omega}{F_g} R_{go} \tag{3.3}$$

$$\frac{dy_{gl}}{dx} = \frac{\rho_c \varepsilon_c \Omega}{F_g} R_{gl} \tag{3.4}$$

$$\frac{dy_{gs}}{dx} = \frac{\rho_c \varepsilon_c \Omega}{F_g} R_{gs} \tag{3.5}$$

$$\frac{dy_{ck}}{dx} = \frac{\rho_c \varepsilon_c \Omega}{F_g} R_{ck} \tag{3.6}$$

The rates of reaction for gas oil R_{go}, gasoline R_{gl}, light gas R_{gs}, and coke R_{ck}, are given as:

$$R_{go} = -(K_1 + K_2 + K_3){y_{go}}^2 \emptyset_c \quad (3.7)$$

$$R_{gl} = \left(K_1 {y_{go}}^2 - K_4 y_{gl} - K_5 y_{gl}\right)\emptyset_c \quad (3.8)$$

$$R_{gs} = \left(K_2 {y_{go}}^2 - K_4 y_{gl}\right)\emptyset_c \quad (3.9)$$

$$R_{ck} = \left(K_3 {y_{go}}^2 - K_5 y_{gl}\right)\emptyset_c \quad (3.10)$$

The rate constants K_i, of reaction path *i* = 1 to 5 and their corresponding frequency factors k_{i0} are given as:

$$K_1 = k_{10} \exp\left(\frac{-E_1}{RT_g}\right) \quad (3.11)$$

$$K_2 = k_{20} \exp\left(\frac{-E_2}{RT_g}\right) \quad (3.12)$$

$$K_3 = k_{30} \exp\left(\frac{-E_3}{RT_g}\right) \quad (3.13)$$

$$K_4 = k_{40} \exp\left(\frac{-E_4}{RT_g}\right) \quad (3.14)$$

$$K_5 = K_{50} \exp\left(\frac{-E_5}{RT_g}\right) \quad (3.15)$$

Q_{react} is the rate of heat generation or heat removal by reaction and can be written as

$$Q_{react} = -\left(\Delta H_1 K_1 {y_{go}}^2 + \Delta H_2 K_2 {y_{go}}^2 + \Delta H_3 K_3 {y_{go}}^2 + \Delta H_4 K_4 y_{gl} + \Delta H_5 K_5 y_{gl}\right)\emptyset_c \quad (3.16)$$

3.1.2 Kinetic equations for six-lumped model developed in this work

The material balance for the reaction showing the six lumps; gas oil, diesel, gasoline, LPG, dry gas and coke are given respectively as Equations (3.17–3.22):

$$\frac{dy_{go}}{dx} = \frac{\rho_c \varepsilon_c \Omega}{F_g} R_{go} \quad (3.17)$$

$$\frac{dy_{dz}}{dx} = \frac{\rho_c \varepsilon_c \Omega}{F_g} R_{dz} \quad (3.18)$$

$$\frac{dy_{gl}}{dx} = \frac{\rho_c \varepsilon_c \Omega}{F_g} R_{gl} \quad (3.19)$$

$$\frac{dy_{lpg}}{dx} = \frac{\rho_c \varepsilon_c \Omega}{F_g} R_{lpg} \quad (3.20)$$

$$\frac{dy_{dg}}{dx} = \frac{\rho_c \varepsilon_c \Omega}{F_g} R_{dg} \quad (3.21)$$

$$\frac{dy_{ck}}{dx} = \frac{\rho_c \varepsilon_c \Omega}{F_g} R_{ck} \quad (3.22)$$

The rates of reaction for gas oil R_{go}, diesel R_{dz}, gasoline R_{gl}, LPG R_{lpg}, dry gas R_{dg}, and coke R_{ck}, are given as

$$R_{go} = -\left(k_{go-dz} + k_{go-g} + k_{go-ck} + k_{go-lpg} + k_{go-dg}\right){y_{go}}^2 \emptyset_c \quad (3.23)$$

$$R_{dz} = \left(\left(k_{go-dz}\, {y_{go}}^2\right) - \left(k_{dz-ck} + k_{dz-gl} + k_{dz-lpg} + k_{dz-dg}\right)y_{dz}\right)\emptyset_c \quad (3.24)$$

$$R_{gl} = \left(k_{go-g}\, {y_{go}}^2 - k_{dz-gl}\, y_{dz} - \left(k_{gl-lpg} + k_{gl-dg} + k_{gl-ck}\right)y_{gl}\right)\emptyset_c \quad (3.25)$$

$$R_{lpg} = \left(k_{go-lpg}\, {y_{go}}^2 + k_{dz-lpg}\, y_{dz} + k_{gl-lpg}\, y_{gl} - \left(k_{lpg-dg} + k_{lpg-ck}\right)y_{lgp}\right)\emptyset_c \quad (3.26)$$

$$R_{dg} = \left(k_{go-dg}\, {y_{go}}^2 + k_{dz-dg}\, y_{dz} + k_{gl-dg}\, y_{gl} + k_{lpg-dg}\, y_{lpg} - k_{dg-ck}\, y_{dg}\right)\emptyset_c \quad (3.27)$$

$$R_{ck} = \left(k_{go-ck}\, {y_{go}}^2 + k_{dz-ck}\, y_{dz} + k_{gl-ck}\, y_{gl} + k_{lpg-ck}\, y_{lpg} - k_{dg-ck}\, y_{dg}\right)\emptyset_c \quad (3.28)$$

The rate constants, reaction path and their corresponding frequency factors are given as:

Overall rate constant for cracking gas oil to diesel is

$$k_{go-dz} = k_{0_{go-dz}} \exp\left(\frac{-E_{go-dz}}{R_g T_g}\right) \quad (3.29)$$

Overall rate constant for cracking gas oil to gasoline is

$$k_{go-gl} = k_{0_{go-gl}} \exp\left(\frac{-E_{go-gl}}{R_g T_g}\right) \quad (3.30)$$

Overall rate constant for cracking gas oil to LPG is

$$k_{go-lpg} = k_{0_{go-lpg}} \exp\left(\frac{-E_{go-lpg}}{R_g T_g}\right) \quad (3.31)$$

Overall rate constant for cracking gas oil to dry gas is

$$k_{go-dg} = k_{0_{go-dg}} \exp\left(\frac{-E_{go-dg}}{R_g T_g}\right) \quad (3.32)$$

Overall rate constant for cracking gas oil to coke is

$$k_{go-ck} = k_{0_{go-ck}} \exp\left(\frac{-E_{go-ck}}{R_g T_g}\right) \quad (3.33)$$

Overall rate constant for cracking diesel to gasoline is

$$k_{dz-gl} = k_{0_{dz-gl}} \exp\left(\frac{-E_{dz-gl}}{R_g T_g}\right) \quad (3.34)$$

Overall rate constant for cracking diesel to LPG is

$$k_{dz-lpg} = k_{0_{dz-lpg}} \exp\left(\frac{-E_{dz-lpg}}{R_g T_g}\right) \quad (3.35)$$

Overall rate constant for cracking diesel to dry gas is

$$k_{dz-dg} = k_{0_{dz-dg}} \exp\left(\frac{-E_{dz-dg}}{R_g T_g}\right) \quad (3.36)$$

Overall rate constant for cracking diesel to coke is

$$k_{dz-ck} = k_{0_{dz-ck}} \exp\left(\frac{-E_{dz-ck}}{R_g T_g}\right) \quad (3.37)$$

Overall rate constant for cracking gasoline to LPG is

$$k_{gl-lpg} = k_{0_{gl-lpg}} \exp\left(\frac{-E_{gl-lpg}}{R_g T_g}\right) \quad (3.38)$$

Overall rate constant for cracking gasoline to dry gas is

$$k_{gl-dg} = k_{0_{gl-dg}} \exp\left(\frac{-E_{gl-dg}}{R_g T_g}\right) \quad (3.39)$$

Overall rate constant for cracking gasoline to coke is

$$k_{gl-ck} = k_{0_{gl-ck}} \exp\left(\frac{-E_{gl-ck}}{R_g T_g}\right) \quad (3.40)$$

Overall rate constant for cracking LPG to dry gas is

$$k_{lpg-dg} = k_{0_{lpg-dg}} \exp\left(\frac{-E_{lpg-dg}}{R_g T_g}\right) \quad (3.41)$$

Overall rate constant for cracking LPG to coke is

$$k_{lpg-ck} = k_{0_{lpg-ck}} \exp\left(\frac{-E_{lpg-ck}}{R_g T_g}\right) \quad (3.42)$$

Overall rate constant for cracking dry to coke is

$$k_{dg-ck} = k_{0_{dg-ck}} \exp\left(\frac{-E_{dg-ck}}{R_g T_g}\right) \quad (3.43)$$

Q_{React} is the rate of heat generation or heat removal by the equation:

$$Q_{react} = -\left(\Delta H_{go-dz}\, k_{go-dz}\, {y_{go}}^2 + \Delta H_{go-gl}\, k_{go-gl}\, {y_{go}}^2 + \Delta H_{go-ck} k_{go-ck} {y_{go}}^2 + \Delta H_{go-lpg}\, k_{go-lpg}\, {y_{go}}^2 + \Delta H_{go-dg}\, k_{go-dg}\, {y_{go}}^2 + \Delta H_{dz-ck}\, k_{dz-ck}\, y_{dz} + \Delta H_{dz-gl}\, k_{dz-gl}\, y_{dz} + \Delta H_{dz-lpg}\, k_{dz-lpg}\, y_{dz} + \Delta H_{dz-dg}\, k_{dz-dg}\, y_{dz} +\right.$$

$$\Delta H_{gl-lpg}\, k_{gl-lpg}\, y_{gl} + \Delta H_{gl-dg}\, k_{gl-dg}\, y_{gl} + \Delta H_{gl-ck}\, k_{gl-ck}\, y_{gl} + \Delta H_{lpg-dg}\, k_{lpg-dg}\, y_{lpg} + \Delta H_{lpg-ck}\, k_{lpg-ck}\, y_{lpg} + \Delta H_{dg-ck}\, k_{dg-ck}\, y_{dg})\emptyset_c \quad (3.44)$$

3.1.3 Hydrodynamic equations of the riser

The gas volume fraction, ε_g, can be obtained from:

$$\varepsilon_g = 1 - \varepsilon_c \quad (3.45)$$

The catalyst volume fraction, ε_c, can be obtained from:

$$\varepsilon_c = \frac{F_c}{v_c \rho_c \Omega} \quad (3.46)$$

The cross-sectional area of the riser, Ω, is given as:

$$\Omega = \frac{\pi D^2}{4} \quad (3.47)$$

The effective interface heat transfer area per unit volume between the catalyst and gas phases (Dixon and Cresswell 1979),

$$A_{ptc} = \frac{6}{d_c} * (1 - \varepsilon_g) \quad (3.48)$$

Coke deposition on catalyst is considered as the main reason of catalyst deactivation and that its consequence is represented by a catalyst deactivation function. The catalyst deactivation is given by:

$$\emptyset_c = \exp(-\alpha_c C_{ck}) \quad (3.49)$$

Where α_c is related to the temperature and the feedstock by Conradson carbon R_{AN} in the virgin feedstock is directly converted to coke at the entrance of the riser and deactivates the catalyst.

$$\alpha_c = \alpha_{c0} \exp\left(\frac{-E_c}{RT_g}\right) (R_{AN})^{\alpha_{c*}} \quad (3.50)$$

In addition, the coke on catalyst is obtained as the sum of the residual coke from the regenerator and the coke generated during the cracking reactions:

$$C_{ck} = C_{ckCL1} + \frac{F_g y_{ck}}{F_c} \quad (3.51)$$

The density of the gas phase is given by:

$$\rho_g = \frac{F_g}{\varepsilon_g v_g \Omega} \quad (3.52)$$

The riser pressure is given by gas law:

$$P = Z\rho_g \frac{RT_g}{M_{wg}} \quad (3.53)$$

The ratio of the mass flowrate of catalyst to the mass flowrate of gas oil is catalyst-to-oil ratio (C/O) ratio and it is given by:

$$\mathrm{C/O\ ratio} = \frac{\mathrm{F_c}}{\mathrm{F_g}} \tag{3.54}$$

The pseudo-reduced temperature is given as:

$$\mathrm{T_{pr}} = \frac{\mathrm{T_g}}{\mathrm{T_{pc}}} \tag{3.55}$$

The pseudo-reduced pressure is given as:

$$\mathrm{P_{pr}} = \frac{\mathrm{P}}{\mathrm{P_{pc}}} \tag{3.56}$$

The momentum balance equations gives catalyst and gas velocity distribution across the riser without radial and axial dispersion:

$$\frac{\mathrm{dv_c}}{\mathrm{dx}} = -\left(\mathrm{G_c}\frac{\Omega}{\mathrm{F_c}}\frac{\mathrm{d\varepsilon_c}}{\mathrm{dx}} - \frac{\mathrm{C_f(v_g - v_c)\Omega}}{\mathrm{F_c}} + \frac{\mathrm{2f_{rc}v_c}}{\mathrm{D}} + \frac{\mathrm{g}}{\mathrm{v_c}}\right) \tag{3.57}$$

$$\frac{dv_g}{dx} = -\left(\frac{\Omega}{F_g}\frac{dP}{dx} - \frac{C_f(v_c - v_g)}{F_g} + \frac{2f_{rg}v_g}{D} + \frac{g}{v_g}\right) \tag{3.58}$$

The stress modulus (Tsuo and Gidaspow 1990) of the catalyst is calculated by:

$$\mathrm{G_c} = 10^{(-8.76\varepsilon_g + 5.43)} \tag{3.59}$$

3.1.4 Feed vaporisation section

The regenerated catalyst meets the feed and vaporises at the bottom of the riser. The section is modelled as a pseudo-heat transfer system where catalyst and feed meet and their operating variables; temperature, pressure, and velocity are evaluated. These variables depend on the process variables such as feed temperature, feed characteristics, feed droplet size, catalyst temperature, and pressure. The volume expansion and temperature variation because of the vaporisation of liquid feed are measured in the modelling of the feed vaporisation section.

Gas phase temperature at the vaporisation section is given as:

$$\mathrm{T_{gFS}} = \frac{\mathrm{B_{lg}}}{\mathrm{A_{lg} - log(P_{FS}y_{goFS})}} - \mathrm{C_{lg}} \tag{3.60}$$

Catalyst temperature at the vaporisation section

$$\mathrm{T_{cFS}} = \mathrm{T_{cCL1}} - \frac{\mathrm{F_{lg}}}{\mathrm{F_{cCL1}C_{pc}}}\left[\mathrm{C}_{plg}\left(\mathrm{T_{gFS}} - \mathrm{T_{lg}}\right) + \frac{\mathrm{F_{ds}C}_{pds}}{\mathrm{F_{lg}}}\left(\mathrm{T_{gFS}} - \mathrm{T_{ds}}\right) + \Delta H_{vlg}\right] \tag{3.61}$$

Pressure at the vaporisation

$$\mathrm{P}_{FS} = \mathrm{P}_{RT} + \Delta\mathrm{P}_{RS} \tag{3.62}$$

Weight fraction of feed (gas oil) at the vaporisation section

$$y_{goFS} = \frac{\mathrm{F_{lg}}}{\mathrm{F_{lg} + F_{ds}}} \tag{3.63}$$

Velocity of gas phase at the vaporisation section

$$v_{gFS} = \frac{\mathrm{F_{lg}} + \mathrm{F_{ds}}}{\rho_{\mathrm{gFS}}(1 - \varepsilon_{cCL1})\Omega_{FS}} \quad (3.64)$$

Velocity of entrained catalyst at the vaporisation section

$$v_{cFS} = \frac{\mathrm{F_{cCL1}}}{\rho_{\mathrm{c}}\, \varepsilon_{cCL1}\Omega_{FS}} \quad (3.65)$$

Gas oil density at the vaporisation section

$$\rho_{gFS} = \frac{\mathrm{P_{FS}M_{wgFS}}}{\mathrm{R}_g\mathrm{T_{gFS}Z_{gFS}}} \quad (3.66)$$

Catalyst phase velocity to the riser from the vaporisation section

$$v_{cRS}^{(0)} = v_{cFS} \quad (3.67)$$

Gas phase velocity to the riser from the vaporisation section

$$v_{gRS}^{(0)} = v_{gFS} \quad (3.68)$$

Catalyst mass flowrate to the riser from the cyclone via the vaporisation section

$$\mathrm{F_{cRS}} = \mathrm{F_{cCL1}} \quad (3.69)$$

Gas phase mass flowrate to the riser from vaporisation section is the sum of the mass flowrate of the liquid feed and the dispersed steam

$$\mathrm{F_{gRS}} = \mathrm{F_{lg}} + \mathrm{F_{ds}} \quad (3.70)$$

Heat of vaporisation of gas oil

$$\Delta H_{vlg} = 0.3843T_{MABP} + 1.0878 * 10^3\, exp\left(\frac{-M_{wm}}{100}\right) - 98.153 \quad (3.71)$$

Z factor of Heidaryan et al., (2010) is used for the first time to model the riser, and the very first time that a Z factor other than unity for riser simulation is used.

$$Z = \ln\left[\frac{\mathrm{A_1} + \mathrm{A_3}\ln(\mathrm{P_{pr}}) + \frac{\mathrm{A_5}}{\mathrm{T_{pr}}} + \mathrm{A_7}(\ln\mathrm{P_{pr}})^2 + \frac{\mathrm{A_9}}{\mathrm{T_{pr}^2}} + \frac{\mathrm{A_{11}}}{\mathrm{T_{pr}}}\ln(\mathrm{P_{pr}})}{1 + \mathrm{A_2}\ln(\mathrm{P_{pr}}) + \frac{\mathrm{A_4}}{\mathrm{T_{pr}}} + \mathrm{A_6}(\ln\mathrm{P_{pr}})^2 + \frac{\mathrm{A_8}}{\mathrm{T_{pr}^2}} + \frac{\mathrm{A_{10}}}{\mathrm{T_{pr}}}\ln(\mathrm{P_{pr}})}\right] \quad (3.72)$$

3.2 Stripper/Reactor/Disengager model equations

This Stripper/Reactor/Disengager section is modelled as a perfectly mixed continuous tank without reaction, with an exponential type stripping function, which considers the catalyst-to-oil coke:

$$C_{ckST} = C_{ckST0} + k_{ss0}\exp\left[\frac{-F_{cRS}F_{ss}E_{ss}}{F_{lg}}\right] \quad (3.73)$$

Where the coke on the catalyst exiting the stripper is estimated as

$$\frac{dC_{ckRT}}{dt} = \frac{F_{cRS}}{w_{cRT}}\left(C_{ckRS}^{(hrg)} + C_{ckST} - C_{ckRT}\right) \quad (3.74)$$

The mass balances for gases in the disengaging-stripping section

$$\frac{dw_{gRT}}{dt} = F_{gRS}\left(\left(1 - y_{ckRS}^{(hrg)}\right) + F_{ss} - F_{gRT} - F_{cRS}C_{ckST}\right) \quad (3.75)$$

The mass balances for catalysts in the disengaging-stripping section

$$\frac{dw_{cRT}}{dt} = (F_{cRS} + F_{cSV2} - F_{cMF}) \quad (3.76)$$

The weight fractions of the gaseous products from the disengager are obtained from the component balance

$$\frac{dy_{iRT}}{dt} = \frac{1}{w_{gRT}}\left\{y_{iRS}^{hrg}\left[F_{gRS} - \frac{F_{gRS}C_{ck_{ST}}}{\sum_{j=go,gl,gs,dz,LPG} y_{iRS}^{hrg}}\right] - y_{iRT}\left[F_{gRT} + \frac{dw_{gRT}}{dt}\right]\right\} \quad (3.77)$$

Where $i = go, gl, gs, dz, LPG$

$$y_{wvRT} = y_{goRT} - y_{glRT} - y_{gsRT} - y_{dzRT} - y_{LPGRT} \quad (3.78)$$

The conversion of the gas oil on fresh feed is

$$Y_{convRT} = 1 - \frac{F_{gRS}y_{goRT}}{F_{lg}} \quad (3.79)$$

The energy balance in the stripper is given by

$$\left(w_{cRT}C_{pc} + w_{gRT}C_{pgRT}\right)\frac{dT_{RT}}{dt} = F_{ss}H_{ss} + F_{ds}H_{ds} - (F_{ss} + F_{ds})H_{wvRT}^{(out)} + F_{cRS}\left(H_{cRT}^{(in)} - H_{cRT}^{(out)}\right) + \left(F_{gRS} - F_{ds}\right)\left(H_{hgRT}^{(in)} - H_{hgRT}^{(out)}\right) - F_{ss}\Delta H_{stripST} + Q_{lossRT} \quad (3.80)$$

Where

$$H_{ss} = \bar{C}_{pwv}\left(T_{ss} - T_{ref}\right) \quad (3.81)$$

$$H_{ds} = \bar{C}_{pwv}\left(T_{gRS}^{(hrs)} - T_{ref}\right) \quad (3.82)$$

$$H_{hgRT}^{(in)} = \bar{C}_{phg}\left(T_{gRS}^{(hrs)} - T_{ref}\right) \quad (3.83)$$

$$H_{hgRT}^{(out)} = \bar{C}_{pc}\left(T_{RT} - T_{ref}\right) \quad (3.84)$$

$$H_{cRT}^{(in)} = \bar{C}_{pc}\left(T_{cRS}^{(hrs)} - T_{ref}\right) \quad (3.85)$$

$$H_{wvRT}^{(out)} = \bar{C}_{pwv}\left(T_{RT} - T_{ref}\right) \quad (3.86)$$

$$Q_{lossRT} = U_{RT}A_{RTe}(T_e - T_{RT}) \quad (3.87)$$

The gas-phase pressure is given by

$$P_{RT} = \frac{w_{gRT}RT_{RT}Z_{gRT}}{M_{wgRT}V_{gRT}} \quad (3.88)$$

Where

$$V_{gRT} = V_{RT} - \frac{w_{cRT}}{\rho_c} \quad (3.89)$$

The pressure at the bottom of the disengaging-stripping section is higher than the pressure at the top by the static head exerted by the catalyst:

$$P_{RTb} = P_{RT} + \frac{(w_{cRT} - w_{cCY1})(h_{RT} - h_{ST})g}{1000V_{RT}} \quad (3.90)$$

3.2.1 Reactor cyclones

The rate of accumulation of catalyst in the cyclones based on a continuous stirred tank (CST) model is

$$0 = \eta_{CY1} v_{cCY1} \Omega_{CY1i} \frac{w_{cRT}}{V_{RT}} - k_{cCY1} \left[\frac{w_{cCY1}\Omega_{CY1d}/N_{CY1}}{\rho_{bCY1}}\right]^{\left(\frac{1}{2}\right)} \quad (3.91)$$

Where

$$w_{cCY1} = \frac{\rho_{bCY1} N_{CY1}}{\Omega_{CY1d}} \left[\eta_{CY1} v_{cCY1} \Omega_{CY1i} \frac{w_{cRT}}{V_{RT} k_{cCY1}}\right]^2 \quad (3.92)$$

The cyclone inlet velocity is obtained by the equation (Rosin et al. 1932)

$$\eta_{CY1} = \frac{9\mu_{gRT}\Omega_{CY1i}}{\pi N_{tCY1} d_{cm}^2 \left(\rho_c - \frac{w_{cRT}}{V_{gRT}}\right) h_{CY1i}} \quad (3.93)$$

The main fractionator receives the products from the disengager and separates the products further. The respective mass flowrates are given as:

$$F_{cMF} = (1 - \eta_{CY1}) v_{cCY1} \Omega_{CY1i} \frac{w_{cRT}}{V_{RT}} N_{CY1} \quad (3.94)$$

$$F_{gRT} = k_{vMF} \sqrt{P_{RT} - P_{MF}} \quad (3.95)$$

$$F_{hgRT} = F_{gRT}(1 - y_{wvRT}) \quad (3.96)$$

3.3 Regenerator model equations

The total mass balance of catalyst and gas in the entire regenerator are given as:

$$\frac{dw_{cRG}}{dt} = F_{cCL2} - F_{cSV1} - F_{cSG} \quad (3.97)$$

$$\frac{dw_{gRG}}{dt} = F_{aD} + F_{cCL2} C_{ckCL2} - F_{cSV1} C_{ckD} - F_{cSG} C_{ckF}^{(hrg)} - F_{gSG} \quad (3.98)$$

And the mass flowrate of gas to the stack is

$$F_{gSG} = k_{vSG} f_v(x_{vSG}) \sqrt{F_{RG}} - P_{SG} \quad (3.99)$$

As coke is burned off, the gas phase increases also with a velocity given by the correlation

$$u_{gRG} = \frac{F_{aD}(1-\delta_{gRG}) + F_{gSG}\delta_{gRG}}{\rho_{gRG}\Omega_{RG}} \quad (3.100)$$

And the relative extend δ_{gRG} by which the gas phase increases are given by

$$\delta_{gRG} = \left[\frac{0.5q\rho_{gRG} - C_{H_2OF}^{(hrg)} M_{wck}}{0.5q\rho_{gRG} - C_{H_2Oi}^{(z)} M_{wck}}\right] \left[\frac{C_{H_2Oi}^{(z)} - C_{H_2OD}^{(0)}}{C_{H_2OF}^{(hrg)} - C_{H_2OD}^{(0)}}\right] \quad (3.101)$$

Where $i = D, F$

And density of the gas phase is

$$\rho_{gRG} = \frac{w_{gRG}}{V_{RG} - \frac{w_{gRG}}{\rho_c}} \quad (3.102)$$

In the literature (Han and Chung 2001a; Han and Chung 2001b), the average regenerator pressure is measure at the dense bed exit and it is given by:

$$P_{RG} = \frac{RT_D \rho_{gRG} Z_{gRG}}{M_{wgRG}{}^{(H_D)}} \quad (3.103)$$

In this model, the pressure of the regenerator is calculated along the height of the regenerator.

$$M_{wgRG} = \sum_i M_{wi} f_{ij} \quad (3.104)$$

$i = O_2, CO, CO_2, H_2O, N_2$

And $j = D, F$

$$f_{ij} = \frac{C_{ij}}{\sum_i C_{ij}} \quad (3.105)$$

$i = O_2, CO, CO_2, H_2O, N_2$

And $j = D, F$

The pressure exerted on the bottom is

$$P_{RGb} = P_{RGb} + \frac{g\rho_c}{1000}\left[\varepsilon_{cD} H_D + \int_{H_D}^{hrg} \varepsilon_{cD}(z) dz\right] \quad (3.106)$$

3.3.1 The dense bed

The dense bed is modelled as a hybrid reactor that employs a mixed-tank model for energy and coke balances but a tubular reactor model for gas component balances. The component balance equations for each gaseous phase are described by the following partial differential equations, respectively:

$$\frac{\partial C_{iE}}{\partial t} + u_{gE}\frac{\partial C_{iE}}{\partial t} = -\frac{C_{iE} S_{gE}}{\varepsilon_{gE}} + \frac{K_I}{\varepsilon_{cE}}(C_{iB} - C_{iE}) + R_{iE} \quad (3.107)$$

$i = O_2, CO, CO_2, H_2O, N_2$

$$R_{O_2E} = -\frac{\rho_c \varepsilon_{cD}}{\varepsilon_{gE}}\left[\frac{(0.5+0.25q) r_{1E}}{M_{wck}} + \frac{(1+0.25q) r_{2E}}{M_{wck}} + 0.5 r_{4E}\right] - 0.5 r_{3E} \quad (3.108)$$

$$R_{COE} = \frac{\rho_c \varepsilon_{cD}}{\varepsilon_{gE}}\left[\frac{r_{1E}}{M_{wck}} - r_{4E}\right] - r_{3E} \quad (3.109)$$

$$R_{CO_2E} = \frac{\rho_c \varepsilon_{cD}}{\varepsilon_{gE}}\left[\frac{r_{2E}}{M_{wck}} + r_{4E}\right] + r_{3E} \quad (3.110)$$

$$R_{H_2OE} = \frac{\rho_c \varepsilon_{cD} q}{\varepsilon_{gE} M_{wck}}[0.5 r_{1E} + 0.5 r_{2E}] \quad (3.111)$$

$$R_{N_2E} = 0 \quad (3.112)$$

$$S_{gE} = \frac{\partial \varepsilon_{gE}}{\partial t} + \frac{\partial (v_{gE} \varepsilon_{gE})}{\partial z} \quad (3.113)$$

I.C.:

$$C_{iE}^{(0,z)} = C_{iE}^{(z)} \quad (3.114)$$

$$i = O_2, CO, CO_2, H_2O, N_2$$

B.C.:

$$C_{iE}^{(t,0)} = \frac{f_{iE}^{(0)} \rho_{gRG}}{M_{wgRG}^{(0)}} \quad (3.115)$$

$$i = O_2, CO, CO_2, H_2O, N_2$$

$$\frac{\partial C_{iB}}{\partial t} = -v_{gB} \frac{\partial C_{iB}}{\partial z} - \frac{C_{iB} S_{gB}}{\varepsilon_{gB}} + \frac{K_I}{\varepsilon_{gB}} (C_{iE} - C_{iB}) + R_{iB} \quad (3.116)$$

$$i = O_2, CO, CO_2, H_2O, N_2$$

$$R_{O_2B} = -0.5 r_{3E} \quad (3.117)$$

$$R_{COB} = -r_{3E} \quad (3.118)$$

$$R_{CO_2B} = r_{3E} \quad (3.119)$$

$$R_{H_2OB} = 0 \quad (3.120)$$

$$R_{N_2B} = 0 \quad (3.121)$$

$$S_{gB} = \frac{\partial \varepsilon_{gB}}{\partial t} + \frac{\partial (v_{gB} \varepsilon_{gB})}{\partial z} \quad (3.122)$$

I.C:

$$C_{iB}^{(0,z)} = C_{iB}^{(z)} \quad (3.123)$$

$$i = O_2, CO, CO_2, H_2O, N_2$$

$$C_{iB}^{(t,0)} = \frac{f_{iB}^{(0)} \rho_{gRG}}{M_{wgRG}^{(0)}} \quad (3.124)$$

$$i = O_2, CO, CO_2, H_2O, N_2$$

Kinetic rates for the bubble and emulsion phases are given as:

$$\mathrm{r_{1E}} = \frac{\mathrm{k_{1RG} C_{ckD} C_{O_2E}}}{1 + \sigma} \quad (3.125)$$

$$\mathrm{r_{2E}} = \mathrm{r_{1E}} \sigma \quad (3.126)$$

$$\mathrm{r_{3E}} = \mathrm{k_{3RG} C_{COE} C_{O_2E}^{0.5} C_{H_2OE}^{0.5}} \quad (3.127)$$

$$\mathrm{r_{3B}} = \mathrm{k_{3RG} C_{COB} C_{O_2B}^{0.5} C_{H_2OB}^{0.5}} \quad (3.128)$$

$$\mathrm{r_{4E}} = \mathrm{k_{4RG} C_{COE} C_{O_2E}^{0.5}} \quad (3.129)$$

The Arrhenius equation is used to describe the temperature dependency of the rate constants as follows:

$$k_{iRG} = k_{i0RG} exp\left(\frac{-E_{iRG}}{RT_j}\right) \quad (3.130)$$

$$i = 1,3,4$$

$$j = D, F$$

The mean molar concentration from the dense bed is given by:

$$C_{iD} = \frac{C_{iE}u_{gE}\varepsilon_{gE} + C_{iB}u_{gB}\varepsilon_{gB}}{u_{gRG}} \quad (3.131)$$

$$i = O_2, CO, CO_2, H_2O, N_2$$

The volume fraction of the emulsion and bubble phases for catalyst and gases must add up to unity for the entire length of the dense bed.

$$\varepsilon_{cD} + \varepsilon_{gE} + \varepsilon_{gB} = 1 \quad (3.132)$$

While the catalyst voidage is

$$\varepsilon_{cD} = 0.3418\exp\left(-0.9751\bar{u}_{gRG}\right) + 0.1592 \quad (3.133)$$

The average velocity is

$$\bar{u}_{gRG} = \frac{1}{H_D}\int_0^{H_D} u_{gRG}(z)dz \quad (3.134)$$

The volume fraction of the bubble phase, the minimum fluidisation velocity and bubble rising velocity are given as (Kunii and Levenspiel 1991)

$$\varepsilon_{gB} = \frac{u_{gRG} - v_{gm}}{v_{gB} - v_{gm}} \quad (3.135)$$

$$v_{gm} = \frac{d_c^2(\rho_c - \rho_{gRG})g\varepsilon_{gm}^3 s_c^2}{150\mu_{gRG}(1-\varepsilon_{gm})} \quad (3.136)$$

$$v_{gB} = u_{gRG} - v_{gm} + 0.711\sqrt{gd_b} \quad (3.137)$$

$$d_b = d_{bm} - (d_{bm} - d_{b0})\exp(-0.3z/D_{RGe}) \quad (3.138)$$

The initial bubble diameter is

$$d_{b0} = \frac{2.78}{g}(u_{gRG}^0 - v_{gm})^2 \quad (3.139)$$

The maximum bubble diameter is

$$d_{bm} = 0.59(u_{gRG}^{(H_D)} - v_{gm})^{0.4} D_{RGe}^{0.8} \quad (3.140)$$

The interstitial emulsion gas velocity is obtained from the mass balance in the dense bed as

$$v_{gE} = \frac{u_{gRG} - \varepsilon_{gB}v_{gE}}{\varepsilon_{gE}} \quad (3.141)$$

The total holdups of the catalyst and gas in the dense bed of the regenerator are given by the equations

$$w_{cD} = w_{cRG} - w_{cF} - w_{cCY2} \quad (3.142)$$

$$w_{cD} = H_D\Omega_{RG}(1-\varepsilon_{cD})\rho_{gRG} \quad (3.143)$$

And the height of the dense bed is obtained as

$$H_D = \frac{w_{cD}}{\Omega_{RG}\varepsilon_{cD}\rho_c} \quad (3.144)$$

The coke on catalyst is uniformly distributed; hence a lumped equation for the coke deposited on catalyst as follows:

$$\frac{dC_{ckD}}{dt} = \frac{F_{cCL2}}{w_{cD}}(C_{ckCL2} - C_{ckD}) + \frac{F_{cCY2}}{w_{cD}}\left(C_{ckF}^{(hrg)} - C_{ckD}\right) + \frac{M_{wck}}{0.5q\rho_{gRG}w_{cD}}\left(F_{ad}C_{H_2OD}^{(0)} - F_{gD}^{(H_D)}C_{H_2OD}^{(H_D)}\right) \quad (3.145)$$

$$F_{ad} = \rho_{gRG}\Omega_{RG}\, u_{gRG} \quad (3.146)$$

The substances in the bed are in thermal equilibrium, hence, a mixed-tank dynamic model for the energy balance is considered for the dense bed:

$$\left(w_{cD}C_{pc} + w_{gD}C_{pcD}\right)\frac{dT_D}{dt} = F_{cCL2}\left(H_{cD}^{(in)} - H_{cD}^{(out)}\right) + F_{ad}\left(H_{gD}^{(in)} - H_{gD}^{(out)}\right) + F_{cCY2}\left(H_{cCY2}^{(in)} - H_{cD}^{(out)}\right) + Q_{lossD} + Q_{reactD} \quad (3.147)$$

Where

$$H_{cD}^{(in)} = \bar{C}_{pc}(T_{cCL2} - T_{ref}) \quad (3.148)$$

$$H_{cD}^{(out)} = \bar{C}_{pc}(T_D - T_{ref}) \quad (3.149)$$

$$H_{gD}^{(in)} = \bar{C}_{pa}(T_{aD} - T_{ref}) \quad (3.150)$$

$$H_{gD}^{(out)} = \bar{C}_{pgD}(T_D - T_{ref}) \quad (3.151)$$

$$H_{cCY2}^{(out)} = \bar{C}_{pc}(T_{CY2} - T_{ref}) \quad (3.152)$$

$$Q_{lossD} = U_D A_{De}(T_e - T_D) \quad (3.153)$$

$$Q_{reactD} = \frac{1}{\rho_{gRG}}\sum_i \left(F_{ad}C_{iD}^{(0)} - F_{gD}^{(H_D)}C_{iD}^{(H_D)}\right)\Delta H_{fi}^{(T_D)} + \frac{1}{0.5q\rho_{gRG}}\left(F_{ad}C_{H_2OD}^{(0)} - F_{gD}^{(H_D)}C_{H_2OD}^{(H_D)}\right)\Delta H_{fck}^{(T_D)} \quad (3.154)$$

$$i = O_2, CO, CO_2, H_2O, N_2$$

3.3.2 Freeboard

The component mass balance giving rise to molar concentrations of gaseous substances in the freeboard are given as:

$$\frac{\partial C_{iF}}{\partial t} = \frac{-u_{gRG}}{\varepsilon_{gF}}\frac{\partial C_{iF}}{\partial z} - \frac{\rho_c\varepsilon_{gF}C_{iF}}{\rho_{gRG}\varepsilon_{gF}}(r_{iE} - r_{iB}) + R_{iF} \quad (3.155)$$

$$i = O_2, CO, CO_2, H_2O, N_2$$

$$R_{O_2F} = -\frac{\rho_c\varepsilon_{cF}}{\varepsilon_{gF}}\left[\frac{(0.5+0.25q)r_{1F}}{M_{wck}} + \frac{(1+0.25q)r_{2F}}{M_{wck}} + 0.5r_{4F}\right] - 0.5r_{3F} \quad (3.156)$$

$$R_{COF} = \frac{\rho_c\varepsilon_{cF}}{\varepsilon_{gF}}\left[\frac{r_{1F}}{M_{wck}} - r_{4F}\right] - r_{3F} \quad (3.157)$$

$$R_{CO_2F} = \frac{\rho_c\varepsilon_{cF}}{\varepsilon_{gF}}\left[\frac{r_{2F}}{M_{wck}} + r_{4F}\right] + r_{3F} \quad (3.158)$$

$$R_{H_2OF} = \frac{\rho_c\varepsilon_{cF}q}{\varepsilon_{gF}M_{wck}}[0.5r_{1F} + 0.5r_{2F}] \quad (3.159)$$

$$R_{N_2F} = 0 \quad (3.160)$$

I.C:

$$C_{iF}^{(0,z)} = C_{iF0}^{(z)} \tag{3.161}$$

$$i = O_2, CO, CO_2, H_2O, N_2$$

$$C_{iF}^{(t,H_D)} = C_{iD}^{(H_D)} \tag{3.162}$$

$$i = O_2, CO, CO_2, H_2O, N_2$$

Kinetic rates for the freeboard phase are given as:

$$r_{1F} = \frac{k_{1RG} C_{ckF} C_{O_2F}}{1+\sigma} \tag{3.163}$$

$$r_{2F} = r_{1F}\sigma \tag{3.164}$$

$$r_{3F} = k_{3RG} C_{COF} C_{O_2F}^{0.5} C_{H_2OF}^{0.5} \tag{3.165}$$

$$r_{3F} = k_{3RG} C_{COF} C_{O_2F}^{0.5} C_{H_2OF}^{0.5} \tag{3.166}$$

$$r_{4F} = k_{4RG} C_{COF} C_{O_2F}^{0.5} \tag{3.167}$$

The volume fraction of the freeboard for catalyst and gases must add up to unity for the entire length of the freeboard.

$$\varepsilon_{cF} + \varepsilon_{gF} = 1 \tag{3.168}$$

The catalyst voidage is based on an exponential decay given by the empirical equation

$$\varepsilon_{cF} = \varepsilon_{cF}^{*} + (\varepsilon_{cD} - \varepsilon_{cF}^{*}) \exp\left(-\beta_c (z - H_D)\right) \tag{3.169}$$

where

$$\varepsilon_{cF}^{*} = \frac{\rho_{gRG}}{\rho_c} 10^{\left(-0.725 - 2.517 (log\chi)^2\right)} \tag{3.170}$$

$$\chi = \frac{\left(u_{gRG}^{(hrg)}\right)^2}{g d_c \rho_c^2} \tag{3.171}$$

The catalyst holdup in the freeboard is

$$w_{cF} = \Omega_{RG} \rho_c \int_{H_D}^{hrg} \varepsilon_{cF}(z) dz \tag{3.172}$$

Where

$$hrg = H_D + H_F \tag{3.173}$$

The catalyst flow rate and the superficial catalyst velocity in the freeboard are assumed constant, and given as:

$$F_{cF} = \frac{F_{cCY2}}{\eta_{cCY2}} \tag{3.174}$$

$$u_{cF} = \frac{F_{cF}}{\rho_c \Omega_{RG}} \tag{3.175}$$

Unlike in the dense bed, a distributed parameter model expresses the coke on catalyst in the freeboard as follows:

$$\frac{\partial C_{ckF}}{\partial t} = \frac{-u_{cF}}{\varepsilon_{cF}}\frac{\partial C_{ckF}}{\partial z} - (r_{1F} + r_{2F}) \quad (3.176)$$

I.C:

$$C_{ckF}^{(0,z)} = C_{ckF0}^{(z)} \quad (3.177)$$

B.C.:

$$C_{ckF}^{(t,H_D)} = C_{ckD} \quad (3.178)$$

Neglecting the heat transfer resistance between the catalyst and gas phases, the temperature distribution in the freeboard region is evaluated by the following partial differential equation:

$$\left(\rho_c \varepsilon_{cF} C_{pc} + \rho_{gRG} \varepsilon_{gF} C_{pgF}\right)\frac{dT_F}{dt} + \left(u_{cF}\rho_c C_{pc} + u_{gRG}\rho_{gRG} C_{pgF}\right)\frac{dT_F}{dz} = Q_{lossF} + Q_{reactF} \quad (3.179)$$

Where

$$Q_{lossF} = \frac{4U_F}{D_{RG}}(T_e - T_F) \quad (3.180)$$

$$Q_{lossF} = \frac{\rho_c \varepsilon_{cF}}{M_{wck}}[r_{1F}\Delta H_{r1} + r_{2F}\Delta H_{r2}] + \varepsilon_{gF} r_{3F}\Delta H_{r3} + \rho_c \varepsilon_{cF} r_{4F}\Delta H_{r4} \quad (3.181)$$

$$\Delta H_{ri} = -\sum_j v_{ij}\Delta H_{fj}^{(T_F)} \quad (3.182)$$

$$i = O_2, CO, CO_2, H_2O, ck$$

I.C:

$$T_F^{(0,z)} = T_{F0}^{(z)} \quad (3.183)$$

B.C.:

$$T_F^{(t,H_D)} = T_D \quad (3.184)$$

3.3.3 Regenerator cyclone

Just like the reactor cyclone, the regenerator cyclone is modelled as a continuous stirred tank, and its rate of accumulation of catalyst is given by

$$w_{cCY2} = \frac{\rho_{bCY2} N_{CY2}}{\Omega_{CY2d}}\left(\frac{F_{cCY2}}{k_{vCY2} N_{CY2}}\right)^2 \quad (3.185)$$

$$F_{cCY2} = \eta_{cCY2} v_{cCY2} \rho_c \varepsilon_{cF}^{(hrg)} \Omega_{CY2i} N_{CY2} \quad (3.186)$$

$$v_{cCY2} = \frac{9\mu_{gRG}\Omega_{CY2i}}{d_{cm}^2 \pi N_{tCY2}(\rho_c - \rho_{gRG})h_{CY2i}} \quad (3.187)$$

The flow rate of the catalyst entering the stack through the cyclone is given by

$$F_{cSG} = \frac{(1-\eta_{CY2})F_{cCY2}}{\eta_{CY2}} \quad (3.188)$$

3.3.4 Catalyst transport lines

The pressure drop determines the flow rate of catalyst through a catalyst transport line across a slide valve. The mass flow rate of the regenerated catalyst through the slide valve is evaluated as

$$F_{cSV1} = k_{vSV1} f_v(x_{cSV1}) \sqrt{P_{RGb} - P_{FS} + \frac{\rho_c(1-\varepsilon_{gCL1}) g l_{CL1} sin\theta_{CL1}}{1000}} \quad (3.189)$$

The flow rate through the transport line is assumed constant because the catalyst bulk density is constant, therefore,

$$F_{cCL1} = F_{cSV1} \quad (3.190)$$

Ignoring the transport lag throughout the catalyst transport lines, the temperature and the coke on catalyst at the outlet of the regenerated catalyst transport line are simply given by

$$T_{cCL1} = T_D \quad (3.191)$$

$$C_{ckCL1} = C_{ckD} \quad (3.192)$$

Related equations can be obtained for the spent catalyst transport line from the reactor to the regenerator as follows:

$$F_{cSV2} = k_{vSV2} f_v(x_{cSV2}) \sqrt{P_{RTb} - P_{RG} + \frac{\rho_{bCL2} g l_{CL2} sin\theta_{CL2}}{1000}} \quad (3.193)$$

$$F_{cCL2} = F_{cSV2} \quad (3.194)$$

$$T_{cCL2} = T_{RT} \quad (3.195)$$

$$C_{ckCL2} = C_{ckRT} \quad (3.196)$$

3.4 A proposed technique for parameter estimation using gPROMS

Parameter Estimation can be achieved for complex models using the parameter estimation platform of gPROMS software. However, it requires a detailed gPROMS process model that captures the system's physical and chemical interactions like the riser model used in this study. The process model representing the system should have parameters that can be tuned to make the model predictions adequately aligned with real data. Such model parameters, particularly in this work, are heat of reactions, frequency factors and activation energies. The more accurate these parameters are, the closer the model's response to reality (gPROMS, 2013). The method used in making these parameters to fit with laboratory or plant/industrial data is called parameter estimation.

gPROMS uses the Maximum Likelihood formulation technique for parameter estimation which estimates parameters in the physical model of the process and the variance model of the measuring instruments. The measuring instrument can be a sensor that is either constant variance for temperature measurement (thermocouple) with an accuracy of +/- 1K, or constant relative variance for measuring of concentration (composition analyser) with an error of +/- 2%, or both measuring instruments, in which case it is called the heteroscedastic variance, combining both constant variance and constant relative variance (gPROMS, 2013).

Model parameters of any developed model and their operating conditions should be evaluated before solving the model equations. Murthy and Gupta (1998) have used the non-linear parameter estimation method of the Box-Kanemasu to evaluate model parameters. Senthilmurugan et al. (2005) adopted the simplex search method for model parameter evaluation. In this research, the estimation of the unknown parameters was carried out using a technique describe in Figure 3.1. In gPROMS parameter estimation is a form of optimisation, which aims to evaluate the values of several parameters depending on the experimental information that gives the best value of the performance criterion. The principle of gPROMS parameter estimation is to minimise the sum of square errors (SSE) between the experimental values of several parameters and the calculated values. This is carried out by changing the model parameters from an initial guesstimate value to optimal values based on experimental data. In other words, the optimisation of these parameters is achieved by fitting the experimental data to the model predicted values by varying certain model parameters to maximise the probability that the model will closely predict the actual values. The gPROMS software uses a mathematical solver tool called Maximum Likelihood formulation technique (MXLKHD) for the parameter estimation.

A description of a parameter estimation technique developed and used for all the other developed kinetic models in this research is presented. The estimation of kinetic parameters using model-based technique along with experimental (generated from model and plant) data is carried out in this work. Specifically, the parameter estimation tool of the gEST in the gPROMS is used to predict the unknown parameters of the developed model. The method involves the use of optimisation technique in gPROMS to the minimise sum of squared errors (SSE) between experimental values y_i^{exp} (generated by using a new technique from

the model having obtained input and output data from the plant) and calculated values y_i^{cal}. This technique has two approaches: firstly, simulation for converging all the equality constraints and satisfying the inequality constraints and secondly, performing the optimisation where the objective function is as summarily written:

$$Obj(SSE) = \sum_{M=1}^{M_t}\left(y_i^{exp} - y_i^{cal}\right)^2 \quad (3.195)$$

Where y is the mass fraction of lumps and i refers to the various lumps in the riser.

The parameter estimation problem statement can be written as:

Given	The fixed riser reactor configuration, feed quality and characteristics, catalyst properties and process operational conditions
Optimise	The kinetics parameters; activation energies E_j, heat of reactions ΔH_j and frequency factors k_{oj} at given process conditions
So as to minimise	The sum of square errors (SSE)
Subject to	Equality and inequality constraints

Mathematically;

$$\min_{\xi_{io},\eta_i,\theta_i} SSE$$

s. t.

$f(x, z'(x), z(x), u(x), v) = 0$ (model equations, equality constraints)

$\xi^l \le \xi \le \xi^u$ (inequality constraints)

$\eta^l \le \eta \le \eta^u$ (inequality constraints)

$\theta^l \le \theta \le \theta^u$ (inequality constraints)

Where $f(x, z'(x), z(x), u(x), v) = 0$ is model equation, x the height of the riser and the independent variable. $u(x)$ is the decision variable; ξ the frequency factors k_{oj} with ξ^u as the upper and ξ^l as lower limits; η the activation energies E_j, with η^u as upper and η^l as lower limits; θ as the heat of reaction ΔH_j, with θ^u as upper and θ^l as lower limits. $z(x)$ the differential and algebraic equations while $z'(x)$ their derivative. v the constants parameters. The decision variables are the model parameters to be estimated and, in this case, they are the frequency factors, heat of reactions and activation energies. The parameter estimation is solved by renewing the decision variables in a way, which satisfies the equality and inequality constraints (Mujtaba 2004).

It is a common practice to obtain experimental data or results from the laboratory or pilot plant to fit with predicted results of the process using parameter estimation. It is different when only the operating conditions and exit conditions of an actual plant are available and a detailed model of the plant is used to estimate unknown parameters. This is the case with this proposed technique. To start with, known parameters of a known unit with detailed mathematical model was used to test the technique. The proposed parameter estimation technique presented in Figure 3.1 describes how input and output data from the plant were used in model simulation to generate online data across the discretised height of the riser, which were used to represent experimental data in the gPROMS software for parameter estimation.

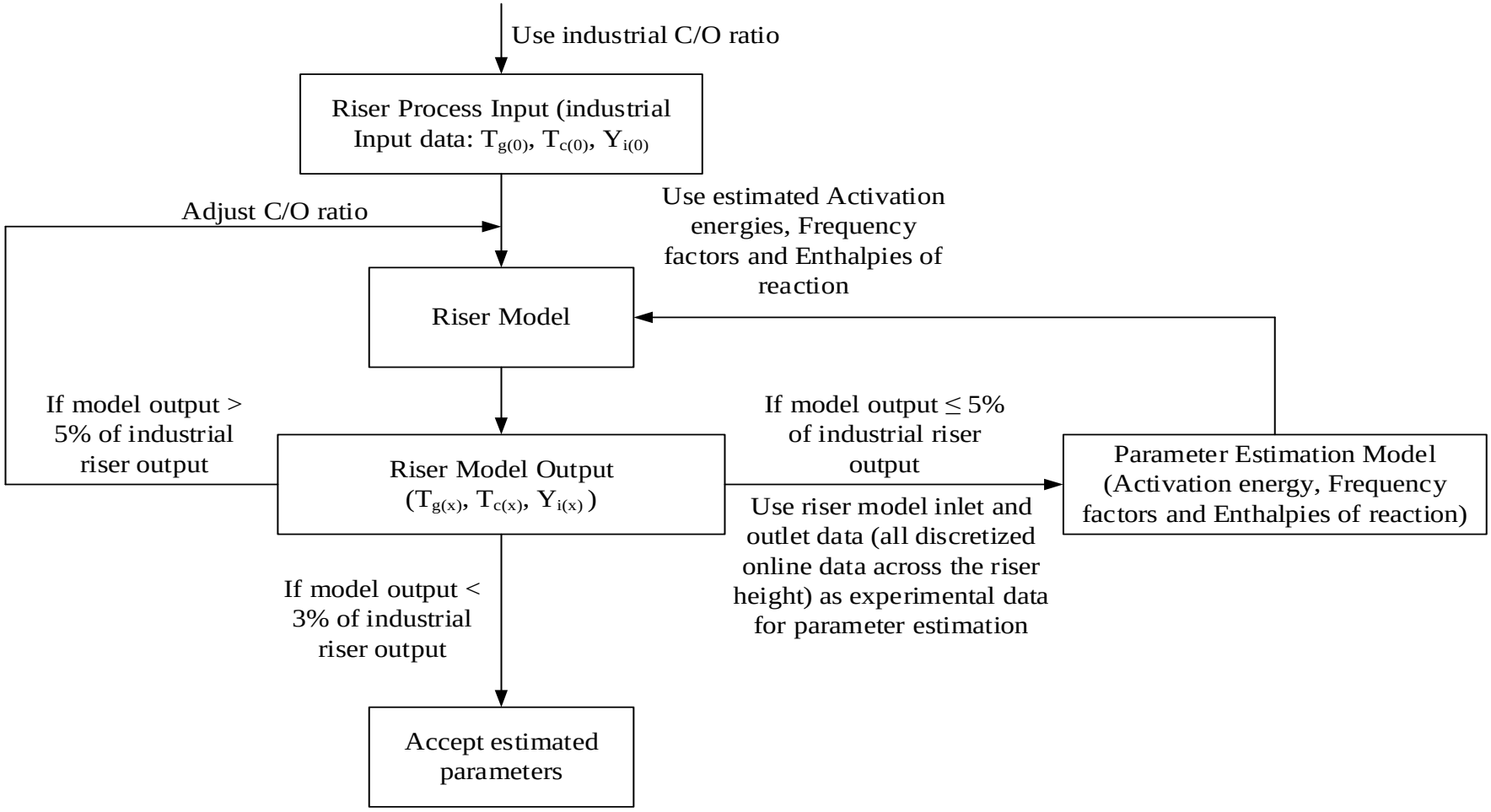

Figure 3.1: Testing of parameter estimation technique

Since estimated parameters of a process can only be trusted if they are obtained from accurate models of that process, the riser mathematical model used for this parameter estimation was validated to ensure that it is not just accurate enough to simulate the riser, but it is able to estimate those kinetic parameters as well. Hence, to generate experimental data through simulation with the riser model, a known four-lump kinetic model of the riser (Han and Chung, 2001a, Han and Chung, 2001b) was used. From Figure 3.1, the procedure requires that the output data from the riser model simulation be compared with the actual plant riser outlet conditions. If the difference between the outputs from the simulation and plant data are less than or equal to 5%, a reasonable limit of error, the values of the lumps and temperatures of the catalyst and gas phases at discrete heights of the riser are taken and used as experimental data on the parameter estimation platform of the gPROMS software. If the outputs from the simulation are more than 5%, the C/O ratio is adjusted to obtain riser output in the simulation almost the same as those of the plant. Once this happen, the values of the estimated parameters are deemed 'estimated' and are used in the riser model, which is expected to eventually predict the riser output to be the same as that of the plant. 5% level of error is accepted because the data generated will be subjected to some optimisation during the parameter estimation process, where the level of error is further reduced as the estimated parameters are obtained.

3.4.1 Testing of parameter estimation technique using four-lumped model

A four-lump kinetic model is chosen for testing the parameter estimation strategy because it is most widely used for FCC unit simulation (Han and Chung 2001a). It also represents the major product classification of the FCC reactant and products and have all the values of its kinetic parameters validated over the years. Additionally, using kinetic models with more than four lumps means more kinetic parameters to estimate. The fewer the lumps the fewer the kinetic parameters needed. The four lumped kinetic data in Table 3.1 are taken from literature and have been used by many authors to simulate the FCC riser. In this section, these kinetic data of the four lumped kinetic model are used as guess values with upper and lower bounds, along with the riser mathematical model on the parameter estimation platform of gPROMS. The parameters to be estimated for the four lump are $[k_{o1}, k_{o2}, k_{o3}, k_{o4}, k_{o5}]$, $[E_1, E_2, E_3, E_4, E_5]$ and $[\Delta H_1, \Delta H_2, \Delta H_3, \Delta H_4, \Delta H_5]$.

The mass and energy balance, and kinetic model equations used for the four-lump model are presented in Equations (3.1 - 3.16) together with the riser hydrodynamic Equations (3.45 - 3.70). The operational parameters and riser configuration used can be found in the same literature from where the riser model was adopted (Han and Chung, 2001a, Han and Chung, 2001b). The riser conditions (temperatures and compositions) at discrete points along the riser height obtained from the procedure in Figure 3.1 were used as experimental data in the parameter estimation platform of the gPROMS software. The values are presented in Table 3.2.

Table 3.1: Kinetic parameters of four-lump model (Han and Chung, 2001b)

Reaction	Frequency Factor (k_i) (s^{-1})	Activation Energy (kJ/kmol) (E_i)	Heat of Reaction (kJ/kmol) ΔH_i
Gas Oil → Gasoline	1457.50	57,359	195
Gas Oil → Gas	127.59	52,754	670
Gas Oil → Coke	1.98	31,820	745
Gasoline → Gas	256.81	65,733	530
Gasoline → Coke	0.000629	66,570	690

Table 3.2: Riser simulation results of the four-lump kinetic model

Riser Height (m)	Gas oil (wt. %)	Gasoline (wt. %)	Gases (wt. %)	Coke (wt. %)	Temperature of gas phase (T_g) (K)	Temperature of catalyst phase (T_c) (K)
0.0	1.0000	0.0000	0.0000	0.0000	679.0	911.6
5.0	0.5945	0.2918	0.0572	0.0295	808.5	833.7
10.0	0.4598	0.3937	0.0846	0.0313	807.6	817.6
15.0	0.3806	0.4403	0.1034	0.0352	802.2	809.1
20.0	0.3333	0.4741	0.1158	0.0348	796.8	801.3
25.0	0.2989	0.4929	0.1240	0.0409	794.6	797.8
*30.0	0.2750	0.5075	0.1365	0.0426	791.1	793.7
**30.0	0.2835	0.5137	0.1332	0.0354	791.5	791.9
% diff.	3.00	1.21	2.48	20.34	0.05	0.23

*this row is riser exit condition obtained from the procedure in Figure 3.1, then used as experimental data

**this row riser exit condition obtained from literature (Han and Chung, 2001a, Han and Chung, 2001b)

From Table 3.2, the percentage errors are within some level of acceptability, 5% and below as described in Figure 3.1. Percentage difference for the coke lump was high (20.34%) because the value of coke was assumed zero in the feed, which is not always the case. The values of the lumps from the simulation are used as true representation of the online-discretised data along the riser height.

They are taken as experimental data input in the parameter estimation platform of the gPROMS software and used for the estimation of the four-lump kinetic parameters. The four-lump kinetic parameters estimated are compared in Tables 3.3, 3.4 and 3.5 with the existing four lumped kinetic data from the literature (Han and Chung, 2001a, Han and Chung, 2001b).

The results of the parameter estimation for the four-lump model denoted with asterisks in Tables 3.3 – 3.5, gives very close estimates as compared with similar values of kinetic data by Han and Chung (2001b) with double asterisks, giving the assurance that the process model can be used for parameter estimation. The results are presented in Tables 3.3 – 3.5.

Table 3.3: Heat of Reaction for four-lump model

Reaction	Heat of Reaction** (kJ/kmol) ΔH_i	Heat of Reaction* (kJ/kmol) ΔH_i	% Difference
Gas Oil → Gasoline	195	189	3.17
Gas Oil → Gas	670	664	0.90
Gas Oil → Coke	745	739	0.81
Gasoline → Gas	530	524	1.14
Gasoline → Coke	690	684	0.87

*Heat of reaction obtained from the procedure in Figure 3.1.

** Heat of reaction from literature (Han and Chung, 2001a, Han and Chung, 2001b)

Table 3.4: Frequency factor for four-lump model

Reaction	Frequency Factor** (k_i) (s^{-1})	Frequency Factor* (k_i) (s^{-1})	% Difference
Gas Oil → Gasoline	1457.50	1468.5	0.74
Gas Oil → Gas	127.59	134.269	4.97
Gas Oil → Coke	1.98	1.99911	0.95
Gasoline → Gas	256.81	253.315	1.38
Gasoline → Coke	0.000629	0.00052	20.96

* Frequency Factor obtained from the procedure in Figure 3.1.

** Frequency Factor from literature (Han and Chung, 2001a, Han and Chung, 2001b)

Table 3.5: Activation energy for four-lump model

Reaction	Activation Energy** (kJ/kmol) (E_i)	Activation Energy* (kJ/kmol) (E_i)	% Difference
Gas Oil → Gasoline	57,359	57,348	0.01
Gas Oil → Gas	52,754	52,765	0.02
Gas Oil → Coke	31,820	31,809	0.03
Gasoline → Gas	65,733	65,723	0.01
Gasoline → Coke	66,570	66,581	0.01

* Activation Energy obtained from the procedure in Figure 3.1.

** Activation Energy from literature (Han and Chung, 2001a, Han and Chung, 2001b)

The differences are 3% and less, except for the percentage differences between the frequency factors of the reaction of gas oil to gas, which is 4.97% and gasoline cracking into coke, which has a difference of about 20.96% as shown in Table 3.4. Although this difference appeared to be very large, it may not be very significant. This is because the frequency factor itself is very small, and even though the activation energy and heat of reaction for the reaction may be large, the frequency factor multiplies the exponential term in the Arrhenius equation, which makes the yield of coke very small. It was also found that even when the heat of reaction was assumed to be 1000 kJ/kmol, the yield of coke is still small because of the value of the frequency factor. Another reason for the high frequency factor could be because gasoline undergo secondary reaction, being favoured by increased heat of reaction of 0.87% in Table 3.3, and being a lighter component, the rate of collision of its molecules in the reacting space to form coke increased.

Using the new kinetic parameters estimated for the riser simulation with four-lumped model, the riser exit conditions are shown in Table 3.6.

Table 3.6: Riser exit results of the four-lump kinetic model using the new estimated parameters

Riser Height (m)	Gas oil (wt. %)	Gasoline (wt. %)	Gases (wt. %)	Coke (wt. %)	Temp. (T_g) (K)	Temp. (T_c) (K)
*30	0.2835	0.5137	0.1332	0.0354	791.5	791.9
**30	0.2803	0.5134	0.1366	0.0354	791.7	792.1
% diff.	1.14	0.06	2.49	0.0000	0.03	0.03

*riser exit conditions for the Han and Chung (2001b) kinetics

**riser exit conditions using the new estimated kinetic parameters for the four lumps

The percentage errors in Table 3.6 are all less than 3%, an acceptable level of marginal error. This low percentage differences in Tables 3.3, 3.4, 3.5 and 3.6

shows that the technique used for the parameter estimation as described in Figure 3.1, is capable of estimating process parameters with very high accuracy. Since the difference of mostly about 3% and less is seen between the estimated parameters and the literature parameters. This confirms the adequacy of the riser model, the parameter estimation technique proposed in Figure 3.1 and the new kinetic data for parameter estimation. As can be seen, the ability of the technique in predicting the exiting kinetic parameters is good. Hence, the parameter estimation technique is used to estimate the kinetic parameters of the new six-lumped kinetic model proposed in this work.

3.5 Optimisation using gPROMS

gPROMS software was used to maximise yield using models of the riser which is a set of nonlinear functions subjected to general nonlinear constraints (Equality and Inequality constraints) of upper and lower limits of operation. Solution of this optimisation functions is carried out by manipulating a set of optimisation decision variables that may be either continuous or discrete. This in turn provides a prediction of the appropriate operating conditions precisely that are proportionate with the objective function. There are several methods used to solve different optimisation problems. This research presents only the Nonlinear Programming problems (NLP), solved using specific methods as described in the next section.

3.5.1 NLP solution technique

The NLP problems are solved using different approaches such as Global Optimisation Problem (GOP) (Marcovecchio et al. 2005), Successive Linear Programming (SLP) method and Sequential Quadratic Programming (SQP) method (Villafafila and Mujtaba 2003). The Mixed Integer Nonlinear Programming (MINLP) (Lu et al. 2006), Genetic Algorithm (GA) method (Murthy and Vengal 2006) and Multi-Objective Optimisation and Genetic Algorithm (MOO+GA) (Guria et al. 2005). For the models developed in this research, the optimisation problem is solved as a Non-Linear Programming (NLP) problem and is solved using the Successive Quadratic Programming (SQP) method.

3.5.2 Successive quadratic programming (SQP) technique

The SQP is incorporated in the gPROMS software suites to function by default. It uses first-order Taylor's series approximation around as initial point specified in

the process to solve optimisation problems. It converts the nonlinear functions into approximate linear functions, which means that the process converges around the equality constraints and specified the inequality constraints. Secondly, the optimisation step reinitializes by updating the values of decision variables. Precise re-initialization of the decision variables locates a new search direction for the decision variables, which is attained using the solution of the last successful iteration (Edgar et al. 2001). The new values of the decision variables will be the initial point (guestimate values) for further linearization to solve the linear problem. The solution goes on until the problem is linearized with specific improvement of the objective function. One of the typical solvers in gPROMS software for optimisation problems is CVP_SS, which works with the DASOLV code. This solver is able to solve steady state and dynamic optimisation problems with both discrete and continuous optimisation decision variables (mixed integer optimisation).

3.6 Summary

This chapter presents the models of the different sections of the FCC unit.

- A new kinetic model of six-lump model was developed and presented, along with a new parameter estimation technique.
- The new parameter estimation technique was used to obtain new kinetic data for the proposed six lump kinetic scheme. The results obtained were accurate representation of the literature and plant data obtained.
- Explanation of optimisation technique for the determination of maximum and minimum values of yields of product was included in this chapter.

Chapter 4

Parameter Estimation of Riser Reaction Kinetics

4.1 Introduction: Kinetic modelling and model parameters for six lumps

The FCC is an important unit that has captured the interest of many authors. Nevertheless, not many achievements have been made when it comes to the precise understanding of the riser unit behaviour. This could be due to the complexity of the riser's feed, which is a complex mixture of extremely large number of unknown compounds. In addition, there is the complex hydrodynamics of the riser owing to the three phases (solid, liquid and gas) nature along with gas-phase volume expansion due to vaporisation and cracking reaction (Kumar and Reddy 2011).

The challenge with the cracking reaction is its characterization. Most research efforts to model cracking kinetics consider components with similar characteristics as a single lump and each lump is considered unique. There are three kinds of such lumping strategy. The first is the parametric strategy that considers a lump, being the feed, which cracks into some lumps such as gasoline, gas and coke as products of cracking reactions (Jacob et al. 1976; Theologos and Markatos 1993). The second type of lumping strategy is pseudo-cracking where the feedstock and products are considered to be a mixture of some hypothetical or pseudo components (Bollas et al. 2004; Gupta et al. 2007) giving rise to many lumps. The third is the structure-oriented lumping, which offers a basis for molecular based modelling of all refinery processes. It creates reaction networks of varying sizes and complexity and treats hydrocarbon molecules as structures that builds continually (Quann and Jaffe 1992). Although each strategy has its advantage and disadvantage, the first lumping strategy has gained acceptability in the characterization of reactants and products from the cracking reactions in the FCC unit, with different number of lumps used by different researchers.

The 3-lump kinetic model (Weekman 1968b) was the first to be presented, where gas oil was cracked into two other lumps; gasoline and gases plus coke. Coke is useful when burnt in the regenerator to provide the heat required for the cracking reactions in the riser. Hence, the 3-lump model was further broken to form the 4-

lump model (Lee et al. 1989a), which includes gas oil, gasoline, gases and coke. Further increment of lumps were added to acquire more detail and to achieve a higher level of accuracy in the lumping strategy. This led to the development of several lumps and although the number of lumps may be the same, the nature of lumps may be different. For instance, the six-lump model of Souza et al. (2011) is different from the six-lump model of Mu et al. (2005). The increase in number of lumps continued to the 5-lump model (Ancheyta et al. 1999; Dupain et al. 2003a); the 6-Lump model (Takatsuka et al. 1987; Du et al. 2014; Xiong et al. 2015; Zhang et al. 2017); 7-lump model (Xu et al. 2006; Heydari et al. 2010b); 8-lump model (Hagelberg et al. 2002; Gao et al. 2014); 9-lump model (You et al. 2006; You 2013); 10-lump model (Jacob et al. 1976); 11 lump model (Mao et al. 1985; Sa et al. 1985; Zhu et al. 1985) and so on. In this work, new kinetic parameters are developed for a new six-lump model.

4.1.1 Six-lumps kinetic parameters

In the FCC unit, the heat balance is controlled by hydrodynamics of the process, which depends on the endothermic heats of the cracking reactions (Arbel et al., 1995) and needs to be sufficiently accounted for. During regeneration, heat produced compensates the heat necessary for the endothermic cracking reactions, resulting in the FCC unit operating under conditions of thermal balance (Arandes et al. 2000). The heat from the feed, the vaporisation steam, regenerated catalyst, and the endothermic reactions in the riser influences these conditions of thermal balance. Most of the heat components are measurable with little difficulty compared to the heat produced or consumed during the endothermic reactions. To account for the endothermic heat of reactions, it is necessary to measure the enthalpy of reaction in the riser, which is important for the effective control, and stability of the FCC unit.

Most of the riser models of the FCC unit found in the literature do not use equations that account for the endothermic heat of reaction in the riser. At best, the temperature profile of the gas phase is presented. A real industrial plant located in Sudan is simulated in this work. It has five products and a feed, making it a six lumped kinetic model; they are gas oil, diesel, gasoline, liquefied natural gas (LPG), dry gas and coke. To simulate this industrial FCC unit, a six lumped kinetic model that adequately represents its product distribution is required.

However, this six-lumped kinetic model is unique and not readily used in the literature. Where this six-lumped kinetic model was used (Du et al. 2014; Xiong et al. 2015; Zhang et al. 2017), the riser model did not account for the heat of reaction, which is the endothermic heat required for the cracking of the feed. This heat of reaction is important and a requirement for the riser model used in this work (Han and Chung 2001a; Han and Chung 2001b). This six-lumped kinetic model (Du et al. 2014; Xiong et al. 2015; Zhang et al. 2017) have their frequency factors and activation energies presented in the literature. Nevertheless, they did not provide their enthalpies; hence, the data they used cannot be used to account for the endothermic heat of reaction.

4.1.2 Six-lump model

Different six-lump models have been used in the modelling of the FCC unit kinetic reactions and all have their unique characteristics. A six-lump kinetic model (Baldessar and Negrão 2005; Souza et al. 2011) was used that cracks gasoil into gasoline, LPG, fuel gas, light cycle oil (LCO) and coke lumps. Mu et al. (2005) presented a different six-lump model; it cracks residual fuel oil (RFO) into heavy fuel oil (HFO), light fuel oil (LFO), gasoline, gas and coke. Besides the fact that their product distributions are different, their respective frequency factors and activation energies are also different and were presented (Mu et al., 2005) without the heat of reaction for each cracking reaction. Hence, these kinetic models may not be suitable for use with the comprehensive model (Han and Chung 2001a; Han and Chung 2001b) of FCC unit used in this study.

Another six-lump model, which is similar and has presented the same lumps as the one developed in this work was presented in the literature (Du et al. 2014; Xiong et al. 2015; Zhang et al. 2017). The difference being the secondary cracking reactions of LPG and dry gas into coke. This difference is significant because many authors assume that the cracking reactions of some lumps into other lumps can be neglected to reduce the total number of kinetic parameters to be accounted for. However, with a powerful tool that performs accurate parameter estimation, all parameters can be estimated, and the data can then be subjected to the decision of whether to neglect some reactions or not. Therefore, the new kinetic model accounts for kinetic data for the secondary cracking reactions of LPG and dry gas into coke. Again, only kinetic data such as the frequency factors

and activation energies are presented (Du et al. 2014; Xiong et al. 2015; Zhang et al. 2017) without the heat of reactions of the kinetic equations involved, which are required by the riser model used in this study.

The six-lump kinetic model developed in this work represents a real industrial product distribution. It cracks gas oil into diesel, gasoline, LPG, dry gas and coke. It estimates the heats of reactions involved in the six-lump cracking reactions and presents kinetic data (frequency factors, activation energies and heats of reaction) for the secondary reactions of the conversion of LPG and dry gas into coke. Figure 4.1 shows a schematic diagram of the kinetic model presented by some authors (Du et al. 2014; Xiong et al. 2015; Zhang et al. 2017), even though Xiong et al. (2015) did not present the secondary cracking of LPG to dry gas. Figure 4.2 shows the proposed kinetic model to be used in this work. As stated earlier, the difference between Figures 4.1 and 4.2 is the secondary cracking reactions of LPG and dry gas into coke.

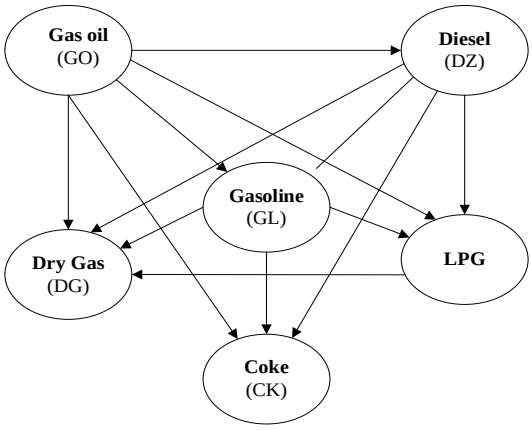

Figure 4.1: Six-lump kinetic model (Du et al. 2014; Xiong et al. 2015; Zhang et al. 2017)

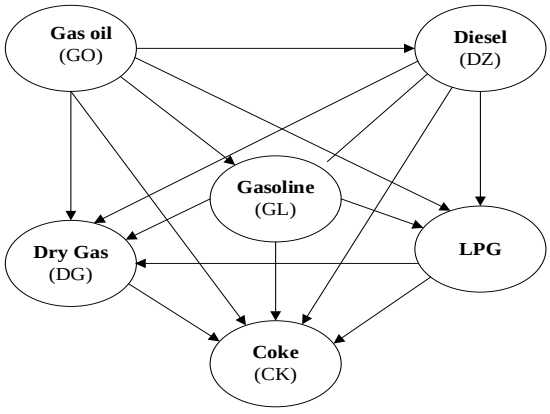

Figure 4.2: Six-lump kinetic model as proposed in this work

In this work, the endothermic heat of reaction will be calculated using a similar but new six lump kinetic reaction scheme, which incorporates the new enthalpies of reaction, frequency factors and activation energies obtained through parameter estimation technique described in Figure 3.1 and implemented using the gPROMS software. These new estimated parameters will make it possible for the simulation of the FCC unit in Sudan using the new kinetic scheme model and the robust riser model of Han and Chung (2001a) and Han and Chung (2001b), which accounts for the endothermic heat of reaction.

4.1.3 Riser simulation with new six-lump kinetic model

Some model equations along with some of their parameters used in this simulation study were adopted from literature (Han and Chung 2001a; Han and Chung 2001b). The feed conditions and other parameters were obtained from an industrial refinery from Sudan and are shown in Appendix Table A.8. Material balance equations for the various lumps showing the six-lump; gas oil, diesel, gasoline, LPG, dry gas and coke are represented by Equations (3.17 – 3.22). The overall rates of reaction for the six lumps: gas oil $\mathrm{R_{go}}$, diesel $\mathrm{R_{gdz}}$, gasoline $\mathrm{R_{gl}}$, LPG $\mathrm{R_{lpg}}$, dry gas $\mathrm{R_{dg}}$, and coke $\mathrm{R_{ck}}$, were developed from the six-lump kinetic reaction scheme and are presented in Equations (3.23 -3.28). These equations are new six lumped model equations since they include the secondary reactions of the cracking of LPG and dry gas to coke which were not in the literature. Each overall rate of reaction is a function of an overall rate constant that is described by the Arrhenius equation given in Equations (3.29 – 3.44), which include the new overall rate constants of the secondary reactions of the cracking of LPG and dry gas to coke. During the catalytic cracking, endothermic heat from the regenerator is utilized in the riser, and the rate of heat removal by reaction, $\mathrm{Q_{react}}$, is estimated by Equation 3.44, a unique feature of the current riser model used in this study. For the six-lump kinetic model proposed in this work, the following are the parameters to be estimated:

$$\begin{bmatrix} \mathrm{k_{dz-gl}}, \mathrm{k_{dz-lpg}}, \mathrm{k_{dz-dg}}, \mathrm{k_{gl-lpg}}, \mathrm{k_{gl-dg}}, \mathrm{k_{gl-ck}}, \mathrm{k_{lpg-dg}}, \mathrm{k_{lpg-ck}}, \mathrm{k_{dg-ck}}, \mathrm{k_{go-dz}}, \\ \mathrm{k_{go-gl}}, \mathrm{k_{go-ck}}, \mathrm{k_{go-lpg}}, \mathrm{k_{go-dg}}, \mathrm{k_{dz-ck}} \end{bmatrix},$$

$$\begin{bmatrix} \mathrm{E_{dz-gl}}, \mathrm{E_{dz-lpg}}, \mathrm{E_{dz-dg}}, \mathrm{E_{gl-lpg}}, \mathrm{E_{gl-dg}}, \mathrm{E_{gl-ck}}, \mathrm{E_{lpg-dg}}, \mathrm{E_{lpg-ck}}, \mathrm{K_{dg-ck}}, \mathrm{K_{go-dz}}, \\ E_{\mathrm{go-gl}}, \mathrm{E_{go-ck}}, \mathrm{E_{go-lpg}}, \mathrm{E_{go-dg}}, E_{\mathrm{dz-ck}} \end{bmatrix} \quad \text{and}$$

$$\begin{bmatrix} \Delta H_{\mathrm{dz-gl}}, \Delta H_{\mathrm{dz-lpg}}, \Delta H_{\mathrm{dz-dg}}, \Delta H_{\mathrm{gl-lpg}}, \Delta H_{\mathrm{gl-dg}}, \Delta H_{\mathrm{gl-ck}}, \Delta H_{\mathrm{lpg-dg}}, \Delta H_{\mathrm{lpg-ck}}, \Delta H_{\mathrm{dg-ck}}, \\ \Delta H_{\mathrm{go-dz}}, \Delta H_{\mathrm{go-gl}}, \Delta H_{\mathrm{go-ck}}, \Delta H_{\mathrm{go-lpg}}, \Delta H_{\mathrm{go-dg}}, \Delta H_{\mathrm{dz-ck}} \end{bmatrix}$$

Hence, in this work, the FCC unit simulation model of (Han and Chung 2001a; Han and Chung 2001b) is used coupled with gPROMS software for parameter estimation to estimate activation energies, frequency factors and enthalpies of a new riser cracking reactions scheme of an industrial FCC plant located in Sudan. This new and comprehensive kinetic model and parameters of the reaction scheme of the industrial plant in Sudan can be used to simulate other FCC units with similar product distribution. It is necessary to obtain the accurate kinetic parameters of the refinery in Sudan using the already validated riser model of Han and Chung (2001a) and Han and Chung (2001b). This result can further be validated with plant data from the Sudan refinery.

Figure 3.1 shows a schematic diagram of the parameter estimation technique used in this work. It describes how input and output data from the plant were used in model simulation to generate online data across the discretised height of the riser which were used to represent experimental data in the gPROMS software for parameter estimation.

The feed condition is assumed to be 100% gas oil and the riser inlet temperatures of the feed (522.9 K) and the catalyst (904.7 K) from the regenerator. Gas oil input flow rate is 62.5 kg/s and that of the catalyst is 400.32 kg/s, which is a catalyst to oil ratio of 6.41. Parameter estimation in gPROMS require industrial data of the yields of all lumps of the riser, which are used as experiments to estimate the unknown parameters. The available industrial data are the yields of the lumps at the exit of the riser, which are used as experimental data on the parameter estimation platform of gPROMS. The kinetic data in Table 2 are used with the riser model along with the only available industrial riser outputs, which are gas oil; 0.0478, diesel; 0.1857, gasoline; 0.4731, LPG; 0.1518, dry gas; 0.0483 and coke; 0.0891. The FCC process model is then simulated in gPROMS software to generate yields at discreet points of the riser height, which gives more data that are then used on the parameter estimation platform of gPROMS. The newly estimated kinetic parameters are taken back into the riser model to obtain yields that are compared with the ones obtained from the industrial plant as described in Figure 3.1.

The overall rate and Arrhenius equations written for the six-lumped model (Equations 3.23 - 3.44) were used with the riser hydrodynamic equations. The kinetic parameters; frequency factors, activation energies and heat of reactions

were estimated using guessed values between minimum and maximum of the respective kinetic parameter values in Table 4.1. In addition, the guess values of the kinetic data used for the cracking of LPG to dry gas and coke and dry gas to coke on the parameter estimation platform were assumed to be between the minimum and maximum of the kinetic data presented in Table 4.1. Similarly, simulated results were generated for the six-lump model using the kinetic and hydrodynamic equations following the same parameter estimation technique described in Figure 3.1. These exit compositions of the simulated riser are then used as experimental data on the parameter estimation platform of the gPROMS software. The values shown in Table 4.2 were generated using the real plant configurations and industrial riser input and output conditions (Table A.8) on the PROMS riser simulation.

Table 4.1: Kinetic parameters of six-lumped model in the literature

Reaction	(Du et al., 2014)		(Xiong et al., 2015)		(Zhang et al., 2017)	
	Frequency Factor (k_{oi})*(s^{-1})	Activation Energy (kJ/kmol) (E_i)	Frequency Factor (k_{oi})* (m^3 kg^{-1} hr^{-1})	Activation Energy (E_i) (kJ/mol)	Frequency Factor (k_{oi})*(s^{-1})	Activation Energy (kJ/kmol) (E_i)
Gas Oil → Diesel	601.7	59.33	31328.5	47.6	6.012×10^4	65.14
Gas Oil → Gasoline	$2.19x10^5$	95.00	52064.7	43.4	2.190×10^5	90.93
Gas Oil → Coke	28.91	177.2	574.4	30.0	0.485×10^3	45.10
Gas Oil → LPG	16.96	38.05	6560.4	38.5	9.053×10^6	70.53
Gas Oil → Dry Gas	1869	176.44	175.6	30.2	1.870×10^3	69.34
Diesel → Coke	$2.7x10^4$	174.4	46291.9	65.0	6.760×10^3	61.40
Diesel → Gasoline	240.46	57.5	14683.7	54.1	2.400×10^3	49.20
Diesel → LPG	46.08	141.95	40140.4	62.9	4.680×10^3	68.65
Diesel → Dry Gas	1560	81.78	18604.8	66.7	1.560×10^4	63.23
Gasoline → LPG	40.39	74.22	494068.4	80.5	4.039×10^4	50.90
Gasoline → Dry Gas	1.6	135.34	245194.8	85.2	9.420×10^3	36.81
Gasoline → Coke	1.22	44.26	241931.9	77.3	0.515×10^3	37.23
LPG → Dry Gas	78.98	89.27	*	*	1.081×10^4	65.80
LPG → Coke*						
Dry Gas → Coke*						

*reactions not available in the authors kinetic schemes

This technique for parameter estimation provides a way to develop new kinetic schemes with just plant data. Once a plant inlet and outlet values (yields and process conditions) are known, along with a robust process model, which describes the process adequately, experimental results can be generated from the process model and be used for parameter estimation. This is a major novel contribution of this work. Another contribution is the development of a new kinetic scheme. Comparing Figures 4.1 and 4.2, the cracking reactions of dry gas to coke, and LPG to coke were added to Figure 4.1 to obtain a new six-lumped kinetic scheme shown in Figure 4.2. Most authors assumed that those reactions added were usually negligible, because it is usually difficult to measure them. With parameter estimation, it can be seen that they do indeed exits in the riser. This technique proved to be useful because the parameters estimated were used in the process model to predict the plants data with minimal percentage of errors as shown in Figures 4.3, 4.4, 4.5, and 4.6. This technique is applicable to both laboratory and plant size processes which is an advantage.

4.1.4 Results and discussions on kinetics of six lumps

The industrial riser simulation results and the estimated kinetic parameters are presented in this section with the view to demonstrate the accuracy of the technique used in the simulation of the plant where real data was obtained. The simulation also demonstrates the capability of the gPROMS software which is used here for solving the FCC riser complex nonlinear DAEs by validating the results against those of the plant. The estimated parameters for six-lump kinetics are also presented.

Table 4.2 shows riser simulation results along the riser height for the six lumps and temperature profiles. These results were used as experimental data on the gPROMS parameter estimation platform to perform parameter estimation.

Table 4.2: Riser simulation results of the six-lump kinetic model

Riser Height (m)	Gas oil (wt. %)	Diesel (wt. %)	Gasoline (wt. %)	LPG (wt. %)	Dry gas (wt. %)	Coke (wt. %)	Temp. (Tg) (K)	Temp. (Tc) (K)
**0.0	1.0000	0.0000	0.0000	0.0000	0.0000	0.0000	523.0	904.7
5.0	0.3479	0.2185	0.2312	0.1073	0.0339	0.0612	706.0	775.5
10.0	0.1537	0.2652	0.3245	0.1385	0.0434	0.0748	734.5	748.2
15.0	0.0971	0.2613	0.3686	0.1476	0.0462	0.0792	738.4	742.2
20.0	0.0724	0.2487	0.3982	0.1516	0.0475	0.0817	738.3	740.2
25.0	0.0587	0.2349	0.4210	0.1538	0.0482	0.0834	737.7	739.1
30.0	0.0499	0.2217	0.4398	0.1552	0.0487	0.0847	737.0	738.2
35.0	0.0438	0.2095	0.4556	0.1562	0.0491	0.0857	736.5	737.5
40.0	0.0393	0.1983	0.4694	0.1570	0.0494	0.0866	736.0	736.9
45.0	0.0358	0.1881	0.4815	0.1576	0.0496	0.0873	735.5	736.4
47.0	0.0346	0.1843	0.4860	0.1578	0.0497	0.0876	735.3	736.2
47.1	0.0346	0.1841	0.4862	0.1578	0.0497	0.0709	735.3	736.2
**47.1	0.0478	0.1857	0.4731	0.1518	0.0483	0.0891	773.2	NA
% error	38.24	0.86	2.69	3.81	2.80	1.70	5.15	

**values in this row are riser conditions from the industrial plant

Table 4.3: Kinetic parameters of six-lump model estimated

Reaction	**Frequency Factor (k_i) (s^{-1})**	**Activation Energy (kJ/kmol) (E_i)**	**Heat of Reaction (kJ/kmol) ΔH_i**
Gas Oil → Diesel	7957.29	53,927.7	190.709
Gas Oil → Gasoline	14,433.4	57,186.6	128.45
Gas Oil → Coke	40.253	32,433.6	458.345
Gas Oil → LPG	2337.1	51,308.6	209.192
Gas Oil → Dry Gas	449.917	48,620.4	44.543
Diesel → Coke	75.282	61,159.4	305.925
Diesel → Gasoline	197.933	48,114.5	513.568
Diesel → LPG	3.506	67,792.9	90.894
Diesel → Dry Gas	3.395	64,266.6	204.381
Gasoline → LPG	2.189	56,194.4	225.082
Gasoline → Dry Gas	1.658	63,319.1	19.667
Gasoline → Coke	2.031	61,785.1	117.212
LPG → Dry Gas	3.411	55,513.0	17.618
LPG → Coke	0.601	52,548.2	11.839
Dry Gas → Coke	2.196	53,046.0	52.863

Table 4.3 shows the new six-lump estimated parameters. Being the first of such six-lumped kinetic model that considered the cracking of LPG and dry gas to coke, as well as the cracking of dry gas to coke. In Table 4.3, the frequency factors, activation energies and heats of reaction of the cracking reactions of LPG to dry gas and coke, and dry gas to coke, for the six-lumped kinetic model are presented. These data were not available in the open literature, which is a contribution of this work. Overall, this new six-lumped kinetic data presented in this work is validated by simulating with the riser process model and exit values were compared with the exit conditions of industrial riser.

The process model was run on the gPROMS simulation platform using the new six-lump kinetic parameters with the new kinetic scheme shown in Figure 4.2. At C/O ratio of 6.405, the feed (gas oil at 62.5 kg/s) meets the regenerated catalyst (400.32 kg/s) at the feed vaporisation section of the riser unit and cracks to produce lumps; diesel, gasoline, LPG, dry gas and coke. The cracking reaction starts at gas oil inlet temperature of 523.0 K and catalyst inlet temperature of 904 K. The profiles of the products are shown in Figures 4.3 and 4.4.

The amount of the gas oil at the exit of the riser is 0.0346 (kg lump/kg feed) which is 3.46% of gas oil left unreacted. It also means that, about 96.54% of gas oil reacted and above 80% of the reacted fraction was consumed in the first 12 m of the riser. In some risers, most of the conversion takes place in the first 10 m. This may not be the same for some short risers. Some of the risers are 30 m high and others are less (Han and Chung 2001b). The riser considered here is 47.1 m high. The amount of diesel at the exit of the riser is 0.1842 (kg lump/kg feed) which is 18.42% of total products formed. The product gasoline formed is 0.4863 (kg lump/kg feed), that is 48.63% of total products formed. Other products formed are LPG; 0.1577 (kg lump/kg feed) which is 15.77% of products formed, dry gas; 0.0497 (kg lump/kg feed) which is 4.97% of total products formed, and coke; 0.0876 (kg lump/kg feed), 8.76% of total product formed in the riser. These outputs from the riser are compared with the riser plant data in Table 4.3. The diesel and gasoline profiles increase from 0 (kg lump/kg feed) at the inlet of the riser to its maximum yield of 0.4863 (kg lump/kg feed) at the riser exit for gasoline and a maximum of 0.2660 (kg lump/kg feed) for diesel in the first 11 m. However, the mass fraction of diesel increases initially and then decreases gradually to 0.1858 (kg lump/kg feed) at the end of the riser. This fraction of diesel decreases after 11 m due to a secondary reaction, which is common for intermediates in a

series – parallel reactions. The endothermic heat was enough to convert the diesel into gasoline and other intermediates. The other products of the riser; LPG, dry gas and coke all started from zero weight fraction as well and rose to their maximum at approximately 11 m height, but essentially levels out at the exit of the riser. The profiles of the lumps in the riser qualitatively compare favourably with the profiles of riser products in the literature (Han and Chung 2001b; Du et al. 2014).

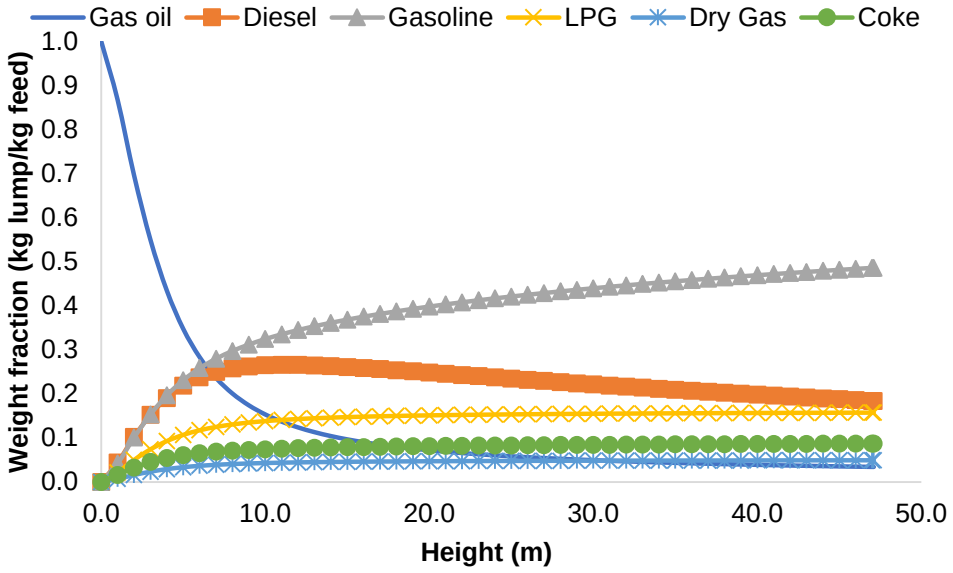

Figure 4.3: Profile of gas oil cracking in the riser

Figure 4.4 shows the temperature profiles of the gas and catalyst phases as a function of riser height. The temperature of the catalyst-phase starts from about 933 K in the feed vaporisation section, decreases for the first 11 m from 904.7 K at the entrance of the riser and then essentially levels out to 736.2 K at the riser exit.

The temperature profile of the gas phase starts from 478.15 K, which is also the temperature of the gas oil coming into the vaporisation section. This temperature was quickly raised by the incoming hot regenerated catalyst to about 522.9 K as can be seen at the riser inlet in Figure 4.4. This gas phase temperature rises from 522.9 K to a peak 738.5 K in the first 17 m of the riser and levels out in the remaining portion of the riser. The difference in both temperature profiles represents the endothermic reaction in the riser with a temperature difference of 382.2 ^{o}C at the riser inlet to 0.95 ^{o}C at the exit. This difference aid the completion of the cracking reaction and represents the heat of removal shown in Figure 4.7, which is accounted for in this work with the help of the estimated heat of reactions

obtained and shown in Table 4.3. The temperature profiles obtained in this work are qualitatively like those obtained in many literatures (Han and Chung 2001b; Du et al. 2014).

To determine the accuracy and validate the capability of this gPROMS model, refinery operational data are used to compare with the results of this simulation work. The results are shown in Table 4.3.

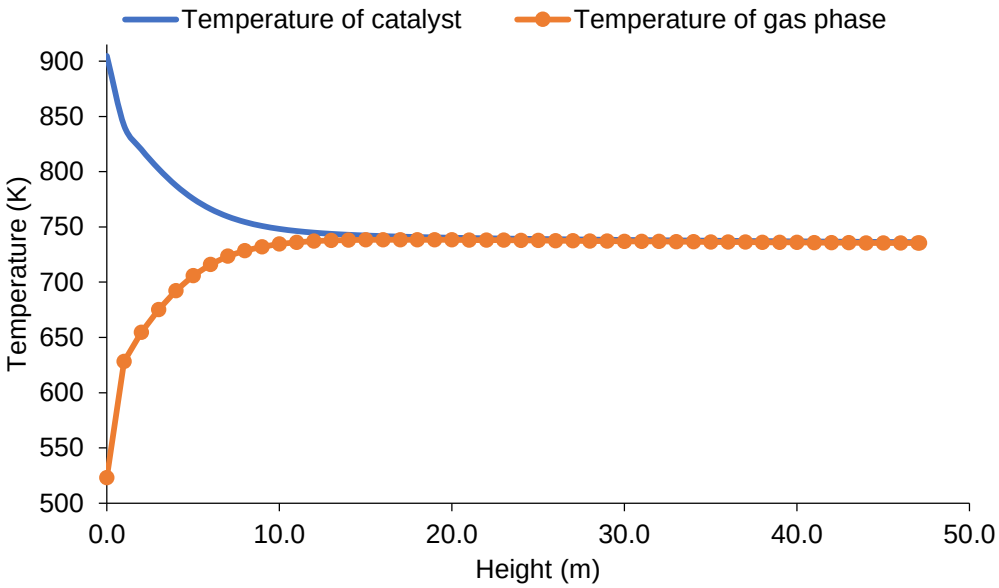

Figure 4.4: Temperature profiles across the riser

Table 4.4: Riser simulation results compared with plant data

Parameter	Input	Riser output	Plant data	% difference
Gas oil Temperature (K)	478.15	735.3	773.2	5.15
Catalyst Temperature (K)	905	736.2		
Gas oil Mass flowrate (kg/s)	62.5	62.5	62.5	
Catalyst Mass flowrate (kg/s)	400.32	400.32	400.32	
Mass fraction of Gas oil (wt. %)	1.0	0.0346	0.0478	38.15
Mass fraction of Diesel (wt. %)	0.0	0.1842	0.1857	0.81
Mass fraction of Gasoline (wt. %)	0.0	0.4863	0.4731	2.71
Mass fraction of LPG (wt. %)	0.0	0.1577	0.1518	3.74
Mass fraction of Dry gas (wt. %)	0.0	0.0497	0.0483	2.28
Mass fraction of Coke (wt. %)	0.0	0.0876	0.0891	1.71

The temperature of the catalyst is 905 K at the inlet of the riser and gradually decreased to 736.2 K at the riser exit due to the endothermic cracking reactions. The decrease in the catalyst temperature increases the temperature of the gas phase from 478.2 K at the riser inlet to 735.3 K at the exit. For the gas phase

temperature at the riser exit, there is a 5.15% difference between the riser exit temperature in this simulation of 735.30 K and that of the plant (773.20 K). The 5.15% difference can be acceptable considering that the yield of products is not only dependent on reaction temperature but also on the hydrodynamics of the riser, C/O ratio, catalyst type, nature of feed and many other operational variables. This temperature difference between plant data and the simulation result is evident in the increased conversion found in this simulation, showing that more heat of the endothermic reaction was utilized. The feed conversion in this work is higher than that obtained in the plant, with a 38.15% increase on the fraction of feed converted. This increase is far above the 3% difference required for the estimated parameter to be accepted. However, most of the values of the six-lump are less than 3% and so the results are acceptable. The most valuable products are the diesel and gasoline and the parameter estimated was able to predict the plant values with about an average of over 98% accuracy. The percentage difference compared with the plant data for the diesel is 0.81% and for gasoline it is 2.71%. The percentage difference between the value for the lighter products LPG and dry gas are 3.74% and 2.28% respectively, which are also acceptable values within margin of difference. The major products are diesel and gasoline and are within acceptable margins of error. Although the difference between the predicted values and plant data for gas oil value at the exit of the riser is large, it can be corrected by optimizing the C/O ratio and other operational variables of the unit. The percentage differences in Table 4.3 shows that the estimated kinetic parameters are accurate and can be used for the simulation of the riser of FCC unit.

Figure 4.5 shows the velocity profiles of the gas and catalyst phase along the riser height. The velocity profile of catalyst rose from 18.8 m/s at the entrance of the riser to 44.94 m/s at the exit. The velocity profile of the gas phase rose sharply from 8.79 m/s to 21.25 m/s in the first 1 m of the riser and increased to 44.81 m/s at the exit of the riser. This gives a slip velocity of 10.01 m/s at the entrance and 0.13 m/s at the exit, giving an average slip velocity of 0.29 m/s across the riser. The slip velocity is very close to 0.25 m/s presented in the literature (Han and Chung 2001b).

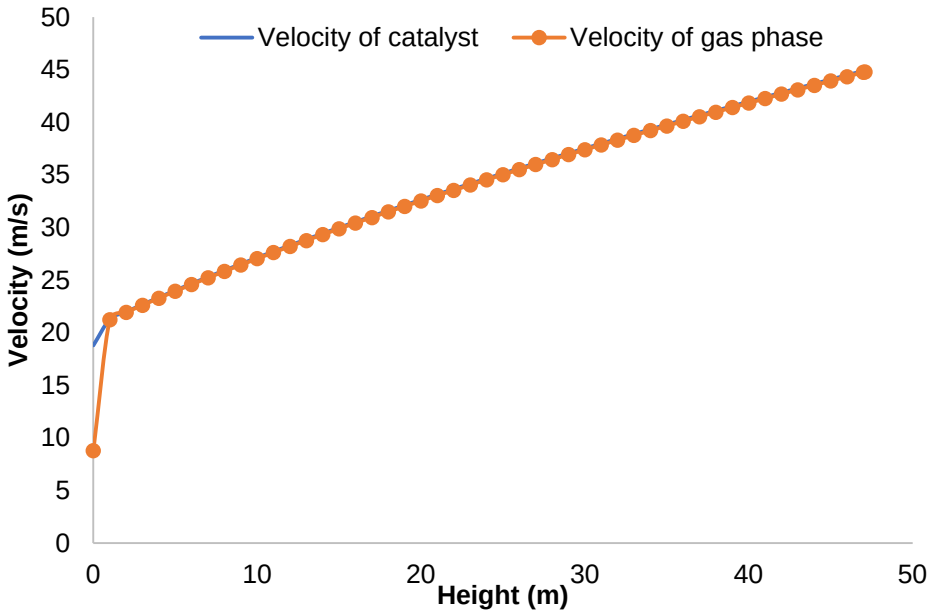

Figure 4.5: Velocity profiles across the riser

Figure 4.6 shows that the profile of pressure in the riser decreases from 340.5 kPa at the entrance to 296.1 kPa at the exit. The pressure drop is thus 44.9 kPa and could be as high as 163 kPa in industrial risers (Chang et al. 2012). Although the model simulation predicts the pressure drop, it is only limited to the riser and the effect of the regenerator pressure was not considered which could be a reason for the variation of pressure drop in this study compared with other predicted pressure drops (Han and Chung 2001b; Chang et al. 2012).

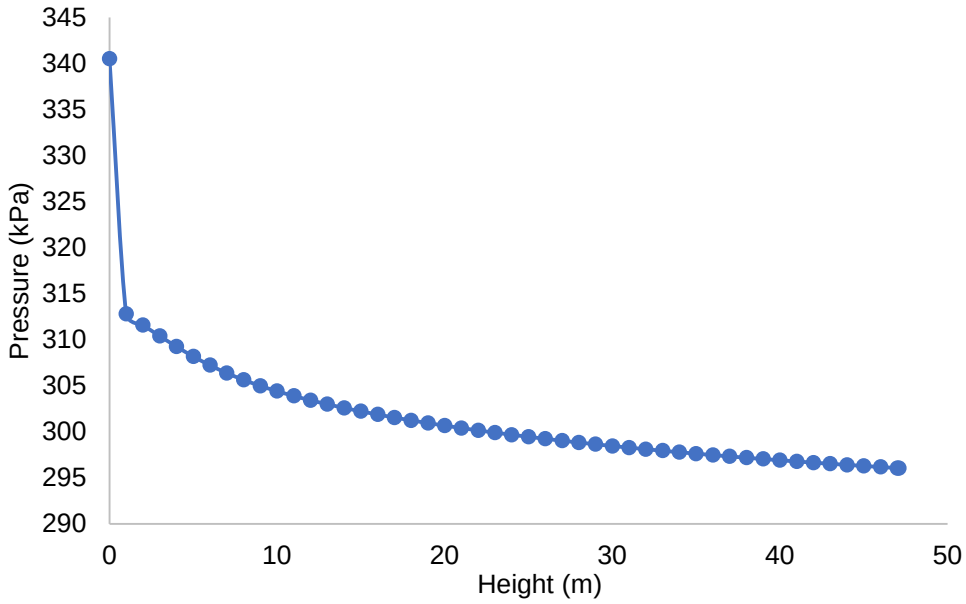

Figure 4.6: Pressure profile along the riser

Another reason could be that, since the pressure of the riser in the plant is measured at the end of the disengaging section, which is not captured in this simulation, greater pressure drop is expected to be recorded in the plant. In addition, product streams are often used for quenching of the cracking reactions at the riser end, which affects the pressure in the disengaging section. Though, the pressure drop is quantitatively different from the pressure drop of the plant (30 kPa), the profile is qualitatively similar to the ones in the literature (Han and Chung 2001b).

The heat released with the catalyst from the regenerator reimburses the heat requirements for the endothermic cracking reactions in the riser, which overall causes the unit to operate under conditions of thermal balance. The heat coming with the regenerated catalyst is useful for heating and evaporating the feed; gas oil, as it moves pneumatically upward into the riser. This process brings about heat removal due to the endothermic heats of the cracking reactions (Arbel et al. 1995) which strongly affects the overall heat balance in the FCC unit. This heat removal is measured as a function of the enthalpies of the various cracking lumps. It is possible to measure the heat removal as shown in Figure 4.7 from the estimated heats of reactions in Table 4.3.

At the entrance of the riser a substantial amount of heat is removed because of the fast cracking reaction and vaporisation. In addition, most of the products are formed in the first few meters of the riser. After about 10 m of the riser, heat removal is almost constant for the remaining parts of the riser.

The simulation was carried out at C/O ratio of 6.405, which means the gas oil mass flowrate at 62.5 kg/s and the regenerated catalyst mass flowrate at 400.32 kg/s. The C/O ratio was changed from 6.405 to 5.405 and compared with the plant data, even though the plant data was only obtained at C/O ratio of 6.405. In the absence of the plant data at the varied C/O ratio of 5.405, its outputs are compared with the plant data at 6.405. The results are shown in Table 4.5.

In varying the C/O ratios, only the mass flowrate of the gas oil was varied while the mass flowrate of catalyst was kept constant. This is because mass flowrate of gas oil can be directly manipulated unlike the mass flow rate of catalyst, which depends on many other variables including fresh catalyst addition.

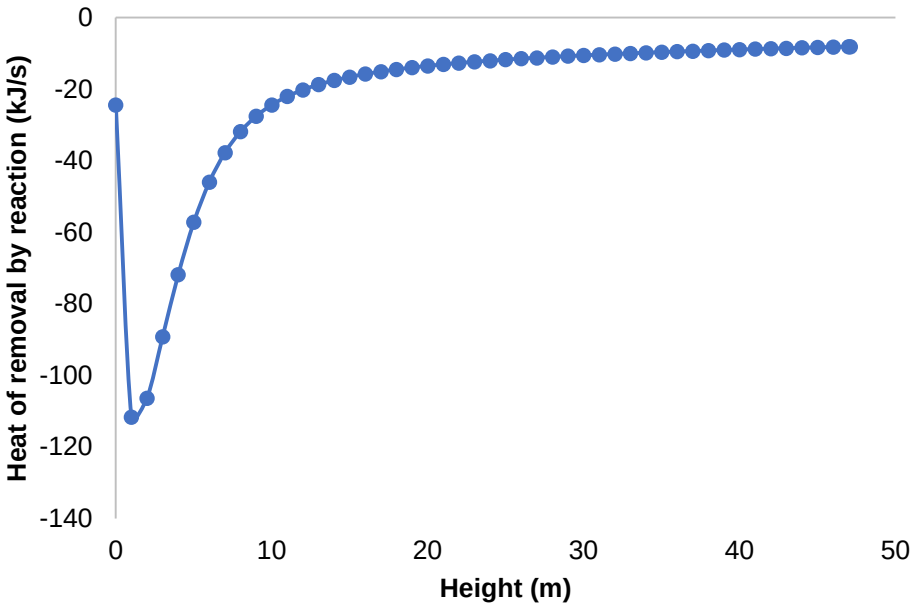

Figure 4.7: Profile of heat removal along the riser

At 74.06 kg/s and a C/O ratio of 5.406, it is a 15.61% increase on mass flowrate of gas oil. This lower C/O ratio compared to 6.405 of the plant brought about 11.15% increase in the converted fraction of gas oil from 0.0478 to 0.0538 kg-lump/kg-feed. This increased conversion leads to 17.80% increase in diesel yield from 0.1857 to 0.2259 kg-lump/kg-feed. However, there is a significant decrease in the yield of gasoline from 0.4731 to 0.4305 kg-lump/kg-feed (9.90% decrease). This is because the riser exit temperature for this simulation being 712.7 K, is 8.49% lower than the temperature (773.2 K) of the plant at the exit of riser, which favours the cracking of heavier products like diesel compared with gasoline. This difference also caused considerable percentage decrease in the lighter products and coke.

At 62.5 kg/s, the C/O ratio is 6.406. The converted fraction of gas oil is 0.0478 kg-lump/kg-feed for the plant and 0.0346 kg-lump/kg-feed for this simulation. This is equivalent to 38.15% increase on the conversion of gas oil. This increase has caused a 0.81% increase of 0.1857 kg-lump/kg-feed of diesel for the industrial plant compared with 0.1842 kg-lump/kg-feed for this simulation at C/O ratio of 6.406. Likewise, the increase caused a 2.71% increase of 0.4731 kg-lump/kg-feed of gasoline for the plant compared to 0.4863 kg-lump/kg-feed for this simulation at C/O ratio of 6.406. This shows that at C/O ratio of 6.406, the percentage conversion of the gas oil is 38.15%, which is higher than 11.15% at C/O ratio of 5.406.

The two simulation outputs shown in Table 4.5 are obtained at C/O ratios of 5.405 and 6.405. Comparing their percentage differences with the plant data, there is a decrease of 8.49 % in gas oil temperature at C/O = 5.405, while, there is a decrease of 5.15 % in gas oil temperature at C/O = 6.405. This shows that increase in C/O ratio could increase the gas phase temperature, which eventually favours conversion as seen; a 38.15 % increase in conversion at C/O = 6.405 as against 11.15 % increase at C/O = 5.405. However, increase in C/O ratio from 5.406 to 6.406 gives a lower diesel yield (17.8 % at C/O = 5.404 and 0.81 % at C/O = 6.404) and higher gasoline yield (a decrease of 9.90 % at C/O = 5.404 and 2.71 % at C/O = 6.404). This means that higher C/O ratios may favour increased gas oil conversion but results in decrease yield of diesel.

Therefore, the plant needs to be operated at lower C/O ratio for increased diesel yield, while increased C/O ratio favours the yield of gasoline. In addition, if the production objective is to produce gasoline, then a higher C/O ratio is appropriate. Increased C/O ratios also increase the temperature of the riser which favours secondary reactions. This is one of the reasons for gasoline yield to increase with increasing C/O ratio. This variation of the C/O ratio, a major influence on the FCC unit, follows a typical FCC riser behaviour (León-Becerril et al. 2004).

Table 4.5: Compare riser output results for different C/O ratio

Riser Parameter	Plant	Simulation Output @ C/O = 5.405	% Diff. @ C/O = 5.405	Simulation Output @ C/O = 6.405	% Diff. @ C/O = 6.405
Catalyst-to-oil ratio (C/O)	6.405	5.405		6.405*	
Catalyst Mass flowrate (kg/s)	400.32	400.32	0.0	400.32	0.0
Gas oil Mass flowrate (kg/s)	62.50	74.06	15.61	62.50	0
Gas oil Temperature (K)	773.2	712.7	-8.49	735.3	-5.15
Catalyst Temperature (K)	N/A	713.6	N/A	736.2	N/A
Mass fraction of Gas oil (wt. %)	0.0478	0.0538	11.15	0.0346	38.15
Mass fraction of Diesel (wt. %)	0.1857	0.2259	17.80	0.1842	0.81
Mass fraction of Gasoline (wt. %)	0.4731	0.4305	-9.90	0.4863	2.71
Mass fraction of LPG (wt. %)	0.1518	0.1550	2.06	0.1577	3.74
Mass fraction of Dry gas (wt. %)	0.0483	0.0488	1.02	0.0497	2.28
Mass fraction of Coke (wt. %)	0.0891	0.0861	-3.48	0.0876	1.71

4.2 Parameter estimation for riser kinetic reaction scheme with propylene as single lump

The FCC unit is mostly used to increase gasoline and diesel yield to meet high demand of fuel, which is due to increase in transportation. However, it is not just to increase gasoline and diesel but middle distillates like the gas lump as well, which comprises light olefins such as ethylene and propylene, a major source of the raw materials for the polyethylene and polypropylene industries. These light olefins are the most important raw materials for many chemicals such as acrylonitrile, propylene oxide and other chemicals that are consumed as substitutes for non-plastic materials (Khanmohammadi et al. 2016).

In recent times, there has been an increase in the demand for propylene, a petrochemical industry feedstock (Li et al. 2007) and it is chiefly sourced from light olefins in the naphtha steam pyrolysis process. Naphtha steam pyrolysis process is a high energy consumption process because it is carried out at about 800 °C and separation of olefins is done at temperatures as low as -100 °C (Li et al. 2007). This makes the naphtha steam pyrolysis process a more capital-intensive one. However, propylene and ethylene are sourced cheaply from the FCC unit due to the abundance and cheapness of the FCC feedstock compared with Naphtha (Li et al. 2007; Khanmohammadi et al. 2016). The recent growth in demand for propylene in the world has maintained focus on the refineries toward FCC technologies for the maximisation of propylene production in order to achieve economic profit (Berrouk et al. 2017). In addition, the FCC operates below 550 °C and does not require extreme ‘cold’ for the separation of propylene from liquefied petroleum gas (LPG) (Li et al. 2007). Therefore, the cost of producing propylene from the FCC is much lower than that from steam pyrolysis (Akah and Al-Ghrami 2015). The FCC unit is thus ideally suited for the manufacture of ethylene and propylene from the light products.

Currently, there is an increasing interest in maximizing propylene yield of FCC units (Liu et al. 2007; Akah and Al-Ghrami 2015). The FCC unit can produce high yields under suitable operating conditions. However, changes in quality, nature of the crude oil feedstock, changes in the environment and the desire to achieve maximum profitability, results in many different operating conditions in the FCC riser unit (Li et al. 2007).

According to Almeida and Secchi (2011), the riser can produce large profits when it runs at maximum capacity with maximum feed rate and power applied to the equipment. Optimisation of the design and operation is crucial to facilitate the constantly changing quality and nature of blends of feedstocks while meeting the maximum capacity requirements. Some factors like the large amount of feed processed, valuable gasoline yield, gas lump yield, the various processes occurring in the riser and its economic operation affects the overall economic performance of the refinery. Thus, it is vital to improve the performance of the riser through process optimisation strategies (Khandalekar 1993).

The production of propylene is mostly achieved using catalytic reactions with special selectivity for propylene (Liu et al. 2007; Inagaki et al. 2010; Haiyan et al. 2012; Akah and Al-Ghrami 2015). A number of lumps for catalytic cracking have been reported in the literature but most of them lumped the gaseous products in a single lump, thereby making it difficult to optimise or maximise a particular gas, for instance propylene. In the FCC unit, the yield of propylene is influenced by the reaction temperature, catalyst to oil ratio (C/O), residence time, nature of feed and the catalyst system (Aitani et al. 2000; Knight and Mehlberg 2011; Parthasarathi and Alabduljabbar 2014) and when any of the foregoing variables is optimised, the yield of propylene can be considerably increased.

Usman et al. (2017) conducted experiments using three different crudes (Super Light, Extra Light and Arab Light) in catalytic cracking to produce light olefins, where they presented propane and propylene as different lumps. They used different catalysts: base equilibrated catalyst and others (Z30 and Z1500), which are the base equilibrated catalyst + MFI Zeoliite at varying Si/Al ratio. The results shows that the total weight fraction of the two lumps; propylene and propane has propylene about 80% to 89% for all the crude oils and catalysts used (Usman et al. 2017). This percentage is high; therefore, a combined lump of propylene and propane can be treated as a single lump of propylene and the kinetic model of Ancheyta and Rogelio (2002) as shown in Figure 4.8 is suitable for this work. Hence, in this study, the FCC riser is simulated based on a six-lumped kinetic model (Ancheyta and Rogelio 2002) consisting of vacuum gas oil, gasoline, C_3's (propane and propene), C_4's (butane and butene), dry gas (H_2, C_1 – C_2) and coke. Vacuum gas oil is the feed whilst gasoline, butylene, propylene and dry gas are products with coke deposited on the catalyst.

Hence, parameter estimation for a six-lump kinetic model that gives propylene as a single lump is carried out. Then, the simulation of the riser with the new six lump kinetic data to obtain results showing the effects of changing variables such as temperature and mass flowrates on the yield of propylene was carried out.

4.2.1 Simulation model description

The riser in this work is of industrial size; 30 m high and 1.0 m diameter and is simulated using a six-lump kinetic model as shown in Figure 4.8. The kinetic data for the various constants in Figure 4.8 are estimated using the parameter estimation technique. The simulation involves many other parameters such as the feed conditions, catalyst properties and riser dimensions, which were obtained from the literature (Ancheyta and Rogelio 2002) and presented in Appendix A, Table A.8. The steady-state model in Appendix A, Table A.9 is derived from mass, energy and momentum balance equations for the catalyst and gaseous phases of the riser, while assuming that there is no loss of heat from the riser to the surrounding (Ali et al. 1997). In addition, it is assumed that the cracking reactions only take place on the catalyst surface.

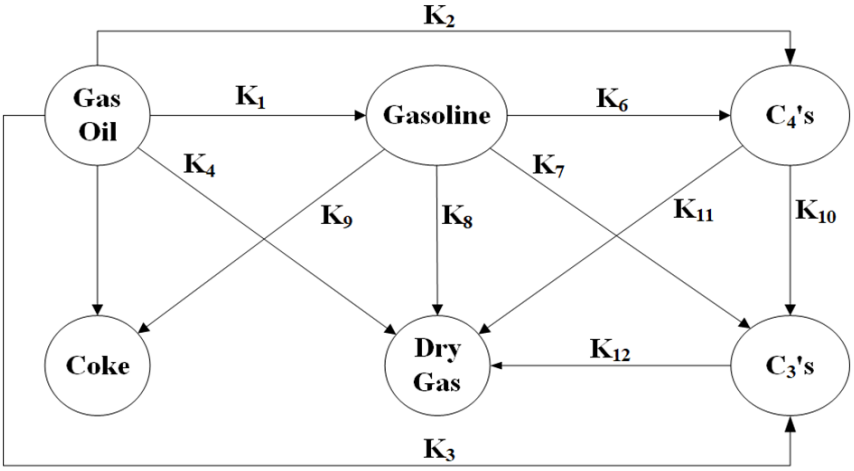

Figure 4.8: Six-lump model (Ancheyta and Rogelio, 2002, Han and Chung, 2001a)

4.2.2 Riser simulation and Kinetic studies for propylene production

The kinetic studies on the production of propylene have been carried out and they are mostly based on catalytic pyrolysis. However, catalytic pyrolysis includes catalytic reactions and thermal reactions (Meng et al. 2006) and the cracking extent of catalytic pyrolysis is more comprehensive than that of catalytic cracking (Meng et al. 2005). In addition, catalytic cracking is favoured over thermal cracking for maximum propylene production especially in high severity FCC units

(Parthasarathi and Alabduljabbar 2014). In addition, just as the catalytic cracking reactions require the understanding of the kinetics of the reaction involved for reactor design, the design of the catalytic pyrolysis reactor would require the understanding of both the thermal and catalytic reactions involved in designing a catalytic pyrolysis reactor. This is true because kinetic study is an essential means for thorough understanding of reactions and catalysis for any catalysed chemical reaction which help in the correct design of chemical reactors and determine the progress of the chemical reaction (Naik et al. 2017). In this study, mathematical and kinetic models used are based on the kinetic lumping approach which catalytic cracking as a form of reaction was employed (Han and Chung 2001a; Han and Chung 2001b).

One of the kinetic lumped models for the production of propylene, based on catalytic pyrolysis of heavy oils, is the 8-lumped model (Meng et al. 2006) which includes ethylene as a lump and a separate propylene lumped with butylene. Where propylene is required as a separate lump, this 8-lumped model may not be useful. Some kinetic models for the propylene production are based on catalytic cracking, such as the four lumped model which include propylene as a component of a gas lump (Hussain et al. 2016); the ten lumped model with propylene as a distinct lump (Du et al. 2015) and 6-lumped model with distinct propylene lump (Ancheyta and Rogelio 2002). To maximise the yield of propylene in a lumped kinetic model, propylene must be a separate lump. The gas lump in Hussain et al. (2016) is a mixture of propylene, butylene and some dry gas. Hence, it is unsuitable for use to maximise propylene because maximizing gas lump would mean maximizing other gases along.

The ten-lumped model of Du et al. (2015) and six-lumped model of Ancheyta and Rogelio (2002) are most suitable for their ability to have propylene as unique lumps. However, the yields of lumps were obtained at a particular constant temperature; 580 ^{o}C (Du et al. 2015) and 500 ^{o}C (Ancheyta and Rogelio 2002), instead of the progressive temperature profile of the catalyst and vapour phases as found in the industrial FCC riser. Specific rate constants for the various cracking reactions and catalyst deactivation in a typical industrial riser also vary along the length of the riser. In this work, the catalyst deactivation is represented by Equation (3.49) which is a function of varying temperature of the gas phase of the riser. Since temperature varies in the riser and has effect on some important kinetic variables such as rate constants and catalyst deactivation, it means that

heat required at every point in the riser varies. This heat requirement is estimated by heat of reaction of all cracking reactions as shown in Equation (A.43).

The riser mathematical model used in this work requires kinetic data that involves activation energy, frequency factor and heat of reaction which vary along the riser. Hence, in this work, heats of reaction, frequency factors and activation energies for varying rate constants are estimated using parameter estimation. Where the kinetic parameters to be estimated are numerous and especially with limited laboratory data available, it poses substantial challenges (Ancheyta-Juarez and Murillo-Hernandez 2000; Zhang et al. 2017). For the parameter estimation and simulation of the riser, the six-lumped model (Ancheyta and Rogelio 2002) is chosen over the ten lumped model because it predicts propylene as a single lump and has less parameters to be estimated, which reduces the complexity of the model.

4.2.3 Parameter estimation of kinetic data involving propylene as single lump

In gPROMS Parameter estimation requires the use of experimental data (Table 4.6) for validation and for the design of experiments. In this work, the experimental data were obtained from the literature (Ancheyta and Rogelio 2002) and used to generate the predicted results. Ancheyta and Rogelio, (2002) presented fifteen sets of fractional yields for the six-lumps obtained at fifteen different weight hourly space velocities (WHSV) from 6 – 48 hr^{-1} and at 773 K. These sets of fractional yields for the six-lumps were read with a software called Webplotdigitizer 3.8 and are presented in Table 4.6. On the gPROMS parameter estimation framework, the fifteen sets of results are used with each set for a single experiment that represents experimental values, y_i^{exp}. Along with the complete riser mathematical model (hydrodynamic, kinetic, mass and energy conservation equations), the calculated values, y_i^{cal} are obtained and the sum of squared errors (SSE) are minimised.

Table 4.6 shows the experimental data obtained from the literature (Ancheyta and Rogelio 2002).

Table 4.6: Six-lumps yields used as experimental data (Ancheyta and Rogelio, 2002).

WHSV (hr^{-1})	Propylene (C_3's)(wt%)	Butylene (C_4's)(wt%)	Gas oil (wt%)	Gasoline (wt%)	Dry gas (wt%)	Coke (wt%)
6	5.38	9.49	23.63	55.19	1.81	4.55
7	5.03	9.15	24.88	55.11	1.63	4.34
10	4.80	8.80	26.16	54.58	1.44	4.20
11	4.94	8.80	26.59	53.96	1.51	4.20
13	4.87	8.66	27.76	53.91	1.40	4.18
15	4.77	8.50	28.54	53.34	1.37	4.09
16	4.75	8.36	28.85	53.12	1.33	4.08
20	4.63	8.27	30.17	52.96	1.28	4.04
24	4.56	8.08	31.02	52.19	1.23	4.01
28	4.45	8.08	31.80	51.62	1.16	3.92
32	4.40	7.82	31.95	51.58	1.09	3.82
36	4.35	7.68	32.02	51.19	1.09	3.87
40	4.28	7.75	32.25	51.26	1.06	3.89
44	4.26	7.52	32.64	50.85	0.99	3.91
48	4.23	7.50	32.55	50.85	0.99	3.93
Average	4.65	8.30	29.39	52.78	1.29	4.07
Range	4.23 – 5.39	7.50 - 9.49	23.63-32.55	50.85-55.19	0.99-1.81	3.82-4.55

There are two approaches here: firstly, simulation for converging all the equality constraints and satisfying the inequality constraints and secondly, carrying out the optimisation where the objective function is:

$$Obj(SSE) = \sum_{M=1}^{M_t} \left(y_i^{exp} - y_i^{cal}\right)^2$$

Where y is the mass fraction of lumps and i the various lumps in the riser.

The parameter estimation problem statement can be written as:

Given	The fixed riser reactor configuration, feed quality and characteristics, catalyst properties and process operational conditions
Optimise	The kinetic parameters; activation energies E, heat of reactions ΔH and frequency factors k_o at given process conditions
So as to minimise	The sum of square errors (SSE)
Subject to	Equality and inequality constraints

Mathematically;

$$\min_{\xi_{io},\eta_i,\theta_i} SSE$$

s. t.

$f(x, z'(x), z(x), u(x), v) = 0$ (model equations, equality constraints)

$\xi^l \leq \xi \leq \xi^u$ (inequality constraints)

$\eta^l \leq \eta \leq \eta^u$ (inequality constraints)

$\theta^l \leq \theta \leq \theta^u$ (inequality constraints)

Where $f(x, z'(x), z(x), u(x), v) = 0$ is model equation, x the height of the riser and the independent variable, $u(x)$ the decision variable, ξ the upper and lower limits of the frequency factors k_{oi}, η the upper and lower limits of the activation energies E_i and θ the upper and lower limits of the heat of reactions ΔH_i. $z(x)$ is the differential and algebraic equations while $z'(x)$ is their derivative. v is the constant parameters.

Upper and lower limits are set for the decision variables which of course are the parameters requiring to be estimated. They are set based on the assumption that the kinetic values will be within the range found in the literature for four, five and six lump models. Since the six lumped model was derived based on the sequential strategy (Ancheyta-Juarez et al. 1997), they assumed that the major

reactant and products of the cracking reactions have similar rate constants, and hence derived the four lumped model from the three lumped model and the six-lumped model from the five lumped model in a sequential strategy. Therefore, it is expected in this work, that the upper and lower limits for the activation energy, heat of reaction and frequency factors should be within the existing range. The values from the literature are: activation energy (31923 - 57278.96 kJ/kg mol) (Ancheyta et al. 1999; Ancheyta-Jua´rez and Sotelo-Boya´s 2000) and (31820 – 66570 kJ/kg mol) (Han and Chung 2001b), heat of reaction (195 – 745 kJ/kg) and frequency factor (0.000629 – 1457.5 s^{-1}) (Han and Chung 2001b). The upper and lower limits are wider apart on the gPROMS parameter estimation framework to allow the software to make the best estimates. Hence, the following upper and lower limits were set; activation energy; 0 – 100,000 kJ/kg mol, heat of reaction; 0 – 1000 kJ/kg and frequency factors; 0 - 2000 s^{-1}. Another reason for widening the limits of the decision variables is to allow for the adjustment of data obtained from the laboratory model to get modified since they are being used on a mathematical model that represents an industrial unit (Du et al. 2015).

4.2.4 Model validation and parameter estimation results

The simulation results will help to determine the capability of gPROMS in handling complex nonlinear DAEs of the riser using the kinetic model of Ancheyta and Rogelio (2002), and to compare the results obtained with those predicted results of the same kinetic model obtained experimentally by Ancheyta and Rogelio (2002). Even though the experimental results were obtained at 773 K, the simulated riser temperature was progressive along the length of the riser.

The mass flowrates for gas oil and catalyst used in this simulation are 51.8 kg/s and 190.9 kg/s respectively, while the C/O ratio is 3.685. These mass flow rates predicted the yields of the six lumps in the range presented by Ancheyta and Rogelio (2002). The estimated kinetic parameters are shown in Table 4.7.

Table 4.7: New kinetic parameters estimated

Rate Constant	Frequency factors (s^{-1})	Activation Energy (kJ/kg mol)	Heat of reaction (kJ/kg)
k1	1233.51	45005.4	284.151
k2	841.36	66364.1	22.452
k3	1333.60	62582.7	103.432
k4	6.019	66568.4	25.596
k5	0.493	66054.1	194.867
k6	26.056	35760.4	675.894
k7	63.008	66426.2	645.963
k8	8.19×10^{-6}	62591.5	250.896
k9	12.048	36983.7	565.387
k10	1367.37	60938.7	496.002
k11	1359.88	57575.9	899.319
k12	8.19×10^{-6}	45880.0	682.498

When gas oil meets the catalyst, it begins to crack to form gasoline, butylene, propylene, dry gas and coke. In this study, the cracking reaction takes place at gas oil inlet temperature of 523.0 K at the vaporisation section rising to 719.9 K at the first 6 m height of the riser and levelling out for the remaining height of the riser with 706.2 K as the exit temperature. The inlet temperature of catalyst from the cyclone is 1010 K, which mixes with regenerated catalyst in the vaporisation section to give a catalyst temperature of 971.4 K at the entrance of the riser. Cracking reactions begin immediately at the riser entrance and the profiles of these cracking reactions are presented in Figure 4.9, while the temperature profiles are presented in Figure 4.10.

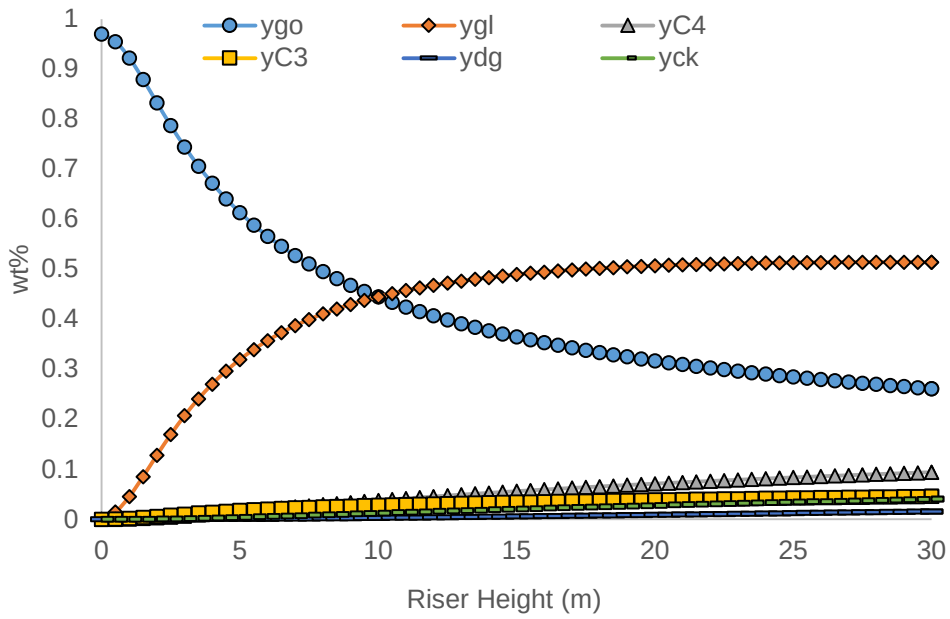

Figure 4.9: Lumps of gas oil cracking

The feed in this study is a 97.00 wt% gas oil and the remaining 3.00 wt% is steam. Figure 4.9 shows that the fraction of gas oil at the exit of the riser is 26.12 wt% which is 26.93% of gas oil unconverted. It also shows that about 73.07% of gas oil was consumed and about 70% of the fraction is consumed in the first 20 m of the riser. Literature results (Ancheyta and Rogelio 2002) show that the fraction of gas oil at the exit was a range of values because it was obtained at varied WHSV and it is between 23.50 – 32.50 wt% which corresponds to 67.5 - 76.5% of gas oil consumed. The value of 26.93 wt% of unconverted gas oil obtained in this simulation at C/O ratio of 3.685 falls within the range of results from Ancheyta and Rogelio (2002).

Likewise, gasoline started yielding as soon as cracking starts at the entrance of the riser. It rises from 0 wt% to 51.36 wt% at the exit of the riser. This accounts for 52.95% of the total product of the riser with about 80% of the gasoline formed in the first 20 m of the riser. The value of 51.36 wt% of gasoline yield in this simulation is within the range of 50.85 – 55.19 wt% presented by Ancheyta and Rogelio (2002).

The butylene lump (C_4's) increases from 0 wt% to 9.39 wt% at the exit of the riser. This accounts for 9.68% of the total product of the riser and it is within the range of 7.50 – 9.49 wt% presented by Ancheyta and Rogelio (2002). Similarly, the propylene lump (C_3's) which is of more interest in this work, also builds up as cracking commences at the riser entrance from 0 wt% to 4.59 wt% at the exit of the riser, accounting for 4.73 wt% of total riser products. The propylene yield of

4.80 wt% is also within the range of 4.23 – 5.38 wt% presented by Ancheyta and Rogelio (2002) and others in the literature (Farshi et al. 2011).

The dry gas lump also rises from 0 wt% to 1.55 wt% at the exit of the riser. This is 1.60 wt% of the total product of the riser and it is within the range of 0.99 – 1.81 wt% presented by Ancheyta and Rogelio (2002). The remainder being coke deposited on the catalyst, which also rises from 0 wt% to 0.0399 wt% and it represents 4.11 wt% of the total product of the riser. It is also found within the range of 3.82 – 4.55 wt% presented by Ancheyta and Rogelio (2002).

In general, the yields of the six lumps are within the range presented by Ancheyta and Rogelio (2002). This shows that the estimated kinetic parameters are a true representation of the cracking reactions. The values also show that the experimental data of Ancheyta and Rogelio (2002) can actually be used for the parameter estimation and the estimated kinetic parameters are useful for simulation of industrial riser. The profiles of the reactant and products are qualitatively consistent with those found in the literature (Han and Chung 2001b).

As cracking takes place, the endothermic reaction gives up heat from the catalyst to the gaseous phase. The endothermic heat, which is determined in this simulation with the aid of the heat of reaction estimated, is represented by the profile of the gas phase temperature and shown along with the profile of the catalyst phase temperature in Figure 4.10. The temperature of the catalyst-phase is about 971.4 K at the entrance of the riser but decreases for the first 5 m and then essentially levels out. The temperature profile of the gas phase at the entrance of the riser is about 523.0 K and rises to a maximum in the first 5 m of the riser and levels out to the exit of the riser. Both profiles start with a difference of about 448.5 K at the entrance of the riser and come very close to the same value with temperature difference of about 4.4 ^{o}C at the exit of the riser.

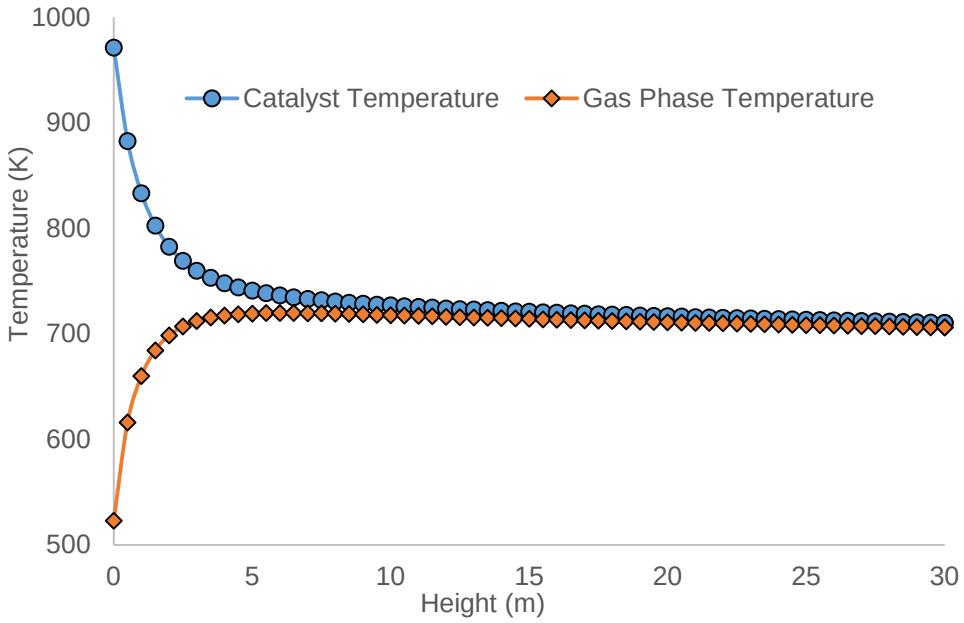

Figure 4.10: Temperature profile across the riser

This temperature difference is required to accomplish the endothermic reaction. The temperature of the cracking reactions in Ancheyta and Rogelio (2002) experimental work is 773 K. This temperature was reached at the riser entrance where both catalyst and oil mixed vigorously. However, the temperature of cracking in a typical riser varies at the entrance to the exit because the reaction is progressive at varied temperatures along the riser as seen in Figure 4.10. The temperature profiles obtained in this work are similar to those obtained in many literatures (Ali et al. 1997; Han and Chung 2001b; Souza et al. 2006).

Table 4.8 shows the comparison of the results obtained in this simulation at C/O ratio 3.685, already presented in Figures 4.9 and 4.10, with the results presented by Ancheyta and Rogelio (2002) experimental work. All the results are within the corresponding range for each lump, which validates the results obtained. With an increment of 50 kg/s of catalyst mass flowrate, the C/O ratio was varied, and the results are also presented for C/O ratios of 4.651, 5.616 and 6.581 in Table 4.8.

Table 4.8: Comparing simulated riser output with that of Ancheyta and Rogelio (2002)

Lump (wt%)	Output Range (Ancheyta and Rogelio 2002)	Riser Output (wt%)						
		C/O = 3.685	C/O = 4.651	Difference	C/O = 5.616	Difference	C/O = 6.581	Difference
Gas oil (wt%)	23.63 - 32.55	26.11	19.50	-6.61	15.58	-10.53	13.06	-13.05
Gasoline (wt%)	50.85 - 55.19	51.36	49.69	-1.67	46.40	-4.96	42.86	-8.5
Butylene (C_4's) (wt%)	7.50 - 9.49	9.39	12.06	2.67	13.37	3.98	13.70	4.31
Propylene (C_3's) (wt%)	4.23 - 5.39	4.59	6.37	1.78	8.22	3.63	10.05	5.46
Dry gas (wt%)	0.99 - 1.81	1.55	3.36	1.81	5.58	4.03	7.92	6.37
Coke (wt%)	3.82 - 4.55	4.00	6.04	2.04	7.86	3.86	9.41	5.41
Cat. Temp. (K)		710.6	734.0	23.4	753.2	42.6	769.6	59.0
Gas Phase Temp. (K)		706.3	729.1	22.8	748.0	41.7	764.1	57.8

The unconverted gas oil yields at the varied C/O ratios are outside and lower than the range of the results by Ancheyta and Rogelio (2002). This is expected because increasing the C/O ratio increases gas oil conversion because of increase in cracking temperature. The absolute difference between the simulated results (C/O = 3.685) and the varied C/O ratios (C/O = 4.651, 5.616 and 6.581) show decrease for both gas oil and gasoline. All other lumps increase due to increase in the C/O ratio and eventual rise in cracking temperature which increases the conversion of the cracking reaction. Gasoline undergoes secondary cracking to add to the butylene, propylene and dry gas lumps with additional coke deposit on the catalyst. This trend shows that increasing the C/O ratio may favour the yield of the light products like butylene, propylene and dry gas. However, the absolute difference for propylene (5.46 wt%) at C/O ratio of 6.581 is more than that of butylene (4.31 wt%), which suggests that it would be necessary to operate the riser at C/O ratio of 6.581 to have more propylene in the light components. To get the best operating condition for propylene yield, optimisation of the unit is necessary.

4.3 Summary

In this work, a steady state detailed industrial FCC riser process model is simulated to carry out parameter estimation of a newly developed six-lump kinetic model for gas oil cracking. The new six-lump model was implemented on gPROMS software to crack gas oil into diesel, gasoline, LPG, dry gas and coke. In another parameter estimation, kinetic data were obtained to simulate the gas oil cracking in an industrial FCC unit to produce propylene as a single lump. The following conclusions are made:

- A new kinetics scheme has been developed which includes the cracking of LPG to coke and dry gas, as well as the cracking of dry gas into coke.
- New activation energies, frequency factors and heat of reactions for a new six-lump kinetic model were estimated.
- The estimated parameters predict the major industrial riser fractions; diesel is 0.1842 kg-lump/kg-feed with a 0.81% error while gasoline is 0.4863 kg-lump/kg-feed with a 2.71% error compared with the plant data.
- With the help of the new kinetic parameters, the heat of cracking reaction was estimated for the six-lumped model for the first time.

- The estimated parameters can be used to simulate any type of FCC riser with a six-lump model since C/O ratios were varied and the results showed agreement with the typical riser profiles.
- New kinetic parameters (frequency factor, activation energies and heat of reactions) were estimated for and used with a six-lumped kinetic model with a separate propylene lump. The yields of the six lumps fall within the range of yields presented in the literature.

Chapter 5

Effects of Compressibility Factor on Fluid Catalytic Cracking Unit Riser Hydrodynamics

5.1 Introduction

The FCC process is effective if the riser hydrodynamics is efficient. Upholding an efficient pressure gradient in the riser is a measure of good riser hydrodynamics that tends to improve product yield. A detailed model of the FCC can capture all the aspects of the unit that improves on the prediction of the performance of FCC risers (León-Becerril et al. 2004). As the feed meets the catalysts at the vaporisation section, it vaporises into the riser forming gas and catalyst phases that flows in a fluid-like manner to the top where it exits. The volume of the products, which is the gas phase, increases as cracking of the feed proceeds bringing about changes in the density, molecular weight, temperature and pressure of the system along the riser height. All the changes in those process variables depend on the type and nature of catalyst and feed.

Due to this, properties like the crude oil American Petroleum Institute (API) gravity, density or specific gravity of feed and catalyst properties are specified in most FCC riser simulation.

One of the process variables not always specified is the compressibility factor. Some authors (Ali et al. 1997; Han and Chung 2001a; Martignoni and de Lasa 2001) have treated the gas compressibility of the vaporised fluid in the riser as unity. Others have assumed that the compressibility or Z factor can be a dimensionless value of one due to the fact that the riser operates at low pressure and high temperature (Ali et al. 1997; Fermoselli 2010), even though, at low pressure, 2 - 3% error is prevalent (Ahmed 2001). There is also an assumption that the density relationship of the gas phase model in the riser behaves as an ideal gas at any position in the riser even for a heavy oil feedstock (Martignoni and de Lasa 2001). Another researcher treated the gas phase in the riser as ideal gas with the assumption of constant enthalpy (Li et al. 2009). However, enthalpy is not constant in the riser (Han and Chung 2001b).

The Z-Factor is very significant in characterising the fluid flow of oil and gas in the upstream and downstream sector of the petroleum industries (Heidaryan et

al. 2010a; Heidaryan et al. 2010b). The process that the fluid undergo describes whether it is compressible or non-compressible, and if there is a density change, as is possible in the riser, then the compressibility factor changes. Hence, treating the gaseous phase as an ideal gas in the case of changing density system will not be accurate. Also, as velocity increases, the density of the fluid varies and can be a compressible fluid (Balachandran 2007). Some process variables such as density (Lopes et al. 2012), viscosity and the void fraction would vary when change in mass (or moles) occur due to cracking reactions and when operating conditions such as temperature, mass flowrate and/or pressure (a function of gas compressibility) are altered. Since these changes in the operating conditions of the riser are considered when modelling risers (León-Becerril et al. 2004), the variation in the compressibility factor of the fluid needs to be considered too. One major operating determinant of the FCC unit is the catalyst circulation between the riser and regenerator, and it accomplishes two simple purposes: preserving the regenerated catalyst activity via regeneration and upholding the heat balance by the endothermic reactions in the riser and other forms of heat removal. The catalyst circulation in the FCC is possible by the overall pressure balance, which also has a relationship with the gas compressibility factor. To get this pressure balance right, accurate conditions of the catalyst, feed and auxiliary equipment must synchronise with proper design of the FCC unit. In this work, the impact of the gas compressibility on the riser pressure, a major hydrodynamic parameter of the riser will be studied. This will identify the adequate compressibility factor at every point in the riser, which may give an accurate estimate of pressure drop and pressure balance in the riser and of the entire FCC unit. This will also determine the need for considering adequate gas compressibility factor to be used in plant design and not the outright assumption that the fluid phase is an ideal gas.

5.2 Gas compressibility factor

The gas compressibility factor (Z-Factor) is a vital process variable in upstream and downstream calculations in petroleum industries (Heidaryan et al. 2010b), and its root equation is:

$$PV=ZnRT \tag{5.1}$$

Equation 5.1 is fit for real gases, and for ideal gas, Z is unity. The concept of ideal gas is mostly theoretical, it does not exist in practice. Hence, an accurate gas

compressibility factor needs to be used in some processes that handle gaseous phase flow or reactions. The compressibility factor is defined as the ratio of the actual volume of gas to the ideal volume of gas, meaning that it is a measure of the extent of deviation from perfect behaviour (Heidaryan et al. 2010b).

Fayazi et al. (2014) said, the Z-Factor can be easily obtained from experimental data, equation of state (EoS) and empirical correlations. Experimental methods are expensive and time consuming and there are numerous petroleum gases to account for (Ahmed 2001), whilst empirical correlations are found to be accurate and less complex than the EoS (Elsharkawy 2004). Having known the pseudo-reduced pressure and pseudo-reduced temperature of the fluid, empirical correlations offer a good estimate of the compressibility factor of the hydrocarbon gases (Fayazi et al. 2014). The model used in this work (Han and Chung 2001a; Han and Chung 2001b), captures the interactions of the pressures and temperatures in the vaporisation and riser sections as functions of the pseudo-reduced pressures and temperatures. They obtain a correlation for the gas phase viscosities of the hydrocarbon lumps into pseudo-reduced viscosity and pseudo-critical viscosity using pseudo-reduced temperature in the range $(0.75 < T_{pr} < 3.0)$ and pseudo-reduced pressure in the range$(0.01 < P_{pr} < 0.2)$. Although, the pseudo-reduced temperature and pressure across the riser height for this simulation work lie outside the range that Han and Chung (2001a); Han and Chung (2001b) used for the derivation of the correlation for the viscosities, the pseudo-reduced pressure from this work as shown in Figure 1 lies within the range of many correlations from the literature and presented in this work. This is to show the variations of the riser hydrodynamic variables with the compressibility factor, and since the pseudo-reduced pressures and pseudo-reduced temperatures vary along the riser, the compressibility factor may not be the same at all points in the riser.

Equations (3.55) and (3.56) are used to obtain the pseudo-reduced temperature and pseudo-reduced pressure respectively and Figure 5.1 shows their profiles along the riser height. The pseudo-reduced pressure in this simulation is in the range

$1.218066 \geq P_{pr} \geq 1.023427$ while the pseudo-reduced temperature is in the range $0.528144 \geq T_{pr} \geq 0.348992$. P_{pr} and T_{pr} may vary depending on the operating pressure and temperature of the riser and regenerator. This means that

as the many process variables that influence the pressure and temperature of the FCC unit change during operation, P_{pr} and T_{pr} will also change. Consequently, the Z factor, which is mostly dependent on the P_{pr} and T_{pr} will change too.

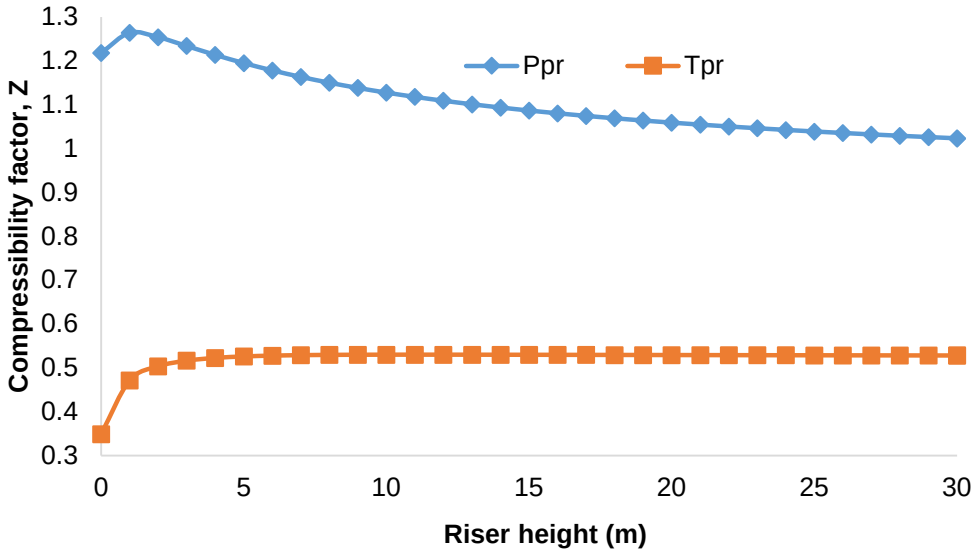

Figure 5.1: Pseudo-reduced pressure and temperature along riser height

There are some common empirical correlations (Beggs and Brill 1973; Kumar 2004) which are not applicable to the pseudo-reduced temperatures equal or less than 0.92. Others that are used in this work accept T_{pr} above 0.92 (Heidaryan et al. 2010a; Sanjari and Lay 2012). To find a suitable correlation that predicts accurately or most closely the compressibility factor of the gas phase in the riser, several correlations were tested in this work. Each Z-factor correlation is inserted in the riser model and tested. Significant riser hydrodynamic variables such as inlet riser pressure and pressure drop will be compared for each Z-factor used. Results from the test will be compared with plant and literature data to determine which correlation estimates the riser Z-factor adequately. The T_{pr} in this simulation is out of the range of many of the correlations tested here, however, the P_{pr} is between $1.218066 \geq P_{pr} \geq 1.023427$ which is consistent with all the ranges for all P_{pr} for all the correlations. The correlations are:

Azizi et al. (2010) Z factor:

Azizi et al. (2010) derived an empirical correlation for the compressibility factor over the range of $0.2 \leq P_{pr} \leq 11$ and $1.1 \leq T_{pr} \leq 2$, using Standing-Katz chart with 3038 points and is presented in Equation (5.2). The Z factor is:

$$Z = A + \frac{B+C}{D+E} \tag{5.2}$$

The coefficients in Equation (5.2) are presented in Equations (5.3 - 5.7)

$$A = a\,T_{pr}^{2.16} + b\,P_{pr}^{1.028} + c\,P_{pr}^{1.58}T_{pr}^{-2.1} + d\,ln\,T_{pr}^{-0.5} \tag{5.3}$$

$$B = e + f\,T_{pr}^{2.4} + g\,P_{pr}^{1.56} + h\,P_{pr}^{0.124}T_{pr}^{3.033} \tag{5.4}$$

$$C = i\,ln\,T_{pr}^{-1.28} + j\,ln\,T_{pr}^{1.37} + k\,ln\left(P_{pr}\right) + l\,ln(P_{pr})^2 + m\,ln\left(P_{pr}\right)ln\left(T_{pr}\right) \tag{5.5}$$

$$D = 1 + n\,T_{pr}^{5.55} + o\,P_{pr}^{0.68}T_{pr}^{0.33} \tag{5.6}$$

$$E = p\,ln\,T_{pr}^{1.18} + q\,ln\,T_{pr}^{2.1} + r\,ln\left(P_{pr}\right) + s\,ln(P_{pr})^2 + t\,ln\left(P_{pr}\right)ln\left(T_{pr}\right) \tag{5.7}$$

The tuned coeffients for Equations (5.3 - 5.7) are presented in Appendix A Table A.2.

Bahadori et al. (2007) Z factor:

Bahadori et al. (2007) presented a Z-factor given in Equation (5.8) and its coefficients are presented in Equations (5.9 - 5.12) (Bahadori et al. 2007). The application range of this correlation is 0.2 < Ppr < 16 and 1.05 < Tpr < 2.4.

$$Z = a - bP_{pr} + cP_{pr}{}^2 + dP_{pr}{}^3 \tag{5.8}$$

$$a = Aa + BaT_{pr} + CaT_{pr}{}^2 + DaT_{pr}{}^3 \tag{5.9}$$

$$b = Ab + BbT_{pr} + CbT_{pr}{}^2 + DbT_{pr}{}^3 \tag{5.10}$$

$$c = Ac + BcT_{pr} + CcT_{pr}{}^2 + DcT_{pr}{}^3 \tag{5.11}$$

$$d = Ad + BdT_{pr} + CdT_{pr}{}^2 + DdT_{pr}{}^3 \tag{5.12}$$

The tuned coeffients for Equations (5.9 - 5.12) are presented in Appendix Table A.3.

Heidaryan et al. (2010a) Z factor:

Heidaryan et al. (2010a) presented a Z-factor is given in Equation (5.13) while the tuned coeffients are presented in Appendix A Table A.4. The range for the pseudo-reduced pressures is $0.2 \leq P_{pr} \leq 3$. The range of the pseudo-reduced pressure in this work is consistent with that of Heidaryan et al. (2010a).

$$Z = \ln\left[\frac{A_1 + A_3\ln(P_{pr}) + \frac{A_5}{T_{pr}} + A_7(\ln P_{pr})^2 + \frac{A_9}{T_{pr}^2} + \frac{A_{11}}{T_{pr}}\ln(P_{pr})}{1 + A_2\ln(P_{pr}) + \frac{A_4}{T_{pr}} + A_6(\ln P_{pr})^2 + \frac{A_8}{T_{pr}^2} + \frac{A_{10}}{T_{pr}}\ln(P_{pr})}\right] \tag{5.13}$$

Heidaryan et al. (2010b) Z factor:

Heidaryan et al. (2010b) presented a Z-factor given in Equation (5.14) while the tuned coeffients are presented in Appendix Table A.5. The range for the pseudo-reduced pressures and temperatures is $0.2 \leq P_{pr} \leq 15$ and $1.2 \leq T_{pr} \leq 3$ (Heidaryan et al. 2010b). The range of the pseudo-reduced pressure in this work is consistent with that of Heidaryan et al. (2010b).

$$Z = \frac{A_1 + A_2 \ln(P_{pr}) + A_3(lnP_{pr})^2 + A_4(lnP_{pr})^3 + \frac{A_5}{T_{pr}} + \frac{A_6}{T_{pr}^2}}{1 + A_7 \ln(P_{pr}) + A_8(lnP_{pr})^2 + \frac{A_9}{T_{pr}} + \frac{A_{10}}{T_{pr}^2}} \quad (5.14)$$

Mahmoud (2014) Z factor:

Mahmoud (2014) presented a Z-factor given in Equation (5.15). It was based on 300 data points of measured compressibility factor and is a function of P_{pr} and T_{pr} only (Mahmoud 2014).

$$Z = \left(0.702e^{(-2.5T_{pr})}\right)P_{pr}^2 - \left(5.524e^{(-2.5T_{pr})}\right)P_{pr} + (0.044T_{pr}^2 + 1.15) \quad (5.15)$$

Papay (1968) Z factor:

The Z-factor correlation of Papay presented in 1968 is described by Equation (5.16) (Li et al. 2014).

$$Z = 1 - \frac{P_{pr}}{T_{pr}}\left[0.3648758 - 0.04188423\left(\frac{P_{pr}}{T_{pr}}\right)\right] \quad (5.16)$$

Sanjari and Lay (2012) Z factor:

Sanjari and Lay (2012) developed a Z-factor model from 5844 experimental data of compressibility factors for a range of 0.01 ≤ Ppr ≤15 and 1 ≤Tpr ≤ 3, and correlation is presented in Equation (5.17), while its tuned coefficients are presented in Appendix Table A.6.

$$Z = 1 + A_1 P_{pr} + A_2 (P_{pr})^2 + \frac{A_3 P_{pr}^{A_4}}{T_{pr}^{A_5}} + \frac{A_6 P_{pr}^{(A_4+1)}}{T_{pr}^{A_7}} + \frac{A_8 P_{pr}^{(A_4+2)}}{T_{pr}^{(A_7+1)}} \quad (5.17)$$

Shokir et al. (2012) Z factor:

Shokir et al. (2012) presented a Z-factor correlation in Equation (5.18), while its various terms are presented in Equations (5.19- 5.23).

$$Z = A + B + C + D + E \quad (5.18)$$

$$A = 2.679562\ \frac{(2T_{pr} - P_{pr} - 1)}{[(P_{pr}^2 + T_{pr}^3)/P_{pr}]} \quad (5.19)$$

$$B = -7.686825\left[\frac{(P_{pr}T_{pr}+P_{pr}^2)}{[(P_{pr}T_{pr}+2T_{pr}^2+T_{pr}^3)]}\right] \quad (5.20)$$

$$C = -0.000624\,(P_{pr}{T_{pr}}^2 - T_{pr}P_{pr}^2 + T_{pr}P_{pr}^3 + 2P_{pr}T_{pr} - 2P_{pr}^2 + 2{P_{pr}}^3) \quad (5.21)$$

$$D = 3.067747\,\frac{(T_{pr}-P_{pr})}{[(P_{pr}^2+T_{pr}+P_{pr})]} \quad (5.22)$$

$$E = \frac{0.068059}{P_{pr}T_{pr}} + 0.139489{T_{pr}}^2 - 0.081873P_{pr}^2 - \left[\frac{0.041098T_{pr}}{P_{pr}}\right] + \left[\frac{8.152325P_{pr}}{T_{pr}}\right] - 1.63028P_{pr} + 0.24287T_{pr} - 2.64988 \quad (5.23)$$

5.3 Results

In this section, the simulation results are presented and compared with literature and plant data (Han and Chung 2001a; Han and Chung 2001b) to demonstrate the capability of gPROMS in solving complex nonlinear DAEs, again, by validating the results against those predicted by the same model but using different solution software as DSim-FCC (Han and Chung 2001b).

5.3.1 Simulation

Gas oil and catalyst vaporises into the riser to form cracked lumps; gasoline, gases and coke. In this study, the cracking reaction is set to take place at gas oil inlet temperature of 535 K and catalyst inlet temperature of 1006.4 K. In addition, the mass flow rate of catalyst and gas oil is 300 kg/s and 49.3 kg/s respectively, which means a catalyst-oil-ratio (C/O) ratio of 6.085 as in the case of Han and Chung (2001a). The profiles of the products are shown in Figure 5.2.

The gas oil comes into the riser at 0.9686 (kg lump/kg feed) fraction and its unconverted fraction at the exit of the riser is 0.3045 (kg lump/kg feed) corresponding to 29.56% unconverted. This shows that 70.44% of gas oil feed was consumed and 60% of the fraction was consumed in the first 18 m of the riser. In Han and Chung (2001a) the fraction of gas oil at the exit of the riser is 0.2735 (kg lump/kg feed) which corresponds to 69.51% of gas oil consumed. This difference can be caused by the difference in the inlet temperature of catalyst to the riser, because increase in catalyst temperature can increase conversion. This would further explain the reason for some differences for the other lumps: gasoline, gases and coke. The profile of gasoline rose from 0 (kg lump/kg feed) at the inlet of the riser to its maximum yield of 0.4998 (kg lump/kg feed) at the exit of the riser. The yield compares well with the value of about 0.5085 (kg lump/kg feed) which is 50.85 wt% obtained by Han and Chung (2001b). The coke

concentration also rose from 0 (kg lump/kg feed) at the inlet to 0.038 (kg lump/kg feed) at the exit of the riser while that reported by Han and Chung (2001b) is 0.0472 (kg lump/kg feed). The yield of the gases rose from 0 (kg lump/kg feed) at the inlet of the riser to a maximum of 0.1262 (kg lump/kg feed) at the exit while that of Han and Chung (2001b) is 0.141 (kg lump/kg feed).

The profile of gases and coke in this work compares qualitatively well with the validated results obtained by Han and Chung (2001a) where the same model was adopted. The difference in the quantity of gasoline produced in this simulation and that of Han and Chung (2001b) is 1.7%, and in the case of the lump, gases, an increase of 10.49% yield was obtained due to higher catalyst inlet temperature as earlier stated.

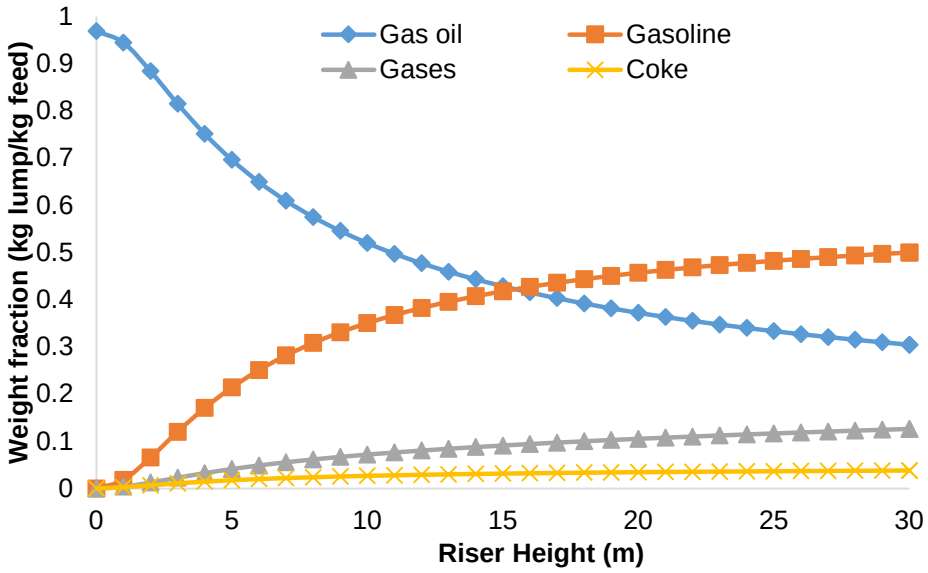

Figure 5.2: Profiles of four lumps along the riser

Figure 5.3 shows the temperature profiles of the gas and catalyst phases as a function of riser height for this simulation. The inlet temperature of the catalyst-phase, which comes from the vaporisation section as 1006.4 K drastically decreases to a minimum in the first 6 m and continue to decrease until it eventually levels out to the riser exit. The inlet temperature of the gas phase, which comes from the vaporisation section at 535 K also rises to a peak in the first 11 m of the riser and levels out for the remaining portion of the riser. Both profiles, with a difference of 483.5 K at the riser inlet, only have a difference of 1.6 K at the exit of the riser. The difference in these temperatures provides the

heat of reaction necessary for completion of the reaction. The temperature profiles obtained in this work are like those obtained in many literatures (Ali et al. 1997; Han and Chung 2001b; Souza et al. 2006).

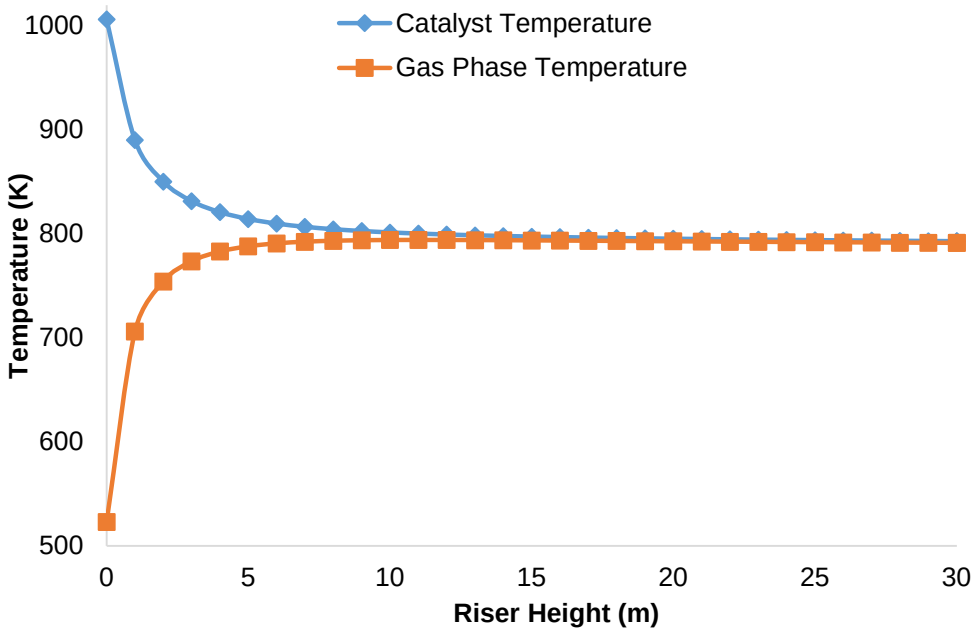

Figure 5.3: Temperature profile along the riser

The velocity profiles of the gas and catalyst phases along the riser height are shown in Figure 5.4. The catalyst and gas velocities emanated from the vaporisation section of the riser unit and rises relatively sharply from about 10.32 m/s at the riser inlet for the gas to about 33.17 m/s at the exit of the riser, and likewise 11 m/s for the catalyst at the inlet to 33.41 m/s at the exit. During the cracking reactions, the slip velocity between the two phases is maintained within 0.675 m/s at the inlet of the riser to 0.246 m/s at the exit of the reactor. The average is comparable to the slip velocity of 0.25 m/s obtained by Han and Chung (2001a).

The velocity profiles of the phases of gas and catalyst show that velocity is not constant along the height of the riser during cracking and it is due to the molar expansion of gases formed as the catalyst moves upward.

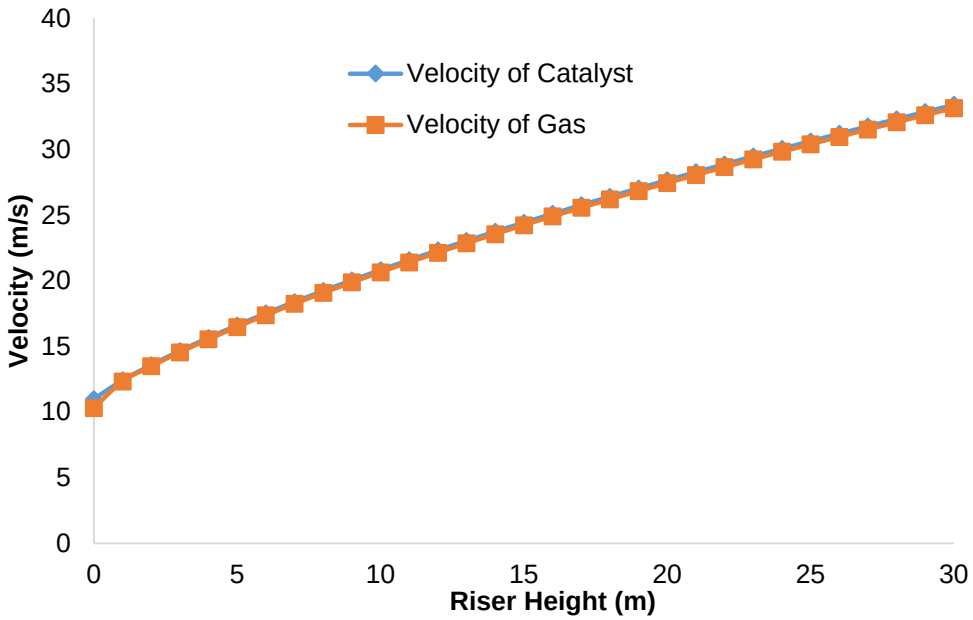

Figure 5.4: Velocity profile of gas and solid phases

Figure 5.5 shows the pressure profile in the riser, which decreases practically linearly from 242.32 kPa at the inlet of the riser coming from the vaporisation section to 203.59 kPa at the exit of the riser. However, in the first 1 m of the riser the pressure rose sharply to 251.49 kPa, mainly due to the vigorous mixing because of the instantaneous vaporisation in the vaporisation section before it steadily decreases towards the outlet of the riser. The total pressure drop is 38.73 kPa for this simulation against 16 kPa, obtained by Han and Chung (2001b). This pressure drop of 38.73 kPa is quite big but can compare closely with operation log data obtained from the Kaduna refinery: 0.28 kg/cm^2 (27.46 kPa) in February 2012; 0.23 kg/cm^2 (22.56 kPa) in April 2014: 0.25 kg/cm^2 (24.52 kPa) in September 2014 and was allowed to have up to 0.31 kg/cm^2 (30.4 kPa). Therefore, the pressure drop in practice could be greater than 16 kPa obtained by Han and Chung (2001a). Another reason for this pressure drop difference is that this simulation only considered part of the riser section of the FCC unit, which is the riser reactor and the vaporisation section. The pressure of the disengaging-stripping section also influences the riser pressure and the pressure of the regenerator section, which were all, considered in the (Han and Chung 2001a; Han and Chung 2001b) simulation but not considered in this simulation. However, the velocities and pressure profiles are qualitatively similar with results obtained by Han and Chung (2001a).

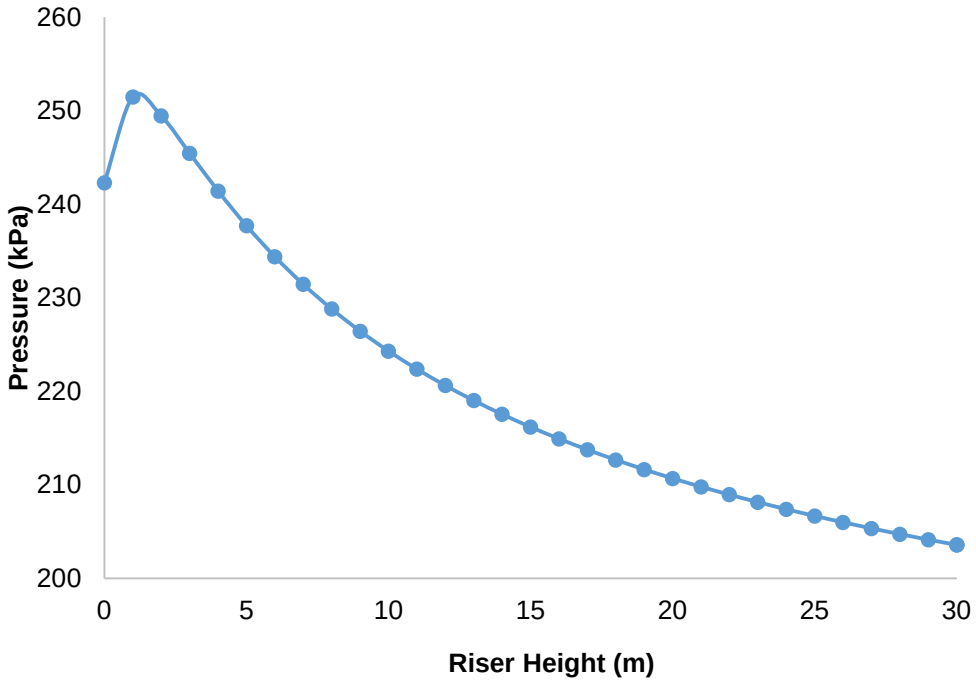

Figure 5.5: Pressure profile along the riser

For the accuracy of this work and to validate the capability of this gPROMS model, results from validated work (Han and Chung 2001a; Han and Chung 2001b) shown in column B of Table 5.1, and Kaduna refinery operational data shown in column C, are used to compare with the results of this simulation work. The catalyst-to-oil ratio (C/O) in this simulation is 6.085, while for the data obtained from Kaduna refinery, the C/O ratio is 7.0. This means that the Kaduna refinery plant data may not be an exact pivot for comparison with this simulation results since the yields from a riser are functions of the feed quality, catalyst type, reaction temperature, catalyst to oil ratio and many other operational variables. However, the deviation may not be too large and small marginal error limits can still be acceptable. Hence, Kaduna refinery data can still be used for validation of this simulation along with the simulated results (Han and Chung 2001a; Han and Chung 2001b) whose plant operational conditions and riser configuration are the same as those used in this simulation.

Table 5.1: Comparison of this riser simulation output results in column A, with (Han and Chung 2001a; Han and Chung 2001b) simulation in column B, and plant data from Kaduna refinery in column C (Chiyoda 1980)

Parameter	Input	Riser output				
		A (This simulation)	B (Han and Chung (2001a, b)	C (Kaduna Refinery)	% Deviation	
					A with B	A with C
Gas oil Temperature (K)	535	791.5	793.5	800.0	-0.25	-1.07
Catalyst Temperature (K)	1006	793.1	796.1		-0.38	
Gas oil mass flowrate (kg/s)	49.3	49.3	49.3			
Catalyst mass flowrate (kg/s)	300	300	300			
Gas oil mass fraction	0.969	0.3045	0.2735	0.236	10.18	22.49
Gasoline mass fraction	0.00	0.4997	0.5085	0.515	-1.76	-3.06
Gases mass fraction	0.00	0.1261	0.1410	0.198	-11.82	-57.01
Coke mass fraction	0.00	0.0381	0.0427	0.051	-12.07	-33.86

The simulation results (Han and Chung 2001a; Han and Chung 2001b) had been validated against plant and literature data, which makes it suitable to be referenced here. From Table 5.1, the deviation (column A with B) between the results of this simulation (column A) and the literature results (Han and Chung 2001a; Han and Chung 2001b) (column B) are within a marginal error of less than 4 %, except for mass fractions of gas oil and coke. The mass fraction of gasoline and temperatures are the most important parameters to compare here and seemed to conform adequately. Hence, it shows that gPROMS is accurate in predicting the results obtained from the literature (Han and Chung 2001a; Han and Chung 2001b) and can be recommended for the simulation of the FCC unit. The deviation between the results of this simulation (column A) and the plant data (column C) for key components like temperatures and gasoline fraction is also within a marginal error limit of 4%. Others are quite wide mainly due to differences in the feed quality, catalyst type, reaction temperature, C/O ratio and other operational variables that differ in the two sets of results. Many literatures however show that the profiles of the yields of gas oil, gasoline, gases, coke and temperatures obtained from this gPROMS simulation are qualitatively consistent (Ali and Rohani 1997; Han and Chung 2001b; Cristina 2015).

5.4 Z Factor analysis

Various Z factor correlations were included in the riser model for the first time to investigate the effect of the compressibility factor on the riser. The simulation is run under the same condition of C/O ratio of 6.085. Figure 5.6 shows the profiles of Z factor along the riser height. Z factor correlation models of Sanjari and Lay (2012) and Shokir et al. (2012) produced negative Z factors along the riser height because of the range of P_{pr} and T_{pr} of this simulation. Hence, their profiles are not included in Figure 5.6. Each Z factor varies along the riser height because of the dependency of some variables such as temperature, pressure, density as well as viscosity, heat of reaction and molar change in composition. At any point for each Z factor model, the Z value is not the same. The Z factor for the assumed ideal gas, being Z = 1, remained constant throughout the riser height while from the Z factors shown in Figure 5.6, Z factor varies along the riser.

From Figure 5.6, not all the Z factor equations can adequately represent the true values of Z factor in the riser. Many of the simulation results are far away from the ideal gas prediction as seen in Figure 5.6, with only the Z factor correlation of

Heidaryan et al. (2010a) coming close. However, this does not mean that the Z factor correlation of Heidaryan et al. (2010a) is the true representation of the Z factor in the riser, there is need to investigate further, how it relates to other process variables in the riser. Many other factors may need to be considered. Factors such as the yield of gasoline and conversion of gas oil for each Z factor correlation, the temperature profiles of the solid and gaseous phases, the pressure profile and pressure drop along the column, the viscosity, which is dependent on P_{pr} and T_{pr} , the C/O ratio and riser diameter.

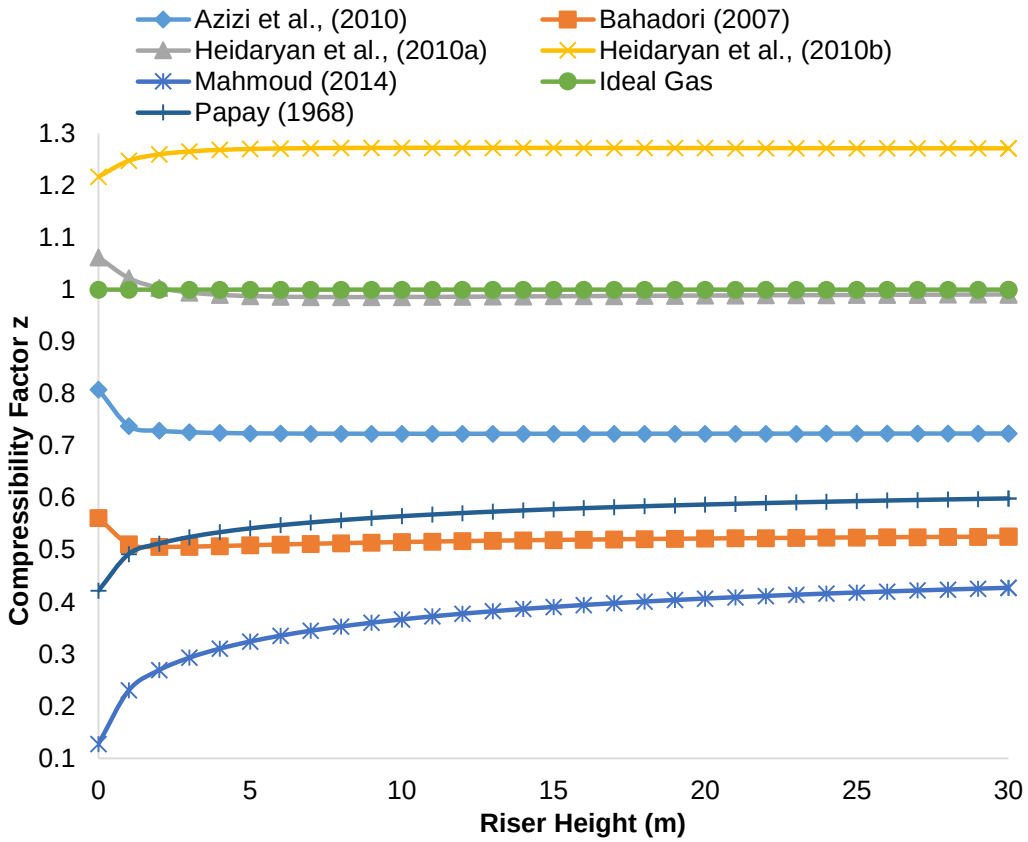

Figure 5.6: Various compressibility factor profiles

Figure 5.7 shows the profiles of viscosity of the gas phase along the riser height. Fluid catalytic cracking breaks down larger hydrocarbon molecules, which due to higher molecular weight have higher viscosity, but when broken-down, the lower molecular weight hydrocarbons tends to have lower viscosity. Hence, the viscosity of the gas oil should be higher at the inlet of the riser and when cracking starts, lower molecular weight hydrocarbons such as gasoline and gases forms the gaseous phase in the riser and the viscosity begins to decrease as seen in Figure 5.7. Although it shows that for ideal gas, the viscosity drops along the riser, one should bear in mind that viscosity is a function of temperature, which

varies along the riser. From Figure 5.7, every Z factor represents a different viscosity profile, which further confirms that Z factor varies along the riser. Unlike the case of the Z factors profiles in Figure 5.6 where the profile for the correlation of Heidaryan et al. (2010a) is very close to the profile of the ideal gas, in Figure 5.7, the profile of viscosity for Bahadori et al. (2007) is the closest to the profile of viscosity for the ideal gas.

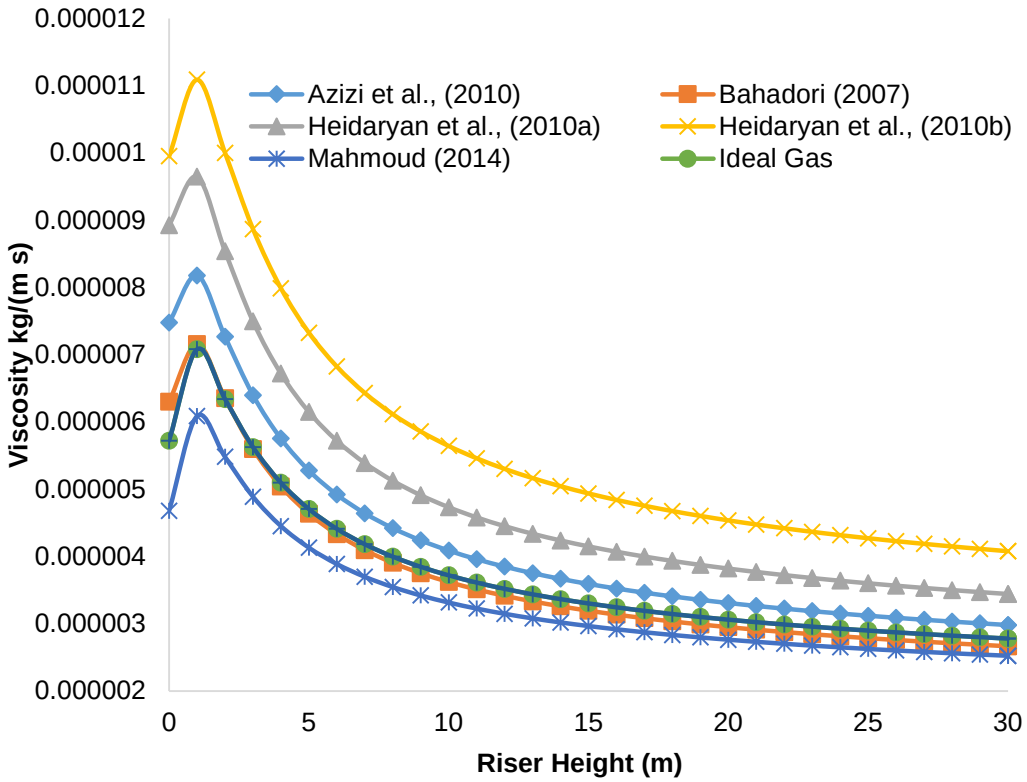

Figure 5.7: Viscosity profile along riser height

Figure 5.8 shows the profiles of the gas and catalyst phase temperatures as a function of the riser height for each Z factor correlation. All of the profiles for both temperature of gas phase and catalyst phase vary from each other in the first 1 m to 5 m height of the riser showing the tendency of each Z factor correlation to be influenced by the temperature change in the riser, which means that different heats of reaction may prevail for different Z factors. This also shows that the heat balance in both the riser and regeneration is altered. However, looking at after a height of 5 m, the profiles tends to come together with almost similar outlet temperatures for both catalyst and gas phases, suggesting that the influence of the Z factor may be felt much only at the first few meters in the riser. The output temperatures are within the limit of acceptability with temperatures of the profile for ideal gas Z factor. Again, it shows that Z factor affects the temperature profile.

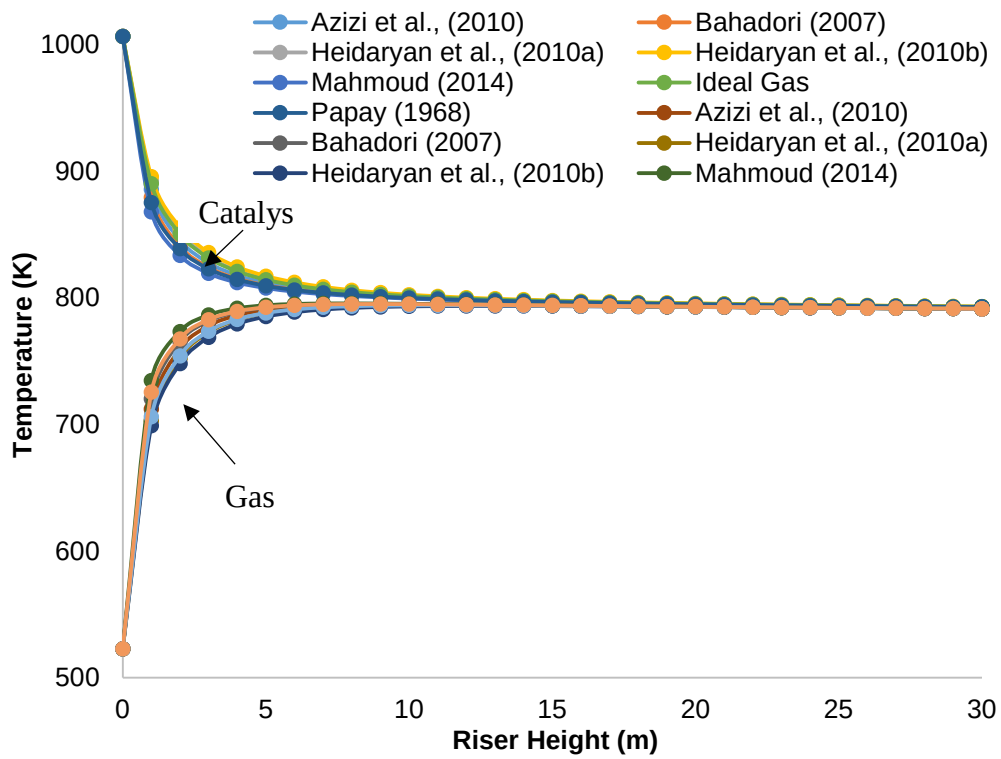

Figure 5.8: Temperature profiles of gas and catalyst phases

The temperature variation with Z factor also affects the yield of products from the cracking reactions. This is because the kinetic reactions are temperature dependent. Therefore, heat of reaction for the different Z factor correlation would eventually change accordingly. Figure 5.9 shows how gasoline and the converted gas oil vary along the riser height for different Z factor correlations. Just as in the case of the temperature, where most of the interactions because of the different Z factors in the riser was centred at the first 5 m of the riser (Figure 5.8), the profiles of both gas oil and gasoline in Figure 5.9 show similar trends. The first few meters of the riser respond differently for different Z factor correlation, confirming that the right Z factor needs to be used in the simulation of the FCC unit. Although the yield of gasoline for all the Z factor correlations show some degree of consistency with the yield of gasoline for the ideal gas Z factor and the plant data, there are still small differences as shown in Table 5.2.

The percentage differences between the gas oil and gasoline with ideal gas Z factor correlation and gas oil and gasoline with other Z factor correlations are an average of 1.21% and 0.51% respectively. If these percentages were achieved on an existing conversion of gas oil and yield of gasoline under optimum operating conditions in the riser, it would amount to more yield of desired product

and eventually increase profitability. These differences shown in Table 5.2 shows that every Z factor used in the riser yields different products.

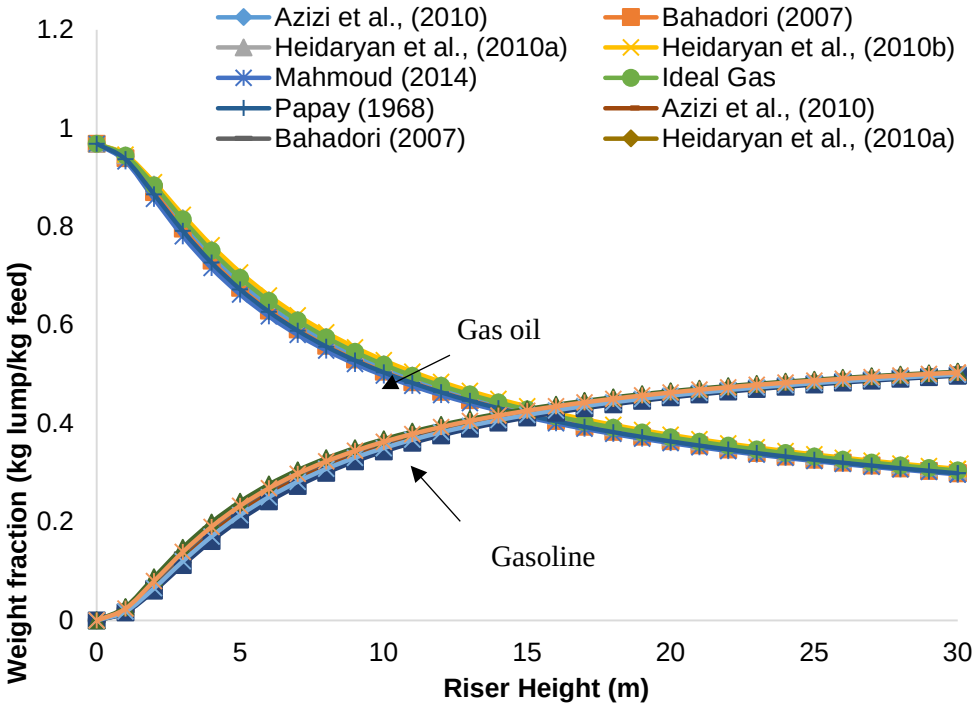

Figure 5.9: Profiles of gas oil and gasoline along the riser

Table 5.2: Gas oil and Gasoline fractions at the exit of the riser

Lump (kg lump/kg feed)	Gas oil	% Difference	Gasoline	% Difference
Azizi et al., (2010)	0.3014	1.02	0.5019	0.42
Bahadori (2007)	0.2991	1.82	0.5036	0.75
Heidaryan et al., (2010a)	0.3046	0.04	0.4996	-0.03
Heidaryan et al., (2010b)	0.3079	1.12	0.4974	-0.48
Mahmoud (2014)	0.2968	-2.60	0.5053	1.10
Ideal gas	0.3045	0.00	0.4998	0.00
Papay (1968)	0.2990	-1.85	0.5037	0.78
Han and Chung (2001b)	0.2735	-11.33	0.5085	1.71

To determine which Z factor correlation is suitable for the riser simulation, an important variable that controls the hydrodynamics of the riser, the riser pressure, was observed. The pressure variation was investigated for all the correlations and compared with the pressures from the models with ideal gas correlations, Kaduna refinery plant and Han and Chung (2001b). The pressures along the riser height for different Z correlations are shown in Figure 5.10, while the inlet and

outlet pressures along with the pressure drops across the riser length for each correlation are shown in Table 5.3.

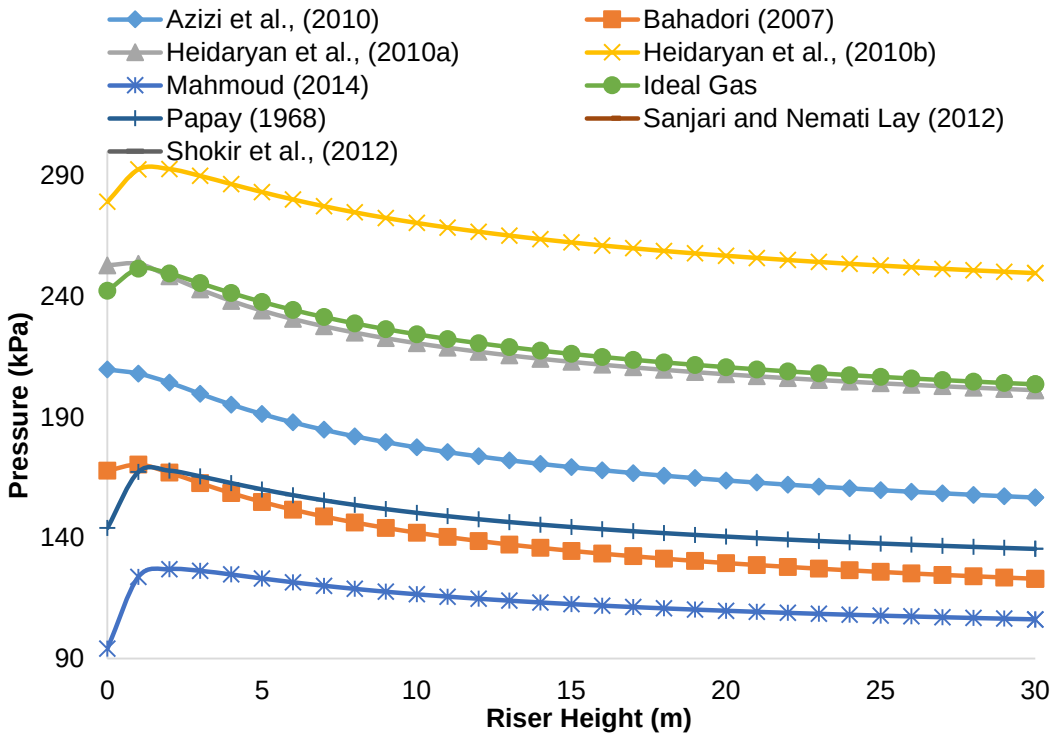

Figure 5.10: Pressure profiles for different Z factor correlations

The pressure profiles in the riser for all the correlations including that with ideal gas, follow a similar pattern. They differ only in the inlet and outlet values. Plant data shows that the riser inlet pressure ranges from 230-270 kPa (Chiyoda 1980), while the simulation of Han and Chung (2001b) shows that the inlet pressure is about 246 kPa. Going by these inlet conditions, Figure 5.10 shows only the correlations with ideal gas Z = 1 and Heidaryan et al. (2010a) fall within the range given by Chiyoda (1980) and come close to 246 kPa. Hence, the model of Heidaryan et al. (2010a) can be considered suitable for the Z factor correlation in the riser simulation. The ideal gas correlation, which considered Z equal to one, even though it predicted the riser inlet pressure to be within the range given by Chiyoda (1980) and the 246 kPa, may not be suitable. This is because, according to the Han and Chung (2001b) simulation, the ideal gas pressure correlation does not vary along the riser length against the fact that the pseudo-reduced temperature and pseudo-reduced pressure (variables that depend on Z factor) do vary along the length of the riser (Pareek et al. 2003).

Another aspect of the pressure profiles in Figure 5.10 to consider is the pressure drop. According to the Han and Chung (2001b) simulation, the pressure drop is 16 kPa as seen in Table 5.3.

Table 5.3: Riser pressure drop (DeltaP) for different Z factor correlations

Pressure (kPa)	Riser inlet	Riser outlet	DeltaP	DeltaP (Han and Chung (2001b))	DeltaP Kaduna refinery
Azizi et al. (2010)	209.75	156.70	53.05	16.000	27.46
Bahadori et al. (2007)	167.83	123.08	44.75	16.000	27.46
Heidaryan et al. (2010a)	252.88	201.18	51.70	16.000	27.46
Heidaryan et al. (2010b)	279.15	249.65	29.50	16.000	27.46
Mahmoud (2014)	94.12	106.27	-12.15	16.000	27.46
Ideal gas	242.32	203.60	38.72	16.000	27.46
Papay (1968)	144.10	135.45	8.65	16.000	27.46

The pressure drop in the industrial riser as seen in Table 5.3 is 27.46 kPa (Chiyoda 1980). Clearly, none of the pressure drops from the correlations in Table 5.3 came close to 16 kPa except that the pressure of 29.50 kPa from Heidaryan et al. (2010b) correlation is close to 27.46 kPa of Kaduna refinery (Chiyoda 1980). Even though the correlation of Heidaryan et al. (2010b) gave a closer pressure drop than the correlation of Heidaryan et al. (2010a), the latter correlation predicts the riser inlet pressure better and follows very closely the pressure profile of Z factor correlations with ideal gas and its Z factor profile as shown in Figure 5.11.

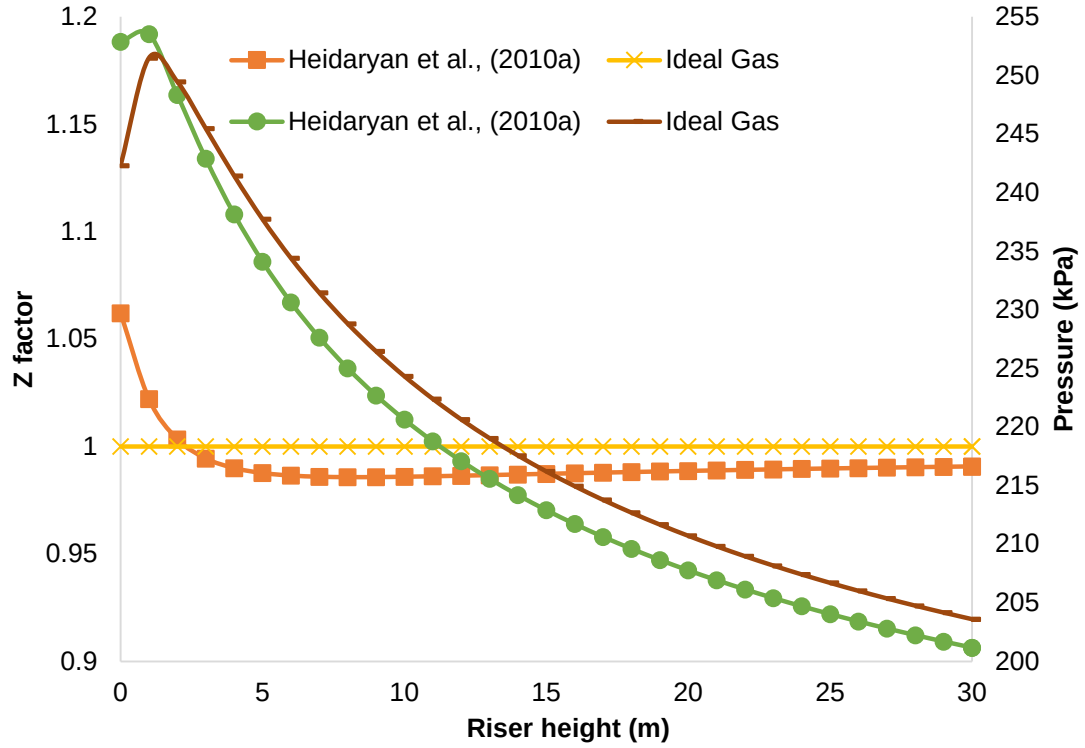

Figure 5.11: Pressure and velocity profiles along the riser

The difference between the pressures predicted by the riser model with Z factor correlation of Heidaryan et al. (2010a) and that of the ideal gas at the inlet of the riser is 10.25 kPa and at the outlet, it is -2.42 kPa. The difference between the Z factor predicted by the riser model with Z factor correlation of Heidaryan et al. (2010a) and that of the ideal gas at the inlet of the riser is 0.062 and at the outlet, it is -0.01. These differences are the least between any of the correlations. It is also the least difference between all the correlations and the two correlations of Heidaryan et al. (2010a) and that of the ideal gas at the inlet of the riser. Heidaryan et al. (2010a) and the ideal gas Z factor correlations predict the inlet pressure much closely to the plant inlet pressure (Chiyoda 1980), and the pressure of Han and Chung (2001b) model. Heidaryan et al. (2010a) Z factor correlation will be used for the riser simulation since it predicts the Z factor across the length of the riser.

To observe the behaviour of the Heidaryan et al. (2010a) Z factor correlation on varying catalyst-to-oil ratio (C/O) and varying riser diameter, four different C/O were used with a riser model that incorporates the Heidaryan et al. (2010a) Z factor correlation. Each C/O ratio was varied against the correlations of Heidaryan et al. (2010a) Z factor and that for the ideal gas to see the impact on the pressures at inlet and the outlet. In addition, since most of the assumptions made in

modelling the riser unit by considering its gas phase as ideal gas came from experiments with very small riser diameters, the Z factor impact is studied over varied industrial riser diameter.

Figure 5.12 shows the variation of pressure for Heidaryan et al. (2010a) Z factor correlations at different C/O ratios.

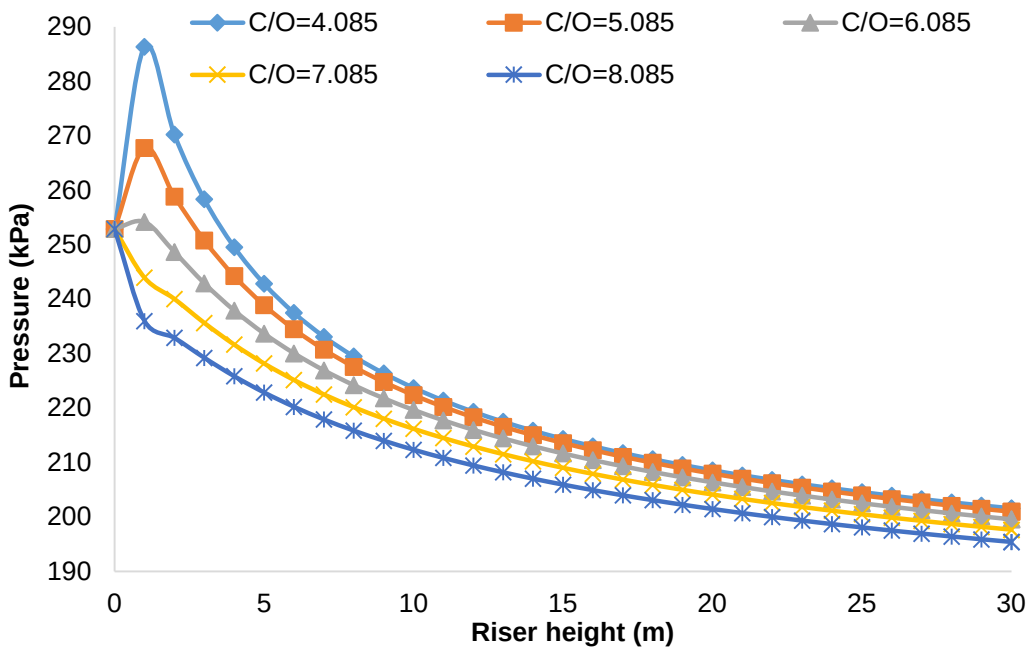

Figure 5.12: Pressure profiles for different C/O with Z factor correlation

All the profiles started at the riser inlet pressure of 252.88 kPa but behaved differently in the first 5 – 10 m of the riser and eventually level out. The varied behaviour at the beginning of the riser is because of the expansion of the gas phase caused by the high temperature and mixing from the vaporisation section. At C/O ratio of 8.085, the pressure decreases immediately after entering the riser. This is because, at higher mass flow rate of catalyst, the residence time is less, and the expansion of the gas phase is distributed along the riser. When the C/O ratio is decreased to 4.085, mass flowrate of catalyst is decreased, causing brief accumulation of catalyst at the bottom of the riser (Das et al. 2007). Hence, the residence time for catalyst at the bottom of the riser slightly increased to allow more heat to be absorbed from the catalyst for the vaporisation, causing the gas oil in contact with the catalyst to expand much more. This is the reason for the rise in the pressure profile.

This trend is also followed in Figure 5.13 for the variation of pressure for the ideal gas Z factor correlations, and at different C/O ratios. The first 5 m of the riser

shows a higher interaction of the pressure for lower C/O ratio 4.085 where the inlet pressure is 242.32 kPa but shoots up to 283.6 kPa in the first 1 m before it decreases and levels out. This is due to brief accumulation of catalyst at the bottom of the riser at this C/O ratio (Das et al. 2007). Unlike the low interaction observed for the higher C/O ratio 8.085 where the inlet pressure 242.32 kPa drops to 233.05 kPa before it eventually levels out. The pressure profiles for the Heidaryan et al. (2010a) Z factor correlation in Figure 5.12 levels out evenly without the overlap observed in Figure 5.13 for the pressure profiles of the ideal's gas Z factor. Therefore, the pressure drops for the two Z factor correlations at different C/O ratio were obtained and presented in Table 5.4.

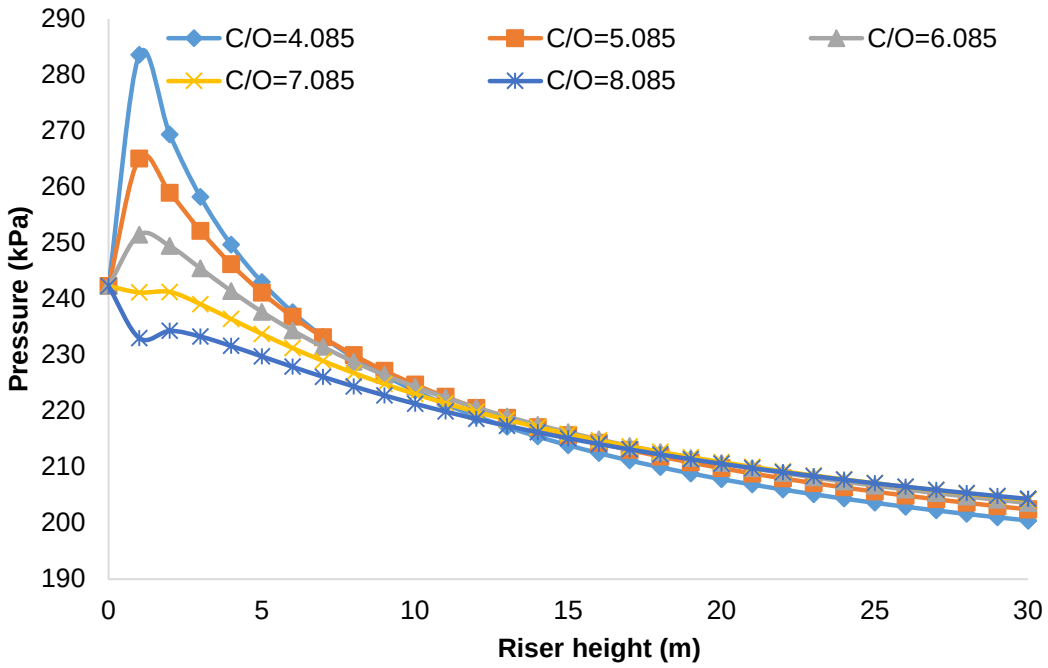

Figure 5.13: Pressure profiles along riser height for different C/O for Z = 1

Table 5.4 shows pressure measurements for two correlations, Heidaryan et al. (2010a) Z factor correlation and the ideal gas Z factor, Z = 1, at different C/O ratios. Values at C/O ratios of 9.085 and 10.085 were obtained to find out if the pressure drop for the ideal gas Z factor correlation, continue to drop after C/O ratio 8.085. The variation of the pressure drop with C/O ratios are presented in Figure 5.14.

Table 5.4: Pressures for different Z factor correlations at different C/O ratio

C/O ratio	Pressure with Heidaryan et al. (2010a)			Pressure with Z factor = 1		
	Riser inlet	Riser outlet	DeltaP	Riser inlet	Riser outlet	DeltaP
4.085	252.88	201.58	51.30	242.32	200.47	41.85
5.085	252.88	200.96	51.92	242.32	202.45	39.87
6.085	252.88	199.57	53.31	242.32	203.60	38.72
7.085	252.88	197.67	55.21	242.32	204.17	38.15
8.085	252.88	195.41	57.47	242.32	204.33	37.99
9.085	252.88	192.91	59.97	242.32	204.20	38.12
10.085	252.88	190.23	62.65	242.32	203.86	38.46

The pressure drop at different C/O for the two correlations were investigated to observe the behaviour of the Z factor as it affects the pressure drop at every C/O. It can be seen from Figure 5.14 that the pressure drops for the ideal gas Z factor correlation decreased nonlinearly from 41.85 kPa across the riser height at C/O ratio of 4.085 to a minimum of 37.99 kPa at 8.085 before rising again. This is not the case with the pressure drop observed with the Z factor correlation of Heidaryan et al. (2010a), where the pressure drop continues to rise polynomially from a value of 51.30 kPa across the riser height at C/O ratio of 4.085 without any minimum. A pressure drop of 163 kPa across the riser height has been reported in the literature (Chang et al. 2012a; Pelissari et al. 2016) and a variation between 200 kPa and 250 kPa across the riser height over a period of 69 hours was also reported (Pinho et al. 2017).

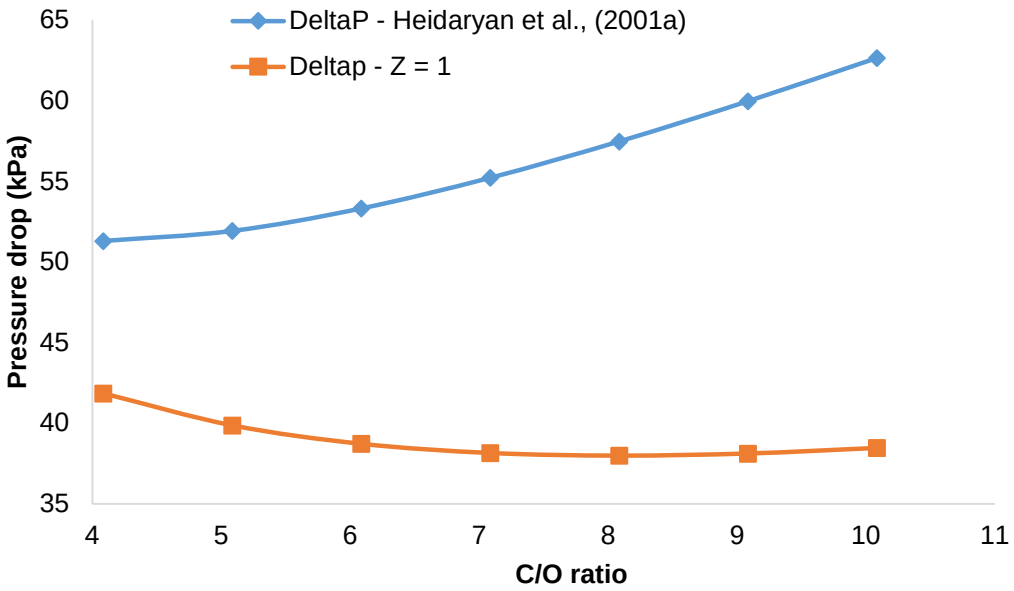

Figure 5.14: Pressure drop at different C/O ratio

Using the statistical modelling approach, trendlines obtained from the curves in Figure 5.14 show that the pressure drop can be predicted as a function of the C/O ratio from the following polynomial equations of fourth order with both equations having a coefficient of determination, $R^2 = 1$.

For the Z factor correlation of Heidaryan et al. (2010a), the equation is

$$\Delta P = 0.0026\,(C/O)^4 - 0.0969\,(C/O)^3 + 1.4539\,(C/O)^2 - 7.5762\,(C/O) + 63.872 \quad (5.24)$$

For the Z factor correlation of ideal gas Z = 1, the pressure drop equation is

$$\Delta P = 0.0025\,(C/O)^4 - 0.0958\,(C/O)^3 + 1.4864\,(C/O)^2 - 10.514\,(C/O) + 65.827 \quad (5.25)$$

Once a C/O ratio is known, these equations can provide the pressure drop values across the riser height in meters.

Figure 5.15 shows the variation of Z factor of Heidaryan et al. (2010a) along the riser for different C/O ratios. The Z factor for an ideal gas would remain constant at 1.0 across the length of the riser. Figure 5.15 shows that the Z factor is not constant across the length of the riser because pseudo-reduced pressure and pseudo-reduced temperature vary from the bottom to the top (Pareek et al. 2003). This understanding may be of particular interest for the engineers when designing the riser.

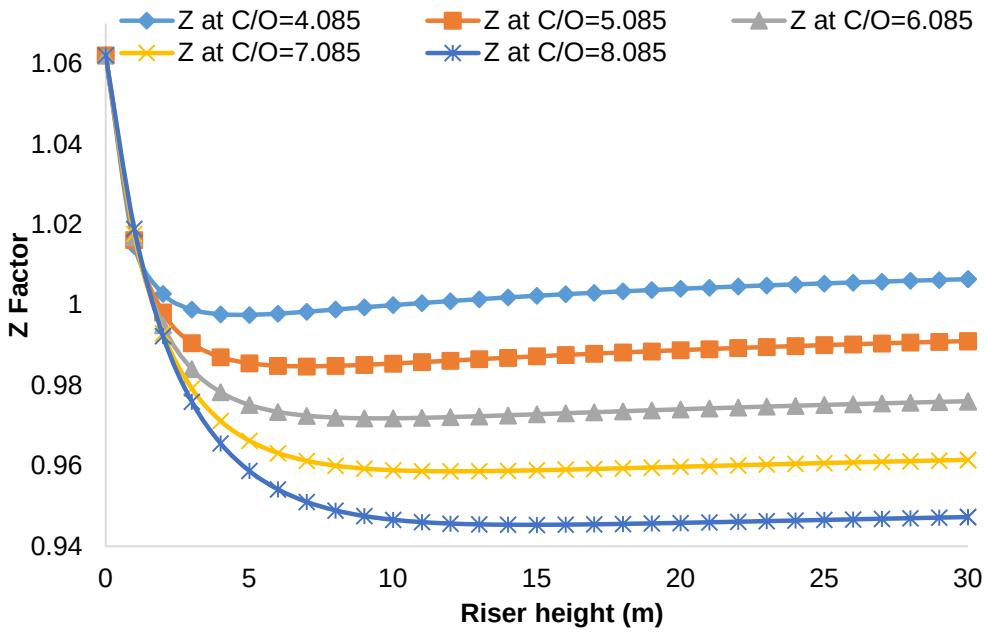

Figure 5.15: Z Factor correlation of Heidaryan et al. (2010a) at different C/O

In Figure 5.15, the Z factor at riser inlet for all C/O ratios is 1.0621, which would be different in the case of the ideal gas being constant Z = 1 at inlet and at any point in the riser. At C/O ratio of 8.085, the Z factor at the exit of the riser is 0.9473 while at C/O ratio 4.085 the Z factor at the exit of the riser is 1.0065. This shows that the higher the C/O ratio, the further the Z factor profile and exit value from other C/O ratios Z factor profiles and exit values. It is also further away from what was considered for the ideal gas Z = 1 constant across the riser length. To obtain a statistical model for this relationship, Z factors at the exit of the riser for C/O ratios 9.085 and 10.085 at the same process conditions were obtained and presented in Table 5.5, along with other C/O ratios.

Table 5.5: Z factor correlation of Heidaryan et al. (2010a) at different C/O ratio

C/O ratio	Z factor of Heidaryan et al. (2010a)		
	Riser inlet	Riser outlet	Delta Z
4.085	1.06	1.01	0.05
5.085	1.06	0.99	0.07
6.085	1.06	0.98	0.08
7.085	1.06	0.96	0.10
8.085	1.06	0.95	0.11
9.085	1.06	0.93	0.13
10.085	1.06	0.92	0.14

The Z factor change for each C/O ratio at the riser inlet and outlet is also present in Table 5.5. It shows that the higher the C/O ratio, the higher the Z factor. This also confirms that Z factor vary with C/O ratios and not constant for all C/O ratios as always considered in the literature. Figure 5.16 shows how change in Z factor varies with the C/O ratios. A statistical correlation with $R^2 = 1$ is obtained for the varying Z factor with C/O ratio and given as:

$$Delta\ Z = -0.0002\ (C/O)^2 + 0.0169\ (C/O) - 0.0104 \quad (5.26)$$

Once the inlet Z factor is known, the change in Z can be obtained at a given C/O ratio, which will eventually lead to the exit Z factor from the difference. It also shows the extent in numerical terms how the real Z factor varies from the ideal gas phase Z factor.

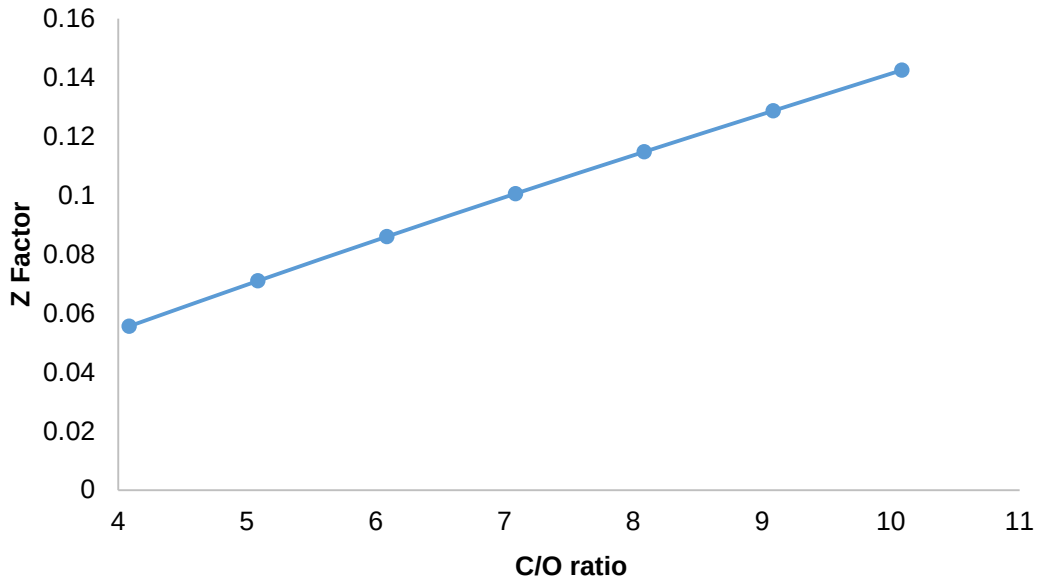

Figure 5.16: Z factor at various C/O

Figure 5.17 presents the pressure profile for different riser diameters for Z factor correlation of Heidaryan et al. (2010a) and Z factor correlation of ideal gas at a C/O ratio of 6.085. This is to find out the pressure drop at larger diameter because experiments that informed the assumptions to treat the gas phase as an ideal gas came from very small diameter risers.

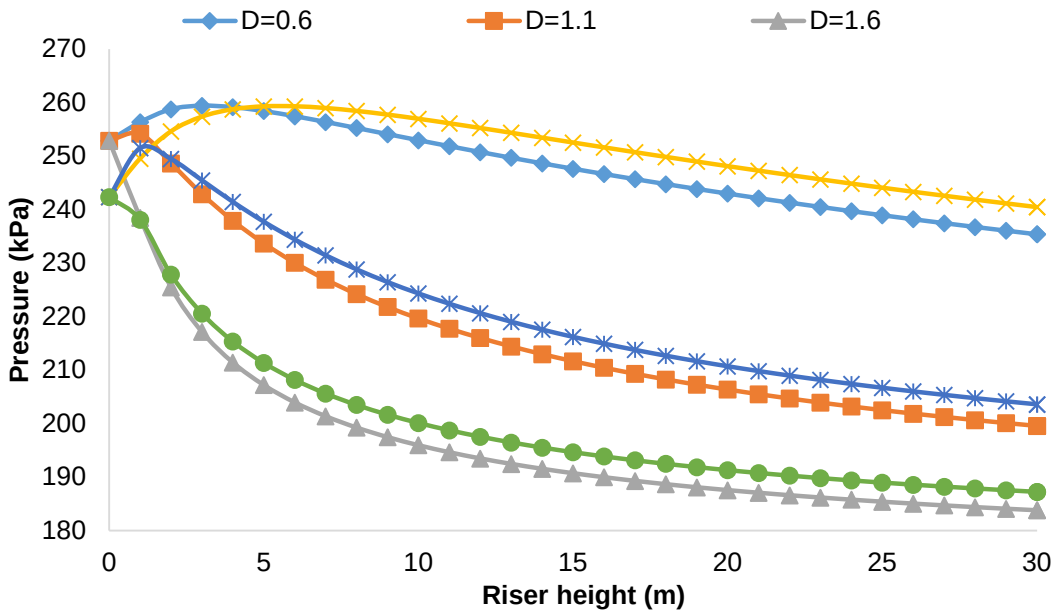

Figure 5.17: Pressure profile for different diameters at different Z factor correlation

At lower riser diameter of 0.6 m, the pressure profiles for both Z factor of ideal gas and Heidaryan et al. (2010a) show lower pressure drops as shown in Table 5.6. When the diameter was increased to 1.1 m and 1.6 m, the pressure drops increased for both profiles and Z factors also shown in Table 5.6.

Table 5.6: Z factor correlation of Heidaryan et al. (2010a) at different C/O ratio

Riser diameter (m)	Z factor	Pressures (kPa)		
		Riser inlet	Riser outlet	Delta P
0.60	Heidaryan et al. (2010a)	252.88	235.38	17.50
	Ideal gas Z = 1	242.32	240.46	1.86
1.1	Heidaryan et al. (2010a)	252.88	199.57	53.31
	Ideal gas Z = 1	242.32	203.60	38.72
1.6	Heidaryan et al. (2010a)	252.88	183.78	69.10
	Ideal gas Z = 1	242.32	187.24	55.08

The pressure drop increases as the diameter increases as stated in the literature (Santos et al. 2007) and as seen in Figure 5.18. The profile of the pressure drop that represents the Z factor of Heidaryan et al. (2010a) has higher pressure drops than the profile for the Z factor of the ideal gas. Though both profiles follow a similar pattern, the Z factor of Heidaryan et al. (2010a) correlation affects the pressure regime in the riser.

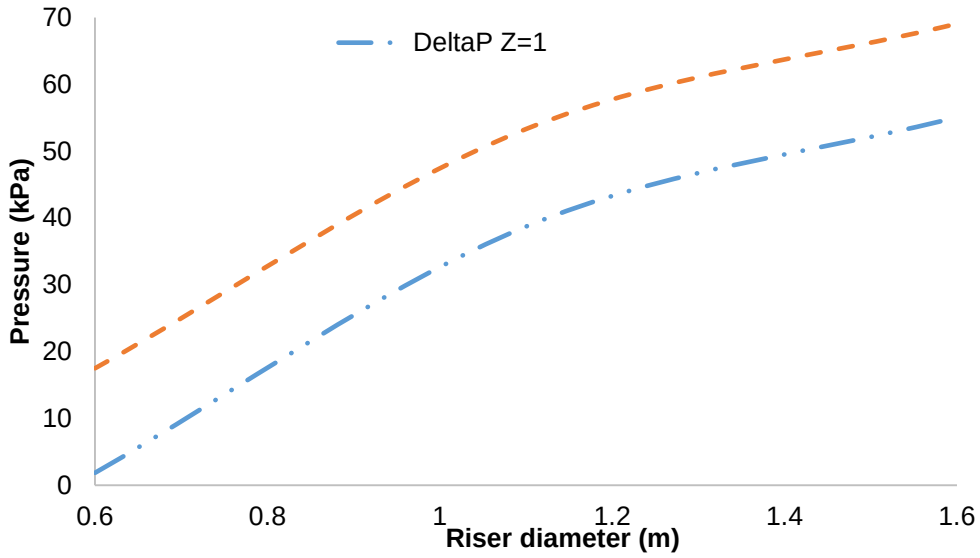

Figure 5.18: Pressure drop across the riser at different diameters for different Z factors

Figure 5.19 shows the Z factor correlations of Heidaryan et al. (2010a) profile for different riser diameters at a C/O ratio of 6.085. For the three risers with different diameters, the Z factor at the entrance of the riser is 1.06 and decreases to an average of Z factor 0.97. The profile for the 0.6 m diameter riser descended smoothly to a Z factor of 0.97 in the first 13 m of the riser. The Z factor profiles for 1.1 m and 1.6 m diameter riser descended sharply and reached the average Z factor of 0.97 in the first 5 m. Clearly, from Figure 5.19, the Z factor correlation of Heidaryan et al. (2010a) behave differently as the diameter of the riser increases. Therefore, every riser may have its different Z factor profile because of its diameter.

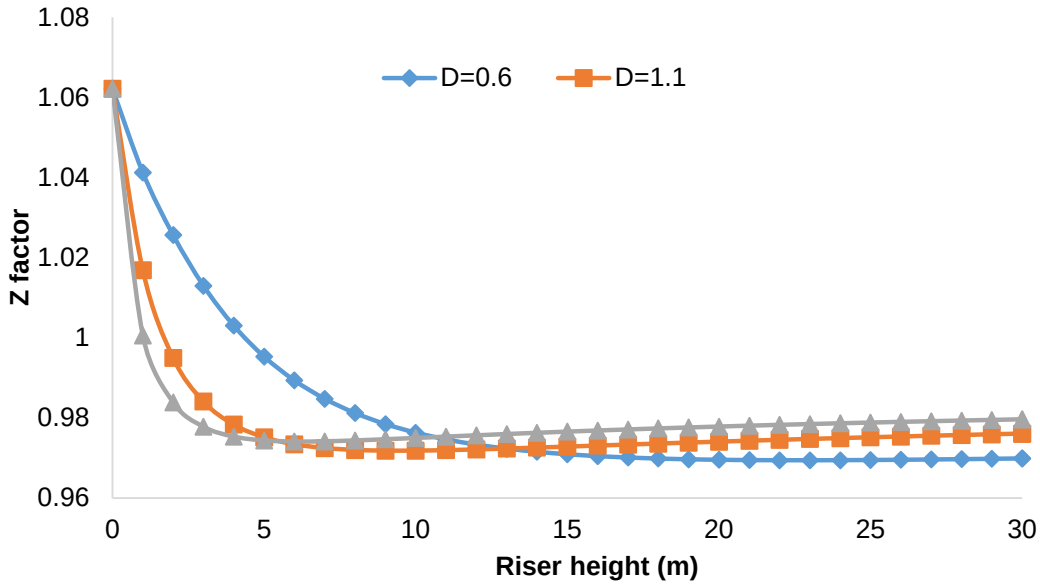

Figure 5.19: Profile of Z factor of Heidaryan et al. (2010a) along the riser

5.5 Summary

A steady state detailed FCC riser process model is for the first time simulated with different Z factor correlations implemented on gPROMS software. A 4-lump kinetic model is used where gas oil cracks to form gasoline, coke and gases. The following conclusions can be made:

- The simulation results from this work compare favourably with the results obtained by Han and Chung (2001b) where the model of the riser was adopted, and with plant data. Thus, demonstrating the capability of the gPROMS software in simulating the riser of the FCC unit. Hence, gPROMS can be recommended for the simulation of the entire FCC unit.
- The Heidaryan et al. (2010a) Z factor correlation is suitable in representing the Z factor across the riser.
- Using different Z factors in the simulation of the riser with the same process conditions yields different profiles for some process variables such viscosity of gas phase, heat of reaction due to varying temperature profiles and varying compositions at every point in the riser.
- The pressure at every point in the riser is different for different C/O ratios. The pressure is also different at every point when the Heidaryan et al. (2010a) Z factor correlation is used as opposed to when the gas phase is treated as an ideal gas.
- When operating an industrial riser, increase in pressure drop follows a polynomial function at varying C/O ratios.
- The higher the C/O ratio, the further away the gas phase behaves from the ideal gas.
- The higher the C/O ratio, the higher the change in Z factor between the inlet and outlet Z factor of the riser.
- A correlation is developed to measure the magnitude of deviation of the gas phase from ideal gas.
- Every riser has a different pressure profile and Z factor profile depending on the riser diameter.

Chapter 6

Optimisation of Operating Conditions to Maximise Yield and Minimise CO_2

6.1 Introduction

Many processes in the downstream sector of the petroleum industry produce gasoline, diesel and propylene; however, not all processes are as good as using the FCC unit to meet the high demand for fuels and other products. For instance, a typical barrel of crude is approximately 20% straight run gasoline, but demand is nearly 50% per barrel, which can be met using an efficient FCC unit. This could be achieved by using the riser to crack gas oil (mostly a product of the atmospheric and vacuum distillation unit) into lighter hydrocarbons such as gasoline.

The riser has a very high profitability and hence operate at maximum capacity, that is, maximum feed rate and maximum power applied to auxiliary equipment like the gas compressor and air blower drivers (Almeida and Secchi 2011). However, the optimal operating conditions of an FCC riser required to operate at the maximum capacity of the plant change with the changes in quality and nature of blends of the feedstock (Almeida and Secchi 2011). Other issues that affect the operating conditions can be environmental changes and the desire to make large profits via increased production of gasoline by cracking the various intermediate fractions into gasoline or by converting the gasoline fractions into LPG.

The riser is a complex unit due to its multivariable nature, nonlinear features, complex dynamics, severe operating restrictions and strong interactions among the process variables. These pose a challenging optimisation problem, though; even little improvements in the optimal operation of the riser can lead to large economic benefits (Zanin et al. 2002; Vieira et al. 2005). In addition, due to the complex nature of the processes involved in the FCC unit, there is not yet an answer to the question of how best to operate it (Zanin et al. 2002; Vieira et al. 2005). Any attempt to optimise the riser is an attempt to establish the best operational route for the unit and that is what this work sets to achieve.

Many optimisation studies have been carried out on the FCC unit and presented in the literature; some of them used single objective function (Sankararao and Gupta 2007). Other techniques that are used to set optimal operating conditions for the FCC unit are the Genetic Algorithm (GA) and Particle Swarm Optimisation (PSO) evolutionary methods. Both algorithms gave good and consistent results for typical FCC optimisation problems (Bispo et al. 2014).

In obtaining solutions to the optimisation problems, some of the techniques used required the writing of codes for complex model equations, but it is time consuming and not void of error. Sometimes, having oversimplified models limit the accuracy of results. To eliminate this challenge, a fast and sufficiently precise model, not too simplified, is required for optimisation. According to Souza et al. (2011) an adequate model used for optimisation should have a fast and sufficiently precise code that can be used to run several simulations (each one for a specific operating condition) and be able to search for the best values for the input variables (mass concentrations, temperatures, etc.). This however is a difficult balance (i.e., a fast and sufficiently precise model) (Souza et al. 2011). The model used in this work is a one-dimensional momentum, energy and mass balance model (Han and Chung 2001a; Han and Chung 2001b). A one-dimensional momentum, energy and mass balance model was considered to be adequate for optimisation studies because it is able to predict the overall performance of the FCC riser unit (Theologos and Markatos 1993). Hence, the model used in this optimisation study is deemed adequate for riser optimisation. This study is an attempt to improve the profitability of the FCC unit, by maximizing the yield of gasoline in a single objective function while optimizing the operating variables of the riser.

In separate optimisation schemes, the same riser model is used with a six-lumped kinetic model in addition to the new kinetic parameters developed in this work to optimise the yield of propylene. Regenerator model (Han and Chung 2001a; Han and Chung 2001b) is used to minimise the CO_2 emission from the regenerator. gPROMS uses a successive reduced quadratic programing (SRQPD), a sequential quadratic programming based solver to maximise the yield of gasoline and propylene in the riser and minimise the CO_2 emission in the regenerator. The optimisation results were compared with the data in several open-literatures (Han and Chung 2001a; Han and Chung 2001b; Ancheyta and Rogelio 2002; Han et al. 2004).

6.2 Optimisation problem formulation

Three different optimisation problem statements were presented. They are for the maximisation of gasoline in the riser, maximisation of propylene in the riser, and minimisation of CO_2 emission from the regenerator.

6.2.1 Optimisation problem statement for gasoline maximisation

In the past, different modelling and optimisation platform/software such as Matlab and Hysys were used for FCC simulation/optimisation but very little with gPROMS, despite its robustness. In this work gPROMS is used for the riser optimisation. Several FCC models have been proposed in the literature for the optimisation of FCC units (Ellis et al. 1998; Han et al. 2004; Souza et al. 2009). Most of the optimisations were based on the maximisation of the production of products with economic objectives, where the best operating conditions (e.g., mass flows, inlet temperatures) were determined for the maximum performance (Souza et al. 2011). In this study, maximisation of gasoline product is considered.

The optimisation problem can be described as:

Given	the fixed volume of the riser
Optimise	the mass flowrate of catalyst, mass flowrate of gas oil and temperature profiles of gas phase and catalyst.
So as to maximise	the yield of gasoline
Subject to	constraints on the mass flowrates of catalyst and gas oil, temperatures of gas phase and catalyst, exit concentrations of gases and coke.

Mathematically, the optimisation problem can be written as;

$$\max_{T(x) or\ F_J(x)} \quad Z$$

$$s.t.$$

$$f(x, z'(x), z(x), u(x), v) = 0 \ (\text{model equations})$$

$$x_f = x_f^*$$

$$T_L \leq T \leq T_U \ or \ F_L \leq F \leq F_U$$

$$Y_{CD} < {Y_{CD}}^*$$

Where Z is the yield of gasoline, the desired product in the riser, *T* the catalyst and gas phase temperature, F_J the mass flow rates of catalyst and gas oil, x_f the height of the riser, Y_{CD} the yield of gases and coke, $T_L \text{ and } T_U$ the lower and upper bounds of the catalyst phase temperature ($788 \leq T_c \leq 933\ K$) and gas phase temperature ($785 \leq T_g \leq 795\ K$) respectively, $F_L \text{ and } F_U$ the lower and upper bounds of the mass flowrate of catalyst ($200 \leq F_{cat} \leq 500 \frac{kg}{s}$) and mass flowrate of gas oil ($20 \leq F_g \leq 100 \frac{kg}{s}$) respectively, x_f^* the fixed height of the riser and $Y_{CD}{}^*$ the maximum allowable limit for gases $Y_C < 0.2$ and coke $Y_D < 0.1$.

In choosing the upper and lower limits of the decision variables, it is well-known that temperature of the reacting phases in the riser and catalyst-to-feed flow ratio, C/O are the dominant cracking intensity indicators (He et al. 2015), they are strong determinants of conversion of feedstock and yield of products (León-Becerril et al. 2004). Hence, the temperatures and mass flowrates of the catalyst and gas oil were chosen as the decision variables. And for the choice of the upper and lower limits for the decision variables, depending on the feed preheat, regenerator bed, and riser outlet temperatures, the ratio of catalyst to oil is normally in the range of 4:1 to 10:1 by weight (Kasat et al. 2002; Sadeghbeigi 2012b). Therefore, the lower and upper bounds of the catalyst flow rate and the feed flow rate which makes the catalyst-to-feed flow ratio, C/O were chosen to lie between 4 and 10.1 at all points during the optimisation run. Below and above these ratios, unnecessary steady states occur that have no relevance in industrial operations. In addition, the upper limit of the feed temperature and lower limit of the catalyst temperature were chosen to avoid the production of more coke, more gases and promote secondary reactions of gasoline. For the same reason the lower limit of the temperature of the catalyst phase was chosen.

6.2.1.1 Results for gasoline maximisation

Both simulation and optimisation results are presented in this section. The purpose of presenting the simulation results is to demonstrate the capability of gPROMS in solving complex nonlinear DAEs by validating the results against those predicted by the same model (Han and Chung 2001b).

6.2.1.1.1 Simulation results

As gas oil encounters the catalyst, it begins to crack to form cracked lumps; gasoline, gases and coke. In this study, the cracking reaction is set to take place at gas oil inlet temperature of 535 K and the inlet temperature of catalyst at 933 K. The profiles of the products are presented in Figure 6.1.

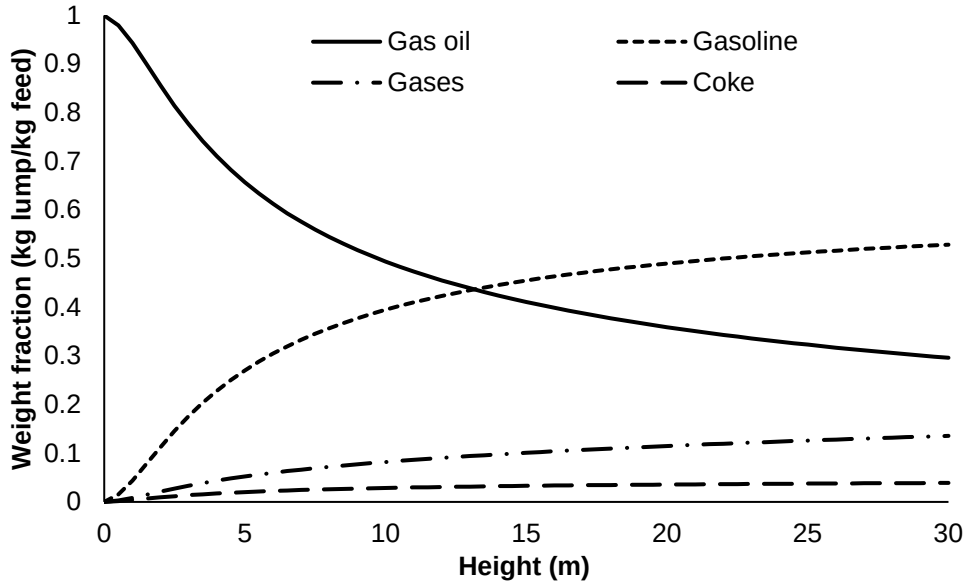

Figure 6.1: Base case steady-state lumps profiles along the riser

The fraction of the gas oil at the exit of the riser is 0.296 (kg lump/kg feed) which is 29.6% of gas oil left unconverted. It also means, about 70.4% of gas oil was consumed and 70% of the fraction is consumed in the first 14 m of the riser. In (Han and Chung 2001b), the fraction of gas oil at the exit of the riser is 0.276 (kg lump/kg feed) which corresponds to 72.4% of gas oil consumed. This difference can be caused by the assumption in this study of using instantaneous vaporisation of gas oil. This explains the reason for some differences which can be noticed for the other lumps; gasoline, gases and coke at the exit of the riser for this study and that of Han and Chung (2001b).

The gasoline profile increases nonlinearly from 0 (kg lump/kg feed) at the inlet of the riser to its maximum yield of 0.529 (kg lump/kg feed) and essentially levels out at the exit of the riser. The catalytic cracking of gas oil is a multiple reaction (Du et al. 2015b), and gasoline being an intermediate is expected to rise to a maximum and then fall due to a secondary reaction as seen in Figure 6.1. The yield almost compares favourably with the value of about 51.2 wt% obtained by Han and Chung (2001b). The coke concentration increases nonlinearly from 0

(kg lump/kg feed) at the inlet to 0.039 (kg lump/kg feed) at the exit of the riser. Coke concentration at the riser exit from Han and Chung (2001b) is 0.047 (kg lump/kg feed). The yield of the gases increases nonlinearly from 0 (kg lump/kg feed) at the inlet of the riser to a maximum of 0.136 (kg lump/kg feed) at the exit. The concentration of gases at the riser exit from Han and Chung (2001b) is 0.142 (kg lump/kg feed). The profile of gases and coke in this work compares qualitatively well with the validated results obtained by Han and Chung (2001b) where the same model was adopted.

Figure 6.2 shows the temperature profiles of the gas and catalyst phases as a function of riser height at base case condition (simulation). The temperature of the catalyst-phase starts from about 933 K and decreases for the first 8 m and then essentially levels out. The temperature profile of the gas phase starts from about 535 K and rises to a peak in the first 6 m of the riser and levels out for the remaining portion of the riser. Both profiles came so close to the same value with temperature difference of about 1 ^{o}C which is necessary for the completion of the reaction. The temperature profiles obtained in this work are like those obtained in many literatures (Ali et al. 1997; Han and Chung 2001b; Souza et al. 2006).

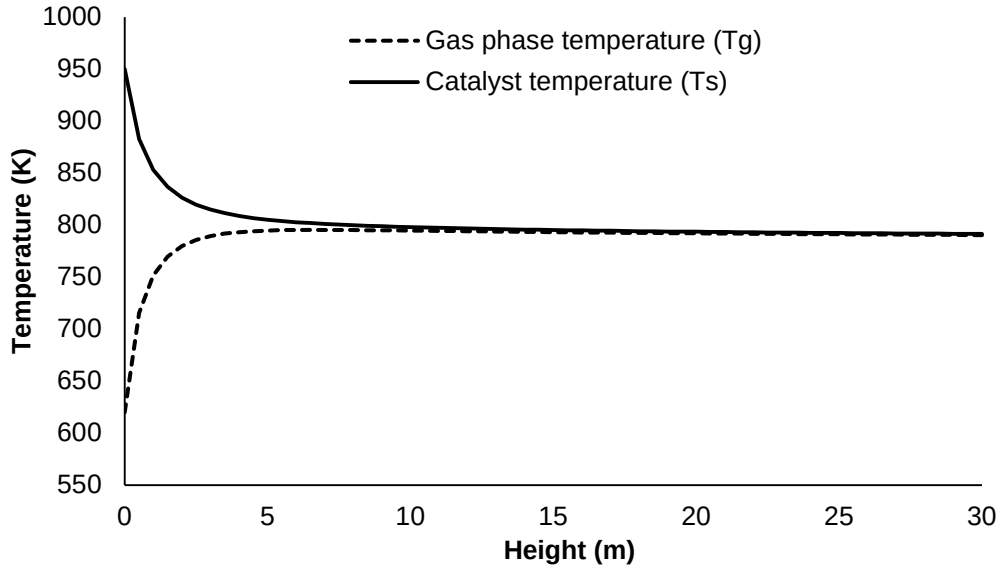

Figure 6.2: Base case temperature profile alone the riser

To determine the accuracy and validate the capability of this gPROMS model, results from validated work of Han and Chung (2001b) shown in column B of Table 6.1, and Kaduna refinery operational data shown in column C, are used to compared with the results of this simulation work. The results are presented in Table 6.1.

Table 6.1: Compare Riser output results with other simulation and plant data

Parameter	Input	Riser output				
		A	B	C	% Deviation	
					A with B	A with C
Gas Oil Temperature (K)	535	790.4	793.1	800	-0.34	-1.21
Catalyst Temperature (K)	933	791.5	796.5		-0.63	
Gas Oil Mass flowrate (kg/s)	49.3	49.3	49.3			
Catalyst Mass flowrate (kg/s)	300	300	300			
Mass fraction of Gas Oil	1	0.296	0.273	0.236	7.77	20.27
Mass fraction of Gasoline	0	0.529	0.514	0.515	2.83	2.64
Mass fraction of Gases	0	0.136	0.136	0.198	0	-45.58
Mass fraction of Coke	0	0.039	0.042	0.051	-7.69	-30.76

The experimental data for comparing this gPROMS model quantitatively and qualitatively are the validated results from Han and Chung (2001b) models where the gPROMS model used in this work was obtained. Han and Chung (2001b) simulation results were validated against plant and literature data, which makes it suitable to be referenced. In addition, yields from the riser are functions of the feed quality, catalyst type, reaction temperature, catalyst to oil ratio and many other operational variables. Since, the input conditions, including the feed quality, catalyst type, reaction temperature, catalyst to oil ratio and riser configuration for Han and Chung (2001b) and this simulation are the same, this simulation results are compared with that of Han and Chung (2001b). It shows from Table 6.1 that, percentage deviation (column A with B) between the results of this simulation (column A) and the Han and Chung (2001b) (column B) are within a marginal error of less than 3 %, except for mass fractions of gas oil and coke which are about +7.77 and -7.69 respectively. This shows that the gPROMS is accurate in predicting the results obtained by Han and Chung (2001b) and can be recommended for the simulation of the FCC unit. The percentage deviation (column A with C) between the results of this simulation (column A) and the plant data (column B) are quite wide mainly due to differences in the feed quality, catalyst type, reaction temperature, catalyst to oil ratio and many other operational variables. The C/O in this simulation is 6.085, while for the data obtained from Kaduna refinery, C/O is 7.0. However, the fractional yield of gasoline for this model is 0.529, while for the plant is 0.515, which is a percentage difference of 2.64% and it is within the reasonable limit of acceptability. The

difference of 2.64% fractional yield of gasoline found in this work is higher than that of Han and Chung (2001b), and higher than that of the plant data. Many literatures however show that the profiles of the yields of gas oil, gasoline, gases, coke and temperatures obtained from this gPROMS simulation are qualitatively consistent (Ali and Rohani 1997; Cristina 2015).

6.2.1.1.2 Optimisation results

The optimisation results for this work are presented in Figures (6.3 to 6.7). Figure 6.3 shows the profiles of the four lumps; gas oil as feed while gasoline, gases and coke as products at both base case conditions and optimised conditions for case 1. It compares the optimised case 1 with the base case simulation results. The base case simulation was also presented earlier to allow a comparison of before and after optimisation. The system was set at gas-oil temperatures of 535 K and catalyst temperature of 933 K. The gas-oil and catalyst flow velocities were at the inlet of the riser are 10 m/s and 11 m/s respectively. The vaporisation of gas oil was instantaneous and hence the vaporisation section was neglected.
In the optimisation case 1, the decision variable (catalyst flow rate) was set to be optimised between 100 kg/s to 500 kg/s, while the gas oil mass flow rate, gas-oil and catalyst temperatures were fixed at 49.3 kg/s, 535 K and 933 K respectively.

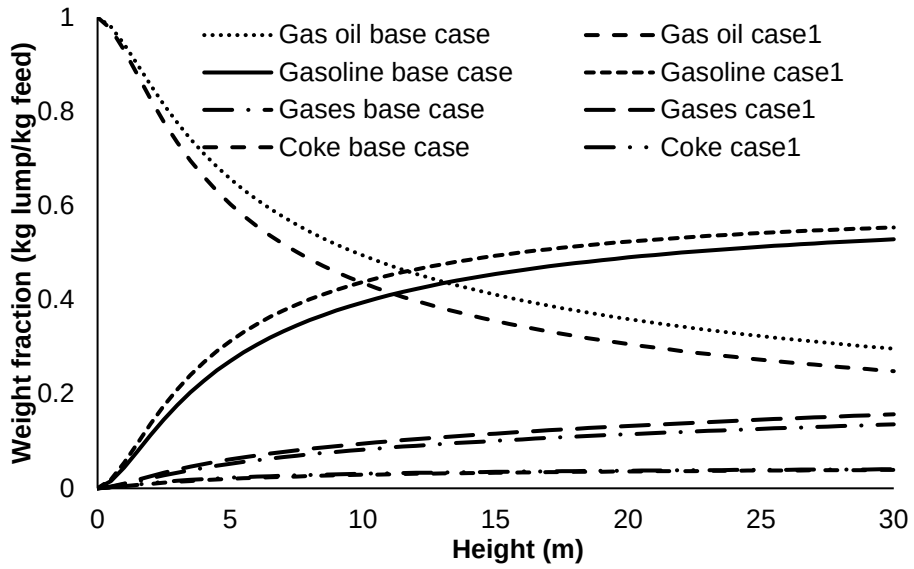

Figure 6.3: Four lump profile base and optimised cases 1

The unconverted gas oil in the base case condition is 0.296 kg-lump/kg-feed, which is about 70.40% conversion while the unconverted for the optimised case 1 is 0.249 kg-lump/kg-feed. This is a difference of 6.26% increased conversion

corresponding to 75.10% conversion of gas oil and resulted in 4.51%, 13.54% and 2.50% increase in gasoline, gases and coke respectively.

Table 6.2 shows the exit mass fractions and operating conditions for the base case and optimised case 1. The percentage increase shown in Tables 6.2 is the improvement made as the system was optimised.

The optimised catalyst mass flowrate is 341.5 kg/s, which is a 12.15% increase on the 300 kg/s base case condition. This would mean additional cost of feedstock to achieve 4.51 % increase in gasoline yield. This is consistent with the riser hydrodynamics where increase in mass flowrate of catalyst can result in increase in the reaction temperature. This is the case where it results in 1.19% increase in the temperature of the gas phase, which in turn causes the increase in the yield of gases and gasoline. This optimisation case shows that at optimised catalyst mass flowrate of 341.5 kg/s corresponding to catalyst-to-oil ratio (C/O) of 6.93, the gasoline throughput increases by 4.51%. The percentage increase may be considered appreciable because any small improvement in the optimal operation of the riser may lead to large economic benefits (Zanin et al. 2002; Vieira et al. 2005). The output riser gas phase temperature in case 1 is 799.9 K, which is 2.9 ^{o}C lower than 802.8 K (Han et al. 2004) in the literature. This shows there is reduced energy needed to achieve the case 1 optimum gasoline yield. Although, there was increase in the feedstock mass flowrate to achieve the 4.51 % increase in gasoline throughput, there was a decrease of 2.9 ^{o}C gas phase temperature at the riser exit which reduces energy consumption in the process.

Table 6.2: Riser output for base case and optimised case 1

Riser Mass Fraction (kg-lump/kg-feed)	Base Case	Case 1	% Increase
Gas oil	0.296	0.249	6.26
Gasoline	0.529	0.554	4.51
Gases	0.136	0.157	13.38
Coke	0.039	0.040	2.50
Mass flowrate of gas oil (kg/s)	49.3	49.3	0.00
Mass flowrate of catalyst (kg/s)	300.0	341.5	12.15
Temperature of gas phase (K)	790.4	799.9	1.19
Temperature of catalyst phase (K)	791.5	800.9	1.17

Figure 6.4 shows weight fraction profiles of the four lumps; gas oil as feed while gasoline, gases and coke as products at both base case conditions and optimised

conditions for case 2. For the optimisation case 2, its decision variable was changed from the mass flow rate of catalyst in case 1 to mass flow rate of gas oil. The gas oil mass flow rate was set to be optimised between 20 kg/s to 100 kg/s, while the catalyst mass flow rate, gas-oil and catalyst temperature were set fixed at 300 kg/s, 535 K and 933 K respectively.

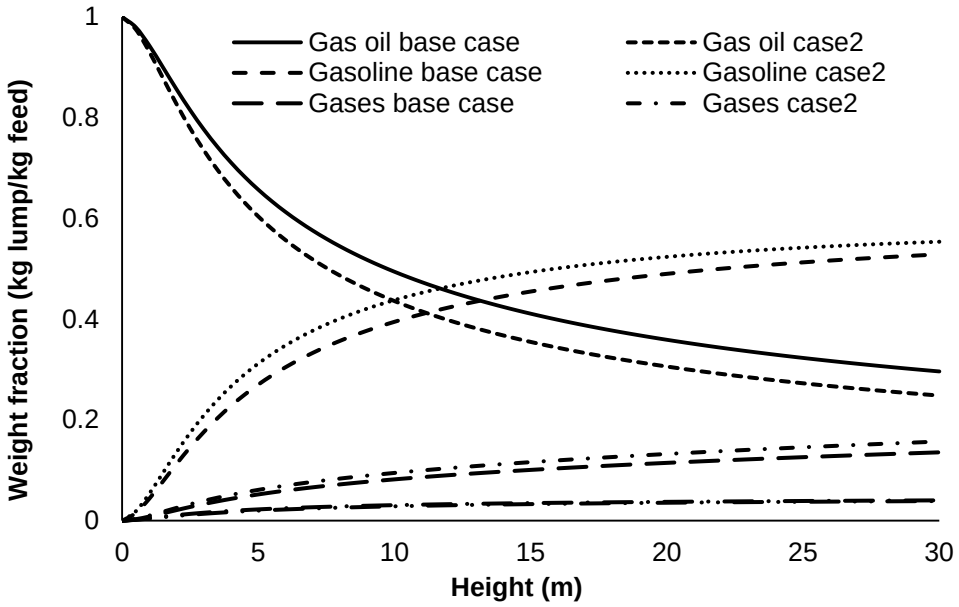

Figure 6.4: Four lump profile base and optimised cases 2

The unconverted gas oil in the base case condition is 0.296 kg-lump/kg-feed which is about 70.40% conversion while the unconverted for the optimised case 2 is 0.248 kg-lump/kg-feed, which gives an increase of 6.38% conversion corresponding to 75.20% conversion of gas oil and results in 4.51%, 13.38% and 2.50% increase in gasoline, gases and coke respectively. Table 6.3 shows the exit mass fractions and operating conditions for the base case and optimised case 2. The percentage increase shown in Tables 6.3 is the improvement made when the system was optimised.

Table 6.3: Riser output for base case and optimised case 2

Riser Mass Fraction (kg-lump/kg-feed)	Base Case	Case 2	% Increase
Gas oil	0.296	0.248	6.38
Gasoline	0.529	0.554	4.51
Gases	0.136	0.157	13.38
Coke	0.039	0.040	2.50
Mass flowrate of gas oil (kg/s)	49.3	43.2	-14.12
Mass flowrate of catalyst (kg/s)	300.0	300.0	0.00
Temperature of gas phase (K)	790.4	800.0	1.20
Temperature of catalyst phase (K)	791.5	801.0	1.19

From Table 6.3, there is approximately 1.2% increase in both catalyst and gas phase temperatures, this means increase in the rate of cracking reaction because of the temperature dependency of the rate of reaction leading to the increased conversion of gas oil by 6.38%, increased yield of gasoline by 4.51%. More gases yield of 13.38 was accompanied including an increase of 2.5% coke deactivation. This is despite the decrease in the mass flowrate of gas oil, the decrease in mass flow rate of gas oil means increase of C/O ratio since the mass flow rate of catalyst was held constant. This is consistent with operational principle of increasing the C/O ratio to the riser to increase gasoline yield in the riser.

Although, the gas oil conversion in case 2 (75.20%) is slightly higher than in case 1 (75.10%), it gave no increase in the yield of gasoline, gases and coke. Even though optimisation cases 1 and 2 gave similar results for all fractions, there was a slight increase (1.2%) in the exit temperature of the gas phase from 790.9 K in case 1 to 800.0 K in case 2.

The optimised gas oil mass flowrate is 43.2 kg/s, which is a 14.12% decrease on the 49.3 kg/s base case condition. This corresponds to a 14.12% cut on the cost of feedstock, which still achieved the same 4.51% increase in the yield of gasoline. In case 2, a higher conversion is obtained as gas oil mass flowrate is used compared with when the catalyst mass flow rate was used in case 1. The riser output temperature in case 2 is 800.0 K, which is 2.8 K lower than the value obtained by Han et al. (2004) (802.8 K). This shows that reduced energy needed to achieve the case 2 optimum gasoline yield. This optimisation case shows that at optimised gas oil flowrate of 43.2 kg/s corresponding to catalyst-to-oil ratio (C/O) of 6.94, gasoline is maximised by 4.51%. Again, a little improvement in the

optimal operation of the riser may lead to large economic benefits (Zanin et al. 2002; Vieira et al. 2005).

Figure 6.5 shows the profiles of the four lumps; gas oil as feed while gasoline, gases and coke as products at both base case conditions and optimised conditions for case 3.

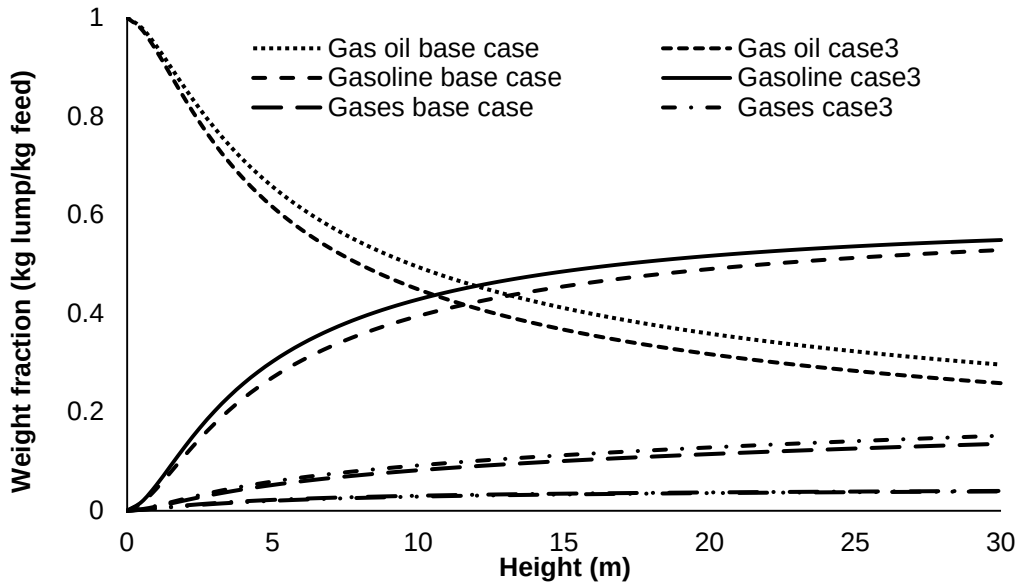

Figure 6.5: Four lump profile base and optimised cases 3

The optimisation case 3 used two decision variables, unlike cases 1 and 2. These were gas oil mass flowrate and catalyst mass flowrate. The gas oil mass flowrate was set to be optimised between 20 kg/s to 100 kg/s as in case 1, while the catalyst mass flow rate was set to be optimised between 100 kg/s to 500 kg/s as in case 2, whilst gas-oil and catalyst temperatures were fixed at 535 K and 933 K respectively.

Table 6.4 shows the exit mass fractions and operating conditions for the base case 3 and optimised case 3 along with percentage increases as the system was optimised.

Table 6.4: Riser output for base case and optimised case 3

Riser Mass Fraction (kg-lump/kg-feed)	Base Case	Case 3	% Increase
Gas oil	0.296	0.259	4.99
Gasoline	0.529	0.549	3.64
Gases	0.136	0.152	10.53
Coke	0.039	0.040	2.5
Mass flowrate of gas oil (kg/s)	49.3	44.8	-10.04
Mass flowrate of catalyst (kg/s)	300.0	310.8	3.47
Temperature of gas phase (K)	790.4	797.8	0.93
Temperature of catalyst phase (K)	791.5	801.0	1.19

The unconverted gas oil in the base case condition is 0.296 kg-lump/kg-feed, which is about 70.40% conversion while the unconverted for the optimised case 3 is 0.259 kg-lump/kg-feed (74.10%), which gives an increase of 4.99% conversion of gas oil and resulted in 3.64%, 10.53% and 2.50% increase in gasoline, gases and coke respectively. Gas oil conversion in case 3 is 74.10% and it is slightly lower than in cases 1 (75.10%) and 2 (75.20%).

The optimised gas oil mass flowrate is 44.8 kg/s, which is a 10.04% decrease on the 49.3 kg/s base case condition. This means a 10.04% cut on the cost of feedstock into the riser. In addition, the optimised catalyst mass flowrate is 310.8 kg/s, which is a 3.47% increase on the 300 kg/s base case condition. It means an additional 3.47% cost of catalyst into the riser. This combination of the two decision variables; catalyst mass flowrate and gas oil mass flowrate are not the best use of operational decision because it produced the lower percentage increase of the yields of gasoline. The yield of gasoline is lower than cases 1 and 2 by 19.29%. Even though the yield of gases is lower in case 3 which is good for plant operation, the yield of gasoline was not favoured due to lower conversion of gas oil compared with cases 1 and 2.

The riser output temperature of the gas phase in case 3 is 797.8 K, which is 5.0 ^{o}C lower than that quoted by (Han et al. 2004) (802.8 K). This also shows a reduced energy needed to achieve the case 3 optimum gasoline yield. This optimisation case shows that at optimised gas oil flowrate of 44.8 kg/s and catalyst mass flowrate 310.8 kg/s, which corresponds to a catalyst-to-oil ratio (C/O) of 6.94, gasoline is maximised by 3.64%.

Table 6.5 shows the yields of gasoline for all three optimisation cases with their corresponding percentage increases.

Table 6.5: The yield of gasoline for cases 1, 2 and 3.

Riser Mass Fraction (kg-lump/kg-feed)	Base Case	Optimised Case	% Increase
Gasoline (Case 1)	0.529	0.554	4.51
Gasoline (Case 2)	0.529	0.554	4.51
Gasoline (Case 3)	0.529	0.549	3.64

In all the three cases, the yield of gasoline was increased by the optimisation. Optimisation case 2 gives the best result because it results in a 14.12% decrease in mass flowrate of feed, which means reducing the cost of feed and achieving a 4.51% improvement on the yield of gasoline. However, case 1 also achieved a 4.51% increase in gasoline throughput; but it has 12.15% increase in catalyst mass flowrate, which may result in increase of the operating cost. Case 3 shows a decrease of 10.04% in mass flowrate of feed but also has 3.47% increase in mass flowrate of catalyst, an additional cost as well with lower gasoline yield compared with case 2.

Figure 6.6 shows exit temperature profiles of the gas phase for the base case condition, which is 790.4 K, and the optimised cases 1, 2 and 3 with temperatures 799.9 K, 800.0 K and 800.0 K respectively.

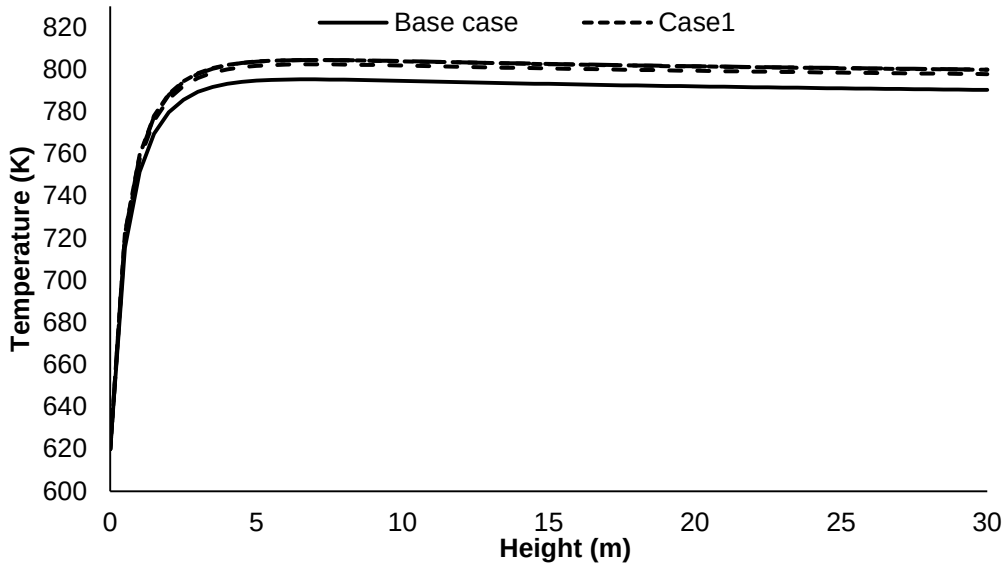

Figure 6.6: Gas phase temperature (base and optimised cases)

The gas phase temperature increases by an average of 10 K due to the slight increase in catalyst mass flowrate. However, the exit temperatures are consistent with the optimum value obtained in the literature (Han et al. 2004).

The profiles in Figure 6.7 are exit temperatures of the catalyst phase for the base case condition (791.5 K) and cases 1, 2 and 3 with temperatures of 800.9 K,

801.0 K and 801.0 K respectively. Here, the catalyst phase temperature increases by an average of 10 K, which is also due to the slight increase in the catalyst mass flowrate. In addition, the exit temperatures are consistent with the optimum value obtained in the literature (Han et al. 2004).

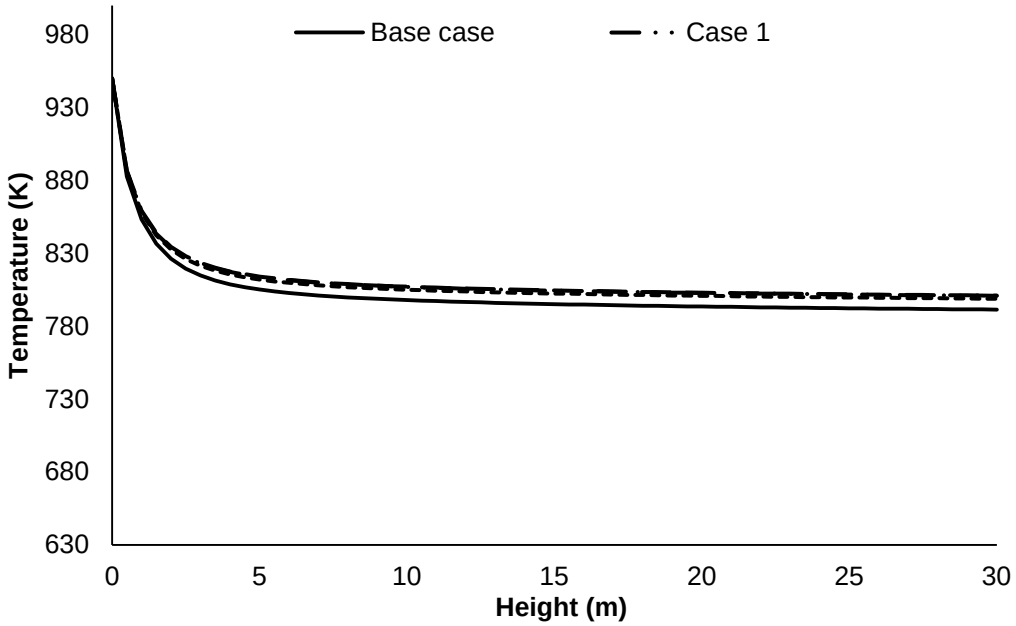

Figure 6.7: Catalyst phase temperature (base and optimised cases)

The exit temperatures of the riser gas phase for the optimised cases 1, 2 and 3 are 799.9 K, 800.0 K and 800.0 K respectively i.e. an average of 800 K. For the optimised cases in Han et al. (2004), the riser exit temperatures of the gas phase for both partial and complete combustion are from 801.6 K to 809.4 K. This is an average of 805 K. Comparing the results, the riser exit temperature of the gas phase for this work is less by an average of 5 ^{o}C, which would result in a substantial reduction in energy consumption for the percentage increase in gasoline yield achieved. The objective of the work of Han et al. (2004) was based on economic optimisation and therefore the optimum yield of the gasoline was not presented as a separate lump. Hence, comparison with the maximised gasoline yield obtained in this work is difficult. However, the maximised gasoline yield of gasoline in this work (0.554 kg feed/kg lump) is a 4.5% increase on the base case condition (0.529 kg feed/kg lump) and 7.6% increase on the gasoline yield of Han and Chung (2001b).

6.2.2 Optimisation problem statement for propylene maximisation

An SQP algorithm was used to maximise propylene yield in a secondary reaction and 16.68 vol% increase was achieved (Zhou et al. 2010). Similarly, SQP is used to maximise propylene in this work. The riser model was used with a new six-lumped kinetic model proposed in this work shown in Table 4.3. The six-lump kinetic scheme is shown in Figure 4.8.

There are three main issues called the constraint triangle for maximizing propylene production, they are the effects of existing FCC technology, operation variables and catalysts on product quality and quantity (Maadhah et al. 2008). Since the alteration of the FCC unit configuration and catalyst development is not the focus of this work, even though they are very important in FCC unit optimisation, only the operation variables are manipulated to maximise the yield of propylene lump (C_3's). Higher propylene production comes at the expense of gasoline. For traditional refiners, maximizing gasoline yield is more important than the propylene yield, while for those interested in petrochemical applications, the target is operating at maximum propylene yield (Akah and Al-Ghrami 2015).

The mass flowrates for gas oil and catalyst used in this simulation are 51.8 kg/s and 190.9 kg/s respectively, while the C/O ratio is 3.685. These mass flow rates predicted the yields of the six lumps in the range presented by Ancheyta and Rogelio (2002) while using the parameters estimated in this research work.

The problem statement for the optimisation of propylene in the riser is:

Optimisation of the yield of propylene

The optimisation problem can be described as:

Given	the fixed volume of the riser
Optimise	the mass flowrate of catalyst, mass flowrate of gas oil and temperatures of gas and catalyst phases.
So as to maximise	the yield of propylene lump (C_3's) y_{C3}
Subject to	constraints on the mass flowrates of catalyst and gas oil, temperatures of gas and catalyst phases, and exit concentration of gasoline.

The optimisation problem can be written mathematically as:

Objective Function: $\underset{T_j,\ FF_j,\ y_{gl}}{\text{Max}} \quad y_{C3}$

Subject to:

Process model: $f(x, \dot{z}(x),\ z(x),\ u(x), v) = 0$

Boundary: $x = x^{max}$

Inequality constraints: $FF_g{}^{min} \leq FF_g \leq FF_g{}^{max}$

$FF_c{}^{min} \leq FF_c \leq FF_c{}^{max}$

$T_g{}^{min} \leq T_g \leq T_g{}^{max}$

$T_c{}^{min} \leq T_c \leq T_c{}^{max}$

Equality constraints: $y_{gl}{}^{min} \leq y_{gl}$

The entire DAE model equations can be written in a compact form as: $f(x, \dot{z}(x), z(x), u(x), v) = 0$, Where x is the independent variable which in this case is the height of riser, $z(x)$ the set of all state variables, $\dot{z}(x)$ the derivatives of $z(x)$ with respect to the height of the riser, $u(x)$ the vector of control variables (mass flowrates of feed and catalyst) and v a vector of invariant parameters, such as design variables (riser diameter and height). Also, y_{C3} the objective function, which is the yield of propylene and the desired product to be maximised in the riser. T_c the catalyst phase temperature, T_g the gas phase temperature, FF_g the mass flow rate of gas oil, FF_c the mass flow rate of catalyst, x the height of the riser, x^{max} the maximum riser height (30 m) and y_{gl} the yield of gasoline. $y_{gl}{}^{min}$ the minimum value of gasoline to be maintained while propylene is maximised. $T_c{}^{min}$ and $T_c{}^{max}$ the minimum and maximum bounds of the catalyst phase temperature ($700 \leq T_c \leq 1000\ K$) and $T_g{}^{min}$ and $T_g{}^{max}$ are the minimum and maximum bounds of the gas phase temperature ($520 \leq T_g \leq 800\ K$). $FF_c{}^{min}$ and $FF_c{}^{max}$ the minimum and maximum bounds of the mass flowrate of catalyst ($20 \leq FF_c \leq 500\frac{kg}{s}$) and $FF_g{}^{min}$ and $FF_g{}^{max}$ the minimum and maximum bounds of the mass flowrate of gas oil ($10 \leq FF_g \leq 100\frac{kg}{s}$). x^{max} the fixed height of the riser; 30 m, and y_{gl} the minimum allowable limit for gasoline $0.40 < Y_{gl}$.

The boundaries for the mass flowrates of gas oil and catalyst are chosen such that it reflects the typical industrial FCC unit limits for C/O ratios of 4:1 to 10:1 by weight (León-Becerril et al. 2004; Sadeghbeigi 2012b; John et al. 2017). C/O

ratios for propylene production in high severity units and riser-downer are higher (Parthasarathi and Alabduljabbar 2014) than the C/O ratios used in conventional FCC units, which vary between 1 and 6 (Aitani et al. 2000; Dupain et al. 2003a; Hussain et al. 2016) and 3 to 25. Hence, the boundaries for the mass flowrates are opened wide enough to accommodate low and high C/O ratio (1 to 25) on the optimisation framework.

Case Studies

- Case 1: optimizing catalyst mass flow rate FF_c, between 20 - 500 kg/s; gas-oil temperature, T_g (520 – 800 K); catalyst temperature, T_c (700 – 1000 K); while gas oil mass flow rate, FF_g, is kept constant at 58.02 kg/s.
- Case 2: optimizing; gas oil mass flow rate FF_g, between 20 - 500 kg/s; gas-oil temperature, T_g (520 – 800 K); catalyst temperature, T_c (700 – 1000 K); while the catalyst mass flow rate, FF_c, is kept constant at 134.94 kg/s.
- Case 3: optimizing catalyst mass flow rate FF_c, between 20 - 500 kg/s; gas-oil temperature, T_g (520 – 800 K); catalyst temperature, T_c (700 – 1000 K); and gas oil mass flow rate FF_g, between 20 - 500 kg/s.

Since FCC's major goal is the production of gasoline, a minimum of 40 wt% of gasoline is imposed as a constraint on all the optimisation cases, else most of the gasoline will deplete due to secondary cracking. The choice of 40 wt% is based on the average gasoline yield presented in the literature; 44.13 - 45.65 wt% (Moustafa and Froment 2003), 44 wt% (Ali et al. 1997; Gupta et al. 2007) and 40 wt% (Lan et al. 2009).

6.2.2.1 Optimisation results for maximizing propylene

Table 6.6 presents the riser exit values of this simulation along with those exit concentrations of the riser from the optimisation cases.

Table 6.6: Propylene optimisation results for cases 1, 2 and 3 and simulation results

Lump	Riser Optimisation Output (wt%)						
	Base case simulation	Case 1	Difference	Case 2	Difference	Case 3	Difference
	C/O = 3.69	C/O = 5.44	1.75	C/O = 5.48	1.79	C/O = 5.45	1.76
Gas oil (wt%)	26.11	14.09	-12.02	14.06	-12.05	14.07	-12.04
Gasoline (wt%)	51.36	43.68	-7.68	43.64	-7.72	43.65	-7.71
Butylene (C_4's) (wt%)	9.39	14.49	5.10	14.50	5.11	14.50	5.11
Propylene (C_3's) (wt%)	4.59	8.93	4.34	8.93	4.34	8.95	4.36
Dry gas (wt%)	1.55	6.81	5.26	6.85	5.30	6.83	5.28
Coke (wt%)	4.00	9.00	5.00	9.00	5.00	9.01	5.01
Cat. Temp. (K)	710.6	737.7	27.1	738.5	27.9	737.7	27.1
Gas Phase Temp. (K)	706.3	733.8	27.5	734.2	27.9	733.8	27.5

The results for both optimisation cases 1, 2 and 3, and base case simulation (Figures 4.9 and 4.10) are presented in Table 6.6, showing the riser exit values of the six lumps; gas oil as feed, while gasoline, butylene, propylene, dry gas and coke as products, and temperatures of the catalyst and gas phases. It compares the base case simulation results with the optimised cases 1, 2 and 3.

In the optimisation case 1, as propylene is maximised, the decision variable (catalyst mass flow rate) was set to be optimised between 20 kg/s to 500 kg/s, while gas-oil temperature, T_g, was between 520 K– 800 K and catalyst temperature, T_c , between 700K - 1000 K. The gas oil mass flow rate was fixed at 51.8 kg/s. The maximised value of propylene is 8.93 wt% at C/O ratio of 5.44 (gas oil mass flowrate is 51.8 kg/s and catalyst mass flowrate is 282.0 kg/s).

The absolute difference between the maximised value and this simulation is 4.34 wt%, an increase from 4.59 wt% to 8.93 wt%. The optimised catalyst mass flowrate is 282.0 kg/s, it is a 47.72% increase on the 190.9 kg/s base case simulation. This increase produced results consistent with the riser hydrodynamics where increase in mass flowrate of catalyst can result in an increase in the reaction temperature and consequent yield of intermediate products (Han and Chung 2001b; Akah et al. 2016). There is 3.81% and 3.89% increase in the temperatures of the gas phase and catalyst respectively, which in turn causes the increase in the yield of a difference of 5.26 wt% of dry gas from 1.55 wt% at C/O ratio of 3.69 to 6.81 wt% at C/O ratio of 5.44. Similarly, the yield of butylene has a difference of 5.10 wt% from 9.39 wt% at C/O ratio of 3.69 to 14.49 wt% at C/O ratio of 5.44. Due to increase in C/O and temperature of reaction, more gas oil cracks, a further 12.02 wt% was achieved from 26.11 wt% at C/O ratio of 3.69 to 14.09 wt% at C/O ratio of 5.44. This is also a reason for more yield of propylene and other intermediate products; butylene and dry gas. Gasoline also cracks in a secondary reaction and depletes from 51.36 wt% at C/O ratio of 3.69 to 43.68 wt% at C/O ratio of 5.44 giving rise to a loss of 7.68 wt%, this secondary reaction was also observed in the literature (Scott and Adewuyi 1996). In optimisation case 1, at C/O ratio of 5.44, 9.00 wt% of coke was deposited on the catalyst, against 4.00 wt% at C/O ratio of 3.69 leading to an addition of 5.00 wt% of coke on catalyst. It is also a consequence of increased C/O ratio and reaction temperature. This increase in coke on catalyst may lead to high deactivation of the catalyst, which is not desirable, however, regeneration

of the catalyst can be achieved, and any eventual consequence is compensated by the much increase in the yield of propylene achieved.

Optimisation cases 2 and 3 presents similar outcomes as optimisation case 1 because their optimum C/O ratios are quite similar; 5.44, 5.48 and 5.45 for cases 1, 2 and 3 respectively, with an absolute average difference of 0.016. This very slight difference is responsible for the slight average variation of 0.01 wt% in the riser outputs for the six lumps.

The optimisation case 2 has its decision variable changed from the mass flow rate of catalyst in case 1 to mass flow rate of gas oil. The gas oil mass flow rate was set to be optimised between 20 kg/s to 500 kg/s, while gas-oil temperature, T_g, between 520 K – 800 K and catalyst temperature, T_c , between 700 K - 1000 K. The catalyst mass flow rate was fixed at 190.9 kg/s. The optimised gas oil mass flowrate is 34.86 kg/s, which is a 32.7% decrease on the 51.8 kg/s of the base case simulation and corresponds to C/O of 5.48, an increase of C/O ratio of 0.04 compared with the C/O ratio of optimisation case 1. This result, as in case 1, is consistent with the riser hydrodynamics where increase in C/O results in increase in the reaction temperature and yield of intermediates products (Akah and Al-Ghrami 2015; Akah et al. 2016). There is 3.90% and 3.95% increase in the temperatures of the gas phase and catalyst respectively. The increase in temperature in cases 1 and 2 are similar, this is because only a difference of 0.04 C/O ratio between cases 1 and 2 exist. Though the optimised conditions in case 2 resulted in increase in the maximum value of propylene by 94.55%, which is the same in case 1 compared with the simulation value of 4.59 wt%, there is no difference between the values of maximised propylene (8.93 wt%) between case 1 and case 2. Similarly, the yield of butylene and dry gas increased respectively by 5.11 wt% and 5.26 wt% due to an increase in C/O ratio of 1.79 (C/O of 3.69 to 5.48). The amount of coke deposited in case 2 is the same in case 1, which is 9.00 wt%. Since maximizing propylene is the main aim of this work, and cases 1 and 2 could achieved the same value of 8.93 wt%, any of the operating conditions of cases 1 or 2 can be used for optimal operation of the riser to produce optimum value of propylene. However, case 2 is preferable because of the difference of C/O ratio of 0.05.

The optimisation case 3 used two decision variables, unlike cases 1 and 2. These are gas oil and catalyst mass flowrates. The gas oil mass flowrate was set to be optimised between 20 kg/s to 500 kg/s as in case 1, and the catalyst mass flow

rate was also set to be optimised between 20 kg/s to 500 kg/s as in case 2. The gas-oil temperature, T_g, was set between 520 K – 800 K and catalyst temperature, T_c , between 700 K - 1000 K.

The optimised gas oil and catalyst mass flowrates are 53.4 kg/s and 290.8 kg/s respectively, showing a 3.09% increase on the 51.8 kg /s base case condition for gas oil mass flowrate and 52.33% increase on the 190.9 kg /s base case condition for catalyst mass flowrate. These optimised flowrates correspond to a C/O of 5.45, an increased C/O of 1.74 on the base case simulation bringing about a 94.99% increase in propylene yield from 4.59 wt% to 8.95 wt%. There is a slight increase of 0.05 wt% of propylene in case 3 over cases 1 and 2, which represents a 0.44% increase. This increase makes optimisation case 3 most preferable because any small improvement to the yield of products in FCC unit amounts to great profitability. In general, the maximised value of propylene is 8.95 wt% achieved at C/O ratio of 5.45, even though, an average of 7.70 wt% of gasoline is lost due to secondary reaction with much coke deposited on the catalyst.

It was observed that the improved yield of propylene is accompanied with increase in some undesirable products such as dry gas and butylene as well as its isomer. It also increased catalyst deactivation. However, FCC units can be modified or operated in a mode shift to produce propylene with less of the consequences. This could be achieved by the harmonious combination of the catalyst, temperature, C/O ratio, time, coke make, and hydrocarbon partial pressure (Akah and Al-Ghrami 2015).

An industrial size conventional FCC riser is simulated in this work to maximise the yield of propylene as a separate lump. The common view is where experimental works were carried out at specific temperature in fixed bed reactors, and propylene mostly considered as part of a general lump of olefins. Instead of using the catalyst additives to improve yield, in this work, only the operational conditions of the riser were used. However, it is recommended that the use of both improved catalyst and optimum operating conditions will greatly increase the yield of propylene.

6.2.3 Optimisation of the regenerator for CO_2 minimisation

There are two major reactors in FCC process: the riser where cracking reactions take place and the regenerator where the burning of coke reactions is accomplished. During this process, which is referred to as regeneration, large

amount of gases called flue gases; CO, CO_2, SO_2, SO_3, NO, N_2O and N_2 are generated (Wauquier 1994). The flue gases are mostly considered as pollutants to the environment, hence, they are required to be found in little quantity in the air. The amount of CO_2 emitted from the FCC unit is about 30% of the total CO_2 emitted from the refinery and it is considered the highest in oil refineries (de Mello et al. 2013). Hence, the refinery is a major contributor to the Green House Gas (GHG), a culprit of global warming. To stop the use of fossil fuels may not be practicable because various projections make clear that fossil fuels will continue to be needed while renewable energy sources are not enough.

A recent report from the Nobel Prize-winning Intergovernmental Panel on Climate Change (IPCC) concluded that global CO_2 emissions must be cut by 50-80% by 2050 to elude the most destructive effects of climate change (CCP 2016).

To cut down on the CO_2 emission, Carbon capture and storage (CCS) is playing a vital role (Metz et al. 2005; de Mello et al. 2013), however, the approach has been proposed for more than 30 years, little is achieved with respect to commercial success of CCS projects. The principal concern is where to stockpile the immense volume of captured pure CO_2 every year (Peng and Zhuang 2012). Therefore, an approach capable of mitigating the emission may be very effective. To achieve this goal, the use of operational changes to bring about emissions reduction can be carried out in the FCC unit to reduce the extent of emission before it is being captured and stored (Moore 2005).

This work will focus on minimizing the yield of CO_2 from FCC regenerator flue-gas as an important step in mitigating CO_2 emission of the refinery. The FCC regenerator is divided into two: the dense bed and freeboard. The dense bed is modelled as a mixed-tank model for energy and coke balances but a plug flow reactor model for gas component balances. The freeboard is modelled as a plug flow reactor. Though, in this work, only the dense bed is considered because most of the solids and gases are much more in the dense bed where almost all reactions take place (Pinheiro et al. 2012), and the fact that the dense bed model can be used for the overall regenerator dynamics (Bollas et al. 2007b).

To carry out the optimisation studies, a single objective function was developed and implemented on gPROMS software, which uses a successive reduced quadratic programming (SRQPD), a sequential quadratic programming based solver to minimise the yield of CO_2. The optimisation is done using the mathematical models (Han and Chung 2001a; Han and Chung 2001b) of the

regenerator and results obtained will be compared with CO_2 emissions from plant and literature data.

6.2.3.1 Optimisation problem statement for CO_2 minimisation

Different modelling and optimisation platform/software such as MATLAB and Hysys were used for FCC regenerator simulation/optimisation but not gPROMS, despite its robustness. The successive reduced quadratic programming (SRQPD) is a nonlinear programming optimisation technique capable of handling the nonlinearity of the partial differential and algebraic equations that described the regenerator. In this work gPROMS is used for the regenerator dense bed optimisation to minimise the yield of CO_2 from the dense bed of the FCC unit regenerator.

The optimisation problem can be described as:

Given	the fixed volume of the dense bed regenerator
Optimise	the mass flowrate of air and hold up of catalyst in the regenerator.
So as to minimise	the yield of CO_2
Subject to	constraints on the yield of CO.

Mathematically, the optimisation problem can be written as;

$$\min_{T(x) or F_J(x)} \quad Z$$

$s.t.$

$f(x, z'(x), z(x), u(x), v) = 0$ (model equations)

$x_f = x_f^*$

$F_L \leq F_{air} \leq F_U$

$Y_{CO} < Y_{CO}{}^*$

Where Z is the yield of carbon-dioxide, F_{air} the mass flow rates of air into the regenerator, x_f the height of the regenerator, Y_{CD} the yield of carbon monoxide, F_L and F_U the lower and upper bounds of the mass flowrate of air ($40 \leq F_{air} \leq 80 \frac{kg}{s}$) and catalyst holdup in the regenerator ($100000 \leq W_c \leq 200000\, kg$) respectively, x_f^* the fixed height of the regenerator and $Y_{CD}{}^*$ the maximum allowable limit for carbon monoxide $Y_{CO} < 0.0002$.

6.2.3.2 Results for CO_2 minimisation

This section shows both simulation and optimisation results for CO_2 minimisation. The results are presented to show the capability of gPROMS in solving complex nonlinear PDAEs by validating the results against those predicted by the same model (Han and Chung 2001b).

6.2.3.2.1 Simulation for CO_2 minimisation

When air meets coke on the surface of the catalyst, the coke is burned, and the catalyst is regenerated under high temperature, which provides enough energy that is required for the endothermic cracking of gas oil in the riser. Figures 6.8 shows the yields of carbon dioxide from the regenerator during coke burning reactions.

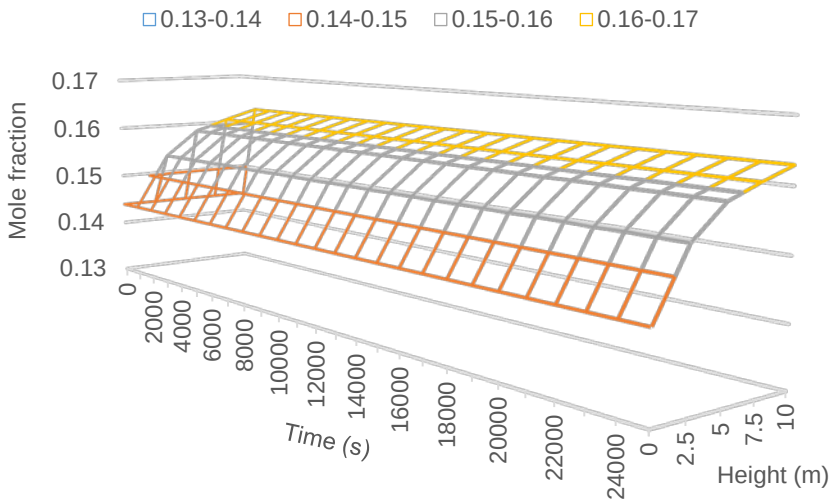

Figure 6.8: Concentration of carbon dioxide from dense bed

At 66.09 kg/s gas flowrate and constant temperature of 991 K, the mole fraction of carbon dioxide at the exit of the dense bed of the regenerator is 0.1629. This is 16.29% carbon dioxide, 0.20% carbon monoxide, 10.95% water, 72.22% nitrogen and 0.33% oxygen. These results are very much closer to gases mole fractions obtained by Han and Chung (2001b). Han and Chung (2001b) obtained 14.805 carbon dioxide, 0.60% carbon monoxide, 9.20% water and 0.20% oxygen. These results agree well with little margin of errors and it is consistent with the literature (Zheng 1994).

Figure 6.9 shows the results of the minimisation of carbon dioxide using the optimised process conditions.

6.2.3.2.2 Optimisation for CO_2 minimisation

The mass flowrate of air for the simulation is 66.09 kg/s, while the optimised mass flowrate of air is 83.09 kg/s. This is a 20 kg/s increase in the mass flowrate of air to the regenerator bringing about a slight reduction on the mole fraction of carbon dioxide, which is 0.1536 at the exit of the dense bed. Compared with the mass fraction of 0.1621 of the simulation results, it shows a decrease of 5.24 % of carbon dioxide emitted at the exit of the reactor. It is expected that with the increase in air mass flowrate, more carbon dioxide should be produced, due to availability of oxygen to burn more coke and CO. However, it was observed that the catalyst holdup decreased slightly, and that could reduce the amount of coke available for the exothermic reaction. This observation is consistent with what was presented by Han and Chung (2001b).

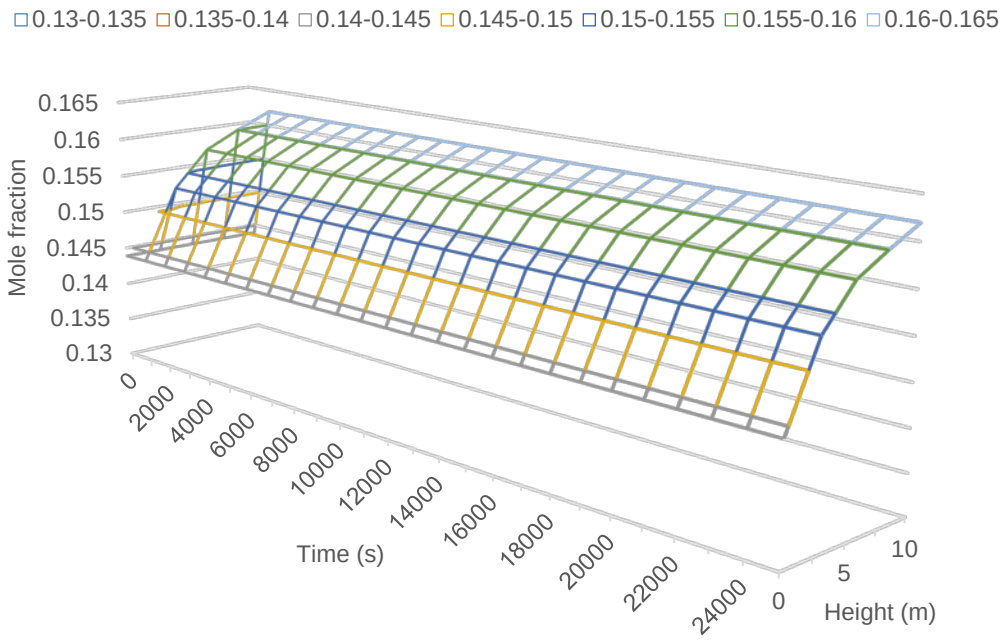

Figure 6.9: Concentration of carbon dioxide from dense bed (Minimum)

6.3 Summary

Three different optimisation problems were solved in this chapter. The maximisation of gasoline and propylene in the riser, and the minimisation of CO_2 in the regenerator.

The optimisation of gasoline has been carried out using a detailed riser process model to maximise the conversion of gas oil to gasoline. A 4-lump kinetic model is assumed where gas oil not only converts to gasoline but to two other undesired

lumps; coke and gases. A steady state optimisation was carried out on an FCC riser and the following were found:

- An optimal value of catalyst mass flowrate (341.5 kg/s) gave a maximised value for gasoline yield as 0.554 kg-gasoline/kg-gas oil corresponding to 4.51% increase.
- An optimal value of gas oil mass flowrate (43.2 kg/s) gave a maximised value for gasoline yield as 0.554 kg-gasoline/kg-gas oil corresponding to 4.51% increase.
- Concurrently using the optimal values of mass flowrates of catalyst (310.8 kg/s) and gas oil (44.8 kg/s) in case 3 gives a lower gasoline yield 0.549 kg-gasoline/kg-gas oil. However, a 10.04% decrease in mass flowrate of gas oil was achieved with 8.68% reduction on the optimum mass flowrate of catalyst in case 1. This shows that a good knowledge of the operation of the riser can reduce cost, because the lost revenue from poorer yield could more than offset any savings in operating costs (Wilson, 1997).

In the optimisation of propylene, a detailed riser process model was used with a six-lumped kinetic model to maximise the conversion of gas oil to propylene, which is a major building block for the polypropylene production. Parameter estimation was also done to estimate new kinetic variables useful in the model used in this simulation. It is a steady state optimisation carried out on an FCC riser and the following were found:

- In the case 1 optimisation, the maximum value of propylene obtained is 8.93 wt% at optimal value of 282.0 kg/s catalyst mass flowrate. Compared with the base case simulation value of 4.59 wt% propylene yield, the maximised value shows an increase by 95%.
- Likewise, in the case 2 optimisation, the maximum value of propylene obtained is the same 8.93 wt% at optimal value of 34.86 kg/s gas oil mass flowrate. When it is compared with the base case simulation value of 4.59 wt% propylene yield, the maximised value shows an increase by 95%, as in case 1.
- When the two optimal values of 290.8 kg/s mass flowrate of catalyst and 53.4 kg/s mass flowrate of gas oil were obtained in case 3, the maximised propylene yield is 8.95 wt%, slightly higher than cases 1 and 2. When it is

compared with the base case simulation value of 4.59 wt% propylene yield, the maximised value shows an increase by 95%.

- The optimisation in all three cases (cases 1, 2 and 3) was achieved at C/O ratios of 5.44, 5.48 and 5.45 respectively. C/O ratio 5.45 gave the higher maximum value of propylene, hence the riser is required to operate at a minimum C/O ratio of 5.44 if optimal operation of the riser is required to maximise propylene yield.

In the third optimisation problem, the regenerator of FCC unit was simulated and optimised to minimise the carbon dioxide exit concentration, to cut down on emission of the greenhouse gas. With an increase of 20 kg/s mass flowrate of air, 5.24 % of carbon dioxide was reduced. On carbon dioxide emission, 5.24 % reduction is good step in cutting down the effect of CO_2 emission from the FCC unit on global warming. With 5.24 % reduction obtained in this simulation, it shows that using operational changes in process variables of the regenerator can bring about great reduction in CO_2 emission.

Chapter 7

Simulation of Varied Diameter Riser and Regenerator

7.1 Introduction

Dynamic and steady state simulations were performed on the riser-regenerator system of the FCC unit using initial and operating conditions to examine the response of major process variables of the model. The riser unit consist of the vaporisation section, the cylindrical riser reactor and the disengager-stripping section, while the regenerator unit consist of the regenerator itself. The riser is modelled as plug flow reactor, while disengaging-stripping section including its cyclones are modelled as a continuous stirred tank (CST). The regenerator model has three phases: the emulsion, bubble and the freeboard. The riser-regenerator schematic diagram is shown in Figure 7.1

The FCC unit operates in a closed circuit, meaning it is a circulating fluidised system. The feed and catalyst enter the riser through the vaporisation section and cracking reaction proceeds in the riser, while the catalyst is deactivated. The spent catalyst flows from the riser to the disengager-stripping section where the product is separated from the spent catalyst, while the spent catalyst is stripped in the stripper from trapped hydrocarbon. The spent catalyst moves to the regenerator to burn off the coke on the catalyst for regeneration. The regenerated catalyst is sent back to the riser via the vaporisation section for cracking of the feed, and the circle continuous. However, most authors simulate the FCC unit as component units. Although, the results obtained are quite meaningful and represent the riser largely, it is expected that when the units are connected, and the simulation is carried out concurrently for riser and regenerator, the expected results should represent the FCC unit adequately.

In this chapter, the concurrent simulation of the riser and regenerator is carried out. In another sensitivity analysis, the riser diameter is varied to investigate the possibility of improving the yield of fuel, and to find out the effect of the varied diameter on the hydrodynamics of the system. The results of the simulation are presented in three subsections; they are the riser, disengager-stripping section and the regenerator.

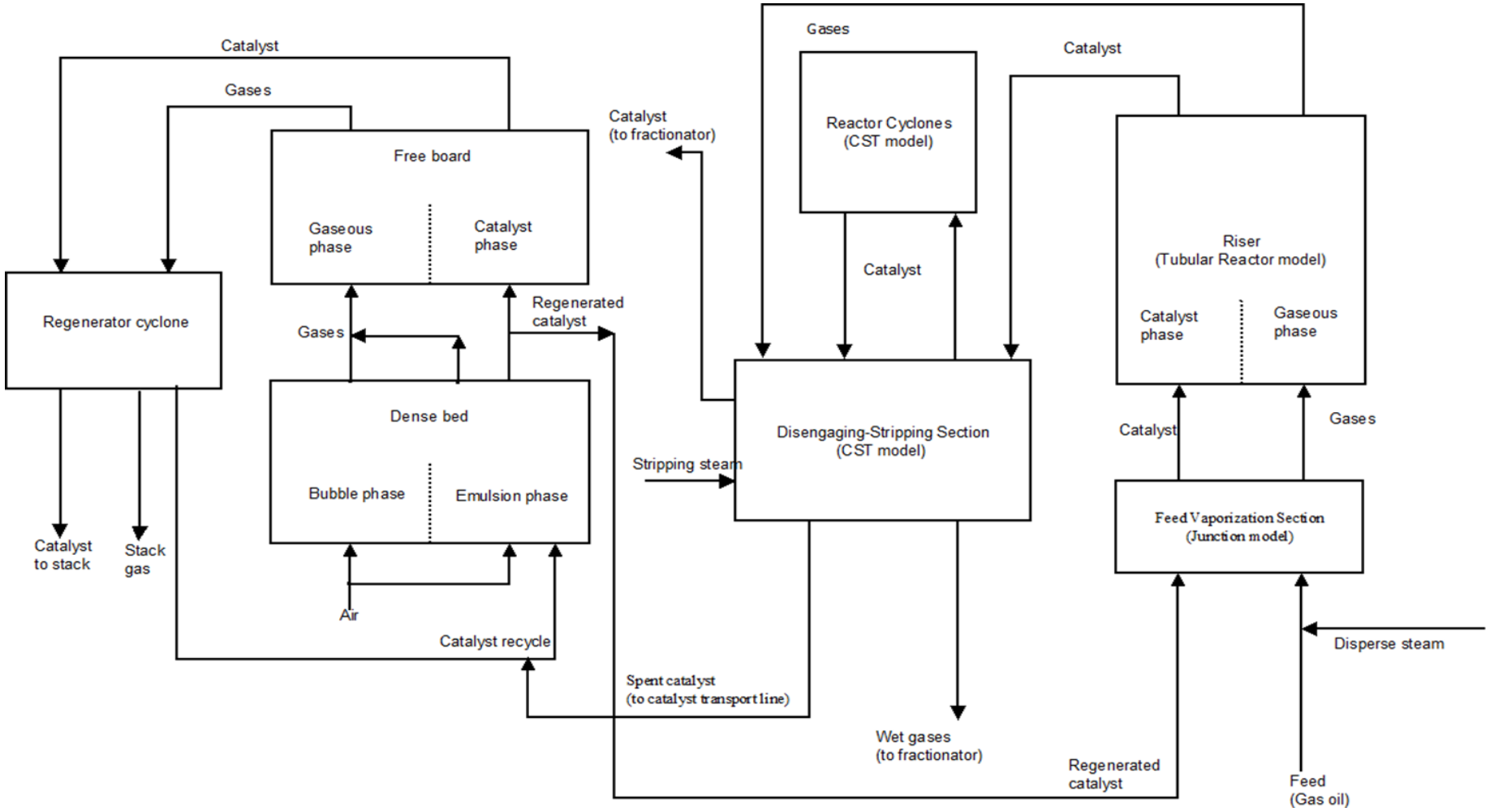

Figure 7.1: Entire FCC unit schematic diagram

7.2 Varied diameter riser

Simulation of the riser is a key approach to increase the yield of gasoline and this is carried out by improving some important success factors like the riser design and operations. To achieve optimum yield of gasoline in the riser, two important factors are considered; having uniform catalyst density and very effective hydrodynamics. In situations where the catalyst activity is excellent, but the yield is poor, the cause would be attributed primarily to the riser hydrodynamics (Kalota and Rahmim 2003), which is a function of riser design. Therefore, riser diameter is an important factor to consider because of its effect on the riser hydrodynamics.

Although a lot of work has been carried out on the modelling of the riser, it is done by considering the riser to be of a uniform cross section (Elshishini and Elnashaie 1990a; Gupta and Subba Rao 2003; Duduku Krishnaiah 2007; Fernandes et al. 2007b). For some, the riser comprises of a number of equal sized compartments (or volume elements) of circular cross section, but not varied diameters (Gupta et al. 2007), and for others it comprises of a cylindrical vertical vessel where cracking of gas oil is carried out using a catalyst in a vaporised upward fashion (Han and Chung 2001a). Even when a comprehensive three-dimensional (3-D) heterogeneous riser model was applied to simulate the turbulent gas–solid flow and reaction in a polydisperse FCC riser, the entire zones of the riser were considered as a uniform cross-sectional tube (Li et al. 2013).

The riser unit has many sections; feed preheater, the vaporisation section and the riser, which are sometimes modelled differently. Although, an attempt to simulate the riser unit with varied diameter (between 1 m at the bottom to 1.4 m at the top) was made (Novia et al. 2007), only a quarter of the riser was considered. This is because they modelled the riser unit in two sections; the vaporisation section (found to have no chemical reactions) as 1 m diameter and the riser section as 1.4 m, a uniform cross section. In some cases, the model of the vaporisation section was included in the riser unit simulation but the length of the riser (uniform cross section) considered did not include the vaporisation section (Han and Chung 2001a; Han and Chung 2001b). It is also clear that the vaporisation section of the riser unit has unique hydrodynamics and can be treated differently, because it takes about 3% of the riser residence time (Ali and

Rohani 1997). For this reason, the riser has been modelled differently from the vaporisation section with the assumption that the gas oil vaporises instantaneously (Al-Sabawi et al. 2006a; Araujo-Monroy and López-Isunza 2006; Ahari et al. 2008a). Therefore, modelling the riser unit by having different diameters for the vaporisation and riser sections is different from modelling the system where the diameter of the riser is varied. This is what this work sets to achieve to model the riser section as a varied diameter with three different cross sections.

The riser unit to be simulated is type of the riser from FCC unit of KRPC in Nigeria. It is a vertical cylinder but with varied diameters. This design is such that the reaction proceeds as the catalyst and vapour mixture flows up through the riser. The lower part of the riser is sized to provide enough pick up velocity and as cracking proceeds, the riser diameter is increased to handle the increasing volume and provide the desired reaction time. The mixture then flows through the remainder of the vertical riser.

This work modelled the riser according to geometric differences of the riser and validated against industrial data. gPROMS software is used for the simulation with C/O ratio, catalyst temperature and gas phase temperature used as manipulating variables. The various effects of the riser geometry on the conversion of gas oil and yield of gasoline were determined. Figure 7.2 presents the riser schematic diagram showing its varied geometry.

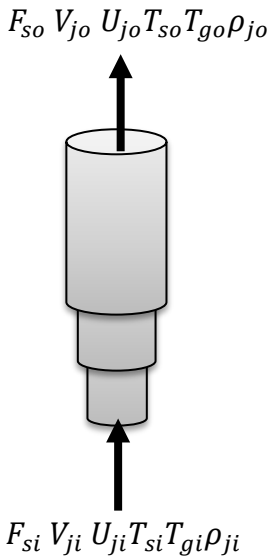

Figure 7.2: The varied diameter riser

It is a vertical cylinder with three different compartments, each of different diameter and height. For simplicity, the connection between each compartment is made flat as shown in Figure 7.2. The first compartment at the bottom has a diameter of 1.0 m and 3.965 m height. The middle compartment has a diameter of 1.35 m and 3.753 m height and the third compartment at the top has a diameter of 1.6 m and 17.6 m height. The entire height of the riser is 25.32 m. A four lump kinetic model shown in Figure 2.2 along with their kinetic parameter in Table 3.1 were used with the riser model equations to simulate the riser.

7.2.1 Results on varied diameter riser

The mass flowrate of catalyst is 300 kg/s while the manipulated variable used for the simulation is catalyst-to-oil ratio (C/O = 7.63, 6.09 and 5.06), for feed flowrate of 39.3 kg/s, 49.3 kg/s and 59.3 kg/s. The inlet temperature of gas oil is maintained at 523 K while the inlet temperature of catalyst after the vaporisation section into the riser is 966.5 K. The results obtained are presented in Figures (7.3 – 7.8) and Tables (7.1 – 7.2).

Figure 7.3 presents the profiles of gas oil (feed) and gasoline along the height of the riser. The fraction of gas oil at the entrance of the riser is 0.9686 mole fraction for all the different C/O ratio used. The gas oil cracks to produce three products: gasoline, gases and coke. However, only the gas oil and gasoline are reported in Figure 7.3, while outlet values of the process variables are presented in Table 7.1.

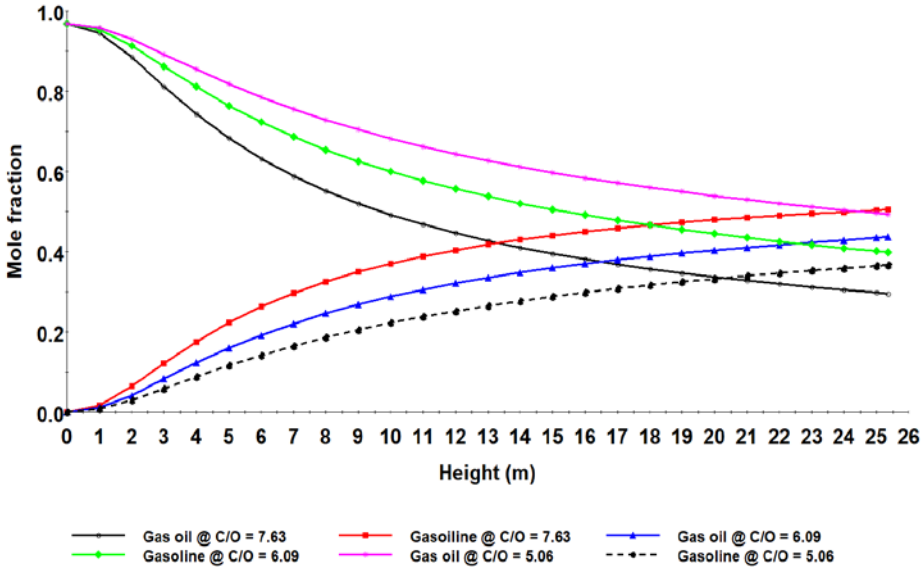

Figure 7.3: Mole fractions of gas oil and gasoline at different C/O ratios

Table 7.1: Weight fractions and temperatures at input different C/O ratios

Parameter	1 m Diameter riser			Plant data
C/O ratio	7.63	6.09	5.06	7.59
Gas phase Temperature, T_g (K)	795.0	772.2	755.1	796.0
Catalyst Temperature, T_s (K)	793.1	774.3	757.3	
Gas oil (wt%)	0.2980	0.4017	0.4935	0.2600
Gasoline (wt%)	0.5028	0.4340	0.3662	0.5080
Pressure (kPa)	200.51	209.34	216.76	

From Table 7.1, gasoline is produced as gas oil cracks from 0.9686 mole fraction at the riser entrance to obtained 69.23 % conversion at C/O ratio of 7.63, 58.53 % conversion at C/O ratio of 6.09 and 49.05 % conversion at C/O ratio of 5.06. Figure 7.3 shows that gasoline yield rises slightly and logarithmically throughout the riser from 0.0 wt% at the riser entrance and reaches to about 50.28 wt% at C/O ratio of 7.63, 43.40 wt% at C/O ratio of 6.09 and 36.62 wt% at C/O ratio of 5.06. This is expected, as the gasoline being a product of a multiple series–parallel reactions, should rise from a minimum to a maximum and then later levels out. The exit of the riser at C/O ratio of 7.63 for gasoline 50.28 wt% compares favourably with the value of 50.10 wt% obtained by (Han and Chung 2001a) and 50.80 wt% in the plant as shown in Table 7.1. At C/O ratio of 6.09 and 5.06, the gasoline yields of respectively 43.40 wt% and 36.62 wt% are far from the average (50.39 wt%) of the yield in this simulation, the yield of the plant and literature (Han and Chung 2001b). the large variation is due to the difference in C/O ratios. The higher the C/O ratio, the higher the conversion of gas oil and the higher the yield of gasoline.

Similarly, the higher the C/O ratio, the higher the outlet temperature of the riser for both catalyst and gas phases as can be seen in Table 7.1 and Figure 7.4. The gas phase temperature at exit of the riser at C/O ratio of 7.63 is 795.0 K, which compares closely with the value of 793.5 K obtained by (Han and Chung 2001a) and 796.0 K in the plant as shown in Table 7.1. At C/O ratio of 6.09 and 5.06, the gas phase temperatures are respectively 772.2 K and 755.1 K and deviate from the average (794.8 K) of the gas phase temperature in this simulation, and that of the plant and literature (Han and Chung 2001b).

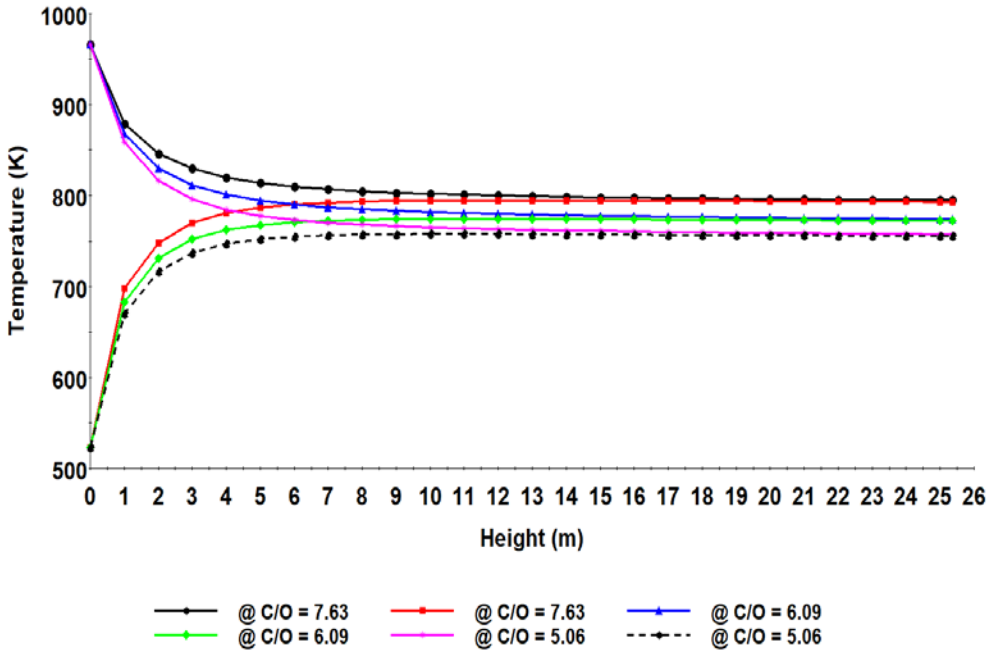

Figure 7.4: Temperature profiles of catalyst and gas phase at different C/O ratios

On a contrary, the higher the C/O ratio, the lower the outlet pressure of the riser as can be seen in Table 7.1 and Figure 7.5. The pressure at exit of the riser at C/O ratio of 7.63, 6.09 and 5.06 is respectively 200.51 kPa, 209.34 kPa and 216.76 kPa.

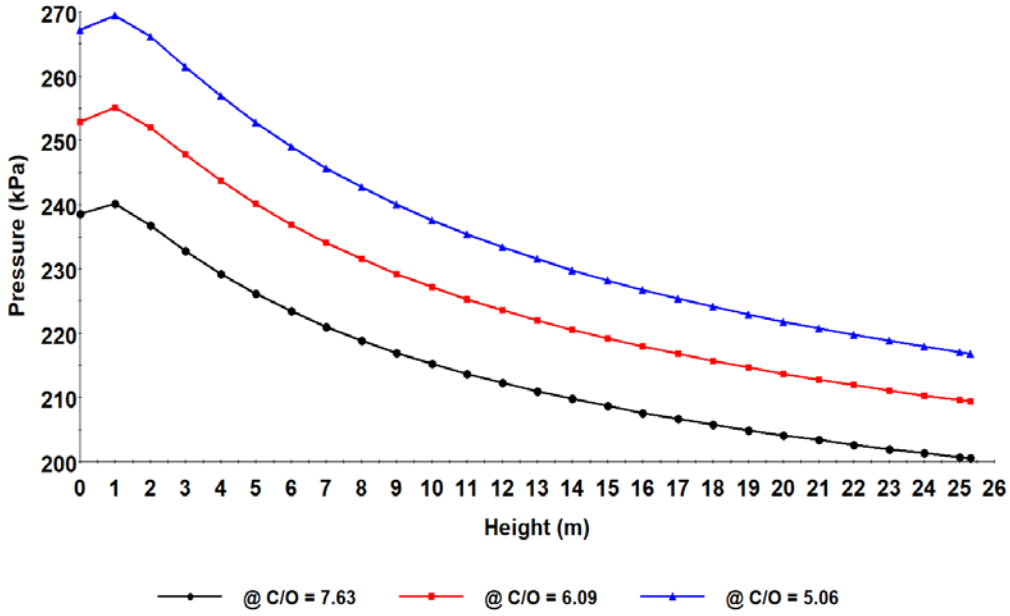

Figure 7.5: Pressure profiles of the riser at different C/O ratios

Similarly, the pressure drop at exit of the riser at C/O ratio of 7.63, 6.09 and 5.06 is respectively 38.06 kPa, 43.54 kPa and 50.46 kPa. The higher the C/O ratio, the lower the pressure drop. This suggests that it is better to operate the riser at

higher C/O ratio, since; higher C/O ratio has the advantage of producing the highest gasoline yield. Lower C/O ratio means more feed to the riser; hence, higher feed is proportional to higher-pressure drop. In addition, lower C/O ratio has higher inlet pressure. This means that the vaporisation section produces more vapour because of increased specific heat from the increased feed mass flowrate, leading to higher pressure.

For the varied diameter riser, the same C/O ratio of 7.63 was used and at gas oil inlet temperature of 523 K. The results obtained are presented in Figures (7.6) and Tables 7.2. In Table 7.2, the results for two different configurations were considered in the simulation; a 1 m diameter riser and a varied diameter riser. This is to enable comparison of the two configurations and to study the effect of the diameter variation on the riser column. The results are presented along with plant data for validation of the model.

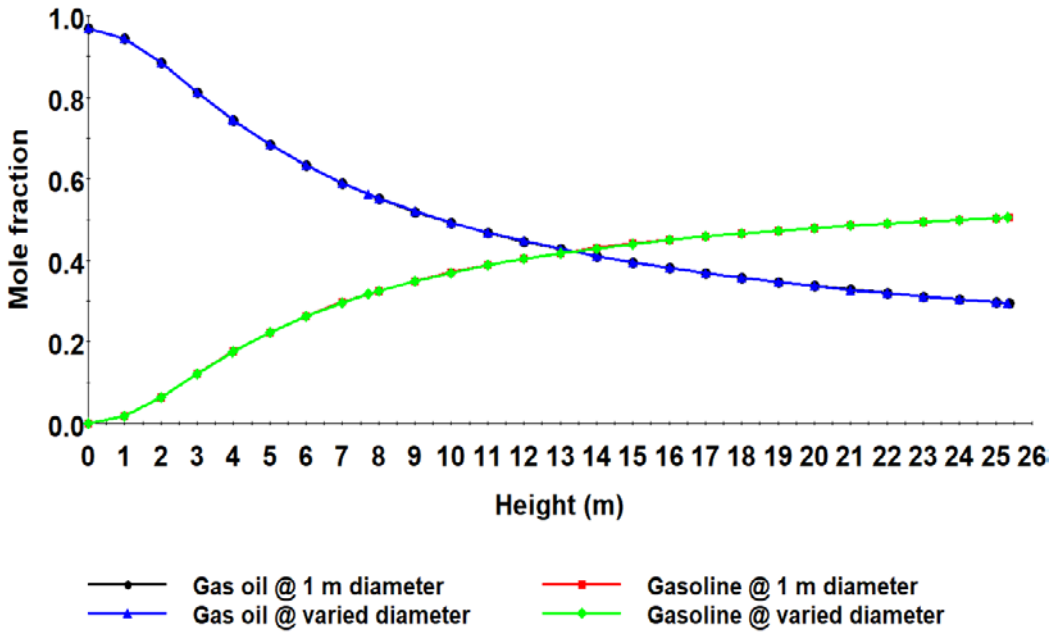

Figure 7.6: Mole fractions of gas oil and gasoline for 1 m and varied diameter riser

It can be seen from Figure 7.6, that the profiles of gas oil for 1 m diameter riser and varied diameter riser are almost the same with just a difference of 0.0007 wt% as shown in Table 7.1, corresponding to 0.23% difference. This is almost an insignificant difference. Similarly, the profiles of the yield of gasoline in Figure 7.6 shows closeness for 1 m diameter riser and varied diameter riser with a difference of 0.0003 wt%, a 0.06% difference. These insignificant differences show that the varying the riser diameter has very little significance on the yield of the products

in the riser. However, if the diameters are varied much more, the impact may be different. The challenge may be the actual data to use for validation since the diameters may not be varied arbitrarily.

Table 7.2: Weight fractions and temperatures at input different C/O ratios

Parameter	1 m diameter	Varied diameter	Absolute difference	Plant data
C/O ratio	7.63	7.63	0.00	7.59
Gas phase Temperature, T_g (K)	795.0	792.6	2.40	796.0
Catalyst Temperature, T_s (K)	793.1	795.2	2.10	
Gas oil (wt%)	0.2980	0.2973	0.0007	0.2600
Gasoline (wt%)	0.5028	0.5031	0.0003	0.5080
Pressure (kPa)	200.514	180.19	20.32	

Figure 7.7 also shows a similar trend for the temperature of the 1 m diameter and the varied diameter riser. The difference for the gas phase temperatures is 2.4 K, and 2.1 K for the catalyst temperature. These differences are not very significant; however, these differences are responsible for the small changes in the yield of gasoline observed.

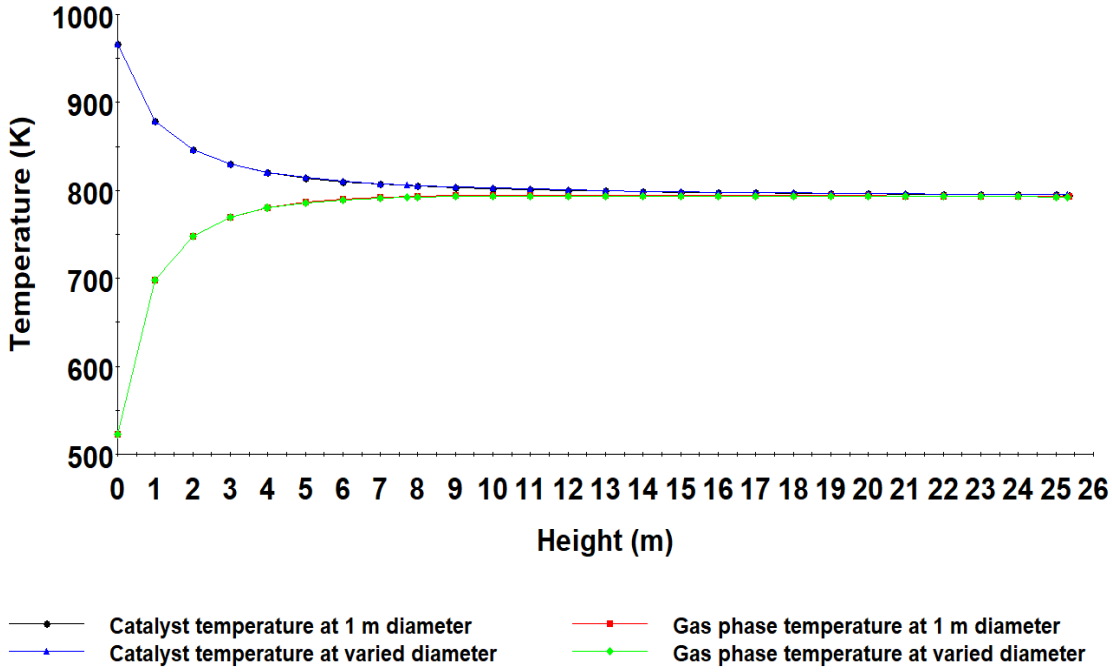

Figure 7.7: Temperature profiles of catalyst and gas phase for 1 m and varied diameter riser

For the pressure of the riser, it behaves differently. This is because the pressure is a function of the area of the riser and responsible for the riser hydrodynamics.

Pressure should be affected by the change in diameter of the system, due to both operational and design conditions of the system. Figure 7.8 shows clearly that the profile of the 1 m diameter continuously declined from a maximum inlet pressure of 238.57 kPa and gradually levels out to 200.51 kPa at the exit of the riser. For the varied diameter riser, the pressure behaves as if there were three riser reactors in series. The pressure declined from a maximum inlet pressure of 238.57 kPa followed the profile of the 1 m diameter to 229.36 kPa at height 3.965 m of the riser where it changed and behaved like a different riser. At this point, the pressure dropped from 229.36 kPa showing a sharp drop to 201.49 kPa. This drop is due to the sharp nature of the diameter change. Further pressure drop due to the diameter change is seen at 7.718 m of the riser height, which is a value of 195.69 kPa to 187.33 kpa, and eventually levels out to 180.19 kPa at the exit of the riser. The total pressure drop is 58.39 kPa for the varied diameter riser while 38.06 kPa. The difference in pressure drop between the two configurations is found to be 20.32 kPa.

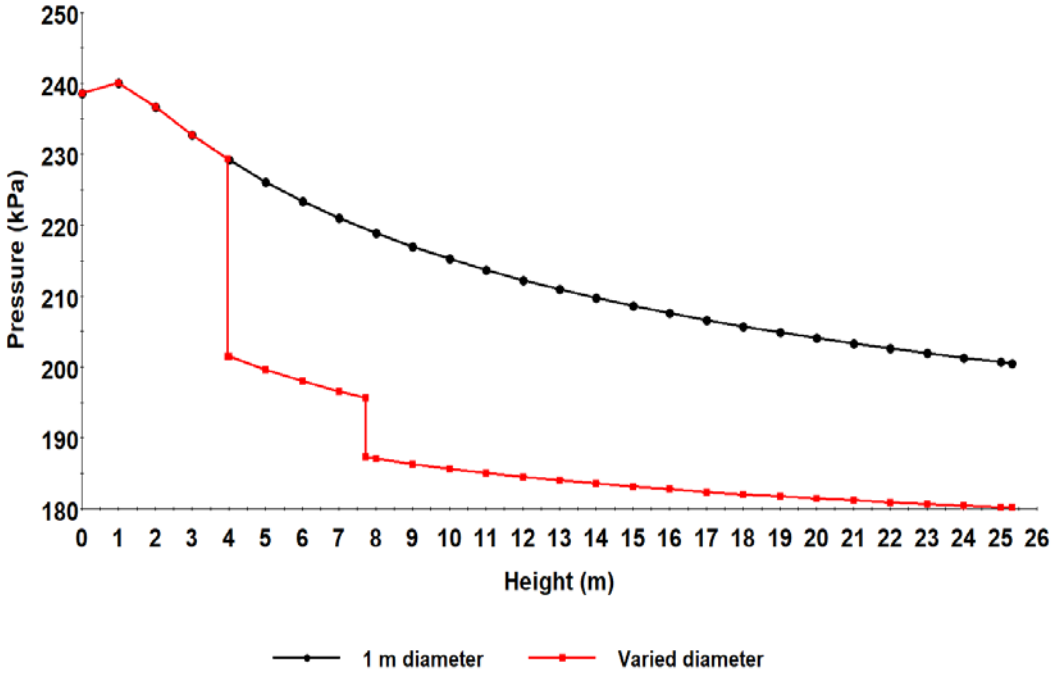

Figure 7.8: Pressure profiles for 1 m and varied diameter riser

7.3 The disengaging stripping section

In the stripper, hydrocarbon vapours from within and around the catalyst particles are moved by steam into the disengager dilute phase, decreasing hydrocarbon carry-under with the spent catalyst to the regenerator. Stripping is a very significant task due to its ability to minimises regenerator bed temperature and

regenerator air requirements, causing an increase in regenerator temperature conversion or air-limited operations.

After cracking of gas oil in the riser, the spent catalyst is immediately separated from the product vapour through the cyclones, in the disengaging-stripping section. The disengaging-stripping model, which consist of the coke, catalyst, gas component, energy, and pressure balances, is used to determine several major state variables: the coke on catalyst after stripping, the catalyst and gas holdups, and the reactor temperature and pressures. The primary function of the disengaging-stripping section is to separate the product gas from the catalyst in the disengager, and to recover the entrained and adsorbed hydrocarbon using minimal amount of steam from the pores and surface of the catalyst. Another advantage of the stripping section is to reduce the amount of hydrocarbon that escapes to the regenerator, because such hydrocarbon causes increase in regenerator temperature. Figures 7.9 – 7.14 shows the responses of the state variables in the disengaging stripping section.

The spent catalyst from the riser coming into the catalyst stripper adsorbs hydrocarbons on its surface and fills the catalyst's pores (Boum et al. 2015). Entrained hydrocarbon vapours also accompany it. The stripping steam is used principally to remove the entrained hydrocarbons between individual catalyst particles. Minimal cracking reactions continue to happen within the stripper and the reactor temperature and the catalyst residence time drive it. The higher temperature and longer residence time allow conversion of adsorbed hydrocarbons into "clean lighter" products (Sadeghbeigi 2012b).

Some quantity of hydrocarbon is trapped in the pores of the catalyst which are converted in the regenerator to coke (it is called catalyst-to-oil coke or occluded coke), this require more air required for regeneration. These hydrocarbons can be stripped by steam stripping the rate of which depends on the catalyst-to-oil ratio and steam injection rate. An exponential type stripping function is used to estimate the catalyst-to-oil coke in the disengaging-stripping section. The coke on the surface of the catalyst from the regenerator and the catalyst-to-oil makes the total coke in the disengaging-stripping section, which after stripping; coke-on-catalyst exiting the stripper is estimated by Equation (111) and shown as Figure 7.9.

Gas oil mass flowrate (49.3 kg/s, this is C/O ratio = 6.085) and dispersed steam mass flowrate (1.1 kg/s) are used as manipulating variables to study the

dynamics of the stripper. Four different cases were considered using 20% reduction on the manipulating variables.

Case 1 which is for the gas oil mass flowrate (49.3 kg/s), and dispersed steam mass flowrate (1.1 kg/s) shown in Figure 7.9. The initial amount of coke on the catalyst is 0.00900 kg-coke/kg-catalyst, but it gradually drops due to steam stripping to a minimum constant value of 0.00197 kg-coke/kg-catalyst in the first 230 s, and remained constant for the remaining total simulation runtime of 24000 s. In case 1, the percentage coke stripped is 78.11%.

Case 2 is also shown in Figure 7.9 for 20% reduction of gas oil mass flowrate (39.44 kg/s, this is C/O ratio = 7.606), while the dispersed steam mass flowrate (1.1 kg/s) is maintained as that of case 1. The initial amount of coke on the catalyst is 0.00900 kg-coke/kg-catalyst, but it gradually drops due to steam stripping to a minimum constant value of 0.00173 kg-coke/kg-catalyst in the first 270 s, and remained constant for the remaining total simulation runtime of 24000 s. In case 2, the percentage coke stripped is 80.78%. The percentage coke stripped for case 2 is 2.67% higher than case 1, even though it was obtained 40 s later. This shows that reducing the mass flowrate of the feed can improve the stripping of the coke-on-catalyst.

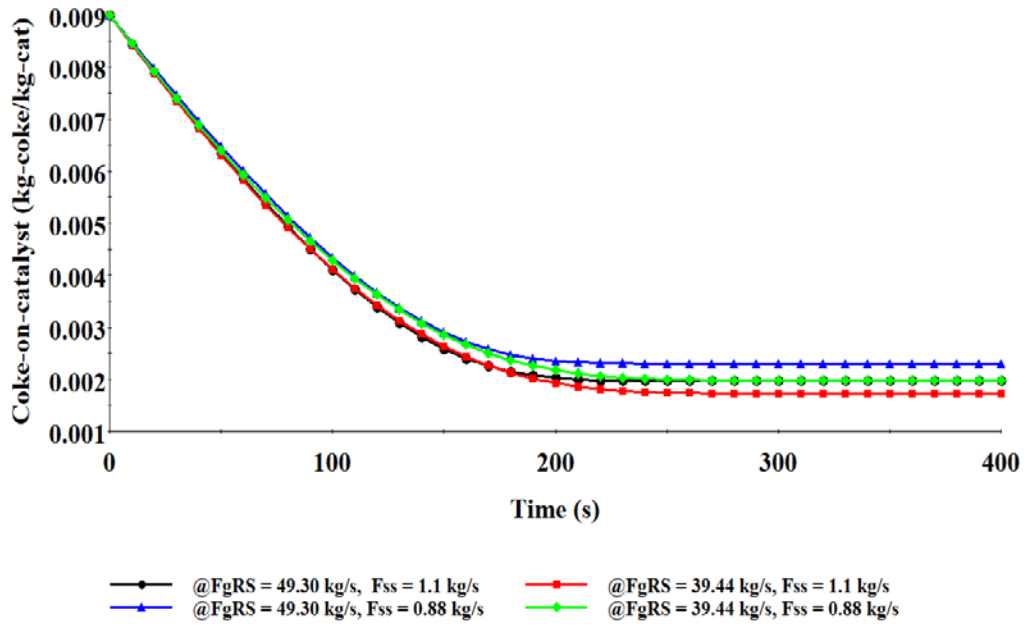

Figure 7.9: Dynamic response of coke-on-catalyst in the stripper

In case 3, there is 20% reduction of the dispersed steam mass flowrate (0.88 kg/s), while gas oil mass flowrate (49.30 kg/s) is maintained as that of case 1. For case 3, the catalyst is steam stripped from 0.009 kg-coke/kg-catalyst to a

minimum constant value of 0.00231 kg-coke/kg-catalyst in the first 270 s and remained constant for the remaining total simulation runtime of 24000 s. Case 3 achieved a constant minimum value of stripped coke at the same time of 270 s as case 2. In case 3, the percentage coke stripped is 74.38%. The percentage coke stripped for case 3 is 3.73% lower than case 1 and 6.40% lower than case 2. This shows that reducing the mass flowrate of the steam can reduce the stripping efficiency of the coke-on-catalyst. Comparing cases 1 and 3 where the mass flowrate of stripping steam differs at constant mass flowrate of feed, it shows that the stripping efficiency can be greatly impacted by reduced steam than reduced feed.

Case 4 shows where both mass flowrates of feed and steam are respectively reduced (39.44 kg/s and 0.88 kg/s) by 20%. The catalyst stripping in case 4 was achieved from 0.009 kg-coke/kg-catalyst to a minimum constant value of 0.00197 kg-coke/kg-catalyst in the first 300 s. This value remained constant for the remaining total simulation runtime of 24000 s. Case 3 achieved a constant minimum value of stripped coke at 300 s, which is longer than all the cases, however, the percentage coke stripped is 78.11%. The percentage coke stripped for case 4 is the same as in case 1 but 3.73% higher than case 3 and 2.67% lower than case 2.

The stripped coke-on-catalyst for cases 1 and 4 is the same, this means that once steady state operating conditions of the stripper are known, to keep the same amount of coke stripped from the catalyst, a corresponding percentage increase is made in the flowrate of steam for any disturbance in the feed flowrate. In addition, increase in the C/O ratio, require decreasing steam flowrate which eventually saves energy and the reverse is the case.

From Figure 7.10, at the maintained mass flowrate of feed, the effect of steam change is negligible. This is consistent with the fact that the flow rate of steam is small, less than about 0.3% of the catalyst flow, therefore, the effect of steam on the energy balance of the reactor is considerably small (Pathanjali et al. 1999). The temperature varies from 787.0 K to 783.2 K and 783.0 K for the cases with the same feed mass flowrate of 39.44 kg/s with only a difference of about 0.2 ^{o}C. The same for cases with the same feed mass flowrate of 49.30 kg/s, which varies from 787.0 K to 780.2 K and 780.0 K with only a difference of about 0.2 ^{o}C. These shows that the mass flowrate of feed is principally responsible for the dynamic response of temperature in the stripping section as shown in Figure 7.9. For the

same reason, change in the mass flowrate of feed in the stripper is also responsible for the dynamic responses for gas phase pressure, heat loss and gases hold up in Figures 7.11 to 7.13 respectively.

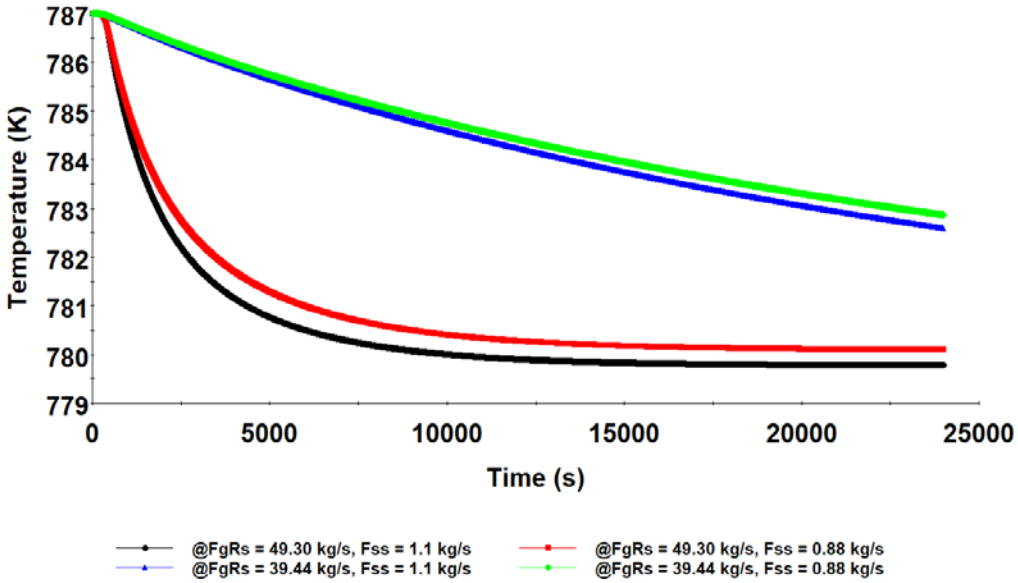

Figure 7.10: Dynamic response of temperature in the stripper

Figure 7.11 presents the dynamic response of the pressure of the stripping section. The mass flowrate of feed affects dynamic response of pressure in the stripping section. The impact of the steam flowrate is minimal.

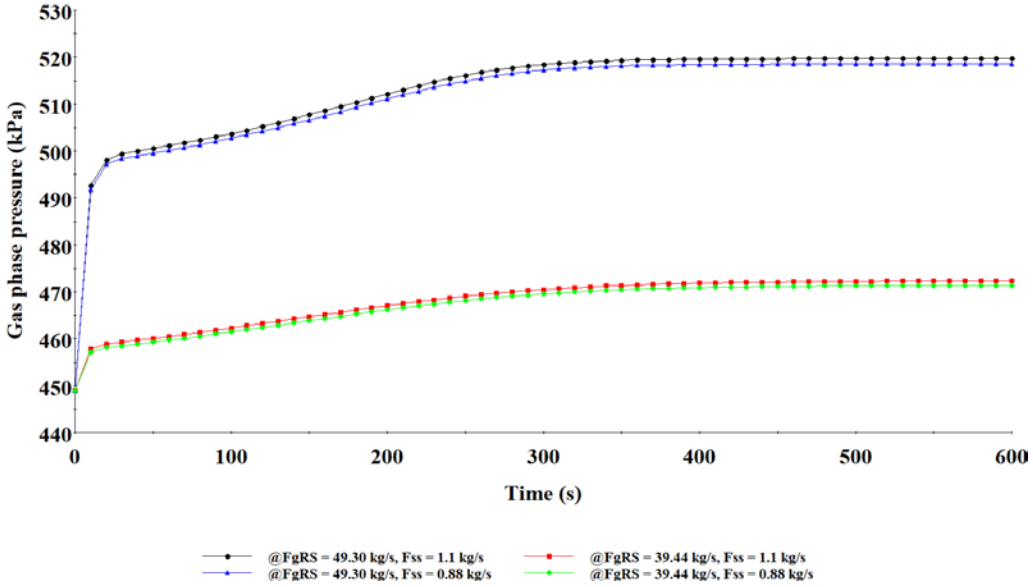

Figure 7.11: Dynamic response of pressure in the stripper

Figure 7.12 shows the dynamic response of the heat loss of the stripping section. Again, the mass flowrate of feed affects dynamic response of heat loss in the

stripping section. The higher the mass flowrate the lower the heat loss. The impact of the steam flowrate is not quite significant.

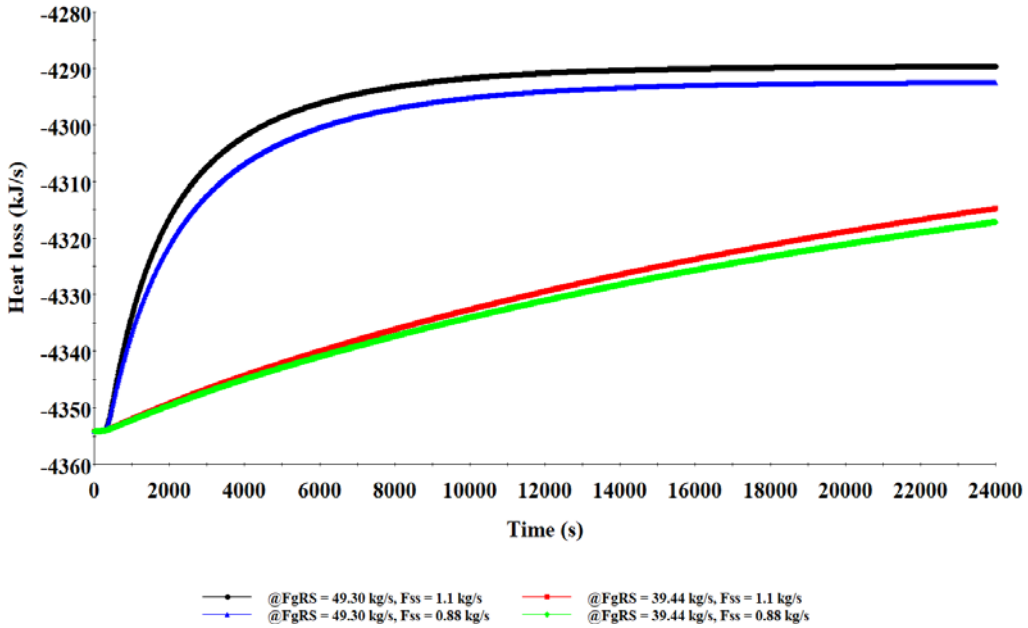

Figure 7.12: Heat loss in the stripper

Figure 7.13 shows the amount of gases in the stripping section, which increases with time at all conditions. However, more gases are formed with increased mass flowrate of feed rather than increase in amount of steam. Therefore, the mass flowrate of feed affects dynamic response of heat loss in the stripping section in a direct proportionality manner.

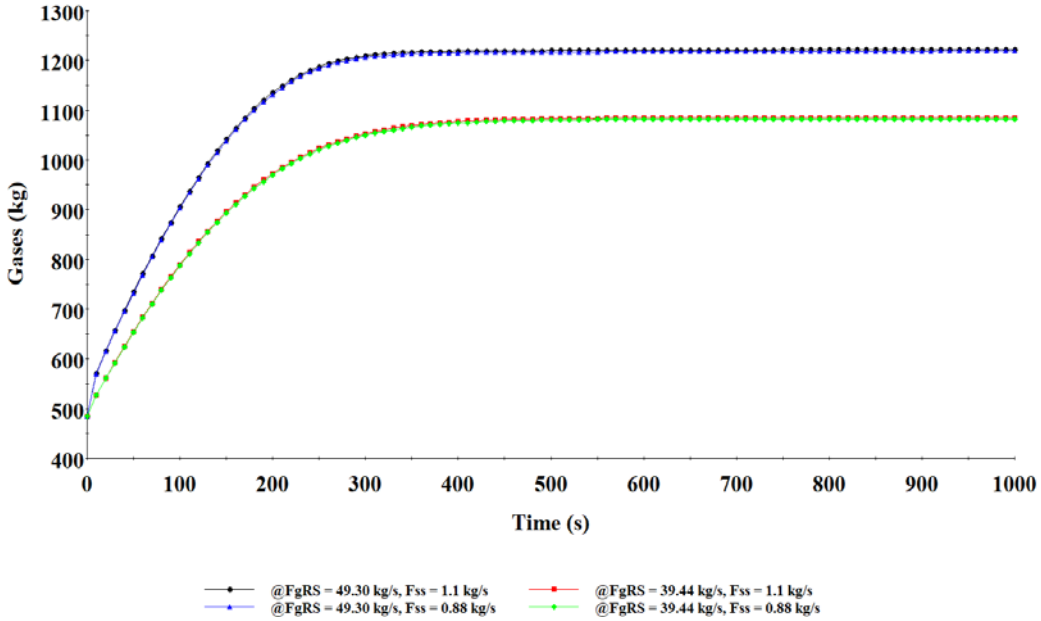

Figure 7.13: Dynamic response of gases in the stripper

Figure 7.14 shows the mass of catalyst in the stripper, which is the flow of spent catalyst to the regenerator. This is frequently regulated by either a slide or plug valve. The slide or plug valve keeps a desired level of catalyst in the stripper, which provides the pressure head to enable the catalyst flow from the reactor to regenerator (Jia et al. 2003). In all FCC units, an adequate catalyst level must be sustained in the stripper to prevent reversal of hot flue gas into the reactor. In this case, the mass falls from 38000 kg being the initial mass in the stripper at time zero, to 278.56 kg/s which is between the range of mass flowrates allowable by the plug/slide valve to the regenerator. This resulting mass flowrate of catalyst is attained after 300 s and remains almost constant throughout the period 24000 s of simulation. According to Pathanjali et al. (1999), the residence time of the catalyst inside the reactor-stripper system is in the order 5 to 6 min (300 s), this is consistent with the time taken in this simulation to have a constant mass flowrate of catalyst to the regenerator. Again, the increase for mass flowrate of steam is in independent of the amount of catalyst flowrate.

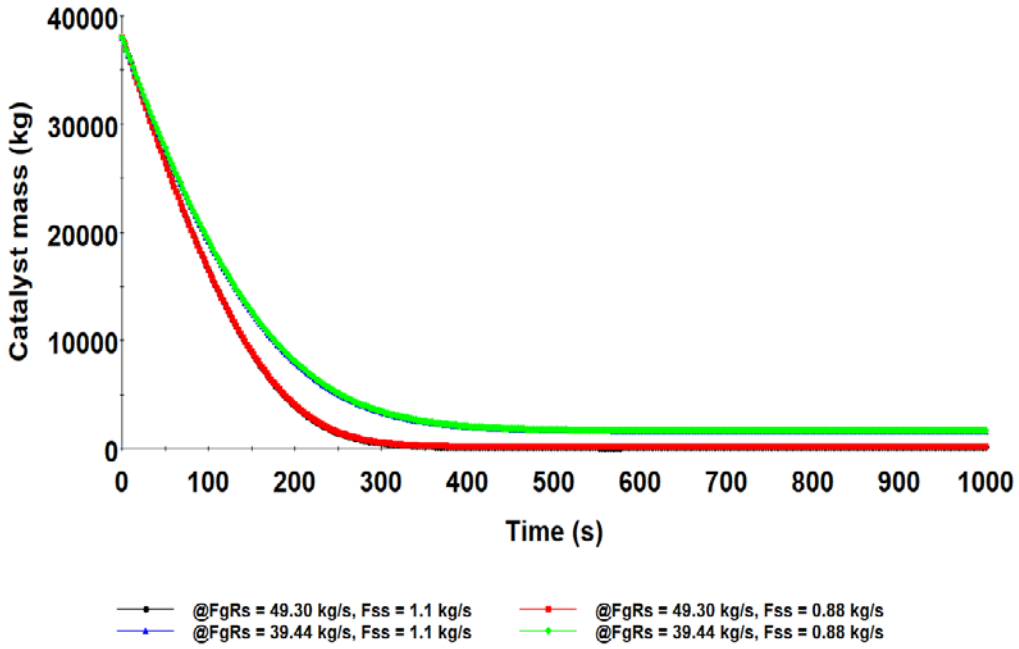

Figure 7.14: Catalyst holdup in the stripper

7.4 The regenerator

In the regenerator, coke is combusted off the catalyst with air in a fluidised bed system to provide the heat requirements of the process and restore the catalyst's activity. The regenerator works in either of two modes: complete or partial CO combustion. One of the main objectives of the regenerator is to burn off coke on spent catalyst to bring back its activity. Other importance includes: to attain low coke on regenerated catalyst, burn more coke at minimum blower air mass flowrate, minimise catalyst deactivation and CO_2 yield, and minimise after burn reaction (Yang 2003).

In partial combustion mode, a less-than-theoretical, or stoichiometric, amount of air is delivered to the regenerator, where little carbon in coke is burnt to carbon dioxide, and the balance of the carbon is burnt to carbon monoxide. Since oxygen is supplied in little amount, all amount of oxygen is expected to be consumed and none should be present in the flue gas. The main parameter to observe in partial combustion regeneration is the CO/CO_2 ratio in the flue gas, which is in the range from 0.5 to 2.0.

Excess air is supplied to the regenerator in total combustion mode, which means all carbon in the coke and carbon monoxide present should be converted to carbon dioxide (Yang 2003).

The coke on regenerated catalyst is a key performance measurement for both partial and total combustion regenerators. For total combustion regenerators, coke on regenerated catalyst is about 0.05 wt% or lower. For partial combustion regenerators, coke on regenerated catalyst is about 0.1 wt% or higher.

Another occurrence in the regenerator is the after-burn reaction, which happens in the partial combustion regenerator because of oxygen that escape the dense bed to the freeboard. When such happens, enormous heat of combustion is generated. Subsequently, due to minute catalyst presence in the freeboard, the heat capacity is low, and the temperature increases rapidly, which is called after-burn. Intense after-burn, results in mechanical damage to the regenerator cyclone system. The most significant advantage of total combustion regenerators is that the CRC is low and catalyst (Yang 2003).

In this work, the regenerator is simulated for 24000 s (400 min) in a closed circuit with the riser and disengaging-stripper section. At mass flowrate of feed 49.3 kg/s, mass flowrate of steam 1.1 kg/s, temperature of air 432 K and mass of air

34 kg/s, a dynamic response of some major state variables of the regenerator is given, with their profiles along the height of the regenerator. Figure 7.15 shows the dynamic response of carbon dioxide along the height of the regenerator.

At the entrance of the regenerator, CO_2 is given as 0.0040 kg mol/m^3 as seen in Figure 7.15. It rose due to combustion of coke or carbon to 0.0059 kg mol/m^3 in the first 2 m of the regenerator height and dropped to a value of 0.0056 kg mol/m^3 before it gradually increased to 0.0058 kg mol/m^3 towards the end of the regenerator dense bed. There is a 45% CO_2 increase in the dense bed. This amount of CO_2 increased goes to the atmosphere and contribute to the global warming. Estimating the amount is important to measure how much reduction can be made through operational changes as well as capture for sequestration.

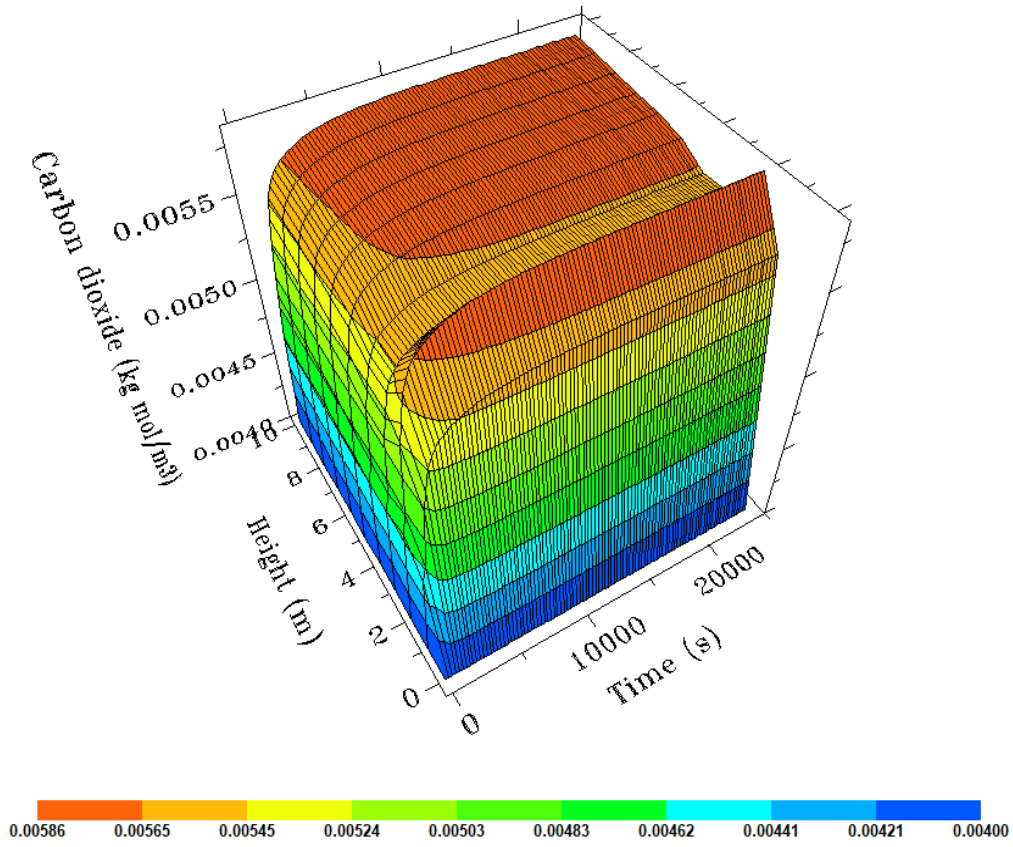

Figure 7.15: Carbon dioxide concentration in the regenerator dense bed

At the entrance of the regenerator, the number of moles of CO is given as 0.0003 kg mol/m^3 as seen in Figure 7.16. It decreased gradually to 7.17 x 10^5 kg mol/m^3 at the exit of regenerator dense bed. The CO/CO_2 ratio is 0.0124, which is very low compared to the range 0.5 -2.0 for partial combustion regenerators. This signifies that complete combustion is mode of combustion in the regenerator, where little or no CO is present in the flue gas (Yang 2003). It also shows that

after-burning reaction in the freeboard is minimised. There is a 76.1% CO decrease in the dense bed. This amount accounts for even the CO that is produced because of combustion of coke, which is eventually reduced, instead of being sent into the atmosphere. For FCC unit that operate the CO boiler unit for generation of energy, this operating condition is not favourable. Estimating the amount is important to measure how much operational changes can result in severe conditions in the freeboard.

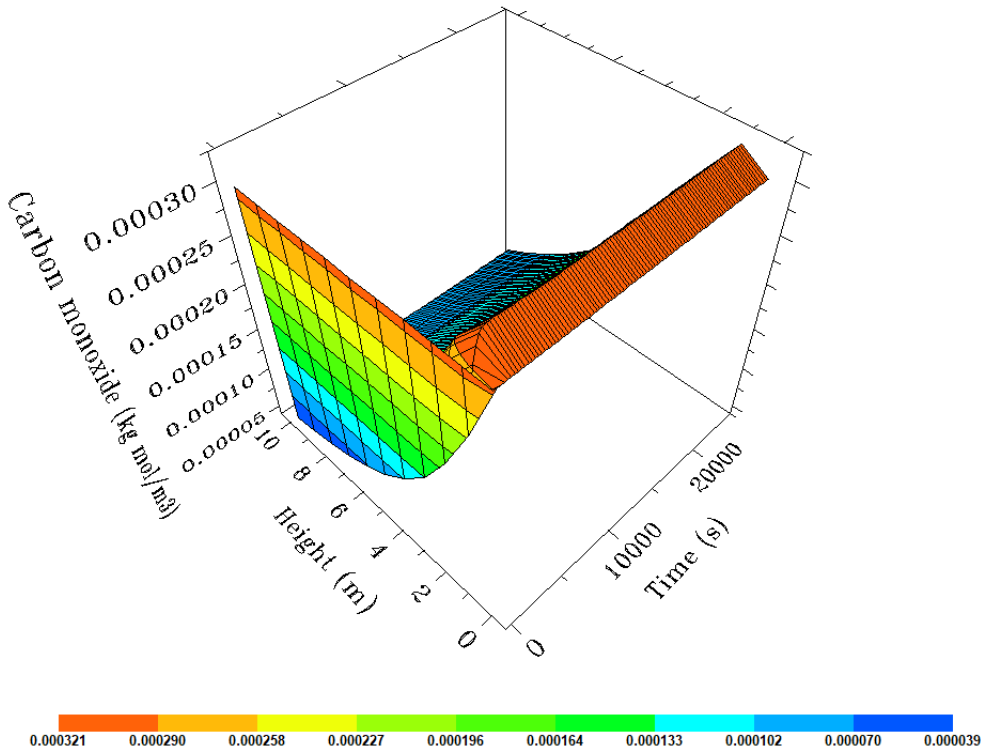

Figure 7.16: Carbon monoxide concentration in the regenerator dense bed

Figure 7.17 presents the oxygen concentration in the regenerator dense bed. It shows the dynamic response of oxygen concentration and along the height of the regenerator.

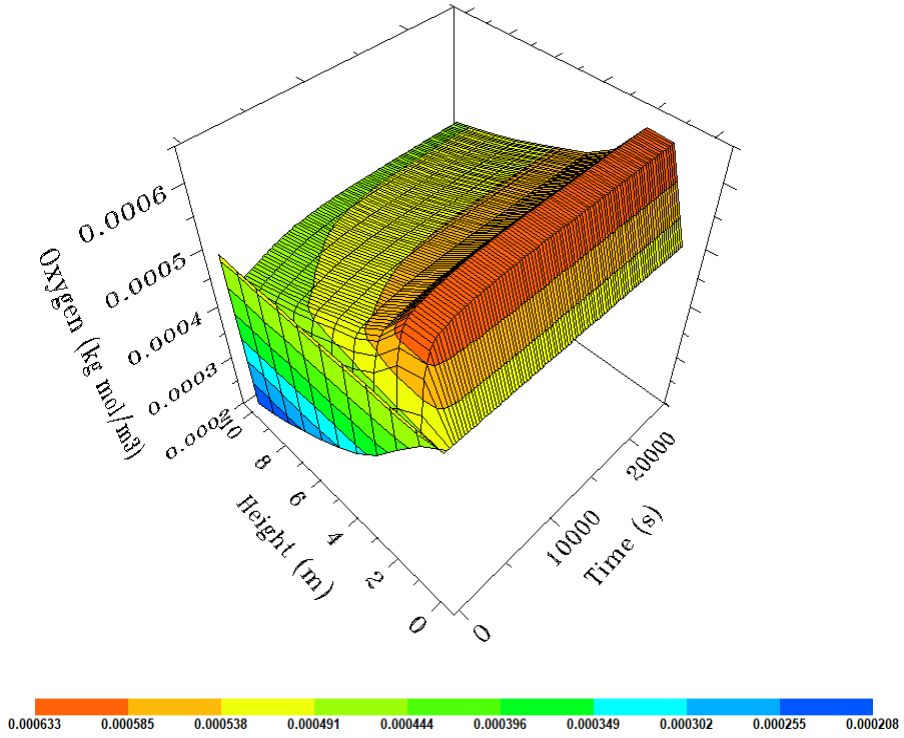

Figure 7.17: Oxygen concentration in the regenerator dense bed

At the entrance of the regenerator, the moles of oxygen is given as 0.0005 kg mol/m^3 as seen in Figure 7.17. It decreased gradually to 0.00048 kg mol/m^3 at the exit of regenerator dense bed. The amount consumed in the regenerator shows that oxygen is much, again signifying the nature of the combustion in the regenerator, which is a complete combustion. There is a 4.0% oxygen concentration decrease in the dense bed.

Figure 7.18 presents Nitrogen concentration in the regenerator dense bed. It shows the dynamic response of nitrogen concentration and along the height of the regenerator.

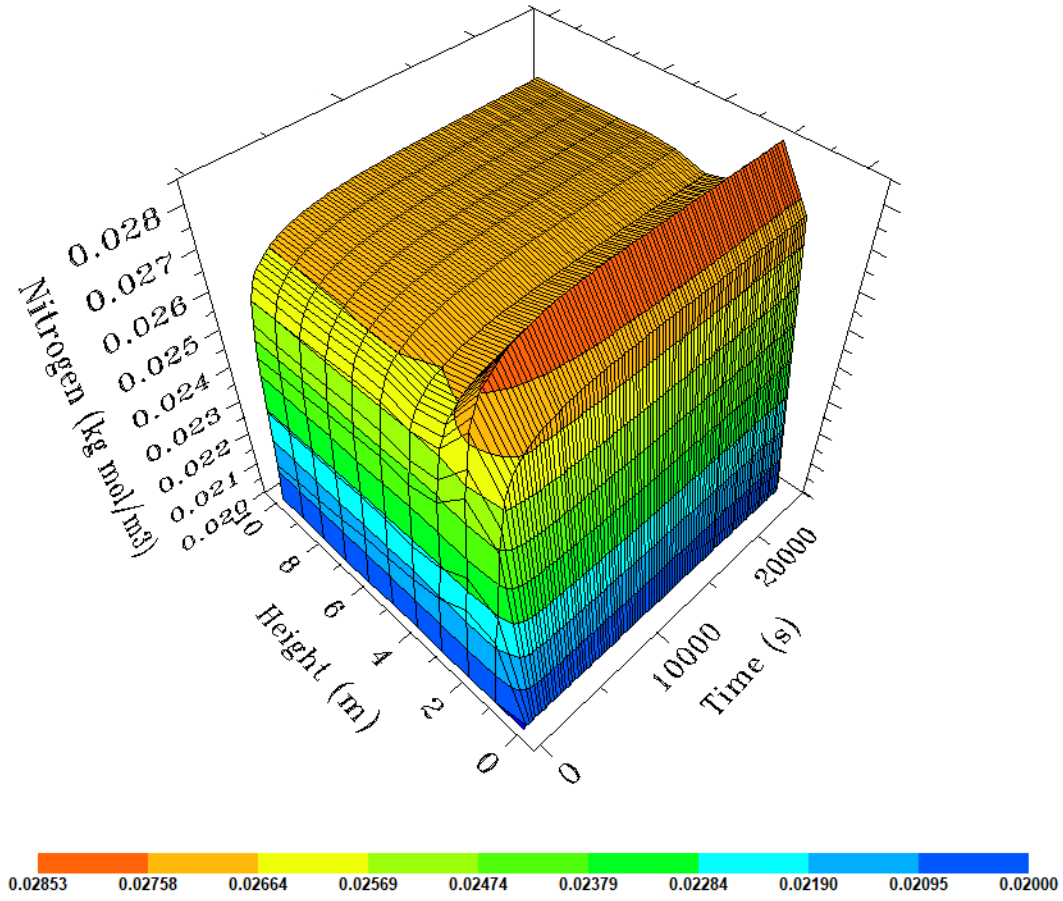

Figure 7.18: Nitrogen concentration in the regenerator dense bed

Subject to the nature of FCC feed, nitrogen levels and regenerator conditions, NO_x concentrations are normally in the range of 50–500 ppm, and they are emitted from the regenerator contributing almost 50% of the total NO_x emissions in a refinery. This contains mainly NO that is formed in the regenerator, while NO_2 is formed only after NO is being released to the air (Zhao et al. 1997). In this simulation, much oxygen is seen in the flue gas, which encourages the formation of NO_x. At the entrance of the regenerator, the moles of nitrogen is 0.02 kg mol/m^3 as seen in Figure 7.18. It increased gradually to 0.027 kg mol/m^3 at the exit of regenerator dense bed. There is a 35% Nitrogen concentration increase in the dense bed. The amount produced in the regenerator shows that, with oxygen is in excess, high nitrogen compounds are produced (Zhao et al. 1997).

Figure 7.19 presents the water concentration in the regenerator dense bed. It shows the dynamic response of water concentration and along the height of the regenerator. The moles of H_2O is 0.0030 kg mol/m^3 at the entrance of the regenerator at time zero, as seen in Figure 7.19. It rose due to combustion of coke to 0.0042 kg mol/m^3 in the first 2 m of the regenerator height and gradually

dropped to a constant value of 0.0041 kg mol/m^3 to the end of the regenerator dense bed. There is a 36.7 % H_2O increase in the dense bed. It is important to estimate the amount H_2O in the regenerator to control the poisoning of the catalyst. In the presence of water vapour, Vanadium oxide can form volatile vanadic acid. Being a strong acid, it destroys zeolite structure (Akah 2017). Hence, the concentration of water needs to be measured and monitored.

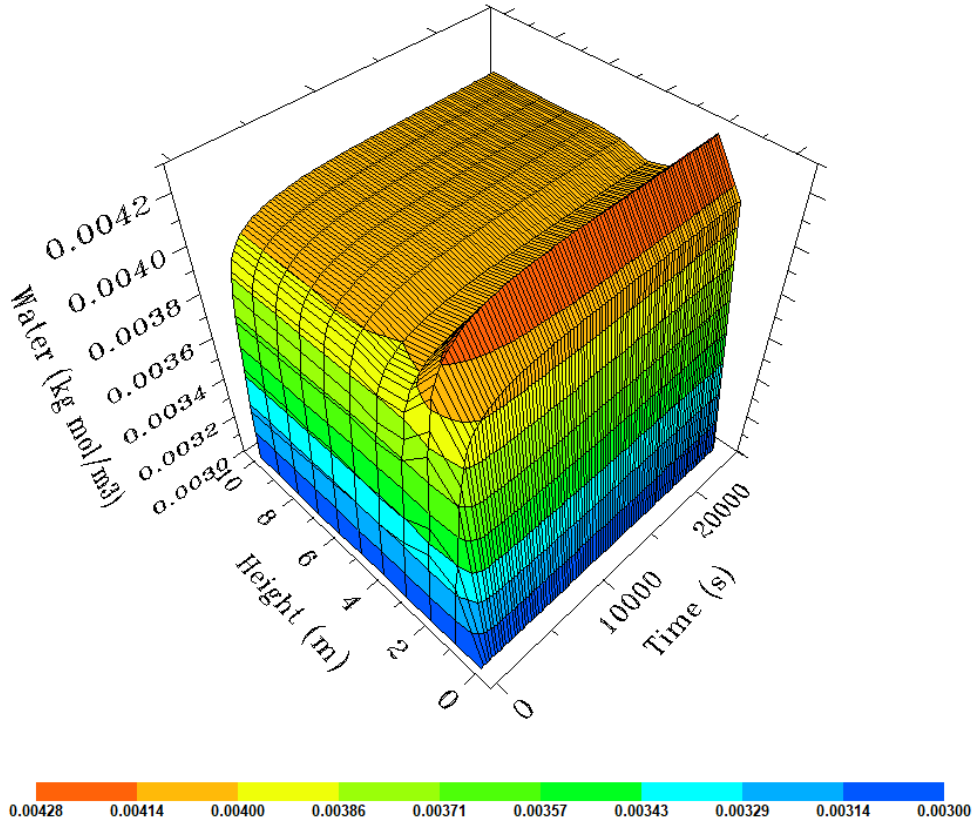

Figure 7.19: Water concentration in the regenerator dense bed.

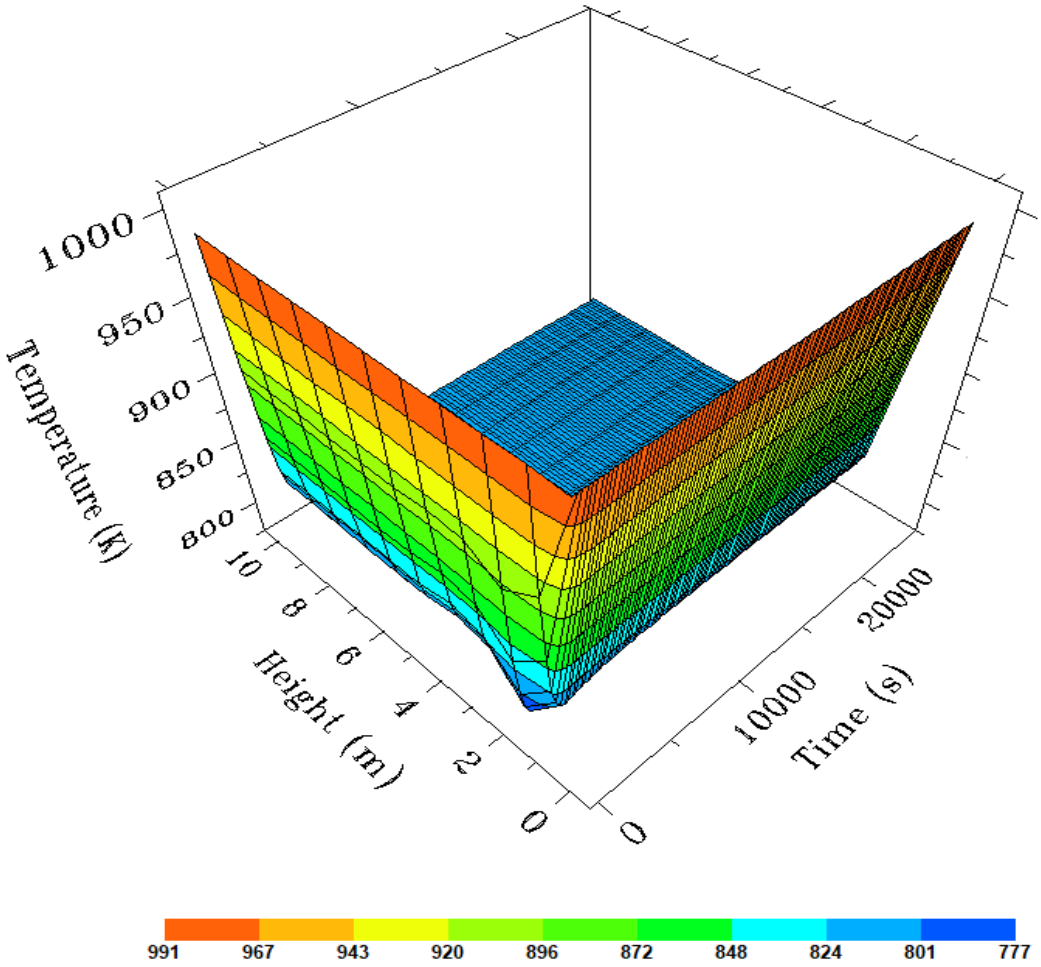

Figure 7.20: Temperature of the regenerator dense bed

Figure 7.20 presents the temperature of the regenerator dense bed. It shows the dynamic response of the temperature and its variation along the height of the regenerator.

At initial condition, the temperature of the regenerator is 991 K as seen in Figure 7.20. It gradually decreased to 819 K at the exit of regenerator dense bed. This is consistent with what was obtained by (Han and Chung 2001b). The temperature of the dense bed is responsible for the riser cracking reactions.

Figure 7.21 presents the pressure of the regenerator dense bed. It shows the dynamic response of the pressure and its variation along the height of the regenerator. At initial condition, the pressure of the regenerator is 289.16 kPa as seen in Figure 7.21, which was the pressure from the disengaging-stripping section. It gradually decreased to 283.50 kPa, a pressure drop of 5.66 kPa at the exit of regenerator dense bed. This is also consistent with the pressure drop across the regenerator given by (Han and Chung 2001b). It is expected that the regenerator pressure drop should be lower than the riser pressure drop which is

usually between 16 -30 kPa. This is to ensure pressure balance between the regenerator and the riser; a driving force that both units depend upon.

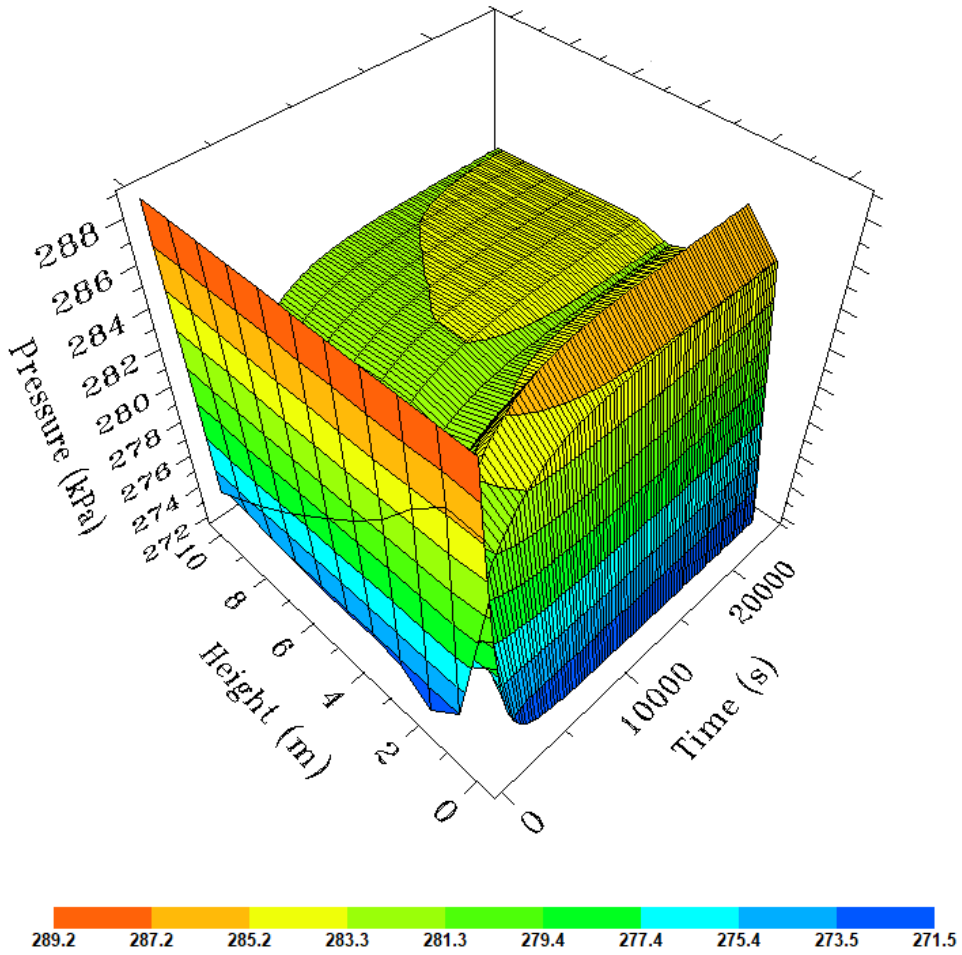

Figure 7.21: Pressure of the regenerator dense bed

Figure 7.22 presents the catalyst hold up in the regenerator. The initial mass of catalyst in the regenerator is 182000 kg, which rapidly decreases to 109580.5 kg in 2000 s and gradually becomes almost steady at 97009.7 kg for the remain part of the 24000 s of the simulation time. It is expected to have such holdup in the regenerator to maintain moderate temperature and pressure required for the burning of coke and regenerating the deactivated catalyst. This fluctuation of the catalyst holdup is responsible for the catalyst bed height as shown in Figure 7.22.

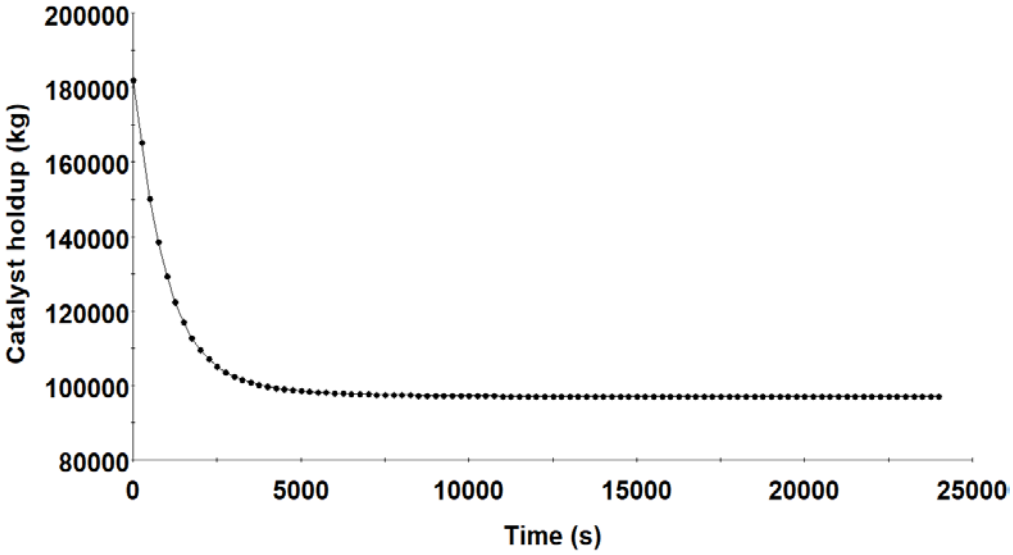

Figure 7.22: Catalyst holdup in the regenerator dense bed

When catalyst fall into the regenerator, the dense bed height increases due to catalyst hold up. However, the dense bed eventually become levelled at steady state. At the beginning of the simulation, the dense bed height is 7.08 m, but at steady state, the height become 3.57 m. This is consistent with the dense bed height reported by Freire de Almeida (2016).

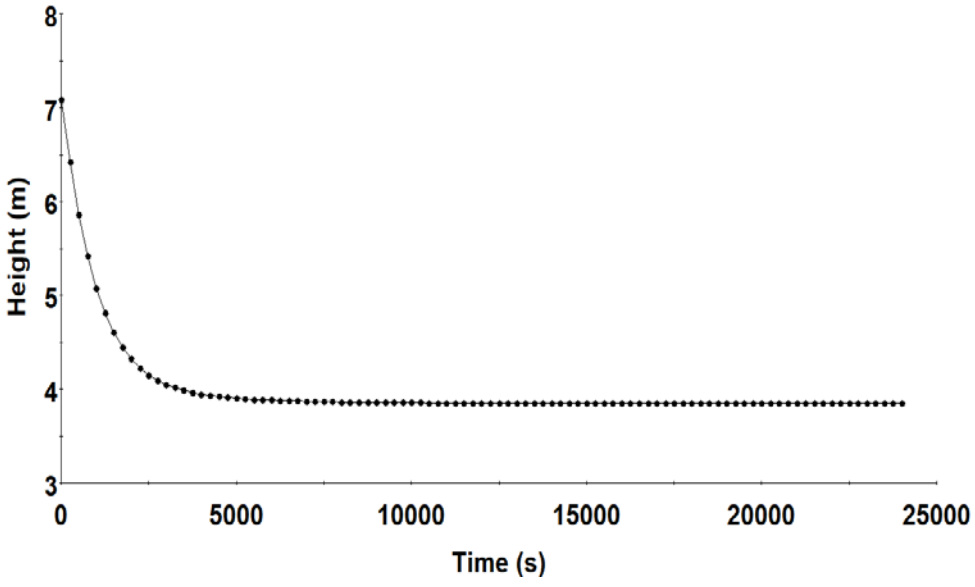

Figure 0.23: Height of catalyst in the regenerator dense bed

Figure 7.24 presents the spent catalyst flowrate from the slide valve after the stripper to the regenerator. At initial condition, the mass flowrate of the regenerated catalyst coming into the riser is 300 kg/s, which is the mass of spent catalyst flowing into the disengager-stripper section. Due to the stripper holdup,

the catalyst leaving the stripper from the slide valve is 301.5 kg/s, just slightly above the mass flowrate in the riser. This eventually drops due to catalyst loss and stripper hold up required to prevent backward flow of air from the regenerator. The spent catalyst mass flowrate dropped to 292.89 kg /s after 6000 s became steady at 292.07 kg/s for the remaining part of the 24000 s of the simulation. The spent catalyst enters the regenerator at 292.07 kg/s. At this point, the spent catalyst is regenerated, but leaves the regenerator back to the riser as regenerated catalyst. At time equal zero, the mass flowrate of the regenerated catalyst is 379.94 kg/s, and after 6000 s, the regenerated catalyst flowrate is 292.89 kg/s. For the remaining part of the simulation, the regenerated catalyst flowrate became steady at 292.07 kg/s. This shows that at steady state, the mass of spent catalyst coming into the riser is the same as the regenerated catalyst coming out of the regenerated and going to the riser. However, the riser and the regenerator were simulated in a closed circuit; the mass flowrate of regenerated catalyst should be 300 kg/s going into the riser. With a difference of 7.93 kg/s of regenerated catalyst, there is need for fresh catalyst addition to make it up to 300 kg/s. This difference is only noticeable when the riser and regenerator are concurrently simulated. Therefore, 7.93 kg/s is the amount of fresh catalyst added to the riser under the current operating conditions. This is a usual industrial practice.

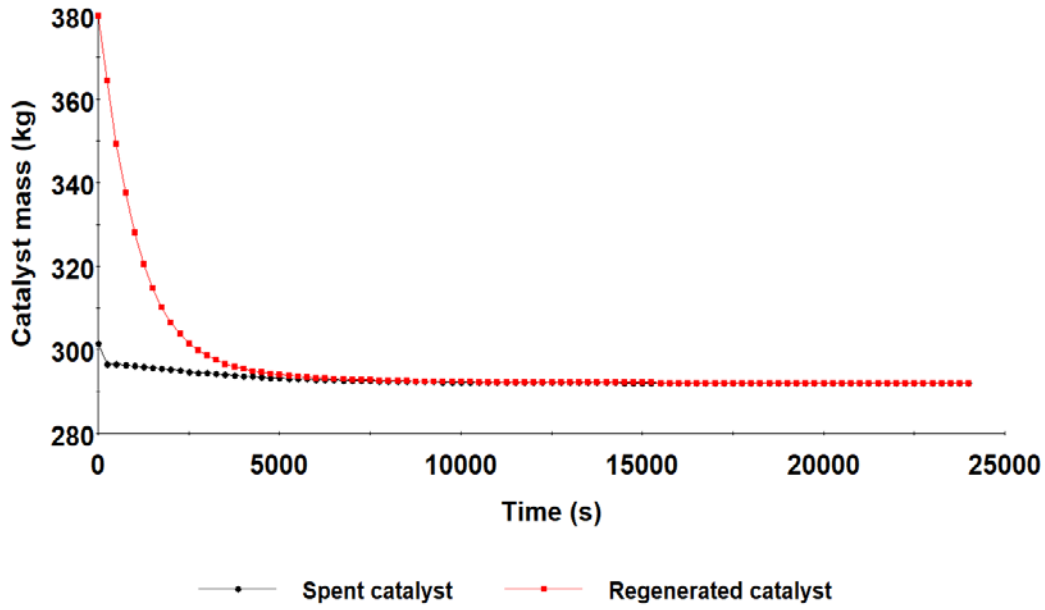

Figure 7.24: Spent and regenerated mass flowrate

7.5 Summary

The riser (1 m diameter and varied diameter), disengaging-stripping section and the regenerator dynamic and distributed model were simulated concurrently in this chapter and the following conclusions were made:

- The higher the C/O ratio, the higher the conversion of gas oil and the higher the yield of gasoline
- The higher the C/O ratio, the higher the outlet temperature of the riser for both catalyst and gas phases
- The higher the C/O ratio, the lower the outlet pressure, but the lower the pressure drop of the riser
- Varying the riser diameter has very little significance on the yield of the products in the riser
- The stripping efficiency can be greatly impacted by reduced steam than reduced feed
- Increase in the C/O ratio, require decreasing steam flowrate which eventually saves energy and the reverse is the case
- The change in mass flowrate of feed has more impact than the mass flow rate of steam on the dynamic change in temperature, pressure, gases hold up and heat loss in the stripping section
- The regenerator operates in a complete combustion mode since CO/CO_2 ratio of 0.0124 is far less than and outside the range 0.5 – 2.0 for combustion partial combustion regenerator mode.
- High concentration of nitrogen and water was found, hence, there is need to operate the regenerator to stifle the production of water and nitrogen.
- The riser and the regenerator were simulated concurrently and found that the mass flowrate of regenerated catalyst has a difference of 7.93 kg/s. It should be 300 kg/s going into the riser. Hence, the fresh catalyst added to the riser is 7.93 kg/s.

Chapter 8:

Conclusions and Recommendation for Future Research

8.1 Conclusions

The FCC unit is described as the workhorse of the petroleum refinery because it accounts for the highest yield of fuels from the unit. Its operation is central to the effective performance of a refinery. The aim of this work was to model, simulate and optimise the FCC unit, which consists of a varied diameter riser, regenerator, stripper and cyclones using gPROMS®. An extensive literature review was carried out and was found that there is always the need to improve on the yield of the fuels such gasoline, diesel, propylene etc, through optimisation and development of new kinetic parameters that represent some kinetic reactions in actual units. This was possible with the development of an adequate model of the FCC unit and the following conclusions were made:

- The model of the FCC riser was improved to include the non-ideality of its gas phase. A correlation was developed to measure the magnitude of deviation of the gas phase from ideal gas. It was also evident that every riser has a different pressure profile and Z factor profile depending on the riser diameter. Therefore, the hydrodynamics of the riser are affected by this model improvement, which in turn affect the design and operations of the FCC unit.
- A new six-lump kinetic scheme, which was based on a real industrial process was developed. With these model improvements, the response and capability of FCC unit can be relied upon and those responsible for planning can confidently generate processing targets knowing that the optimised solution is being used.
- A new parameter estimation technique was proposed and used to estimate new kinetic parameters for the new six lump kinetic scheme. The results obtained were a good representation of the FCC unit cracking reactions. This new scheme can be used to estimate process parameters for all kinds of processes, not just the FCC unit.
- Using the new parameter estimation technique, a set of new kinetic parameters such as frequency factor, activation energy and heat of

reaction of FCC reactions were estimated for a six-lumped kinetic model with a separate propylene lump. To the best knowledge of the author, this is believed to be the first attempt to produce propylene as a single lump in a conventional FCC unit. Hence, making it cost effective for FCC operators and other propylene producers to obtain propylene, which may not require further separation from other components.

- Three different optimisation problems were solved. They are the maximisation of gasoline, maximisation of propylene in the riser, and the minimisation of CO2 in the regenerator. An increase of 4.51% gasoline, 8.93 wt.% increase in propylene as a single lump and 5.24 % reduction of carbon dioxide emission were achieved. The increase in the yields of gasoline and propylene means an increase in profitability of the FCC unit, while the percentage reduction of the CO2 is a good step in cutting down the effect of CO2 emission from the FCC unit on global warming. With 5.24% reduction obtained in this simulation, it shows that using operational changes in process variables of the regenerator can bring about great reduction in CO2 emission.
- The riser diameter was varied to study the effect of change in diameter on the yield of fuels in the riser. It was found that when the riser diameter was varied, it had very little effect on the yield of the products.

8.2 Recommendations for future research

- Concurrent simulation of the riser and a two-stage regenerator would be benefit from a further investigation. There exists already a simulation of the two-stage regenerator of Orthoflow FCC unit, but this model is not comprehensive. Hence, a comprehensive riser model as used in this work could potentially be used with a detailed model of the Orthoflow regenerator.
- The diameter of riser studied in this work was varied according to industrial unit; hence, the diameter variation was limited to the industrial design. It was found that the impact on the yield of products was minimal. Further variation of the diameter can be considered to further study the impact on the yield and other process variables.
- When the riser-regenerator was concurrently simulated, there was need to keep adding fresh catalyst to maintain a constant input to the riser. this

can easily be achieved with the use of controllers. Hence, it is recommended that control studies be carried out on the compressive riser-regenerator system.

- Due attention to description of the catalyst deactivation was not given in this research. Although the chosen reaction network predicts the coke formation and describes the catalyst deactivation by coke, it does not consider the influence of the raw materials composition and heavy metals. Therefore, it is recommended that the description of the catalyst deactivation incorporate the effects of different types of FCC feeds.
- The weight fractions of the lumps were determined in this research, but it does not consider the reactivity of hydrocarbons inside the lumps and the group characteristics of vacuum gas oil, which significantly affect the coke yield, catalyst activity, products yield and composition. This is recommended for further study in other to improve the quality of the products from the riser.
- It is recommended to study the different mechanisms for catalyst deactivation by coke and heavy metals, as well as their impact on product distribution.

References

Ahari, J. S., Farshi, A. and Forsat, K. (2008a) A Mathematical Modeling of the Riser Reactor in Industrial FCC Unit. *Petroleum & Coal* 50 (2) 15-24.

Ahari, J. S., Farshi, A. and Forsat, K. (2008b) A Mathematical Modeling of the Riser Reactor in Industrial FCC Unit. *Petroleum & Coal* 50 (2) 15-24.

Ahmed, T. (2001) *Reservoir Engineering Handbook (2nd Edition).* Elsevier.

Ahsan, M. (2012) Computational fluid dynamics (CFD) prediction of mass fraction profiles of gas oil and gasoline in fluid catalytic cracking (FCC) riser. *Ain Shams Engineering Journal* 3 (4) 403-409.

Ahsan, M. (2015) Prediction of gasoline yield in a fluid catalytic cracking (FCC) riser using k-epsilon turbulence and 4-lump kinetic models: A computational fluid dynamics (CFD) approach. *Journal of King Saud University - Engineering Sciences* 27 (2) 130-136.

Aitani, A., Yoshikawa, T. and Ino, T. (2000) Maximisation of FCC light olefins by high severity operation and ZSM-5 addition. *Catalysis Today* 60 (1) 111-117.

Akah, A. (2017) Application of rare earths in fluid catalytic cracking: A review. *Journal of Rare Earths* 35 (10) 941-956.

Akah, A. and Al-Ghrami, M. (2015) Maximizing propylene production via FCC technology. *Applied Petrochemical Research* 5 (4) 377-392.

Akah, A., Al-Ghrami, M., Saeed, M. and Siddiqui, M. A. B. (2016) Reactivity of naphtha fractions for light olefins production. *International Journal of Industrial Chemistry*.

Al-Khattaf, S. and de Lasa, H. (1999) Activity and Selectivity of Fluidized Catalytic Cracking Catalysts in a Riser Simulator: The Role of Y-Zeolite Crystal Size. *Ind. Eng. Chem. Res.* 38 1350-1356.

Al-Sabawi, M., Atias, J. A. and de Lasa, H. (2006a) Kinetic Modeling of Catalytic Cracking of Gas Oil Feedstocks: Reaction and Diffusion Phenomena. *Ind. Eng. Chem. Res.* 45 (1583-1593).

Al-Sabawi, M., Atias, J. A. and de Lasa, H. (2006b) Kinetic Modeling of Catalytic Cracking of Gas Oil Feedstocks: Reaction and Diffusion Phenomena. *Ind. Eng. Chem. Res.* 45 1583-1593.

Ali, H. and Rohani, S. (1997) Dynamic Modeling and Simulation of a Riser-Type Fluid Catalytic Cracking Unit. *Chemical Engineering Technology* 20 118-130.

Ali, H., Rohani, S. and Corriou, J. P. (1997) Modelling and Control of a Riser Type Fluid Catalytic Cracking (FCC) Unit. *Chemical Engineering Research and Design* 75 (4) 401-412.

Almeida, N. E. and Secchi, A. R. (2011) Dynamic Optimisation of a FCC Converter Unit: Numerical Analysis. *Brazilian Journal of Chemical Engineering* 28 (01) 117-136.

Alvarenga Baptista, C. M. L. and Cerqueira, H. S. (2004) Feedstock effect on FCC catalyst stripping. In Occelli, M. (editor) *Studies in Surface Science and Catalysis.* Vol. 149. Elsevier. 287-295.

Alvarez-Castro, H. C., Armellini, V., Mori, M., Martignoni, W. P. and Oconec, R. (2015a) The Influence on Products Yield and Feedstock Conversion of Feedstock Injection Position along the Industrial Riser. *Chemical Engineering Transactions; The Italian Association of Chemical Engineering* 43.

Alvarez-Castro, H. C., Matos, E. M., Mori, M., Martignoni, W. and Ocone, R. (2015b) Analysis of Process Variables via CFD to Evaluate the Performance of a FCC Riser. *International Journal of Chemical Engineering* 2015 1-13.

Ancheyta-Jua´rez, J. and Sotelo-Boya´s, R. (2000) Estimation of Kinetic Constants of a Five-Lump Model for Fluid Catalytic Cracking Process Using Simpler Sub-models. *Energy & Fuels* 14 1226-1231.

Ancheyta-Juarez, J., Lopez-Isunza, F. and Aguilar-Rodriguez, E. (1999) 5-Lump kinetic model for gas oil catalytic cracking. *Applied Catalysis A: General* 177 (2) 227-235.

Ancheyta-Juarez, J., Lopez-Isunza, F., Aquilar-Rodriquez, E. and Moreno-Mayorga, J. C. (1997) A Strategy for Kinetic Parameter Estimation in the Fluid Catalytic Cracking Process. *Ind. Eng. Chem. Res.* 36 5170-5174.

Ancheyta-Juarez, J. and Murillo-Hernandez, J. A. (2000) A Simple Method for Estimating Gasoline, Gas, and Coke Yields in FCC Processes. *Energy & Fuels* 14 373-379.

Ancheyta, J. r. J., Felipe, L.-I. and Aquilar-Rodriquez, E. (1999) 5-Lump Kinetic Model for Gas Oil Cracking. *Applied Catalysis A: General* 177 227-235.

Ancheyta, J. r. J. and Rogelio, S. (2002) Kinetic modeling of vacuum gas oil catalytic cracking. *Revista de la Sociedad Química de México* 46 (1) 83-42.

Arandes, J. M., Azkoiti, M. J., Bilbao, J. and de Lasa, H. I. (2000) Modelling FCC Units under Steady and Unsteady State Conditions. *The Canadian Journal of Chemical Engineering* 78.

Araujo-Monroy, C. and López-Isunza, F. (2006) Modeling and Simulation of an Industrial Fluid Catalytic Cracking Riser Reactor Using a Lump-Kinetic Model for a Distinct Feedstock. *Industrial & Engineering Chemistry Research* 45 (1) 120-128.

Arbel, A., Huang, Z., Rinard, I. H. and Shinnar, R. (1995a) Dynamic and Control of Fluidized Catalytic Crackers. 1. Modeling of the Current Generation of FCC's. *Ind. Eng. Chem. Res.* 34 1228-1243.

Arbel, A., Rinard, I. H. and Shinnar, R. (1995b) Dynamics and Control of Fluidized Catalytic Crackers. 2. Multiple Steady States and Instabilities. *Znd. Eng. Chem. Res.* 34 3014-3026.

Azizi, N., Behbahani, R. and Isazadeh, M. A. (2010) An efficient correlation for calculating compressibility factor of natural gases. *Journal of Natural Gas Chemistry* 19 (6) 642-645.

Bahadori, A., Mokhatab, S. and Towler, B. F. (2007) Rapidly Estimating Natural Gas Compressibility Factor. *Journal of Natural Gas Chemistry* 16 (4) 349-353.

Balachandran, P. (2007) *Fundamentals of Compressible Fluid Dynamics.* New Delhi: Prentice-Hall of India.

Baldessar, F. and Negrão, C. O. R. (2005) Simulation of fluid catalytic cracking risers – a six lump model. *18th International Congress of Mechanical Engineering Ouro Preto, MG*.

Baudrez, E., Heynderickx, G. J. and Marin, G. B. (2010) Steady-state simulation of Fluid Catalytic Cracking riser reactors using a decoupled solution method with feedback of the cracking reactions on the flow. *Chemical Engineering Research and Design* 88 (3) 290-303.

Beggs, D. H. and Brill, J. P. (1973) A Study of Two-Phase Flow in Inclined Pipes. *Journal of Petroleum Technology*.

Behie, L. A. and Kehoe, P. (1973) The grid region in a fluidized bed reactor. *AIChE Journal* 19 1070-1072.

Behjat, Y., Shahhosseini, S. and Marvast, M. A. (2011) Simulation study of droplet vaporisation effects on gas–solid fluidized bed. *Journal of the Taiwan Institute of Chemical Engineers* 42 (3) 419-427.

Benyahia, S., Arastoopour, H., Knowlton, T. M. and Massah, H. (2000) Simulation of particles and gas flow behavior in the riser section of a circulating fluidized bed using the kinetic theory approach for the particulate phase. *Powder Technology* 112 (1) 24-33.

Berrouk, A. S., Pornsilph, C., Bale, S. S., Du, Y. and Nandakumar, K. (2017) Simulation of a Large-Scale FCC Riser Using a Combination of MP-PIC and Four-Lump Oil-Cracking Kinetic Models. *Energy & Fuels* 31 (5) 4758-4770.

Bispo, V. D. S., Silva, E. S. R. L. and Meleiro, L. A. C. (2014) Modeling, Optimisation and Control of a FCC Unit Using Neural Networks and Evolutionary Methods. *Engevista* 16 (1) 70 - 90.

Blazeck, J. J. (1993) Catalytic Cracking- Part One, History and fundamentals. *The Davidson Chemical Guide to Catalytic Cracking*.

Bolkan-Kenny, Y. G., Pugsley, T. S. and Berruti, F. (1994) Computer Simulation of the Performance of Fluid Catalytic Cracking Risers and Downers. *Industrial & Engineering Chemistry Research* 33 (12) 3043-3052.

Bollas, G. M., Lappas, A. A., Iatridis, D. K. and Vasalos, I. A. (2007a) Five-lump kinetic model with selective catalyst deactivation for the prediction of the product selectivity in the fluid catalytic cracking process. *Catalysis Today* 127 (1-4) 31-43.

Bollas, G. M., Vasalos, I. A., Lappas, A. A., Iatridis, D. K. and Tsioni, G. K. (2004) Bulk Molecular Characterization Approach for the Simulation of FCC Feedstocks. *Ind. Eng. Chem. Res.* 43 3270-3281.

Bollas, G. M., Vasalos, I. A., Lappas, A. A., Iatridis, D. K., Voutetakis, S. S. and Papadopoulou, S. A. (2007b) Integrated FCC riser—regenerator dynamics studied in a fluid catalytic cracking pilot plant. *Chemical Engineering Science* 62 (7) 1887-1904.

Bonvin, D. (1998) Optimal operation of batch reactors—a personal view. *Journal of Process Control* 8 (5) 355-368.

Boum, A. T., Latifi, A. and Corriou, J. P. (2015) Multivariable Control and Online State Estimation of an FCC Unit. *Journal of Engineering Science and Technology Review* 8 (3) 158-168.

Carlisle, R. (2004) *Scientific American IInventions and Discoveries.* (All the Milestones in Ingenuity—from the Discovery of Fire to the Invention of the Microwave Oven) Hoboken, New Jersey: John Wiley & Sons, Inc.

CCP (2016) *What is CO2 Capture & Storage? http://www.co2captureproject.org/what_is_co2_capture_storage.html* Accessed 27/09/2016.

Chang, J., Meng, F., Wang, L., Zhang, K., Chen, H. and Yang, Y. (2012a) CFD investigation of hydrodynamics, heat transfer and cracking reaction in a heavy oil riser with bottom airlift loop mixer. *Chemical Engineering Science* 78 128-143.

Chang, J., Zhang, K., Meng, F., Wang, L. and Wei, X. (2012b) Computational investigation of hydrodynamics and cracking reaction in a heavy oil riser reactor. *Particuology* 10 (2) 184-195.

Chen, G.-Q., Luo, Z.-H., Lan, X.-Y., Xu, C.-M. and Gao, J.-S. (2013) Evaluating the role of intraparticle mass and heat transfers in a commercial FCC riser: A meso-scale study. *Chemical Engineering Journal* 228 352-365.

Chiyoda (1980) *Operating and Unit Manual for the Nigerian National Petroleum Corporation.*

Christensen, G., Apelia, M. R., Hickey, K. J. and Jaffe, S. B. (1999) Future directions in modeling the FCC process: An emphasis on product quality. *Chemical Engineering Science* 54 2753-2764.

Clough, M., Pope, J. C., Xin Lin, L. T., Komvokis, V., Pan, S. S. and Yilmaz, B. (2017) Nanoporous materials forge a path forward to enable sustainable growth: Technology advancements in fluid catalytic cracking. *Microporous and Mesoporous Materials* 254 45-58.

Corella, J., Bilbao, R., Molina, J. A. and Artigas, A. (1985) Variation with Time of the Mechanism, Observable Order, and Activation-Energy of the Catalyst Deactivation by Coke in the Fcc Process. *Industrial & Engineering Chemistry Process Design and Development* 24 (3) 625-636.

Corella, J. and Frances, E. (1991a) *On the Kinetic Equation of Deactivation of Commercial Cracking (Fcc) Catalysts with Commercial Feedstocks.* Vol. 68. Elsevier Science & Technology.

Corella, J. and Frances, E. (1991b) *On the Kinetic Equation of Deactivation of Commercial Cracking (FCC)Catalysts with Commercial Feedstocks.* Vol. 68. Elsevier Science & Technology.

Corella, J. and Francés, E. (1991) Analysis of the Riser Reactor of a Fluid Cracking Unit. 452 165-182.

Corella, J. and Monzon, A. (1988) Modeling of the deactivation kinetics of solid catalysts by two or more simultaneous and different causes. *Industrial & Engineering Chemistry Research* 27 (3) 369-374.

Coxson, P. G. and Bischoff, K. B. (1987) Lumping Strategy. 1. Introductory Techniques and Applications of Cluster Analysis. *Ind. Eng. Chem. Res.* 26 (6) 1239-1248.

Cristina, P. (2015) Four – Lump Kinetic Model vs. Three - Lump Kinetic Model for the Fluid Catalytic Cracking Riser Reactor. *Procedia Engineering* 100 602-608.

Cuadros, J. F., Melo, D. C., Filho, R. M. and Maciel, M. R. W. (2012) Fluid Catalytic Cracking Environmental Impact: Factorial Design Coupled with Genetic Algorithms to Minimise Carbon Monoxide Pollution. *Chemical Engineering Transactions; The Italian Association of Chemical Engineering* 26.

Cuadros, J. F., Melo, D. C., Filho, R. M. and Maciel, M. R. W. (2013) Fluid catalytic cracking optimisation using factorial design and genetic algorithm techniques. *The Canadian Journal of Chemical Engineering* 91 (2) 279-290.

Das, A. K., Baudrez, E., Marin, G. B. and Heynderickx, G. J. (2003) Three-Dimensional Simulation of a Fluid Catalytic Cracking Riser Reactor. *Ind. Eng. Chem. Res.* 42 2602-267.

Das, B. S., Saha, R. K. and Gupta, S. P. (2007) Study of Feedstock Injection to Improve Catalyst Homogenization in the Riser of a FCC. *Indian Journal of Chemical Technology* 14 473-480.

Davidson, J. F. and Harrison, D. (1963) *Fluidized Particles.* New York: Cambridge university Press.

de Carvalho, M. C. N. A., Morgado, E., Cerqueira, H. S., de Resende, N. S. and Schmal, M. (2004) Behavior of Fresh and Deactivated Combustion

Promoter Additives. *Industrial & Engineering Chemistry Research* 43 (12) 3133-3136.
de Lasa, H. I., Errazu, A., Barreio, E. and Solioz, S. (1981) Analysis of fluidized bed catalytic cracking regenerator models in an industrial scale unit. . *Can. J. Chem. Eng.,* 59 549-553.
de Lasa, H. I. and Grace, J. R. (1979) The influence of the freeboard region in a fluidized bed catalytic cracking regenerator. *AIChE Journal* 25 (6) 984-991.
de Mello, L. F., Gobbo, R., Moure, G. T. and Miracca, I. (2013) Oxy-combustion Technology Development for Fluid Catalytic Crackers (FCC) – Large Pilot Scale Demonstration. *Energy Procedia* 37 7815-7824.
Deng, R., Wei, F., Liu, T. and Jin, Y. (2002) Radial behavior in riser and downer during the FCC process. *Chemical Engineering and Processing: Process Intensification* 41 (3) 259-266.
Derouin, C., Nevicato, D., Forissier, M., Wild, G. and Bernard, J.-R. (1997) Hydrodynamics of Riser Units and Their Impact on FCC Operation. *Ind. Eng. Chem. Res.* 36 4504-4515.
Dewachtere, N. V., Santaella, F. and Froment, G. F. (1999) Application of a single-event kinetic model in the simulation of an industrial riser reactor for the catalytic cracking of vacuum gas oil. *Chemical Engineering Science* 54 3653-3660.
Dixon, A. G. and Cresswell, D. L. (1979) Theoretical Prediction of Effective Heat-Transfer Parameters in Packed-Beds. *Aiche Journal* 25 (4) 663-676.
Dobre, T. G. and Marcano, J. G. S. (2007) *Chemical Engineering Modelling Simulation and Similitude.* Germany: WILEY-VCH Verlag GmbH & Co. KGaA, Weinheim.
Du, Y., Yang, Q., Zhang, C. and Yang, C. (2015a) Ten-lump kinetic model for the two-stage riser catalytic cracking for maximizing propylene yield (TMP) process. *Applied Petrochemical Research* 5 (4) 297-303.
Du, Y., Zhao, H., Ma, A. and Yang, C. (2015b) Equivalent Reactor Network Model for the Modeling of Fluid Catalytic Cracking Riser Reactor. *Industrial & Engineering Chemistry Research* 54 (35) 8732-8742.
Du, Y. P., Yang, Q., Zhao, H. and Yang, C. H. (2014) An integrated methodology for the modeling of Fluid Catalytic Cracking (FCC) riser reactor. *Applied Petrochemical Research* 4 (4) 423-433.
Duduku Krishnaiah, V. G., Awang Bono, Rosalam Sarbatly (2007) Steady State Simulation of a Fluid Catalytic Cracking Unit. *Journal of Applied Sciences* 7 (15) 2137-2145.
Dupain, X., Gamas, E. D., Madon, R., Kelkar, C. P., Makkee, M. and Moulijn, J. A. (2003a) Aromatic gas oil cracking under realistic FCC conditions in a microriser reactor☆. *Fuel* 82 (13) 1559-1569.
Dupain, X., Makkee, M. and Moulijn, J. (2006) Optimal conditions in fluid catalytic cracking: A mechanistic approach. *Applied Catalysis A: General* 297 (2) 198-219.
Dupain, X., Rogier, L. J., Gamas, E. D., Makkee, M. and Moulijn, J. A. (2003b) Cracking behavior of organic sulfur compounds under realistic FCC conditions in a microriser reactor. *Applied Catalysis A: General* 238 223–238.
Dutta, A., Constales, D. and Heynderickx, G. J. (2012) Applying the direct quadrature method of moments to improve multiphase FCC riser reactor simulation. *Chemical Engineering Science* 83 93-109.

Edgar, T. F., Himmelblau, D. M. and Lasdon, L. S. (2001) *Optimisation of chemical processes.* 2nd edition*.* London;Boston;: McGraw-Hill.

Ekpo, E. E. (2006) *Dynamic optimisation and control of batch polymerisation process: the dynamic optimisation and on line control of free radical batch . neural networks and advanced control strategies*. Dissertation/Thesis. Bradford U6

Ellis, R. C., Li, X. and Riggs, J. B. (1998) Modeling and optimisation of a model IV fluidized catalytic cracking unit. *AIChE Journal* 44 (9) 2068-2079.

Elsharkawy, A. M. (2004) Efficient methods for calculations of compressibility, density and viscosity of natural gases. *Fluid Phase Equilibria* 218 (1) 1-13.

Elshishini, S. S. and Elnashaie, S. S. E. H. (1990a) Digital simulation of industrial fluid catalytic cracking units—II. Effect of charge stock composition on bifurcation and gasoline yield. *Chemical Engineering Science* 45 (9) 2959-2964.

Elshishini, S. S. and Elnashaie, S. S. E. H. (1990b) Digital simulation of industrial fluid catalytic cracking units: bifurcation and its implications. *Chemical Engineering Science* 45 (2) 553-559.

Elshishini, S. S., Elnashaie, S. S. E. H. and Alzahrani, S. (1992) Digital simulation of industrial fluid catalytic cracking units—III. Effect of hydrodynamics. *Chemical Engineering Science* 47 (12) 3152-3156.

Errazu, A. F., De Lasa, H. Z. and Sarti, F. (1979) A Fluidized Bed Catalytic Cracking Regenerator Model Grid Effects. *The Canadian Journal of Chemical Engineering* 57 (2) 191-197.

Faltsi-Saravelou, O. and Vasalos, I. A. (1991) FBSim: A model for fluidized bed simulation—I. Dynamic modeling of an adiabatic reacting system of small gas fluidized particles. *Computers & Chemical Engineering* 15 (9) 639-646.

Farshi, A., Shaiyegh, F., Burogerdi, S. H. and Dehgan, A. (2011) FCC Process Role in Propylene Demands. *Petroleum Science and Technology* 29 (9) 875-885.

Fayazi, A., Arabloo, M. and Mohammadi, A. H. (2014) Efficient estimation of natural gas compressibility factor using a rigorous method. *Journal of Natural Gas Science and Engineering* 16 8-17.

Feng, W., Vynckier, E. and Froment, G. F. (1993) Single-Event Kinetics of Catalytic Cracking. *Ind. Eng. Chem. Res. 1993,32, 2997-3005* 33 2997-3005.

Fermoselli, N. E. G. (2010) Predicting the Impact of a FCC Turbo Expander on Petroleum Refineries. *Technology* 9 (1) 40-46.

Fernandes, J., Verstraete, J. J., Pinheiro, C. C., Oliveira, N. and Ribeiro, F. R. (2005) Mechanistic Dynamic Modelling of an Industrial FCC Unit. In *European Symposium on Computer Aided Process Engineering - 15.* Elsevier Science B. V.

Fernandes, J. L., Pinheiro, C. I. C., Oliveira, N. M. C., Neto, A. I. and Ramôa Ribeiro, F. (2007a) Steady state multiplicity in an UOP FCC unit with high-efficiency regenerator. *Chemical Engineering Science* 62 (22) 6308-6322.

Fernandes, J. L., Verstraete, J. J., Pinheiro, C. I. C., Oliveira, N. M. C. and Ramôa Ribeiro, F. (2007b) Dynamic modelling of an industrial R2R FCC unit. *Chemical Engineering Science* 62 (4) 1184-1198.

Filho, R. M., Lona Batista, L. M. F. and Fusco, M. (1996) A fast fluidized bed reactor for industrial FCC regenerator. *Chemical Engineering Science* 51 (10) 1807-1816.

Fligner, M., Schipper, P. H., Sapre, A. V. and Krambeck, F. J. (1994) Two phase cluster model in riser reactors: impact of radial density distribution on yields. *Chemical Engineering Science* 49 (24, Part 2) 5813-5818.

Freire de Almeida, M. A. (2016) *Modelling of regenerator units in fluid catalytic cracking processes*. Masters Thesis. Tecnico Lisboa.

Froment, G. F., Bischoff, K. B. and De Wilde, J. (2011) *Chemical Reactor Analysis and Design.* USA: John Wiley & Sons, Inc.

Gan, J., Zhao, H., Berrouk, A. S., Yang, C. and Shan, H. (2011) Numerical Simulation of Hydrodynamics and Cracking Reactions in the Feed Mixing Zone of a Multiregime Gas–Solid Riser Reactor. *Industrial & Engineering Chemistry Research* 50 (20) 11511-11520.

Gao, H., Wang, G., Xu, C. and Gao, J. (2014) Eight-Lump Kinetic Modeling of Vacuum Residue Catalytic Cracking in an Independent Fluid Bed Reactor. *Energy & Fuels* 28 6554−6562.

Gao, J., Xu, C. and Lin, S. (2006) Advanced Reaction-Terminating Technique for FCC Riser Reactor. *Petroleum Science and Technology* 24 (3-4) 367-378.

Geldart, D. (1973) Types of Gas Fhidization. *Powder Technology* 7 285-292.

gPROMS (2013) Model Validation Guide. *Process Systems Enterprise Limited*.

Grace, J. R., Abba, I. A., Bi, H. and Thompson, M. L. (1999) Fluidized bed catalytic reactor modeling across the flow regimes. *The Canadian Journal of Chemical Engineering* 77 (2) 305-311.

Grace, W. R. (1993) *Guide to fluid catalytic cracking.* Columbia, MD: W.R. Grace & Co.-Conn.

Grosdidier, P., Mason, A., Aitolahti, A., Heinonen, P. and Vanhamaki, V. (1993) FCC Unit Reactor Regenerator Control. *Computers & Chemical Engineering* 17 (2) 165-179.

Guisnet, M. and Magnoux, P. (2001) Organic chemistry of coke formation. *Applied Catalysis A-General* 212 (1-2) 83-96.

Gupta, A. and Rao, U. (2001) Model for the performance of a fluid catalytic cracking (FCC) riser reactor: effect of feed atomization. *Chemical Engineering Science* 56 4489-4503.

Gupta, A. and Subba Rao, D. (2003) Effect of feed atomization on FCC performance: simulation of entire unit. *Chemical Engineering Science* 58 (20) 4567-4579.

Gupta, R., Kumar, V. and Srivastava, V. K. (2005) Modeling and Simulation of Fluid Catalytic Cracking Unit. *Reviews in Chemical Engineering* 21 (2).

Gupta, R. K., Kumar, V. and Srivastava, V. K. (2007) A new generic approach for the modeling of fluid catalytic cracking (FCC) riser reactor. *Chemical Engineering Science* 62 (17) 4510-4528.

Gupta, R. K., Kumar, V. and Srivastava, V. K. (2010) Modeling of Fluid Catalytic Cracking Riser Reactor: A Review. *International Journal of Chemical Reactor Engineering* 8 (1) 1-40.

Guria, C., Bhattacharya, P. K. and Gupta, S. K. (2005) Multi-objective optimisation of reverse osmosis desalination units using different adaptations of the non-dominated sorting genetic algorithm (NSGA). *Computers & Chemical Engineering* 29 (9) 1977-1995.

Hagelberg, P., Eilos, I., Hiltunen, J., Lipiainen, K., Niemi, V. M., Aittamaa, J. and Krause, A. O. I. (2002) Kinetics of catalytic cracking with short contact times. *Applied Catalysis A-General* 223 (1-2) 73-84.

Haiyan, L., Liyuan, C., Baoying, W., Yu, F., Gang, S. and Xaojun, B. (2012) In-situ Synthesis and Catalytic Properties of ZSM-5/Rectorite Composites as

Propylene Boosting Additive in Fluid Catalytic Cracking Process. *Chinese Journal of Chemical Engineering* 20 (1) 158-166.

Han, I. S. and Chung, C. B. (2001a) Dynamic modeling and simulation of a fluidized catalytic cracking process. Part I: Process modeling. *Chemical Engineering Science* 56 (5) 1951-1971.

Han, I. S. and Chung, C. B. (2001b) Dynamic modeling and simulation of a fluidized catalytic cracking process. Part II: Property estimation and simulation. *Chemical Engineering Science* 56 (5) 1973-1990.

Han, I. S., Riggs, J. B. and Chung, C. B. (2004) Modeling and optimisation of a fluidized catalytic cracking process under full and partial combustion modes. *Chemical Engineering and Processing* 43 (8) 1063-1084.

Harriott, P. (2003) *Chemical Reactor Design.* New York, USA: Marcel Dekker, Inc.

Hassan, R., Cohanim, B., de Weck, O. and Venter, G. (2005) A Comparison of Particle Swarm Optimisation and the Genetic Algorithm. In *46th AIAA/ASME/ASCE/AHS/ASC Structures, Structural Dynamics & Materials Conference.* Austin, Texas: 18-21 April 2005. USA: American Institute of Aeronautics and Astronautics.

He, P., Zhu, C. and Ho, T. C. (2015) A two-zone model for fluid catalytic cracking riser with multiple feed injectors. *AIChE Journal* 61 (2) 610-619.

Heidaryan, E., Moghadasi, J. and Rahimi, M. (2010a) New correlations to predict natural gas viscosity and compressibility factor. *Journal of Petroleum Science and Engineering* 73 (1–2) 67-72.

Heidaryan, E., Salarabadi, A. and Moghadasi, J. (2010b) A novel correlation approach for prediction of natural gas compressibility factor. *Journal of Natural Gas Chemistry* 19 (2) 189-192.

Hernandez-Barajas, J. R., Vazquez-Roman, R. and Felix-Flores, M. G. (2009) A comprehensive estimation of kinetic parameters in lumped catalytic cracking reaction models. *Fuel* 88 (1) 169-178.

Hernández-Barajas, J. R., Vázquez-Román, R. and Salazar-Sotelo, D. (2006) Multiplicity of steady states in FCC units: effect of operating conditions. *Fuel* 85 (5–6) 849-859.

Heydari, M., AleEbrahim, H. and Dabir, B. (2010a) Modeling of an Industrial Riser in the Fluid Catalytic Cracking Unit. *American Journal of Applied Sciences* 7 (2) 221-226.

Heydari, M., AleEbrahim, H. and Dabir, B. (2010b) Study of Seven-Lump Kinetic Model in the Fluid Catalytic Cracking Unit. *American Journal of Applied Sciences* 7 (1) 71-76.

Hussain, A. I., Aitani, A. M., Kubů, M., Čejka, J. and Al-Khattaf, S. (2016) Catalytic cracking of Arabian Light VGO over novel zeolites as FCC catalyst additives for maximizing propylene yield. *Fuel* 167 226-239.

Inagaki, S., Takechi, K. and Kubota, Y. (2010) Selective formation of propylene by hexane cracking over MCM-68 zeolite catalyst. *Chemical Communications* 46 (15) 2662.

Jacob, S. M., Gross, B., Voltz, S. E. and Weekman, V. W. (1976) A lumping and reaction scheme for catalytic cracking. *AIChE Journal* 22 (4) 701-713.

James, H. G. and Glenn, E. H. (2001) *Petroleum Refining Technology and Economics.* New York. Basel: Marcel Dekker, Inc.

Jarullah, A. T. (2011) *kinetic Modelling Simulation and Optimal Operation of Trickle Bed Reactor for Hydrotreating of Crude Oil* PhD. University of Bradford, United Kingdom *https://bradscholars.brad.ac.uk/handle/10454/5363*

Jarullah, A. T., Awad, N. A. and Mujtaba, I. M. (2017) Optimal design and operation of an industrial fluidized catalytic cracking reactor. *Fuel* 206 657-674.

Jarullah, A. T., Mujtaba, I. M. and Wood, A. S. (2011) Kinetic parameter estimation and simulation of trickle-bed reactor for hydrodesulfurization of crude oil. *Chemical Engineering Science* 66 (5) 859-871.

Jia, C., Rohani, S. and Jutan, A. (2003) FCC unit modeling, identification and model predictive control, a simulation study. *Chemical Engineering and Processing: Process Intensification* 42 (4) 311-325.

Jiménez-García, G., Quintana-Solórzano, R., Aguilar-López, R. and Maya-Yescas, R. (2010) Modelling Catalyst Deactivation by External Coke Deposition during Fluid Catalytic Cracking. *International Journal of Chemical Reactor Engineering* 8 (1).

John, Y. M., Patel, R. and Mujtaba, I. M. (2017) Maximisation of Gasoline in an Industrial Fluidized Catalytic Cracking Unit. *Energy & Fuels* 31 5645−5661.

Kalota, S. A. and Rahmim, I. I. (2003) Solve the Five Most Common FCC Problems. AIChE Spring National Meeting: Expertech Consulting Inc., Irvine and E-MetaVenture, Inc., Houston.

Kasat, R. B., Kunzru, D., Saraf, D. N. and Gupta, S. K. (2002) Multiobjective Optimisation of Industrial FCC Units Using Elitist Nondominated Sorting Genetic Algorithm. *Industrial & Engineering Chemistry Research* 41 (19) 4765-4776.

Khalfalla, H. A. (2009) *Modelling And Optimisation Of Oxidative Desulphurization Process For Model Sulphur Compounds And Heavy Gas Oil*. PhD. University of Bradford, UK. *http://hdl.handle.net/10454/4247*

Khandalekar, P. D. (1993) *Control and Optimisation of Fluidized Catalytic Cracking Process*. Masters. Texas Tech University.

Khanmohammadi, M., Amani, S., Garmarudi, A. B. and Niaei, A. (2016) Methanol-to-propylene process: Perspective of the most important catalysts and their behavior. *Chinese Journal of Catalysis* 37 (3) 325-339.

Knight, J. and Mehlberg, R. (2011) Maximise propylene from your FCC unit. *Hydrocarbon Process* 90 (9) 91-95.

Koon, C. L., Akbar, F., Hughes, R., Tyagi, Y. R., Castro Diaz, M., Martin, S. C., Hall, P. J. and Snape, C. E. (2000) Development of an Experimental Protocol to Evaluate FCC Stripper Performance in Terms of Coke Yield and Composition. *Chemical Engineering Research and Design* 78 (5) 738-744.

Kordabadi, H. and Jahanmiri, A. (2005) Optimisation of methanol synthesis reactor using genetic algorithms. *Chemical Engineering Journal* 108 (3) 249-255.

Krishna, A. S. and Parkin, E. S. (1985a) Modeling the regenerator in commercial fluid catalytic cracking units. *Chem. Eng. Prog* 81 (4).

Krishna, A. S. and Parkin, E. S. (1985b) Modeling the Regenerator in Commercial Fluid Catalytic Cracking Units. *Chemical Engineering Progress* 81 (4) 57-62.

Kumar, N. (2004) *Compressibility Factors for Natural and Sour Reservoir Gases by Correlations and Cubic Equations of State*. Texas Tech University.

Kumar, S., Chadha, A., Gupta, R. and Sharma, R. (1995) CATCRAK: A Process Simulator for an Integrated FCC-Regenerator System. *Industrial & Engineering Chemistry Research* 34 (11) 3737-3748.

Kumar, V. and Reddy, A. S. K. (2011) Why FCC riser is taller than model predictions? *AIChE Journal* 57 (10) 2917-2920.

Kunii, D. and Levenspiel, O. (1969) *Fluidization Engineering.* New York: Wiley.

Kunii, D. and Levenspiel, O. (1990) Fluidized reactor models. 1. For bubbling beds of fine, intermediate, and large particles. 2. For the lean phase: freeboard and fast fluidization. *Industrial & Engineering Chemistry Research* 29 (7) 1226-1234.

Kunii, D. and Levenspiel, O. (1991) *Fluidization Engineering.* SECOND EDITION edition*.* London: Butterworth Heinemann Seris in Chemical Engineering.

Kuo, J. C. W. and Wei, J. (1969) A Lumping Analysis in Monomolecular Reaction Systems-Analysis of Approximately Lumpable System. *I&EC Fundamentals* 8 (1).

Lan, X., Xu, C., Wang, G., Wu, L. and Gao, J. (2009) CFD modeling of gas–solid flow and cracking reaction in two-stage riser FCC reactors. *Chemical Engineering Science* 64 (17) 3847-3858.

Larocca, M., De Lasa, H., Farag, H. and Ng, S. (1990) Cracking catalysts deactivation by nickel and vanadium contaminants. *Industrial & Engineering Chemistry Research* 29 (11) 2181-2191.

Larocca, M., S. Ng and Delasa, H. (1990) Deactivation of cracking catalyst in short contact time reactors. *Ind. Eng. Chem. Res.* 69 355-360.

Lee, L.-S., Chen, Y.-W. and Huang, T.-N. (1989a) Four-Lump Kinetic Model for Fluid Catalytic Cracking Process. *The Canadian Journal of Chemical Engineering* 67.

Lee, L.-S., Yu, S.-W. and Cheng, C.-T. (1989b) Fluidized-bed Catalyst Cracking Regenerator Modelling and Analysis. *The Chemical Engineering Journal* 40 71-82.

Lee, L. S., Yu, S. W., Cheng, C. T. and Pan, W. Y. (1989c) Fluidized-Bed Catalyst Cracking Regenerator Modeling and Analysis. *Chemical Engineering Journal and the Biochemical Engineering Journal* 40 (2) 71-82.

Lee, W. and Kugelman, A. M. (1973) Number of Steady-State Operating Points and Local Stability of Open-Loop Fluid Catalytic Cracker. *Industrial & Engineering Chemistry Process Design and Development* 12 (2) 197-204.

León-Becerril, E., Maya-Yescas, R. and Salazar-Sotelo, D. (2004) Effect of modelling pressure gradient in the simulation of industrial FCC risers. *Chemical Engineering Journal* 100 (1) 181-186.

Li, C., Peng, Y. and Dong, J. (2014) Prediction of compressibility factor for gas condensate under a wide range of pressure conditions based on a three-parameter cubic equation of state. *Journal of Natural Gas Science and Engineering* 20 380-395.

Li, C., Yang, C. and Shan, H. (2007) Maximizing Propylene Yield by Two-Stage Riser Catalytic Cracking of Heavy Oil. *Ind. Eng. Chem. Res.* 46 4914-4920.

Li, J., Luo, Z.-H., Lan, X.-Y., Xu, C.-M. and Gao, J.-S. (2013) Numerical simulation of the turbulent gas–solid flow and reaction in a polydisperse FCC riser reactor. *Powder Technology* 237 569-580.

Li, T., Pougatch, K., Salcudean, M. and Grecov, D. (2009) Numerical simulation of single and multiple gas jets in bubbling fluidized beds. *Chemical Engineering Science* 64 (23) 4884-4898.

Liu, H., Zhao, H., Gao, X. and Ma, J. (2007) A novel FCC catalyst synthesized via in situ overgrowth of NaY zeolite on kaolin microspheres for maximizing propylene yield. *Catalysis Today* 125 (3-4) 163-168.

Lopes, G. C., Rosa, L. M., Mori, M., Nunhez, J. R. and Martignoni, W. P. (2012) CFD Study of Industrial FCC Risers: The Effect of Outlet Configurations on Hydrodynamics and Reactions. *International Journal of Chemical Engineering* 2012 1-16.

Lu, Y.-y., Hu, Y.-d., Xu, D.-m. and Wu, L.-y. (2006) Optimum design of reverse osmosis seawater desalination system considering membrane cleaning and replacing. *Journal of Membrane Science* 282 (1) 7-13.

Ma, C. G. and Weng, H. X. (2009) Application of Artificial Neural Network in the Residual Oil Hydrotreatment Process. *Petroleum Science and Technology* 27 (18) 2075-2084.

Ma, W., Liu, B., Zhang, R., Gu, T., Ji, X., Zhong, L., Chen, G., Ma, L., Cheng, Z. and Li, X. (2018) Co-upgrading of raw bio-oil with kitchen waste oil through fluid catalytic cracking (FCC). *Applied Energy* 217 233-240.

Maadhah, A. G., Fujiyama, Y., Redhwi, H., Abul-Hamayel, M., Aitani, A., Saeed, M. and Dean, C. (2008) A new catalytic cracking process to maximise refinery propylene. *Arabian Journal for Science and Engineering* 33 (1 B) 17-28.

Magee, J. S. (1993) A Guide to Davidson Catalytic Cracking. *The Davidson Guide to Catalytic Cracking*.

Mahmoud, M. (2014) Development of a New Correlation of Gas Compressibility Factor (Z-Factor) for High Pressure Gas Reservoirs. *Journal of Energy Resources Technology-Transactions of the Asme* 136 (1).

Mao, X., Weng, H., Zhu, Z., Wang, S. and Zhu, K. (1985) Investigation of the lumped kinetic model for catalytic cracking: III. Analyzing light oil feed and products and measurement of kinetic constants. *Acta Pet. Sin. (Pet. Process Sect.)* 1 (11).

Marcovecchio, M. G., Aguirre, P. A. and Scenna, N. J. (2005) Global optimal design of reverse osmosis networks for seawater desalination: modeling and algorithm. *Desalination* 184 (1) 259-271.

Martignoni, W. and de Lasa, H. I. (2001) Heterogeneous reaction model for FCC riser units. *Chemical Engineering Science* 56 (2) 605-612.

Martin, M. P., Derouin, C., Turlier, P., Forissier, M., Wild, G. and Bernard, J. R. (1992) Catalytic cracking in riser reactors: core-annulus and elbow effects. *Chemical Engineering Science* 47 (9-11) 2319-2324.

McFarlane, C. R., Rhineman, R. C., Bartee, J. F. and Georgakis, C. (1993) Dynamic Simulator Catalytic Cracking for a Model IV Fluid Catalytic Cracking Unit. *Computers Chem. Engng* 17 (3) 275-300.

Menéndez, R., Martínez, J., Prieto, M., Barcia, L. and Sánchez, J. (2014) A Novel Modeling of Molten-Salt Heat Storage Systems in Thermal Solar Power Plants. *Energies* 7 (10) 6721-6740.

Meng, X., Xu, C., Gao, J. and Li, L. (2005) Studies on catalytic pyrolysis of heavy oils: Reaction behaviors and mechanistic pathways. *Applied Catalysis A: General* 294 (2) 168-176.

Meng, X., Xu, C., Gao, J. and Li, L. (2006) Catalytic pyrolysis of heavy oils: 8-lump kinetic model. *Applied Catalysis A: General* 301 (1) 32-38.

Metz, B., Davidson, O., Coninck, H. d., Loos, M. and Meyer, L. (Metz, B., Davidson, O., Coninck, H. d., Loos, M. and Meyer, L.(Metz, B., Davidson, O., Coninck, H. d., Loos, M. and Meyer, L.s.) (2005) *CARBON DIOXIDE CAPTURE AND STORAGE.* Cambridge University Press. 40 West 20th Street, New York, NY 10011–4211, USA: Cambridge University Press.

Mircea V. Cristea, S. P. A. a. V. M. (2003) Simulation and model predictive control of a UOP fluid catalytic cracking unit. *Chemical Engineering and Processing* 42 67-91.

Montgomery, J. A. (1993) Catalytic Cracking- Part Two "The evolution of the Fluid Catalytic Cracking Unit". *The Davidson Chemical Guide to Catalytic Cracking*.

Moore, I. (2005) Reducing CO_2 emissions. *REFINING*. *http://www.eptq.com/view_article.aspx?intAID=211* Accessed 28/09/2016

Morley, K. and de Lasa, H. I. (1987) On the determination of kinetic parameters for the regeneration of cracking catalyst. *The Canadian Journal of Chemical Engineering* 65 (5) 773-777.

Moro, L. F. L. (2003) Process technology in the petroleum refining industry—current situation and future trends. *Computers & Chemical Engineering* 27 (8) 1303-1305.

Moro, L. F. L. and Odloak, D. (1995) Constrained multivariable control of fluid catalytic cracking converters. *Journal of Process Control* 5 (1) 29-39.

Moustafa, T. M. and Froment, G. F. (2003) Kinetic Modeling of Coke Formation and Deactivation in the Catalytic Cracking of Vacuum Gas Oil. *Ind. Eng. Chem. Res.* 42 14-25.

Mu, S.-J., Su, H.-Y., Li, W. and Chu, J. (2005) Reactor model for industrial residual fluid catalytic cracking based on six-lump kinetic model. *Gao Xiao Hua Xue Gong Cheng Xue Bao/Journal of Chemical Engineering of Chinese Universities* 19 (5) 630-635.

Mujtaba, I. M. (2004) *Batch distillation: Design and operation.* Imperial College Press, London, UK.

Murthy, Z. V. P. and Gupta, S. K. (1998) Thin Film Composite Polyamide Membrane Parameters Estimation for Phenol-Water System by Reverse Osmosis. *Separation Science and Technology* 33 (16) 2541-2557.

Murthy, Z. V. P. and Vengal, J. C. (2006) Optimisation of a Reverse Osmosis System Using Genetic Algorithm. *Separation Science and Technology* 41 (4) 647-663.

Muske, K. R. and Rawlings, J. B. (1995) *Nonlinear moving horizon state estimation.* Berber R. (Ed.), Methods of model based process control. Netherlands: Kluwer Academic Publisher.

Naik, D. V., Karthik, V., Kumar, V., Prasad, B. and Garg, M. O. (2017) Kinetic modeling for catalytic cracking of pyrolysis oils with VGO in a FCC unit. *Chemical Engineering Science* 170 790-798.

Nam, I. S. and Kittrell, J. R. (1984) Use of catalyst coke content in deactivation modeling. *Industrial & Engineering Chemistry Process Design and Development* 23 (2) 237-242.

Nayak, S. V., Joshi, S. L. and Ranade, V. V. (2005) Modeling of vaporisation and cracking of liquid oil injected in a gas–solid riser. *Chemical Engineering Science* 60 (22) 6049-6066.

Novia, N., S. Ray, M. and Pareek, V. (2007) Three-Dimensional Hydrodynamics and Reaction Kinetics Analysis in FCC Riser Reactors. *Chemical Product and Process Modeling* 2 (2) 4.

Nowee, S. M., Abbas, A. and Romagnoli, J. A. (2007) Optimisation in seeded cooling crystallization: A parameter estimation and dynamic optimisation study. *Chemical Engineering and Processing: Process Intensification* 46 (11) 1096-1106.

Oliveira, L. L. and Biscaia, E. C. (1989) Catalytic Cracking Kinetic Models. Parameter Estimation and Model Evaluation. *Ind. Eng. Chem. Res.,* 28 (3).

Pareek, V. K., Adesina, A. A., Srivastava, A. and Sharma, R. (2003) Modeling of a non-isothermal FCC riser. *Chemical Engineering Journal* 92 (1-3) 101-109.

Parthasarathi, R. S. and Alabduljabbar, S. S. (2014) HS-FCC High-severity fluidized catalytic cracking: a newcomer to the FCC family. *Applied Petrochemical Research* 4 (4) 441-444.

Pathanjali, M., Sohrab, R. and J., M. B. (1999) The modified dynamic model of a riser type fluid catalytic cracking unit. *The Canadian Journal of Chemical Engineering* 77 (1) 169-179.

Peixoto, F. C. and de Medeiros, J. L. (2001) Reactions in multiindexed continuous mixtures: Catalytic cracking of petroleum fractions. *Aiche Journal* 47 (4) 935-947.

Pelissari, D. C., Alvarez-Castro, H. C., Mori, M. and Martignoni, W. (2016) Study of Feedstock Injection to Improve Catalyst Homogenization in the Riser of a Fcc. *Brazilian Journal of Chemical Engineering* 33 (3) 559-566.

Peng, P. and Zhuang, Y. (2012) The Evaluation and Comparison of Carbon Dioxide Capture Technologies Applied to FCC Flue Gas. *Renewable and Sustainable Energy, Pts 1-7* 347-353 1479-1482.

Pinheiro, C. I. C., Fernandes, J. L., Domingues, L., Chambel, A. J. S., Graca, I., Oliveira, N. M. C., Cerqueira, H. S. and Ribeiro, F. R. (2012) Fluid Catalytic Cracking (FCC) Process Modeling, Simulation, and Control. *Industrial & Engineering Chemistry Research* 51 (1) 1-29.

Pinho, A. d. R., de Almeida, M. B. B., Mendes, F. L., Casavechia, L. C., Talmadge, M. S., Kinchin, C. M. and Chum, H. L. (2017) Fast pyrolysis oil from pinewood chips co-processing with vacuum gas oil in an FCC unit for second generation fuel production. *Fuel* 188 462-473.

Pitault, I., Nevicato, D., Forissier, M. and Bernard, J.-R. (1994) Kinetic model based on a molecular description for catalytic cracking of vacuum gas oil. *Chemical Engineering Science* 49 (24) 4249-4262.

Process System Enterprise Ltd, P. S. E. L., London. (2001) gPROMS Introductory User Guide.

Quann, R. J. and Jaffe, S. B. (1992) Structure-oriented lumping: describing the chemistry of complex hydrocarbon mixtures. *Industrial & Engineering Chemistry Research* 31 (11) 2483-2497.

Régnier, N., Defaye, G., Caralp, L. and Vidal, C. (1996) Software sensor based control of exothermic batch reactors. *Chemical Engineering Science* 51 (23) 5125-5136.

Robertson, D. G., Lee, J. H. and Rawlings, J. B. (1996) A Moving Horizon-Based Approach for Least-Squares Estimation *A.I.Ch.E.* 42 (2) 2209-2224.

Roman, R., Nagy, Z. K., Cristea, M. V. and Agachi, S. P. (2009) Dynamic modelling and nonlinear model predictive control of a Fluid Catalytic Cracking Unit. *Computers & Chemical Engineering* 33 (3) 605-617.

Rosin, P., Rammler, E. and Intelmann, W. (1932) Principles and limits of cyclone dust removal. *Zeit. Ver. Deutscher Ing.* 76 (18) 433-437.

Sa, Y., Chen, X., Liu, J., Weng, H., Zhu, Z. and Mao, X. (1985) Investigation of the lumped kinetic model for catalytic cracking and establishment of the physical model. *Acta Pet. Sin. (Pet. Process Sect.)* 1 (3).

Sa, Y., Liang, X., Chen, X. and Liu, J. (1995) Study of 13-lump kinetic model for residual catalytic cracking. *Selected papers in memorial of 30th*

anniversary of fluid catalytic cracking process in China, Luoyan. Luoyang, China. Petrochemical Engineering Corporation, Luoyang, China. 145.
Sadeghbeigi, R. (2000) *Fluid Catalytic Cracking Handbook: Design, Operation and Troubleshooting of FCC Facilities.* Gulf Professional Publishing.
Sadeghbeigi, R. (2012a) *Fluid Catalytic Cracking Handbook.* Third Edition edition. (An Expert Guide to the Practical Operation, Design, and Optimisation of FCC Units) UK: The Boulevard, Langford Lane, Kidlington, Oxford, OX5 1GB, UK.
Sadeghbeigi, R. (2012b) *Fluid Catalytic Cracking Handbook.* Third Edition edition. (An Expert Guide to the Practical Operation, Design, and Optimisation of FCC Units) UK: The Boulevard, Langford Lane, Kidlington, Oxford, OX5 1GB, UK.
Sadighi, S. (2013) Modeling a Vacuum Gas Oil Hydrocracking Reactor Using Axial- Dispersion Lumped Kinetics. *Petroleum & Coal* 55 (3) 156-168.
Sanjari, E. and Lay, E. N. (2012) Estimation of natural gas compressibility factors using artificial neural network approach. *Journal of Natural Gas Science and Engineering* 9 220-226.
Sankararao, B. and Gupta, S. K. (2007) Multi-objective optimisation of an industrial fluidized-bed catalytic cracking unit (FCCU) using two jumping gene adaptations of simulated annealing. *Computers & Chemical Engineering* 31 (11) 1496-1515.
Santos, V. A. d., Dantas, C. C., Luna, C. L., Silva, J. M. F., Lima, A. C., Macieira, R. P. and Verçosa, B. (2007) Simulation of the fluid dynamic parameters in a cold Riser with catalyst density measured by gamma ray Transmission. In *2007 International Nuclear Atlantic Conference - INAC 2007.* Santos, SP, Brazil. Associação Brasileira De Energia Nuclear - Aben.
Scott, B. J. and Adewuyi, Y. G. (1996) Effects of high temperature and high ZSM-5 additive level on FCC olefins yields and gasoline composition. *Applied Catalysis A: General* 134 (2) 247-262.
Senthilmurugan, S., Ahluwalia, A. and Gupta, S. K. (2005) Modeling of a spiral-wound module and estimation of model parameters using numerical techniques. *Desalination* 173 (3) 269-286.
Shayegh, F., Farshi, A. and Dehgan, A. (2012) A Kinetics Lumped Model for VGO Catalytic Cracking in a Fluidized Bed Reactor. *Petroleum Science and Technology* 30 (9) 945-957.
Shokir, E. M. E.-M., El-Awad, M. N., Al-Quraishi, A. A. and Al-Mahdy, O. A. (2012) Compressibility factor model of sweet, sour, and condensate gases using genetic programming. *Chemical Engineering Research and Design* 90 (6) 785-792.
Shuyan, W., Yurong, H., Huilin, L., Ding, J., Lijie, Y. and Wentie, L. (2008) Simulation of Performance of Cracking Reactions of Particle Clusters in FCC Risers. *Industrial & Engineering Chemistry Research* 47 (14) 4632-4640.
Soroush, M. (1997) Nonlinear state-observer design with application to reactors. *Chemical Engineering Science* 52 (3) 387-404.
Soroush, M. (1998) State and parameter estimations and their applications in process control. *Computers & Chemical Engineering* 23 (2) 229-245.
Souza, J. A., Vargas, J. V. C., Ordonez, J. C., Martignoni, W. P. and von Meien, O. F. (2011) Thermodynamic optimisation of fluidized catalytic cracking (FCC) units. *International Journal of Heat and Mass Transfer* 54 (5–6) 1187-1197.

Souza, J. A., Vargas, J. V. C., Von Meien, O. F. and Martignoni, W. (2003) Numerical simulation of FCC risers. *Tecnologia/Technology* 4 17-21.

Souza, J. A., Vargas, J. V. C., Von Meien, O. F., Martignoni, W. and Amico, S. C. (2006) A two-dimensional model for simulation, control, and optimisation of FCC risers. *AIChE Journal* 52 (5) 1895-1905.

Souza, J. A., Vargas, J. V. C., von Meien, O. F., Martignoni, W. P. and Ordonez, J. C. (2009) The inverse methodology of parameter estimation for model adjustment, design, simulation, control and optimisation of fluid catalytic cracking (FCC) risers. *Journal of Chemical Technology & Biotechnology* 84 (3) 343-355.

Sugungun, M. M., Kolesnikov, I. M., Vinogradov, V. M. and Kolesnikov, S. I. (1998) Kinetic Modeling of FCC Process. *Catalysis Today* 43 (3-4) 315-325.

Takatsuka, T., Sato, S., Morimoto, Y. and Hashimoto, H. (1987) A reaction model for fluidized-bed catalytic cracking of residual oil. *Int Chem Eng* 27 107-116.

Tatiraju, S. and Soroush, M. (1997) Nonlinear State Estimation in a Polymerization Reactor. *Industria & Engineering Chemistry Research* 36 (7) 2679-2690.

Tatiraju, S. and Soroush, M. (1998) Parameter Estimator Design with Application to a Chemical Reactor. *Ind. Eng. Chem. Res.* 37 455-463.

Theologos, K. N., Lygeros, A. I. and Markatos, N. C. (1999) Feedstock atomization e!ects on FCC riser reactors selectivity. *Chemical Engineering Science* 54 (22) 5617-5625.

Theologos, K. N. and Markatos, N. C. (1993) Advanced modeling of fluid catalytic cracking riser-type reactors. *AIChE Journal* 39 (6) 1007-1017.

Tjoa, I. B. and Biegler, L. T. (1992) Reduced successive quadratic programming strategy for errors-in-variables estimation. *Computers & Chemical Engineering* 16 (6) 523-533.

Tsuo, Y. P. and Gidaspow, D. (1990) Computation of flow patterns in circulating fluidized beds. *A.I.Ch.E.* 36 885.

Usman, A., Siddiqui, M. A. B., Hussain, A., Aitani, A. and Al-Khattaf, S. (2017) Catalytic cracking of crude oil to light olefins and naphtha: Experimental and kinetic modeling. *Chemical Engineering Research and Design* 120 121-137.

Vieira, R. C., Pinto, J. C., Biscaia, E. C., Baptista, C. M. L. A. and Cerqueira, H. S. (2004) Simulation of Catalytic Cracking in a Fixed-Fluidized-Bed Unit. *Industrial & Engineering Chemistry Research* 43 (19) 6027-6034.

Vieira, W. G., Santos, V. M. L., Carvalho, F. R., Pereira, J. A. F. R. and Fileti, A. M. F. (2005) Identification and predictive control of a FCC unit using a MIMO neural model. *Chemical Engineering and Processing: Process Intensification* 44 (8) 855-868.

Villafafila, A. and Mujtaba, I. M. (2003) Fresh water by reverse osmosis based desalination: simulation and optimisation. *Desalination* 155 (1) 1-13.

Villafuerte-Macías, E. F., Aguilar, R. and Maya-Yescas, R. (2004) Towards modelling production of clean fuels: sour gas formation in catalytic cracking. *Journal of Chemical Technology & Biotechnology* 79 (10) 1113-1118.

Voorhies, A. (1945) Carbon Formation in Catalytic Cracking. *Industrial and Engineering Chemistry*.

Wang, L., Yang, B. and Wang, Z. (2005) Lumps and kinetics for the secondary reactions in catalytically cracked gasoline. *Chemical Engineering Journal* 109 (1-3) 1-9.

Wauquier, J.-P. (1994) *Petroleum Refining. Crude oil. Petroleum Products. Process Flosheets.* Editions Technip edition. Vol. 1. Paris, France.: IFP Publications.

Weekman, V. W. (1968a) Model of Catalytic Cracking Conversion in Fixed, Moving, and Fluid-Bed Reactors. *Industrial & Engineering Chemistry Process Design and Development* 7 (1) 90-95.

Weekman, V. W. and Nace, D. M. (1970) Kinetics of Catalytic Cracking Selectivity in Fixed, Moving, and Fluid Bed Reactors. *Aiche Journal* 16 (3) 397-404.

Weekman, V. W. J. (1968b) A Model of Catalytic Cracking Conversion in Fixed, Moving, and Fluid-Bed Reactors. *I&EC Process Design and Development* 7 (1) 90-95.

Wei, J. and Kuo, J. C. W. (1969) A Lumping Analysis in Monomolecular Reaction Systems-Analysis of the Exactly Lumpable System. *I&EC Fundamentals* 8 (1).

Wei, J. and Prater, C. D. (1962) The Structure and Analysis of Complex Reaction Systems. In Eley, D. D., et al. (editors) *Advances in Catalysis.* Vol. 13. Academic Press. 203-392.

Weisz, P. B. (1966) Combustion of Carbonaceous Deposits within Porous Catalyst Particles III. The CO_2/CO Product Ratio. *Journal of Catalysis* 6 425-430.

Weisz , P. B. and Goodwin, R. B. (1966) Combustion of Carbonaceous Deposits within Porous Catalyst Particles II. Intrinsic Burning Rate. *Journal of Catalysis* 6 227-236.

Weisz , P. B. and Goodwin, R. D. (1963) Combustion of Carbonaceous Deposits within Porous Catalyst Particles I. Diffusion-Controlled Kinetics. *Journal of Catalysis* 2 397-404.

Wilson, J. W. (1997) *Fluid catalytic cracking technolgy and operations.* Tulsa, OK: PenWell Pub. Co.

Wu, F. Y., Weng, H. X. and Luo, S. X. (2008) Study on lumped kinetic model for FDFCC I. Establishment of model. *China Petroleum Processing & Petrochemical Technology* (2) 45-52.

Xie, C., Wei, X., Gong, J. and Long, J. (2018) Novel FCC technologies based on reaction chemistry of catalytic cracking. *Hydrocarbon Processing* 69-72.

Xiong, K., Lu, C., Wang, Z. and Gao, X. (2015) Kinetic study of catalytic cracking of heavy oil over an in-situ crystallized FCC catalyst. *Fuel* 142 65-72.

Xu, O.-g., Su, H.-y., Mu, S.-j. and Chu, J. (2006) 7-lump kinetic model for residual oil catalytic cracking. *Journal of Zhejiang University-SCIENCE A* 7 (11) 1932-1941.

Yang, W.-C. (2003) *Handbook of Fluidization and Fluid-Particle Systems.* New York. Basel: Marcel Dekker, Inc.

You, H. (2013) The Forecast of Nine Lumped Kinetic Models of FCC Gasoline Under Aromatization Reaction Conditions. *Energy Sources, Part A: Recovery, Utilization, and Environmental Effects* 36 (1) 54-63.

You, H., Xu, C., Gao, J., Liu, Z. and Yan, P. (2006) Nine lumped kinetic models of FCC gasoline under the aromatization reaction conditions. *Catalysis Communications* 7 (8) 554-558.

Zahran, M., Ammar, M. E., Ismail, M. M. and Hassan, M. A. M. (2017) Fluid catalytic cracking unit control using model predictive control and adaptive neuro fuzzy inference system: Comparative study. Cairo, Egypt.

Computer Engineering Conference (ICENCO), 2017 13th International: IEEE.
Zanin, A. C., Tvrzská de Gouvêa, M. and Odloak, D. (2002) Integrating real-time optimisation into the model predictive controller of the FCC system. *Control Engineering Practice* 10 (8) 819-831.
Zeydan, M. (2008) The Comparison of Artificial Intelligence and Traditional Approaches In FCCU Modeling. *International Journal of Industrial Engineering* 15 (1) 1-15.
Zhang, Y.-c., Wang, Z.-b., Jin, Y.-h., Li, Z.-h. and Yi, W.-m. (2017) Kinetic study of catalytic cracking on the effect of reaction parameters in short-contact cyclone reactors. *Chemical Engineering Research and Design* 119 188-197.
Zhao, X., Peters, A. W. and Weatherbee, G. W. (1997) Nitrogen Chemistry and NOx Control in a Fluid Catalytic Cracking Regenerator. *Industrial & Engineering Chemistry Research* 36 (11) 4535-4542.
Zheng, Y.-Y. (1994) Dynamic Modeling and Simulation of a Catalytic Cracking Unit. *Computers & Chemical Engineering* 18 (1) 39-44.
Zhou, X., Yang, B., Yi, C., Yuan, J. and Wang, L. (2010) Prediction model for increasing propylene from FCC gasoline secondary reactions based on Levenberg-Marquardt algorithm coupled with support vector machines. *Journal of Chemometrics* 24 574–583.
Zhu, C., Jun, Y., Patel, R., Wang, D. and Ho, T. C. (2011) Interactions of flow and reaction in fluid catalytic cracking risers. *AIChE Journal* 57 (11) 3122-3131.
Zhu, K., Mao, X., Weng, H., Zhu, Z. and Liu, F. (1985) Investigation of the lumped kinetic model for catalytic cracking: II. A prior simulation for experimental planning. *Acfa Pet. Sin. (Pet. Process Sect.)* 1 (47).
Zong, G., Ning, H., Jiang, H. and Ouyang, F. (2010) The Lumping Kinetic Model for the Heavy Oil Catalytic Cracking MIP Process. *Petroleum Science and Technology* 28 (17) 1778-1787.

Appendix A: Correlations, equations and parameters

Table A.1 – A.8 and Equations A1 – A24 are correlations of physical and transport parameters adopted from the plant and literature (Han and Chung 2001a; Han and Chung 2001b).

Table A.1: Distillation Coefficients

Volume % distilled	10	30	50	70	90
a	0.5277	0.7429	0.8920	0.8705	0.9490
b	1.0900	1.0425	1.0176	1.0226	1.0110

Table A.2: Tuned coefficients for Z factor (Azizi et al. 2010)

Coefficient	Tuned Coefficient	Coefficient	Tuned Coefficient
a	0.0373142485385592	k	−24449114791.1531
b	−0.0140807151485369	l	19357955749.3274
c	0.0163263245387186	m	−126354717916.607
d	−0.0307776478819813	n	623705678.385784
e	13843575480.943800	o	17997651104.3330
f	−16799138540.763700	p	151211393445.064
g	1624178942.6497600	q	139474437997.172
h	13702270281.086900	r	−24233012984.0950
i	−41645509.896474600	s	18938047327.5205
j	237249967625.01300	t	−141401620722.689

Table A.3: Tuned coefficients for Z factor (Bahadori et al. 2007)

Coefficient	Tuned coefficients
Aa	0.969469
Ba	−1.349238
Ca	1.443959
Da	−0.36860
Ab	−0.107783
Bb	−0.127013
Cb	0.100828
Db	−0.012319
Ac	0.018481
Bc	0.052341
Cc	−0.050688
Dc	0.01087
Ad	−0.000584
Bd	−0.002146
Cd	0.002096
Dd	−0.000459

Table A.4: Tuned coefficients for $0.2 \leq P_{pr} \leq 3$ (Heidaryan et al. 2010a)

Coefficient	Tuned Coefficient
A1	2.827793
A2	-0.4688191
A3	−1.262288
A4	−1.536524
A5	−4.535045
A6	0.06895104
A7	0.1903869
A8	0.6200089
A9	1.838479
A10	0.4052367
A11	1.073574

Table A.5: Tuned coefficients for Z factor (Heidaryan et al. 2010b)

Coefficient	Tuned Coefficient
A1	1.11532372699824
A2	−0.07903952088760
A3	0.01588138045027
A4	0.00886134496010
A5	−2.16190792611599
A6	1.15753118672070
A7	−0.05367780720737
A8	0.01465569989618
A9	−1.80997374923296
A10	0.95486038773032

Table A.6: Tuned coefficients for Z factor (Sanjari and Lay 2012)

Coefficient	Tuned Coefficient
A1	0.007698
A2	0.003839
A3	−0.467212
A4	1.018801
A5	3.805723
A6	−0.087361
A7	7.138305
A8	0.083440

Heat capacity of gas,C_{pg}, is

$$C_{pg} = \beta_1 + \beta_2 T_g + \beta_3 T_g^2 \quad \text{(A.1)}$$

Where β_1, β_2, β_3 and β_4 catalyst decay constant given as

$$\beta_1 = -1.492343 + 0.124432K_f + \beta_4\left(1.23519 - \frac{1.04025}{S_g}\right) \quad \text{(A.2)}$$

$$\beta_2 = (-7.53624 \times 10^{-4})\left[2.9247 - (1.5524 - 0.05543K_f)K_f + \beta_4\left(6.0283 - \frac{5.0694}{S_g}\right)\right] \quad \text{(A.3)}$$

$$\beta_3 = (1.356523 \times 10^{-6})(1.6946 + 0.0884\beta_4) \quad \text{(A.4)}$$

$$\beta_4 = \left[\left(\frac{12.8}{Kf} - 1\right)\left(1 - \frac{10}{Kf}\right)(S_g - 0.885)(S_g - 0.7)(10^4)\right]^2 \text{ For } 10 < Kf < 12.8 \quad \text{(A.5)}$$

Else $\beta_4 = 0$ for all other cases

Kf is the Watson characterization factor written as

$$Kf = \frac{(1.8T_{MeABP})^{\frac{1}{3}}}{S_g} \quad \text{(A.6)}$$

Where M_{wg} is the molecular weight of the gas and can be calculated using

$$M_{wg} = 42.965\left[\exp\left(2.097 \times 10^{-4}T_{MeABP} - 7.787S_g + 2.085 \times 10^{-3}T_{MeABP}S_g\right)\right](T_{MeABP}^{1.26007}\ S_g^{4.98308}) \quad \text{(A.7)}$$

$$T_{MeABP} = T_{VABP} - 0.5556\exp[-0.9440 - 0.0087(1.8T_{VABP} - 491.67)^{0.6667} + 2.9972(Sl)^{0.3333} \quad \text{(A.8)}$$

Where T_{VABP} , the volume average boiling temperature and (Sl) is slope given as

$$(Sl) = 0.0125(T_{90ASTM} - T_{10ASTM}) \quad \text{(A.9)}$$

$$T_{VABP} = 0.2(T_{10ASTM+}\ T_{30ASTM+}T_{50ASTM+}\ T_{70ASTM+}\ T_{90ASTM}) \quad \text{(A.10)}$$

The ASTM D86 distillation temperatures are calculated using

$$T_{10ASTM} = a_{10}^{-\frac{1}{b_{10}}}(T_{10TBP})^{\frac{1}{b_{10}}} \quad \text{(A.11)}$$

$$T_{30ASTM} = a_{30}^{-\frac{1}{b_{30}}}(T_{30TBP})^{\frac{1}{b_{30}}} \quad \text{(A.12)}$$

$$T_{50ASTM} = a_{50}^{-\frac{1}{b_{50}}}(T_{50TBP})^{\frac{1}{b_{50}}} \quad \text{(A.13)}$$

$$T_{70ASTM} = a_{70}^{-\frac{1}{b_{70}}}(T_{70TBP})^{\frac{1}{b_{70}}} \quad \text{(A.14)}$$

$$T_{90ASTM} = a_{90}^{-\frac{1}{b_{90}}}(T_{90TBP})^{\frac{1}{b_{90}}} \quad \text{(A.15)}$$

Where a_i and b_i are distillation coefficients (Table A.1) and T_{iTBP} is the TBP distillation temperature.

Interface heat transfer coefficient between the catalyst and gas phases, h_p,

$$h_p = 0.03 \frac{K_g}{d_c^{\frac{2}{3}}} \left[\frac{|(v_g - v_c)|\rho_g \varepsilon_g}{\mu_g} \right]^{\frac{1}{3}} \quad \text{(A.16)}$$

Thermal conductivity of hydrocarbons

$$K_g = 1 \times 10^{-6}(1.9469 - 0.374M_{wm} + 1.4815 \times 10^{-3}M_{wm}^2 + 0.1028T_g) \quad \text{(A.17)}$$

M_{WM} is the mean molecular weight of the combined catalyst and gas

$$M_{WM} = \frac{1}{\left(\frac{ygo}{M_{wgo}} + \frac{ygl}{M_{wgl}} + \frac{ygs}{M_{wgs}} + \frac{yck}{M_{ck}}\right)} \quad \text{(A.18)}$$

$$M_{wgo} = M_{wg} \quad \text{(A.19)}$$

$$M_{wgs} = 0.002M_{wH_2} + 0.057M_{wC_1} + 0.078M_{wC_2} + 0.297M_{wC_3} + 0.566M_{wC_4} \quad \text{(A.20)}$$

The viscosity of the gas

$$\mu_g = 3.515 \times 10^{-8}\mu_{pr} \frac{\sqrt{M_{WM}P_{pc}^{\frac{2}{3}}}}{T_{pc}^{\frac{1}{6}}} \quad \text{(A.21)}$$

$$\mu_{pr} = 0.435 \exp\left[\left(1.3316 - T_{pr}^{0.6921}\right)P_{pr}\right] T_{pr} + 0.0155 \quad \text{(A.22)}$$

$$T_{pc} = 17.1419\left[\exp\left(-9.3145 \times 10^{-4}T_{MeABP} - 0.5444S_g + 6.4791 \times 10^{-4}T_{MeABP}S_g\right)\right] \times T_{MeAB}^{-0.4844}S_g^{4.0846} \quad \text{(A.23)}$$

$$P_{pc} = 4.6352 \times 10^6\left[\exp\left(-8.505 \times 10^{-3}T_{MeABP} - 4.8014S_g + 5.749 \times 10^{-3}T_{MeABP}S_g\right)\right] \times T_{MeAB}^{-0.4844}S_g^{4.0846} \quad \text{(A.24)}$$

Table A.7 summarizes the variables, feed and catalyst characteristic and other parameters used in this simulation. Most of the parameters were obtained from the industry and literature (Han and Chung 2001b; Ahari et al. 2008b).

Table A.7: Specifications of parameters for four lump model (Han and Chung 2001a; Han and Chung 2001b)

Variable	Value
Riser Height, *x* (m)	30
$T_g(0)$ (Temperature of gas oil, K)	535
$T_c(0)$ (Temperature of gas catalyst, K)	933
$v_c(0)$ Velocity of catalyst (m/s)	12
$v_g(0)$ Velocity of gas oil (m/s)	10

D Riser Diameter (m)	1.1
F_c (Catalyst mass flowrate, kg/s)	300
F_g (Gas oil mass flowrate, kg/s)	49.3
$y_{go}(0)$ Mass fraction of gas oil	1.0
$y_{gl}(0)$ Mass fraction of gas oil	0.0
$y_{gs}(0)$ Mass fraction of gas oil	0.0
$y_{ck}(0)$ Mass fraction of gas oil	0.0
M_{wgo} Molecular weight gas oil (kg/k mol)	371
M_{wgl} Molecular weight gasoline (kg/k mol)	106.7
M_{wck} Molecular weight coke (kg/k mol)	14.4
d_c (Average particle diameter, m)	0.00007
S_c (Average sphericity of catalyst particles)	0.72
S_g (Specific gravity)	0.897
C_{ckCL1} (Coke on catalyst, kg coke/kg catalyst)	0.001
α_{c0} (pre-exponential factor of α_c)	1.1e-5
α_{c^*} (Catalyst deactivation coefficient)	0.1177
C_{pc} (Heat capacity of catalyst, kJ/kg K)	1.15
ρ_c (Density of catalyst, kg/m^3)	1410
R_{AN}(Aromatics/Naphthenes in liquid feedstock)	2.1
T_{10TBP} TBP distilled 10 volume%, ^{o}C	554.3
T_{30TBP}, TBP distilled 30 volume %, ^{o}C	605.4
T_{50TBP}, TBP distilled 50 volume %, ^{o}C	647.0
T_{70TBP} TBP distilled 70 volume %, ^{o}C	688.2
T_{90TBP} TBP distilled 90 volume %, ^{o}C	744.8
a_{10} Distillation Coefficients 10 volume%	0.5277
a_{30} Distillation Coefficients 30 volume %	0.7429
a_{50} Distillation Coefficients 50 volume %	0.8920
a_{70} Distillation Coefficients 70 volume %	0.8705
a_{90} Distillation Coefficients 90 volume %	0.9490
b_{10} Distillation Coefficients 10 volume %	1.0900
b_{30} Distillation Coefficients 30 volume %	1.0425
b_{50} Distillation Coefficients 50 volume %	1.0176
b_{70} Distillation Coefficients 70 volume %	1.0226
b_{90} Distillation Coefficients 90 volume %	1.0110
k_{10} Frequency factor (s^{-1})	1457.50
k_{20} Frequency factor (s^{-1})	127.59
k_{30} Frequency factor (s^{-1})	1.98
k_{40} Frequency factor (s^{-1})	256.81
k_{50} Frequency factor (s^{-1})	6.29e-4
E_1 Activation Energy (kJ/kg mol)	57,359
E_2 Activation Energy (kJ/kg mol)	52,754

E_3 Activation Energy (kJ/kg mol)	31,820
E_4 Activation Energy (kJ/kg mol)	65,733
E_5 Activation Energy (kJ/kg mol)	66,570
E_c Catalyst Activation Energy (kJ/kg mol)	49,000
ΔH_1 Heat of reaction (kJ/kg)	195
ΔH_2 Heat of reaction (kJ/kg)	670
ΔH_3 Heat of reaction (kJ/kg)	745
ΔH_4 Heat of reaction (kJ/kg)	530
ΔH_5 Heat of reaction (kJ/kg)	690
M_{wH_2} Molecular weights of hydrogen (kg/k mol)	2
M_{wC_1} Molecular weights of methane (kg/k mol)	16
M_{wC_2} Molecular weights of ethane (kg/k mol)	30
M_{wC_3} Molecular weights of propane (kg/k mol)	44
M_{wC_4} Molecular weights of butane (kg/k mol)	58
g, acceleration due to gravity (m/s^2)	9.8
R, ideal gas constant (kPa m3/kg mole K)	8.3143

Table A.8: Specifications of parameters and conditions for Sudan Refinery.

Variable	Value
Riser Height, *x* (m)	47.1
$T_g(0)$ (Temperature of gas oil, K)	478.15
$T_c(0)$ (Temperature of gas catalyst, K)	905
D Riser Diameter (m)	1.36
F_c (Catalyst mass flowrate, kg/s)	400.32
F_g (Gas oil mass flowrate, kg/s)	62.5
$y_{go}(0)$ Mass fraction of gas oil (kg lump/kg feed)	1.0
$y_{gl}(0)$ Mass fraction of gasoline (kg lump/kg feed)	0.0
$y_{dz}(0)$ Mass fraction of diesel (kg lump/kg feed)	0.0
$y_{dg}(0)$ Mass fraction of dry gas (kg lump/kg feed)	0.0
$y_{lpg}(0)$ Mass fraction of LPG (kg lump/kg feed)	0.0
$y_{ck}(0)$ Mass fraction of coke (kg lump/kg feed)	0.0
M_{wgo} Molecular weight gas oil (kg/k mol)	371
M_{wgl} Molecular weight gasoline (kg/k mol)	106.7
M_{wdz} Molecular weight diesel (kg/k mol)	178.6
M_{wck} Molecular weight coke (kg/k mol)	14.4
d_c (Average particle diameter, m)	0.000065
S_c (Average sphericity of catalyst particles)	0.72
S_g (Specific gravity)	0.9019
C_{ckCL1} (Coke on catalyst, kg coke/kg catalyst)	0.001
α_{c0} (pre-exponential factor of α_c)	1.1e-5

α_{c^*} (Catalyst deactivation coefficient)	0.1177
C_{pc} (Heat capacity of catalyst, kJ/kg K)	1.15
ρ_c (Density of catalyst, kg/m^3)	720
R_{AN}(Aromatics/Naphthenes in liquid feedstock)	2.1
T_{10TBP} TBP distilled 10 volume%, ^oC	368
T_{30TBP}, TBP distilled 30 volume %, ^oC	453
T_{50TBP}, TBP distilled 50 volume %, ^oC	472
T_{70TBP} TBP distilled 70 volume %, ^oC	528
T_{90TBP} TBP distilled 90 volume %, ^oC	644
E_c Catalyst Activation Energy (kJ/kg mol)	49,000
M_{wH_2}Molecular weights of hydrogen (kg/k mol)	2
M_{wC_1}Molecular weights of methane (kg/k mol)	16
M_{wC_2}Molecular weights of ethane (kg/k mol)	30
M_{wC_3}Molecular weights of propane (kg/k mol)	44
M_{wC_4}Molecular weights of butane (kg/k mol)	58
g, acceleration due to gravity (m/s^2)	9.8
R, ideal gas constant (kPa m3/kg mole K)	8.3143

Table A.9: Kinetic equations for the simulation of propylene lump

Equations and descriptions		
Description of variable	Equations	Eq.No
Kinetic model equations for the six-lump model		
Gas oil R_{go} reaction rate	$R_{go} = -(K_1 + K_2 + K_3 + K_4 + K_5){y_{go}}^2 \emptyset_c$	(A.25)
Gasoline R_{gl} Reaction rate	$R_{gl} = \left(K_1 {y_{go}}^2 - K_6 y_{gl} - K_7 y_{gl} - K_8 y_{gl} - K_9 y_{gl}\right)\emptyset_c$	(A.26)
Butylene R_{C4} Reaction rate	$R_{C4} = \left(K_2 {y_{go}}^2 + K_6 y_{gl} - K_{10} y_{C4} - K_{11} y_{C4}\right)\emptyset_c$	(A.27)
Propylene R_{C3} Reaction rate	$R_{C3} = \left(K_3 {y_{go}}^2 + K_7 y_{gl} + K_{10} y_{C4} - K_{12} y_{C3}\right)\emptyset_c$	(A.28)
Light gas R_{dg} Reaction rate	$R_{dg} = \left(K_4 {y_{go}}^2 + K_8 y_{gl} + K_{11} y_{C4} + K_{12} y_{C3}\right)\emptyset_c$	(A.29)
Coke R_{Ck} Reaction rate	$R_{ck} = \left(K_5 {y_{go}}^2 + K_9 y_{gl}\right)\emptyset_c$	(A.30)
Gas oil to gasoline overall rate constant	$K_1 = k_{10} \exp\left(\frac{-E_1}{RT_g}\right)$	(A.31)
Gas oil to butylene overall rate constant	$K_2 = k_{20} \exp\left(\frac{-E_2}{RT_g}\right)$	(A.32)
Gas oil to propylene overall rate constant	$K_3 = k_{30} \exp\left(\frac{-E_3}{RT_g}\right)$	(A.33)
Gas oil to dry gas overall rate constant	$K_4 = k_{40} \exp\left(\frac{-E_4}{RT_g}\right)$	(A.34)
Gas oil to coke overall rate constant	$K_5 = k_{50} \exp\left(\frac{-E_5}{RT_g}\right)$	(A.35)
Gasoline to butylene overall rate constant	$K_6 = k_{60} \exp\left(\frac{-E_6}{RT_g}\right)$	(A.36)

Gasoline to propylene overall rate constant	$K_7 = k_{70} \exp\left(\frac{-E_7}{RT_g}\right)$	(A.37)
Gasoline to dry gas overall rate constant	$K_8 = K_{80} \exp\left(\frac{-E_8}{RT_g}\right)$	(3.38)
Gasoline to coke overall rate constants	$K_9 = k_{90} \exp\left(\frac{-E_9}{RT_g}\right)$	(A.39)
Butylene to propylene overall rate constant	$K_{10} = k_{100} \exp\left(\frac{-E_{10}}{RT_g}\right)$	(A.40)
Butylene to dry gas overall rate constant	$K_{11} = k_{110} \exp\left(\frac{-E_{11}}{RT_g}\right)$	(A.41)
Propylene to dry gas overall rate constant	$K_{12} = k_{120} \exp\left(\frac{-E_{12}}{RT_g}\right)$	(A.42)
Q_{react} is the rate of heat generation or heat removal by reaction	$Q_{react} = -(\Delta H_1 K_1 {y_{go}}^2 + \Delta H_2 K_2 {y_{go}}^2 + \Delta H_3 K_3 {y_{go}}^2 + +\Delta H_4 K_4 {y_{go}}^2 + \Delta H_5 K_5 {y_{go}}^2 + \Delta H_6 K_6 y_{gl} + \Delta H_7 K_7 y_{gl} + \Delta H_8 K_8 y_{gl} + \Delta H_9 K_9 y_{gl} + \Delta H_{10} K_{10} y_{C4} + \Delta H_{11} K_{11} y_{C4} + \Delta H_{12} K_{12} y_{C4}) \emptyset_c$	(A.43)
Riser equations from material balance		
Gas oil fractional yield	$\frac{d_{y_{go}}}{dx} = \frac{\rho_c \varepsilon_c \Omega}{F_g} R_{go}$	(A.44)
Gasoline fractional yield	$\frac{d_{y_{gl}}}{dx} = \frac{\rho_c \varepsilon_c \Omega}{F_g} R_{gl}$	(A.45)
Butylene fractional yield	$\frac{d_{y_{C4}}}{dx} = \frac{\rho_c \varepsilon_c \Omega}{F_g} R_{C4}$	(A.46)
Propylene fractional yield	$\frac{d_{y_{C3}}}{dx} = \frac{\rho_c \varepsilon_c \Omega}{F_g} R_{C3}$	(A.47)

Dry gas fractional yield	$\frac{d_{y_{dg}}}{dx} = \frac{\rho_c \varepsilon_c \Omega}{F_g} R_{dg}$	(A.48)
Coke fractional yield	$\frac{d_{y_{ck}}}{dx} = \frac{\rho_c \varepsilon_c \Omega}{F_g} R_{ck}$	(A.49)

Appendix B: List of publications

Journals

1. John, Y. M., Mustafa, M. A., Patel, R. and Mujtaba, I. M. (2019) Parameter estimation of a six-lump kinetic model of an industrial fluid catalytic cracking unit. Fuel 235 1436-1454. Impact Factor: 5.908
2. John, Y. M., Patel, R. and Mujtaba, I. M. (2017) Maximisation of Gasoline in an Industrial Fluidized Catalytic Cracking Unit. Energy & Fuels 31 5645−5661. Impact Factor: 3.024
3. John, Y. M., Patel, R. and Mujtaba, I. M. (2017) Modelling and simulation of an industrial riser in fluid catalytic cracking process. Computers & Chemical Engineering 106 730-743. Impact Factor: 3.113
4. John, Y. M., Patel, R. and Mujtaba, I. M. (2018) Effects of compressibility factor on fluid catalytic cracking unit riser hydrodynamics. Fuel 223 230-251.
5. John, Y. M., Patel, R. and Mujtaba, I. M. (2018) Maximisation of propylene in an industrial FCC unit. Applied Petrochemical Research.

Conferences

1. John, Y. M., Patel, R. and Mujtaba, I. M. (2017) Optimisation of Fluidized Catalytic Cracking Unit Regenerator to Minimise CO_2 Emissions. Chemical Engineering Transactions; The Italian Association of Chemical Engineering 57
2. John, Y. M., Patel, R. and Mujtaba, I. M. (2016) Modelling and Simulation of an Industrial Riser in Fluid Catalytic Cracking Process. Maribor, Slovenia, Elsevier.